

A Novel Heat Recovery/Desiccant Cooling System

Thesis by

Shuli Liu, BEng, MSc

Thesis submitted to the University of Nottingham

For the degree of Doctor of Philosophy

May 2008

Contents

Abstract..... III

Acknowledgement III

Nomenclature IV

List of Figures VII

List of Tables XII

Chapter 1. Introduction..... - 1 -

 1.1 Background..... - 1 -

 1.2 Description of the Novel Heat Recovery/Desiccant Cooling System..... - 5 -

 1.3 Work Involved in This Thesis - 8 -

Chapter 2. Review of previous work of Heat/Mass Exchangers and Desiccant Dehumidification/Cooling Systems..... - 12 -

 2.1 Purpose and Regions Employing Desiccant Cooling - 12 -

 2.1.1 Purpose of Utilizing Heat/Mass Recovery and Adsorption/ Absorption..... - 12 -

 2.1.2 Regions Employing Desiccant Cooling..... - 13 -

 2.2 Enthalpy (Energy) Exchanger..... - 14 -

 2.2.1 Enthalpy Plate Exchanger - 15 -

 2.2.2 Enthalpy Wheel Exchanger - 15 -

 2.2.3 Hydrophilic Membranes Exchanger - 17 -

 2.3 Adsorption - 18 -

 2.3.1 Categories of Solid Desiccant - 19 -

 2.3.2 Solid Desiccant Carriers - 21 -

 2.3.3 Regeneration Energy Source - 24 -

 2.3.4 Solid Desiccant Hybrid Cooling Systems - 27 -

 2.4 Absorption - 30 -

 2.4.1 Categories of Liquid Desiccant - 30 -

 2.4.2 Liquid Desiccant Carriers..... - 33 -

 2.4.3 Regenerator Energy Source - 38 -

 2.4.4 Cooling Energy..... - 40 -

 2.4.5 Solution Flowing Direction to Air Flow - 41 -

2.4.6 Liquid Desiccant Hybrid Cooling Systems	- 42 -
2.5 Summary	- 47 -
Chapter 3. Optimal Study of Heat/Mass Recovery Materials.....	- 49 -
3.1 Introduction.....	- 49 -
3.2 Theoretical Analyses of the Heat/mass Transfer	- 50 -
3.2.1 Sensible Heat Transfer Analyses.....	- 52 -
3.2.2 Latent Heat Transfer Analyses	- 53 -
3.3 Characteristics Considered in Selecting the Heat/mass Recovery Materials.....	- 56 -
3.4 Comparative Analyses of Potential Heat/mass Transfer Materials	- 58 -
3.4.1 Metal Type	- 58 -
3.4.2 Fibre Type	- 61 -
3.4.3 Ceramics Type.....	- 63 -
3.4.4 Zeolite Type	- 65 -
3.4.5 Carbon Type.....	- 66 -
3.5 Comparison of the Material Types and Results Discussion	- 68 -
3.6 Summary.....	- 69 -
Chapter 4. Performance Investigations of Fibre Heat/mass Exchanger.....	- 70 -
4.1 Introduction.....	- 70 -
4.2 Theoretical Analyses of Cellulose Fibre Membranes	- 70 -
4.2.1 Description of the Selected Heat/Mass Transfer Membranes.....	- 70 -
4.2.2 Heat/mass Transfer Mechanisms.....	- 73 -
4.2.3 Analyses of Heat/mass Transfer.....	- 74 -
4.3 Numerical Simulation of Cellulose Fibre Membrane.....	- 76 -
4.3.1 Description of the Fibre Exchanger Configuration	- 76 -
4.3.2 Grids Distribution and Assumptions	- 78 -
4.3.3 Heat/Mass Transfer Balance and Efficiencies.....	- 79 -
4.3.4 Calculation Method and Cell Element	- 80 -
4.3.5 Base conditions for Numerical Simulation.....	- 81 -
4.3.6 Numerical Simulation Results.....	- 81 -
4.4 Experimental Testing of the Fiber Membrane Exchanger.....	- 82 -
4.4.1 Prototype of the Fibre Membrane Exchanger.....	- 82 -
4.4.2 Air Environment Control System.....	- 84 -
4.4.3 Fibre Exchanger Test Rig.....	- 85 -
4.4.4 Comparison of Solid Desiccant-Coated and Liquid Desiccant-Soaked FPPEM.....	- 87 -

4.4.5 Comparison of Simulation and Experimental Results.....	- 88 -
4.5 Modelling Based on the Corrected Heat/mass Transfer Coefficients.....	- 90 -
4.5.1 Modelling Results.....	- 90 -
4.5.2 Summary of Simulation Results.....	- 94 -
4.6 Comparison between the Experimental and Correction Modelling Results.....	- 97 -
4.6.1 Airflow Speed Influencing the Energy Recovery Effectiveness.....	- 97 -
4.6.2 Moisture Content Difference Influencing the Energy Recovery Effectiveness.....	- 98 -
4.6.3 Reasons Causing the Errors between Simulations and Testing Results.....	- 99 -
4.7 Summary.....	- 99 -
Chapter 5. Performance Investigations of Desiccant Dehumidifier	- 102 -
5.1 Introduction.....	- 102 -
5.2 Description of the Dehumidifier Core Operation	- 102 -
5.3 Mathematical Theory.....	- 104 -
5.3.1 Heat Transfer between Air and Desiccant Solution	- 104 -
5.3.2 Mass Transfer between Air and Desiccant Solution	- 105 -
5.3.3 Heat and Mass Transfer Performance	- 105 -
5.4 Numerical Modelling.....	- 106 -
5.4.1 Channels Distribution and Assumptions	- 106 -
5.4.2 Calculation Method and Cell Element	- 107 -
5.4.3 Heat and Mass Transfer.....	- 108 -
5.4.4 Base Conditions for Numerical Simulation.....	- 108 -
5.4.5 Modelling Results.....	- 109 -
5.5 Experimental Testing	- 118 -
5.5.1 Test Rig and Dehumidifier Core	- 118 -
5.5.2 Measuring Equipments.....	- 120 -
5.5.3 Testing Results	- 122 -
5.6 Comparisons between the Numerical Simulation and Testing Results	- 125 -
5.6.1 Desiccant Temperature Influence on Dehumidifier Performance	- 125 -
5.6.2 Humid Air Temperature Influence on Dehumidifier Performance	- 126 -
5.6.3 Air Relative Humidity Influence on Dehumidifier Performance	- 127 -
5.6.4 Desiccant Concentration Influence on Dehumidifier Performance.....	- 128 -
5.6.5 Reasons Causing the Errors between Simulations and Testing Results.....	- 129 -
5.7 Summary.....	- 130 -

Chapter 6. Performance Investigations of Desiccant Regenerator.....	133 -
6.1 Introduction.....	133 -
6.2 Description of the Regenerator and Working Mathematical Theory.....	134 -
6.2.1 Description of the Regenerator.....	134 -
6.2.2 Mass and Heat Transfer between Air Stream and Desiccant Film.....	135 -
6.2.3 Performance Definition of the Regenerator.....	135 -
6.3 Numerical Model.....	136 -
6.3.1 Channel Distribution and Assumptions of Air-to-Air Cross-flow Exchanger	136 -
6.3.2 Simulation Base Conditions for Air-to-Air Heat Exchanger.....	138 -
6.3.3 Air-to-Air Heat Exchanger Modelling Results.....	138 -
6.3.4 Simulation Base Conditions for the Regenerator	140 -
6.3.5 Regenerator Modelling Results	141 -
6.3.6 Summary of Simulation Results.....	151 -
6.4 Experimental Testing.....	151 -
6.4.1 Test Rig	152 -
6.4.2 Air-to-Air Heat Recovery Testing Results	153 -
6.4.3 Desiccant Regenerator Testing Result.....	154 -
6.5 Comparisons of the Modelling and Experimental Results	157 -
6.5.1 Comparisons for the Air-to-air Heat Exchanger.....	157 -
6.5.2 Comparisons for the Desiccant Regenerator	158 -
6.6 Summary.....	162 -
Chapter 7. Performance of the Heat Recovery/Desiccant Cooling System.....	167 -
7.1 Description of Heat Recovery/Desiccant Cooling System.....	167 -
7.2 Heat and Mass Transfer and COP of Whole System.....	169 -
7.2.1 Desiccant Circle Thermal Process on Duhring Diagram.....	169 -
7.2.2 Air Circle Thermal Process on Psychrometric Chart	170 -
7.2.3 Heat and Mass Transfer.....	171 -
7.3 Theoretical Modelling	175 -
7.3.1 Modelling Set-up.....	175 -
7.3.2 Base Conditions for Whole System Theoretical Modelling.....	176 -
7.3.3 Modelling Results of Heat Recovery/Desiccant Cooling System.....	177 -
7.3.4 Summary of Theoretical Simulation Results.....	183 -
7.4 Experimental Testing of Heat Recovery/desiccant Cooling System	185 -
7.4.1 Test Rig of Heat Recovery/desiccant Cooling System.....	185 -
7.4.2 Tests of Flat Plate Heat Exchanger	186 -

7.4.3 Testing Results of Heat Recovery/Desiccant Cooling System.....	- 186 -
7.5 Comparison of Theoretical Simulation and Testing Results.....	- 192 -
7.6 Summary.....	- 193 -
Chapter 8. Economic Analysis of the Whole System	- 199 -
8.0 Introduction.....	- 199 -
8.1 Required Cooling and Heating energy.....	- 199 -
8.2 Equipments Capital and Running Cost.....	- 202 -
8.3 Summary.....	- 204 -
Chapter 9. Conclusion	- 205 -
9.1 Conclusions.....	- 205 -
9.1.1 Optimal Material Selection for Heat/mass Transfer.....	- 205 -
9.1.2 Performance of the Air-to-Air Heat/Mass Exchanger.....	- 205 -
9.1.3 Performance of the Liquid Desiccant Dehumidifier.....	- 206 -
9.1.4 Performance of the Liquid Desiccant Regenerator.....	- 207 -
9.1.5 Performance of the Whole Heat Recovery/Desiccant Cooling System.....	- 208 -
9.1.6 Economic Analysis of the Whole System	- 208 -
9.2 Further Work	- 208 -
References.....	- 210 -
Appendixes.....	- 221 -
Appendix I —Thermal Parameters of Air.....	- 221 -
Appendix II —Thermal Parameters of LiCl, CaCl ₂ and LiBr Solutions	- 221 -
Appendix III —Henry’s Law Constant of the Aqueous Solutions.....	- 227 -

Abstract

The global air temperature has increased by 0.74 ± 0.18 °C since 1905 and scientists have shown that CO₂ accounts for 55 percentages of the greenhouse gases. Global atmospheric CO₂ has been sharply increased since 1751, however the trend has slowed down in last fifty years in the Western Europe. UK and EU countries have signed the Kyoto agreement to reduce their greenhouse gas emissions by a collective average of 12.5% below their 1990 levels by 2020. In the EU, 40% of CO₂ emission comes from the residential energy consumption, in which the HVAC system accounts for 50%, lighting accounts for 15% and appliances 10%. Hence, reducing the fossil-fuel consumption in residential energy by utilizing renewable energy is an effective method to achieve the Kyoto target. However, in the UK renewable energy only accounts for 2% of the total energy consumption in 2005.

A novel heat recovery/desiccant cooling system is driven by the solar collector and cooling tower to achieve low energy cooling with low CO₂ emission. This system is novel in the following ways:

- Uses cheap fibre materials as the air-to-air heat exchanger, dehumidifier and regenerator core
- Heat/mass fibre exchanger saves both sensible and latent heat from the exhaust air
- The dehumidifier core with hexagonal surface could be integrated with windcowls/catchers draught
- Utilises low electrical energy and therefore low CO₂ is released to the environment

The cooling system consists of three main parts: heat/mass transfer exchanger, desiccant dehumidifier and regenerator. The fibre exchanger, dehumidifier and regenerator cores are the key parts of the technology.

Owing to its proper pore size and porosity, fibre is selected out as the exchanger membrane to execute the heat/mass transfer process. Although the fibre is soft and difficult to keep the shape for long term running, its low price makes its frequent replacement feasible, which can counteract its disadvantages. A counter-flow air-to-air heat /mass exchanger was investigated

and simulation and experimental results indicated that the fibre membranes soaked by desiccant solution showed the best heat and mass recovery effectiveness at about 89.59% and 78.09%, respectively.

LiCl solution was selected as the working fluid in the dehumidifier and regenerator due to its advisable absorption capacity and low regeneration temperature. Numerical simulations and experimental testing were carried out to work out the optimal dehumidifier/regenerator structure, size and running conditions. Furthermore, the simulation results proved that the cooling tower was capable to service the required low temperature cooling water and the solar collector had the ability to offer the heating energy no lower than the regeneration temperature 60°C.

The coefficient-of-performance of this novel heat recovery/desiccant cooling system is proved to be as high as 13.0, with a cooling capacity of 5.6kW when the system is powered by renewable energy. This case is under the pre-set conditions that the environment air temperature is 36°C and relative humidity is 50% (cities such as Hong Kong, Taiwan, Spain and Thailand, etc). Hence, this system is very useful for a hot/humid climate with plenty of solar energy. The theoretical modelling consisted of four numerical models is proved by experiments to predict the performance of the system within acceptable errors.

Economic analysis based on a case (200m² working office in London) indicated that the novel heat recovery/desiccant cooling system could save 5134kWh energy as well as prevent 3123kg CO₂ emission per year compared to the traditional HVAC system. Due to the flexible nature of the fibre, the capital and maintenance cost of the novel cooling system is higher than the traditional HVAC system, but its running cost are much lower than the latter. Hence, the novel heat recovery/desiccant cooling system is cost effective and environment friendly technology.

Acknowledgement

I would like to thank my supervisor Professor Saffa B. Riffat who offered me the scholarship and unlimited support for my research. I also sincerely appreciate the kind help from my second supervisor, Dr. XuDong Zhao, who guided and advised me through the whole process of my research.

Special thanks to my parents and aunt who supported and encouraged me throughout my life and studies. I am grateful to all the staff in the school for their invaluable assistance and particular thanks to Dr ShenYi Wu and Dr XiaoLi Ma who give me help and advice in the writing process. Thanks to all the technicians in the school especially to Mr Dave Oliver and Mr Dave Taylor for their unlimited help in the laboratory.

I also thank the School of the Built Environment, the University of Nottingham for their financial support for the tuition fees and living expenses.

Nomenclature

Symbol	Term	Unit
A	Heat and mass transfer area	m^2
c	Specific heat capacity	J/kg K
C	Mass quantity multiplying specific heat capacity	J/kg K
d_{Pore}	Pore diameter of the porous membrane	cm
d_{solute}	Solute molecular diameter	cm
d	Moisture content of the air stream	kg/kg dry air
D	Equivalent diameter of the exchanger tunnel	m
D_{AB}	Mass diffusivity	m^2/s
ΔF	Fluid flowing cross annular section acreage	kg/kg (dry air)
$F_1(\xi), F_2(\xi)$	Correction factor of the solute diffusion coefficient through solvent-filled pores	
g	Acceleration of gravity	m^2/s
h	Enthalpy of materials	J/kg
H	Henry's law constant	
k^s	Convective heat transfer coefficient	$W/m^2 K$
k^l	Convective mass transfer coefficient	m/s
k	Thermal conductivity	W/m K
k'_{mass}	Solute diffusion coefficient in the solvent	m^2/s
k_{mass}	Moisture infiltration coefficient through exchanger membrane	m^2/s
L	Length of the exchanger tunnel	m
m	Mass quantity of materials	kg
M_A	Molecular weight of air (29.0)	kg/mole
P	Atmospheric Pressure	Pa
p	Vapour Pressure	Pa
q	Sensible heat transfer energy	J
Q	Input or output energy	J
r	Solute particle radius	cm
R	The ideal gas constant (=8.314)	J/mol K

R_m	The molar gas constant for water (=461)	J kg/K
t	Temperature	°C
T	Absolute temperature	K
u	Air flow speed	m/s
V	Volume flow speed	m ³ /s
V'	Volume of materials	m ³
z	Distance in the z direction	m
α	Thermal diffusivity of air	m ² /s
ν	Kinematic viscosity	m ² /s
μ	Dynamic viscosity	Ns/m ²
ρ	Density	kg/m ³
\mathcal{G}	Porosity of materials	%
θ	Mass concentration of desiccant solution	%
λ	Free path length of the diffusing species	cm
κ	Boltzmann's constant (1.38×10^{-16})	ergs/K
γ	Lennard-Jones diameter of spherical molecule (for air it is 3.617×10^{-8})	cm
ε	Energy recovery effectiveness	
ξ	Reduced pore diameter	
$\omega_{floater}$	Coefficient of the flow meter (determined by floater shape)	
ϖ	Fluid expand coefficient as gaseous, for liquid is 1.0	
δ	Heat recovery membrane's thickness	m
η_1, η_2, η_3	Heat recovery effectiveness of the weak desiccant-to-hot water, weak-to-strong desiccant and strong desiccant-to-cold water plate heat exchanger respectively.	
COP_1	Coefficient of system performance when renewable energy is not utilised	
COP_2	Coefficient of system performance when renewable energy is utilised	
Nu	Nusselt Number	
Pe	Peclet Number	
Pr	Prandtl Number	
Re	Reynolds Number	
Le	Lewis Number	
Kn	Knudsen Number	
Sc	Schmidt Number	

Subscript Term

<i>f</i>	Fresh air
<i>e</i>	Exhaust air
<i>s</i>	Supply air
<i>air</i>	Air stream
<i>b</i>	Bulk temperature of the fluent materials in the exchanger tunnel
<i>w</i>	Wall temperature of the exchanger tunnel membrane's surface
<i>Ex</i>	Air-to-air heat/mass fibre exchanger
<i>De</i>	Desiccant dehumidifier
<i>Re</i>	Desiccant regenerator
<i>Cr</i>	Air-to-air cross-flow heat recovery in regenerator unit
<i>min</i>	The minimal value
<i>material</i>	Materials used as the working heat/mass transfer membrane
<i>wall</i>	Heat/mass transfer wall
<i>d</i>	Desiccant solution
<i>floater</i>	Floater in the flow meter
<i>fluid</i>	Fluid such as air stream, desiccant solution, water
<i>weak</i>	Diluted solution out of dehumidifier
<i>strong</i>	Condensed solution out of regenerator
<i>hot</i>	Hot water heating the dilute solution
<i>cold</i>	Cold water cooling the condensed solution
<i>absorb</i>	Strong desiccant solution absorbed heat/mass from the air stream
<i>desorb</i>	Weak desiccant solution desorbed heat/mass into the air stream
<i>condense</i>	Condensed solution from the regenerator
<i>output</i>	Cooling capacity of the system
<i>electric</i>	Electric energy

Superscript Term

<i>air</i>	Air stream in the tunnel
<i>Se</i>	Sensible heat energy
<i>La</i>	Latent heat energy
<i>En</i>	Total energy (enthalpy) including sensible and latent heat energy
<i>b</i>	Bulk temperature of the fluent materials in the exchanger
<i>in</i>	In to the plate heat exchanger
<i>out</i>	Out of the plate heat exchanger
<i>moisture</i>	Moisture absorbed/desorbed by the desiccant solution

List of Figures

Chapter.1

Figure 1-1 Air conditioning processes: (a) traditional HVAC (b) desiccant cooling with efficient heat recovery.....	- 3 -
Figure 1-2 Thermal processes: (a) traditional HVAC (b) desiccant cooling with efficient heat recovery.....	- 3 -
Figure 1-3 Schematic diagram of the heat recovery/desiccant cooling system	- 7 -

Chapter.2

Figure 2-1 Enthalpy plat heat exchangers: (a) flat-pipe exchanger (b) flat exchanger and (c) spiral plate.....	- 15 -
Figure 2-2 Rotary heat and moisture exchanger	- 16 -
Figure 2-3 Schematic diagram of desiccant exchanger wheel	- 16 -
Figure 2-4 Plate-fine heat and mass exchanger.....	- 18 -
Figure 2-5 Cross-flow air-to-air heat exchanger	- 18 -
Figure 2-6 Silica gel and molecular sieve coated desiccant wheel.....	- 22 -
Figure 2-7 Activated carbons granular.....	- 22 -
Figure 2-8 Experimental apparatus of silica gel bed.....	- 23 -
Figure 2-9 Schematic of desiccant dehumidification/rooftop cooling system	- 25 -
Figure 2-10 Schematic of solar air collector utilized for regenerator	- 26 -
Figure 2-11 Schematic of solar water collector utilized for regenerator.....	- 26 -
Figure 2-12 Desiccant air cycle refrigerator system	- 27 -
Figure 2-13 Chilled–ceiling with desiccant cooling	- 28 -
Figure 2-14 Polypropylene sandwich dehumidifier/regenerator cores	- 34 -
Figure 2-15 Stainless steel internal dehumidifier/regenerator cores	- 34 -
Figure 2-16 Polymer pall rings/ spheres carrier for regenerator.....	- 36 -
Figure 2-17 Sandy bed impregnated with Calcium Chloride.....	- 36 -
Figure 2-18 Honeycomb paper.....	- 36 -
Figure 2-19 Celdek structure pack.....	- 36 -
Figure 2-20 Parallel-flow desiccant–solar regenerator.....	- 39 -
Figure 2-21 Counter-flow desiccant–solar regenerator.....	- 39 -
Figure 2-22 Cross-flow dehumidification/indirect evaporative cooling unit	- 42 -
Figure 2-23 Hybrid desiccant and air vapour compression cooling.....	- 44 -
Figure 2-24 Evaporative-cool greenhouse assisted by liquid desiccant and solar energy	- 45 -

Figure 2-25 Heat pump desiccant cooling system	- 46 -
Figure 2-26 Schematic of the reverse osmosis dehumidification/cooling system	- 46 -
<u>Chapter.3</u>	
Figure 3-1 Schematic diagram showing the principle of the heat/mass transfer.....	- 50 -
Figure 3-2 Pore diameter size of the heat/mass transfer membrane.....	- 56 -
Figure 3-3 Heat exchange copper tube with the micro-structured surface.....	- 59 -
Figure 3-4 Metal foams.....	- 60 -
Figure 3-5 Metal wools.....	- 60 -
Figure 3-6 Fibre structure of hardwood.....	- 61 -
Figure 3-7 Structure overviews of ceramics	- 63 -
Figure 3-8 Performs structure of three kinds of carbon fibre: (a) laminated short fibre felt (b) laminated carbon cloth felt (c) needle picked long fibre felt	- 66 -
<u>Chapter.4</u>	
Figure 4-1 Schematic diagram of three types of cellulose fibre membranes: (a) Clean fibre membrane (b) Solid desiccant-coated fibre membrane (c) Liquid desiccant-soaking fibre membrane.....	- 71 -
Figure 4-2 Schematic diagram of cellulose fibre stack exchanger.....	- 77 -
Figure 4-3 Air flow layers and channels.....	- 78 -
Figure 4-4 Simplified fresh and exhaust air channels and calculation cell	- 80 -
Figure 4-5 Heat/mass recovery efficiency vs. fresh air temperature.....	- 82 -
Figure 4-6 Prototypes of solid desiccant coated and liquid desiccant soaked FPDM	- 82 -
Figure 4-7 (a) Prototype of cellulose fibre exchanger (b) Schematic diagram of one layer of the fresh air tunnel (c) Schematic diagram of C side	- 83 -
Figure 4-8 Schematic diagram of the airflow control system	- 85 -
Figure 4-9 Prototype of the airflow control system	- 85 -
Figure 4-10 Heat/mass exchanger testing rig.....	- 86 -
Figure 4-11 Humidity sensors.....	- 86 -
Figure 4-12 Thermocouples.....	- 86 -
Figure 4-13 TA 45 thermal anemometer and measure method.....	- 87 -
Figure 4-14 Energy recovery performances vs. fresh air temperature	- 88 -
Figure 4-15 Comparison of experimental and simulation results of FPDM recovery.....	- 89 -
Figure 4-16 Energy recovery effectiveness vs. channel length.....	- 95 -
Figure 4-17 Energy recovery effectiveness vs. channel height.....	- 95 -
Figure 4-18 Energy recovery effectiveness vs. fresh air temperature.....	- 95 -
Figure 4-19 Energy recovery effectiveness vs. fresh air flow speed.....	- 95 -

Figure 4-20 Energy recovery effectiveness vs. moisture content difference.....	- 96 -
Figure 4-21 Moisture content vs. fresh air relative humidity.....	- 96 -
Figure 4-22 Energy recovery effectiveness vs. air flow speed ratio.....	- 96 -
Figure 4-23 Supply air parameters vs. air flow speed ratio.....	- 96 -
Figure 4-24 Experimental and modelling energy recovery effectiveness vs. air flow rate.....	- 97 -
Figure 4-25 Experimental and modelling energy recovery effectiveness vs. air moisture content difference.....	- 98 -
<u>Chapter.5</u>	
Figure 5-1 Sketch diagram of desiccant dehumidifier pack and desiccant film.....	- 103 -
Figure 5-2 Calculate channel sketch diagram of the dehumidifier core.....	- 106 -
Figure 5-3 Calculate cell sketch diagram of one air channel.....	- 107 -
Figure 5-4 Dehumidifier performances vs. desiccant solution mass concentration.....	- 110 -
Figure 5-5 Dehumidifier performances vs. dehumidifier channel height.....	- 115 -
Figure 5-6 Air moisture content vs. dehumidifier channel height.....	- 115 -
Figure 5-7 Dehumidifier performances vs. dehumidifier channel length.....	- 115 -
Figure 5-8 Dehumidifier performances vs. solution temperature.....	- 115 -
Figure 5-9 Dehumidifier performances vs. solution flow rate.....	- 116 -
Figure 5-10 Supply air parameters vs. solution flow rate.....	- 116 -
Figure 5-11 Dehumidifier performances vs. humid air flow speed.....	- 116 -
Figure 5-12 Dehumidifier performances vs. humid air temperature.....	- 116 -
Figure 5-13 Dehumidifier performances vs. humid air relative humidity.....	- 117 -
Figure 5-14 Schematic diagram showing the principle and layout of the test rig.....	- 119 -
Figure 5-15 View of test rig — Liquid desiccant dehumidifier.....	- 119 -
Figure 5-16 Schematic diagram of dehumidifier core.....	- 120 -
Figure 5-17 Prototype of dehumidifier core.....	- 120 -
Figure 5-18 Schematic structure and view of liquid flow indicator.....	- 121 -
Figure 5-19 Stainless thermocouples.....	- 121 -
Figure 5-20 GP hydrometers.....	- 121 -
Figure 5-21 Dehumidification performance vs. desiccant temperature.....	- 124 -
Figure 5-22 Dehumidification performance vs. fresh air temperature.....	- 124 -
Figure 5-23 Dehumidification performance vs. air relative humidity.....	- 124 -
Figure 5-24 Dehumidification performance vs. desiccant concentration.....	- 124 -
Figure 5-25 Comparison of testing and simulation results — moisture absorption capacity vs. desiccant temperature.....	- 125 -

Figure 5-26 Comparison of testing and simulation results — heat recovery effectiveness .vs. desiccant temperature..... - 126 -

Figure 5-27 Comparison of testing and simulation results — heat recovery effectiveness .vs. humid air temperature..... - 126 -

Figure 5-28 Comparison of testing and simulation results — moisture absorption capacity .vs. humid air temperature..... - 127 -

Figure 5-29 Comparison of testing and simulation results — moisture absorption capacity .vs. humid air relative humidity..... - 127 -

Figure 5-30 Comparison of testing and simulation results — heat recovery effectiveness .vs. humid air relative humidity..... - 128 -

Figure 5-31 Comparison of testing and simulation results — moisture absorption capacity .vs. desiccant concentration..... - 128 -

Chapter.6

Figure 6-1 Sketch diagram of the desiccant regenerator..... - 134 -

Figure 6-2 Wetted - wall column for mass transfer between gas and liquid..... - 137 -

Figure 6-3 Calculating cell sketch diagram of air-to-air heat exchanger - 137 -

Figure 6-4 Heat recovery efficiency vs. ratio of fresh air to exhaust air channel length..... - 138 -

Figure 6-5 Heat recovery efficiency vs.exhaust and fresh air channel length..... - 138 -

Figure 6-6 Heat recovery efficiency vs.air flow speed..... - 139 -

Figure 6-7 Heat recovery efficiency vs.air temperature..... - 139 -

Figure 6-8 Heat recovery efficiency vs. material thermal conductivity..... - 140 -

Figure 6-9 Regeneration capacity vs. desiccant solution mass concentration - 142 -

Figure 6-10 Regeneration capacity vs. channel length - 143 -

Figure 6-11 Regeneration capacity vs. channel height - 143 -

Figure 6-12 Regeneration capacity vs. desiccant temperature - 145 -

Figure 6-13 Regeneration capacity vs. desiccant flow rate..... - 146 -

Figure 6-14 Regeneration capacity vs. air flow speed - 147 -

Figure 6-15 Regeneration capacity vs. fresh air temperature(relative humidity 30%) - 147 -

Figure 6-16 Regeneration capacity vs. fresh air relative humidity at 35°C - 148 -

Figure 6-17 Regeneration capacity vs. hot water temperature..... - 149 -

Figure 6-18 Regeneration capacity vs. hot water flow speed..... - 150 -

Figure 6-19 View of the test rig — liquid desiccant regenerator - 152 -

Figure 6-20 Testing results of the air-to-air heat exchanger - 153 -

Figure 6-21 Comparisons of testing and simulation results of the air-to-air heat exchanger- 158 -

Figure 6-22 Comparisons of testing and simulation results of desiccant regenerator..... - 161 -

Chapter.7

Figure 7-1 Schematic diagram of the heat recovery/desiccant cooling system	- 168 -
Figure 7-2 (a) Sketch diagram of the desiccant cycle (b) the process on Duhring diagram .-	169 -
Figure 7-3 (a) Sketch diagram of the air processes (b) Air conditioning processes on the psychrometric chart.....	- 171 -
Figure 7-4 COP of the system vs. air temperature	- 178 -
Figure 7-5 COP of the system vs. fresh air relative humidity	- 179 -
Figure 7-6 COP of the system vs. fresh air flow speed.....	- 180 -
Figure 7-7 COP of the system vs. working solution mass concentration.....	- 181 -
Figure 7-8 COP of the system vs. working solution flow speed.....	- 182 -
Figure 7-9 Comparisons of the different factors influencing on the system COP	- 184 -
Figure 7-10 View of the testing rig — whole system	- 185 -
Figure 7-11 COP comparisons between the theoretical and testing results of the heat recovery/desiccant cooling system.....	- 194 -
Figure 7-12 Cooling capacity comparisons between the theoretical and testing results of the heat recovery/desiccant cooling system.....	- 195 -

Chapter.8

Figure 8-1 Monthly mean Irradiation for 45° inclination in London area and gained energy by 3.58m ² solar collector.....	- 203 -
---	---------

List of Tables

Chapter.2

Table 2.1 Results of the energy analysis using real meteorological data.....	- 14 -
Table 2.2 Comparisons of adsorbent–adsorbate pairs.....	- 21 -
Table 2.3 Comparison of several aqueous solutions from seawater	- 32 -

Chapter.3

Table 3.1 Air parameters and calculated Re	- 53 -
Table 3.2 Porosities, pores size and membranes thicknesses of wicked metal, metal foams and wools	- 59 -
Table 3.3 Porosities, pores size and membranes thicknesses of various fibres.....	- 62 -
Table 3.4 Porosities, pores size and membranes thicknesses of porous ceramics	- 64 -
Table 3.5 Porosities, pores size and membranes thicknesses of porous zeolite.....	- 65 -
Table 3.6 Porosities, pores size and membranes thicknesses of porous carbons	- 67 -
Table 3.7 Properties summaries of the selected material types.....	- 68 -

Chapter.5

Table 5.1 Parameters of three kinds of desiccant solution.....	- 109 -
Table 5.2 Factors and their influence on dehumidifier thermal performance	- 118 -

Chapter.6

Table 6.1 Parameters of three kinds of desiccant solutions	- 141 -
Table 6.2 Factors and their influences on regenerator performance	- 151 -
Table 6.3 Testing performance of regenerator vs. desiccant flow rate	- 154 -
Table 6.4 Testing performance of regenerator vs. air flow speed.....	- 155 -
Table 6.5 Testing performance of regenerator vs. air temperature and humidity	- 156 -
Table 6.6 Testing performance of regenerator vs. desiccant mass concentration.....	- 157 -

Chapter.7

Table 7.1 Tested flat plate heat exchanger effectiveness	- 186 -
Table 7.2 Influence of fresh air temperature changing to the COP of the system	- 188 -
Table 7.3 Influence of fresh air moisture content changing to the COP of the system.....	- 189 -
Table 7.4 Influence of fresh air flow speed changing to the COP of the system	- 190 -
Table 7.5 Influence of working solution mass concentration to the COP of the system	- 191 -

Chapter.8

Table 8.1 Recommended comfort criteria for specific applications	- 199 -
Table 8.2 Design outdoor and indoor air parameters	- 200 -
Table 8.3 Monthly mean daily irradiation on inclined planes: London area	- 201 -
Table 8.4 Equipments capital and running cost	- 202 -

Chapter 1. Introduction

1.1 Background

Since 1905, the average global air temperature near the Earth's surface has increased by 0.74 ± 0.18 °C during the last hundred years (Web1.1). Scientists have proved that 55% greenhouse gases is CO₂, which keeps extremely high increasing rate since 1751 (Web 1.2). Residential energy accounts for 40% percent of the primary energy consumptions relative to the CO₂ emission in the EU, of this HVAC (heating, ventilation and air conditioning) systems consume approximately 50%, lighting accounts for 15% and appliances 10% (J. Ortiz and C. Pout, 2006).

UK and EU countries have Kyoto targets for reducing their greenhouse gas emissions by a collective average of 12.5% below their 1990 levels by 2020 (DTI 2006). Reducing the consumption of fossil-fuel energy is significant in controlling the CO₂ emission and slowing down global warming. Renewable energy utilization is an effective method of achieving this target. However, in the UK renewable energy application is only 2% to the total energy consumption in 2005 (Web 1.3).

With the increasing requirements for indoor cooling, sustainable cooling systems have recently gained prominence. These novel cooling systems utilize renewable energy gained from solar collector, cooling tower, ground thermal source etc, and avoid CFC and CO₂ emissions.

Desiccant cooling system is one kind of innovative technologies which employs renewable energy to produce the desired air for comfortable working/living spaces. These systems have little dependency on fossil-fuel energy and are environment friendly. Three main parts are currently included in these systems: air-to-air heat exchanger, desiccant dehumidifier and regenerator.

Air-to-air heat exchangers have been employed to save energy for a long time, most are tube, and flat pipe, flat plate, plate-fin heat exchanger only execute sensible heat exchange. Since the end of last century, enthalpy plate and wheel exchangers are widely researched and utilized for recovery of heat/mass energy from the exhaust air synchronously. However, the mass recovery effectiveness is lower than 60% and accompanied with lots of problems such as: overtaking air, electrical power consumption for driving wheel, and discontinuous running, etc, (Francey, J. L. A. Golding, 1981). Therefore, an innovative high hydrophilic membrane heat/mass exchanger is proposed in this thesis.

Dehumidification and regeneration are the mutually contrary processes of the moisture condensation/evaporation out/into the air stream. Hence, the dehumidifier and regenerator are similar to each other. But the desiccant types are diversiform used for absorbing/adsorbing moisture. It is generally classed into two categories: solid desiccant and liquid desiccant.

Solid desiccant is attached on the enthalpy plate/wheel exchanger increasing the mass transfer efficiency and also separately used for dehumidification. The generally used solid desiccants such as silica gel, natural and synthetic zeolites, activated alumina, and titanium silicate et al, have strong adsorption capacity but the regeneration temperatures of them are higher than 100 °C. In this case, it is difficult for the solar, waste and others low-grade energy to provide so high temperature energy for the regeneration and assisted energy such as electrical, gas or oil is demanded. Hence, the coefficient performance (COP) of solid desiccant cooling is very low even the most hybrid system using part natural energy is lower than 1.0 (J. L. Niu, et al, 2002, and A. Kodama, 2005). Only when special waste energy with high temperature at about 150°C is available, the COP has the possibility value over 1.5 (S. S. Elsayed, et al, 2005).

Liquid desiccant cooling systems substitute the solid desiccant and relative technologies are developed quickly recently years owing to the following advantages. Firstly, the liquid desiccants' lower regeneration temperature is superior to employ low-grade energy (with the

temperature no high than 100°C), this will improve the COP of system greatly; secondly, the liquid desiccants are more convenient to cooperate with other kinds cooling system; thirdly, there are no overtaking air and discontinuous running problems in the whole system. However, in previous research, the desiccant dehumidification cooling systems are all combined with other kinds of HVAC system, and the solar energy only accounts for a small part of the dehumidification capacity. In this research, solar collector and cooling tower are proposed to service the main driving energy and the dehumidification/ regeneration coefficient are targeted to be enhanced greatly to improve the system COP.

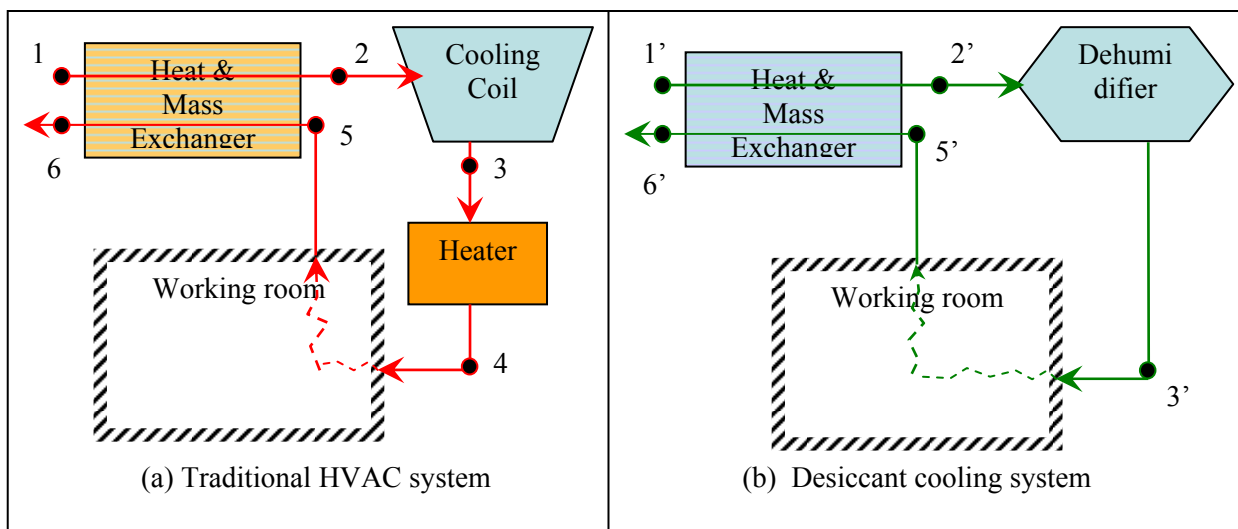


Figure 1-1 Air conditioning processes: (a) traditional HVAC (b) desiccant cooling with efficient heat/mass recovery

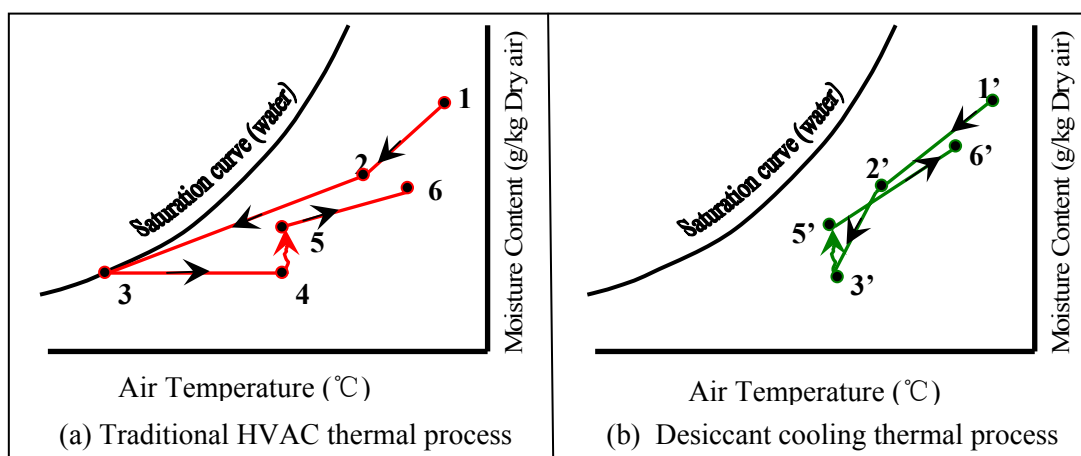


Figure 1-2 Thermal processes: (a) traditional HVAC (b) desiccant cooling with efficient heat recovery

Traditional HVAC and desiccant cooling air conditioning processes diagrams are shown in Figure 1-1 and their thermal processes on the psychrometric chart are shown in Figure 1-2. In this two air conditioning system, the fresh air only take the latent heat load in the serving room. For the conventional refrigerant vapour compression system, the fresh air at point 1 has heat/mass exchanger to point 2, from here it is cooled until below its dew point to point 3, in this process the superfluous moisture is condensed out, and then excess energy is required to reheat it to supply point 4, which mixes with the indoor air to point 5. In this process, overcooling and reheating energy is wasted and more by-product of CO₂ is released. For the proposed effective heat recovery/desiccant cooling system, fresh air from point 1' releases heat/mass effectively to the releasing air until point 2', from here it is further cooled and dehumidified by the cold desiccant to supply point 3'. The treated fresh air deals with the indoor cooling and dehumidification load to point 5', where some air exits out and carries the redundant heat/mass from the entering fresh air until reaching point 6'. This is the novel air treatment circle using less energy to achieve the same air conditioning target. Additionally the special desiccant soaked fibre heat/mass exchanger is utilized in the desiccant cooling system for high recovery effectiveness.

Hence, adsorption and absorption technologies have been developed and applied to dehumidify the humid air in the last twenty years. During the advancement of dehumidification technologies, the regeneration energy developed from fossil-fuel energies oil, gas & electrical to renewable energy such as solar and waste energy. Owing to the adsorbent/absorbent characteristics, the liquid desiccant has the advantage to utilize the solar energy due to its lower regeneration temperature. However, the existing desiccant cooling system is mostly integrated with other HVAC technologies with low performance coefficients. In this thesis, a novel and efficient heat recovery/ desiccant cooling system is researched to produce the desired air condition using natural energy.

The purpose of this research is to develop a novel heat recovery/desiccant cooling system installed into a windcowl/catcher to provide desired air for living/working buildings. An innovative heat/mass transfer fibre membrane is utilized to recover the maximal exhaust energy firstly. Then the pre-cooled/dehumidified air stream is further cooled and dehumidified by the cold/strong liquid desiccant in the dehumidifier. Solar energy is designed to regenerate the dilute desiccant solution and cooling tower is employed to cool the hot condensed solution. Wind cowl/catcher is planned to service the natural ventilation for the fresh and exhaust air, which requires the dehumidifier core to be designed into an octahedron shape with hexagon surfaces. This system only utilizes a small quantity of electrical power to drive the fans in the regenerator and cooling tower and pumps allowing desiccant solution delivery, hence the COP of the system is anticipated to be high. Furthermore, the proposed cost of this system is low, since the cheapest material —fibre is used as the heat/mass exchanger, dehumidifier and regenerator core and the desiccant solution wastage is small in the running. The system does not depend on fossil-fuel energy and has low CO₂ emission, so it's the optimal clean technology servicing good indoor air quality for comfortable working/living conditions.

The research is novel in the following ways:

- i. Uses an effective heat/mass fibre exchanger to save both sensible and latent heat from the exhaust air
- ii. The dehumidifier core could be integrated in a windcowl/catcher
- iii. Uses cheap fibre materials as the air-to-air heat exchanger, dehumidifier and regenerator core
- iv. Utilises low electrical energy and so emits little CO₂ to the environment
- v. The system has a high COP

1.2 Description of the Novel Heat Recovery/ Desiccant Cooling System

The novel heat exchanger/desiccant cooling system mainly includes five parts: solar collector, desiccant regenerator, heat/mass exchanger and dehumidifier, and cooling tower, wind

cowl/catcher as shown in Figure 1-3. Solar collector is designed to service hot water to regenerate the dilute cold desiccant solution, cooling tower is planned to offer cold water to cool the condensed hot solution and wind cowl/catcher is proposed to afford natural ventilation. Because the technologies of solar collector and cooling tower have been developed adequately, they are not the primary units to be researched and will be substituted by electrical boiler and cold water provisionally in the experimental testing. And the windcowl/catcher is mainly to service the natural ventilation for the fresh and exhaust air, which are mature technologies. Hence, this thesis mainly focuses on the performances of heat/mass exchanger, desiccant dehumidifier and desiccant regenerator in this system.

There are one desiccant circle and two air processes between the regenerator and dehumidifier units. The desiccant cycle consists of a desiccant dehumidifier, a desiccant regeneration and store system (DRSS), a solar driven heater, a desiccant to desiccant exchanger, and a desiccant cooling coil, two arrangements of desiccant sprayers, strong/weak solution sinks and piping connections. For the desiccant circle, the dilute solution is preheated by some degree in the desiccant to desiccant heat exchanger on the returning route to the regenerator unit, and then it is heated up by the hot water in a plate heat exchanger, which obtains hot water from the solar collector. And then the weak/hot solution is sprayed from the top of the regenerator core. With the overflow solution flowing down by gravitation, it contacts directly with the counter flowing air stream at the fibre membranes' surface and desorbs moisture to the dry air stream. In this progress, the dilute solution releases moisture as well as latent heat and it turns into strong and warm solution. Then the concentrated and warm solution is pumped forward to the dehumidifier unit through a desiccant-to-desiccant heat exchanger where it transfers some heat to the upcoming diluted desiccant solution, resulting in a certain degree of temperature drop. The strong liquid is then passed through a desiccant-to-water heat exchanger where it loses more heat to the water flow circulated around the cooling tower and the heat exchanger, thus creating natural cooling utilizing ambient energy.

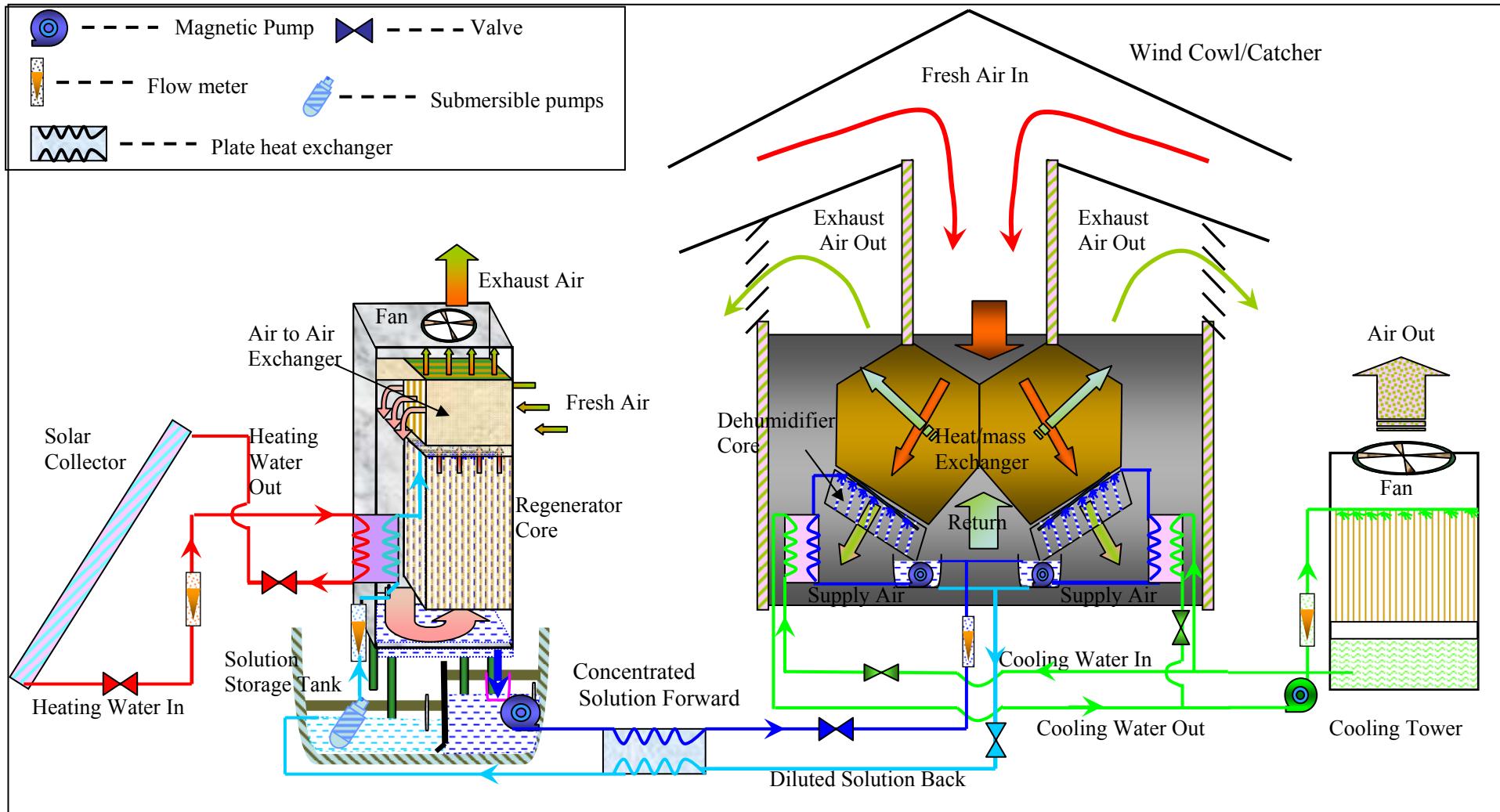


Figure 1-3 Schematic diagram of the heat recovery/desiccant cooling system

Thereafter, the strong solution is delivered to the strong solution sink beneath the dehumidifier and then pumped to the top of the fibre paper core and sprayed over along the fibre paper stack. The strong desiccant soaked by the fibre membranes absorbs the moisture from the passing humid air and flows back to a separate desiccant sink, where the diluted solution is accumulated and ready to be delivered back to the DRSS for regeneration.

In the regenerator unit, fresh air from the environment is forced into the regenerator and has sensible heat exchange with the hot exhaust air. Then preheated air stream flows down to the bottom of the regenerator unit and forwards up through the air tunnel in the fibre core again. Hot and dry air stream at a low vapour pressure evaporates superabundant moisture from the weak desiccant solution at the fibre membrane surface as well as absorbs sensible heat. Thereafter, the hot and humid air transfers sensible heat to the forced in environment air via the air to air cross-flow heat exchanger, and then exits out.

In the dehumidifier unit, the fresh air from the environment has heat/mass exchanger with the return air exiting out of the air conditioning room in a novel fibre heat/mass exchanger. And then the pre-heated and pre-dehumidified air stream is forced into the dehumidifier unit, where it contacts directly with the falling down strong solution film at the fibre membranes' surface and loses moisture to the solution. In the moisture condensation progress, latent heat is released, and designed to be take away by the falling cold desiccant solution. Hence, the cooling tower is required to provide enough cooling energy to cool the strong desiccant before it is pumped to the top of the dehumidifier core.

1.3 Work Involved in This Thesis

The research involves 7 technical chapters:

Chapter 2: Review of existing research work on heat/mass exchangers and desiccant dehumidification/cooling systems;

Chapter 3: Optimal study of heat/mass recovery materials;

Chapter 4: Numerical and experimental investigation of the innovative heat/mass fibre exchanger;

Chapter 5: Numerical and experimental investigation of the liquid desiccant dehumidifier;

Chapter 6: Numerical and experimental investigation of the liquid desiccant regenerator;

Chapter 7: Theoretical and experimental investigation of the whole novel heat recovery/desiccant cooling system;

Chapter 8: Economic analysis of the novel heat recovery/desiccant cooling system.

The work in chapter 2 includes a review of previous work on heat/mass exchanger and absorbent/adsorbent applications in the relevant technical areas, including the reasons of employing desiccant dehumidification/cooling; heat/mass exchanger development history and its performance; adsorbents' type, carriers, working performance and their application assisted with other HVAC systems; and absorbents' type, carriers, working performance and their application cooperated with other HVAC systems.

In chapter 3, the optimal material for heat/mass transfer was selected from five types of materials namely metal, fibre, ceramics, and zeolite, carbons based on the five evaluating criterions such as, thermal conductivity, porosity and pore size, durability, Young's modulus and cost. Mathematical analysis proved that the thermal conductivity slightly affected the heat transfer and the moisture diffusion coefficient through the thin membrane determined the mass transfer. Fibre, ceramics and zeolite, carbons thin membranes all could afford the proper pore size to allow the moisture across and prevent air penetration. However, the economic analysis enhanced the fibre membrane superiority to other materials and it was selected as the optimal heat/mass transfer material.

Chapter 4 is concerned with the performance investigation of air-to-air heat/mass exchanger based on the numerical simulation and experimental researches. Three types of fibre membranes

were referred in this chapter, and the theoretical analysis revealed that the liquid desiccant soaked fibre membrane should perform the best thermal transfer. Numerical modelling was set up according to the heat/mass transfer mechanism of clean fibre membranes, and comparisons with the experimental results were carried out. Corrections of heat transfer resistance and moisture diffusion coefficient across the soaked fibre membranes were made to the original heat/mass transfer coefficient of the clean fibre membrane based on the experimental results. Then a further numerical modelling was developed and it could predict the relationships between the dehumidification performance and the dehumidifier structure, size and fresh/exhaust air parameters. Its acceptance was validated by the experimental results.

Chapter 5 investigated the performance of desiccant dehumidifier based on numerical simulation and experimental results. Three numerical models were developed in this section and the results indicated that LiCl solution was the most suitable material for this system owing to its high absorption capacity. The factors influencing thermal performance of the working performance, such as the dehumidifier structure and size, air stream and solution parameters were all investigated by the numerical modelling. Some affecting factors were further tested through the set-up testing rig, and experimental results proved that the numerical simulation could rightly predict the performance under an acceptable error. Hence, the numerical model could design the proper dehumidifier size and running condition for a given air climate.

Work in chapter 6 includes the numerical simulation and experimental investigation on the air-to-air cross-flow heat exchanger, and the performance of regenerator for three types of desiccant solutions. Regeneration is the reverse process of dehumidification, so the numerical simulation is carried out based on the dehumidifier model. The affecting factors were investigated according to the regenerator core structure and size, air stream parameters and solution parameters, hot water temperature and flow rate. Experimental testing and comparisons with the

simulation results were carried out. Reasons causing the contrast between the numerical simulation and testing results were found, illuminated and corrected.

Chapter 7 is concerned with the prototype system which is integrated by the five parts: air-to-air heat/mass exchanger, dehumidifier core, air-to-air cross-flow exchanger and regenerator core, connecting pipes and ducts. A theoretical model constituted of four numerical simulation modules and two flat plate exchangers' modules was developed. The COP (Coefficient of Performance) of the novel heat recovery/desiccant cooling system was investigated according to the varying influencing factors such as air temperature, humidity, and flow speed, and desiccant concentration, temperature, flow rate etc. Experimental testing was performed and comparisons with the theoretical modelling results were carried out. The reasons inducing the differences between the theoretical simulations and testing results were analyzed.

In chapter 8, the costing comparisons between the traditional HVAC system and the novel heat recovery/desiccant cooling system were carried out. A case based on a 200m² working office in London was studied and the results indicated that the latter was an economical and clean technology to utilizing natural energy producing cooling energy in summer.

A number of conclusions were derived from the research and the advantages of the proposed system were highlighted. The existing problems of the system were illuminated and the further work to improve the system performance and cover the disadvantages was pointed out.

Chapter 2. Review of Previous Work of Heat/Mass Exchangers and Desiccant Dehumidification/Cooling Systems

2.1 Purpose and Regions Employing Desiccant Cooling

2.1.1 Purpose of Utilizing Heat/Mass Recovery and Adsorption/ Absorption

It is a common practice to recover energy from the exhaust air using an air-air heat exchanger. There are several types of heat exchangers currently available for this application, including flat plate exchanger, rotary wheel, etc. These exchangers are able to achieve efficiency up to 60% (J.L.A. Francey & P. Golding, 1981) and exchange both sensible and latent heat between the two airstreams. Recently one type of hydrophilic membranes enthalpy exchanger has been developed, which can achieve efficiency as high as 90% (L.Z. Zhang, 2008).

Most adsorbents and absorbents are used to dry humid air for some specially required places such as paper factory, spinning mill, food factory and storage, and beverage factory (W. Tanthapanicharkoon, et al, 2002; Y.J. Dai, et al, 2002; P.A. Davies, 2005). However, recently, they have become more popularly used to treat environment air to create desired living conditions for residential/working buildings (D. Pietruschka, 2006).

Substituting the overcooling condensing dehumidification systems, adsorbents/absorbents are more popularly used for dehumidifying humid air in people's living/working place and solar energy, waste and other kinds of low grade heat are also employed to regenerate the saturated adsorbents/absorbents. These technologies can save a large amount of cooling energy in the summer.

At present, adsorbents/absorbents used for dehumidification purposes are mostly combined with the conventional HVAC system (Y.J. Dai, et al, 2001; J.R. Sand & J.C. Fischer, 2005; P.A. Davies, 2005). Experiments estimated that up to 52% cooling energy could be saved as well as

air pollution reduced (P. Mazzei, 2002). However, in most of the hybrid cooling systems, normal energy such as electric and gas is consumed to bear the majority of the cooling load. In the purposed novel heat recovery/desiccant cooling system, only a small quantity of electric energy is used to drive the pumps and fans, whilst natural energy such as solar energy to run the system.

2.1.2 Regions Employing Desiccant Cooling

Air-to-air heat/mass recovery is suitable for the case with a large temperature/humidity difference between the indoor and outdoor air environments. Adsorbent/absorbent-assisted dehumidification and cooling systems perform excellently in those regions with humid air and plenty of solar energy such as southern Europe, South America, South Asia, etc.

S. Alizadeh (2002) carried out experiments and proved that the solar collector/regenerator system performed well under summer conditions in Australia.

K. Gommed's (2004) experiments found that liquid desiccant cooling systems had good cooling performance in the hot and humid climates such as in Mediterranean countries to solve the problem of shortage of cooling energy.

J.L. Niu, et al (2002) successfully applied a desiccant combined chilled-ceiling cooling system in a typical office in Hong Kong by saving 44% primary energy consumption. Desiccant cooling experiments were also processed in the south of China, Taiwan, Korea and Japan, as well as Thailand, etc (Y.J. Dai, et al and Qun Cui et al, 2005).

P. Mavroudaki and C.B. Beggs (2002) reviewed the application of desiccant dehumidification/cooling systems in northern Europe and concluded that there was potential to utilize these technologies in the southern European countries. They summarized the saved energy by

utilizing the solar energy-driven desiccant cooling system in the summer in the European countries in Table 2.1.

Table 2.1 Results of the energy analysis using real meteorological data

City	Mode	Max. dry bulb temp. (°C)	Min. dry bulb temp. (°C)	Latent gain (W/m ²)	Solar water temp. (°C)	Supply air volume flow (l/s/m ²)	Gas consumed (kW h/m ²)	Electricity consumed (kW h/m ²)	Daily cost (p/m ²)	Gas saved (%)
Oslo	Non-solar	25.4	13.6	5.86	n.a.	18	0.376	0.016	0.65	93.0
	Solar	25.4	13.6	5.86	50	18	0.026	0.016	0.12	
London	Non-solar	26.9	17.6	10.92	n.a.	18	0.887	0.063	1.64	25.1
	Solar	26.9	17.6	10.92	55	18	0.665	0.063	1.31	
Budapest	Non-solar	30.4	17.8	8.99	n.a.	18	0.826	0.065	1.57	33.9
	Solar	30.4	17.8	8.99	60	18	0.546	0.065	1.15	
Lyon	Non-solar	28.8	17.1	7.91	n.a.	18	0.724	0.048	1.33	39.7
	Solar	28.8	17.1	7.91	55	18	0.436	0.048	0.90	
Lisbon	Non-solar	35.1	21.8	9.60	n.a.	18	0.977	0.075	1.84	38.5
	Solar	35.1	21.8	9.60	70	18	0.601	0.075	1.28	
Athens	Non-solar	36.6	26.4	9.72	n.a.	28	1.015	0.093	1.99	46.5
	Solar	36.6	26.4	9.72	70	28	0.544	0.093	1.28	
Sofia	Non-solar	35.1	21.8	9.96	n.a.	38	1.601	0.145	3.13	29.1
	Solar	35.1	21.8	9.96	70	38	1.136	0.145	2.43	

€1 = 100 p.

A large number of solar energy could be gained in the regions such as Southern Europe, South America and South Asia, etc. Hence, technologies to improve the efficiency of desiccant cooling as well as use of solar energy are the main research topics.

2.2 Enthalpy (Energy) Exchanger

Common exchangers can be classified into two categories: sensible heat exchangers and enthalpy exchangers. The first one, including fixed plates, sensible heat exchanger wheels (the materials making the wheel are high thermal capacity but low porosity), heat pipes and coil run-around loop heat exchangers, can only recover sensible heat with no moisture recovery (L.Z. Zhang, 2007). The latter, mainly involving an enthalpy plate and wheel exchanger, can recover both sensible and latent heat from the exhaust air. Because the enthalpy exchanger is most popular used in air conditioning systems recently, it is the main objective of our project. The development history, working mechanism and performance of this technology are researched in details.

2.2.1 Enthalpy Plate Exchanger

In 1997, solid adsorbents such as activated carbon-methanol, zeolite-water, $\text{CaCl}_2\text{-NH}_3$ and hydride-hydrogen had been integrated with shell, tube, flat pipe, flat plate, and plate-fin heat exchanger to carry out the heat and mass recovery synchronously (R.Z. Wang, et al, 1998; A. Hachemi, 1999). The enthalpy flat-pipe and flat exchangers shown in Figure 2-1 (a) and (b), the sandwiched configuration were employed to produce the cooling energy. The main disadvantages of these earlier plate enthalpy exchangers are the huge thermal resistance between adsorbents and fins, lower adsorption and intermittence of regenerating of the saturated adsorbents. R.Z. Wang, et al (1998) developed one type of spiral plate type adsorber exchanger made of two parallel stainless steel welded plates and adsorbents shown in Figure 2-1(c), with the advantages of higher adsorption, compact size, higher thermal transfer, easier manufacturing, and cheaper price. This is the rudiment of enthalpy wheels.

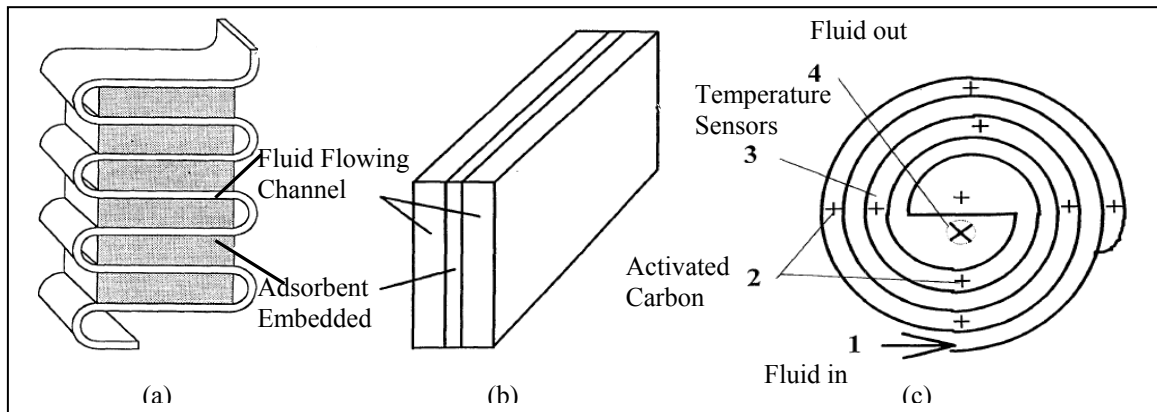


Figure 2-1 Enthalpy plat heat exchangers: (a) flat-pipe exchanger (b) flat exchanger and (c) spiral plate

2.2.2 Enthalpy Wheel Exchanger

Enthalpies wheels are more efficiency compared to the normal adsorbent-plate exchangers and are mostly utilized to maintain current heat/mass transfer. Further technical and theoretical studies were carried out to improve the recovery efficiency.

S. Bilodeau, et al investigated one type of frosting rotary heat and mass exchanger wheel to save the energy from the existing air out of the warm room in Canada in 1998, as shown in Figure 2-2. The rotary wheel adsorbs heat and moisture from the warm exhausting air when it locates at the up exhaust air channel and brings them to the cold supplying air when it turns down to the supply channel. In this process, all the heat and mass transfer occurrences recur in the honeycomb structure to contain heat and mass, and no additional energy is utilized. This is the key difference with the solid desiccant wheel shown in Figure 2-3, which needs extra energy to produce regeneration air to keep it working.

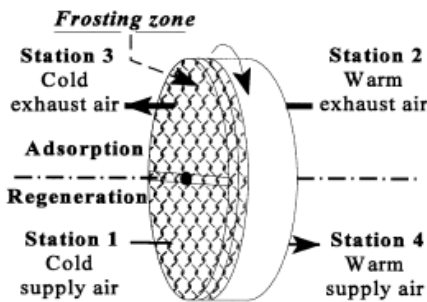


Figure 2-2 Rotary heat and moisture exchanger

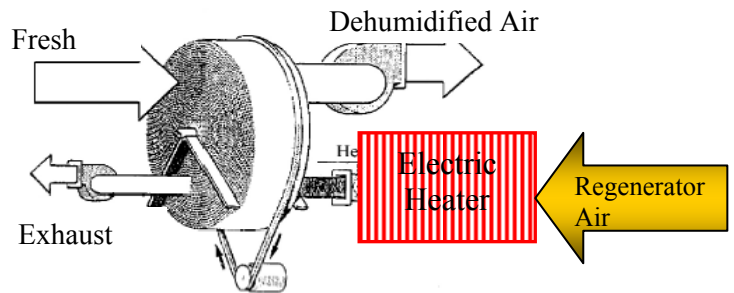


Figure 2-3 Schematic diagram of desiccant wheel

Numerical studies of the enthalpy wheel were carried out by Sankar Nair, et al in 1995 by an axial heat dispersion and longitudinal matrix conduction method to solve the wheel heat/mass exchanger problems using a finite difference approach. The predicated recovery effectiveness was founded to be about 75%. Rotating factors of the enthalpy were considered in the calculating method by Jörg Frauhammer, et al in the report about moving discontinuities model equations describing the efficiency of condensation and evaporation in a regenerative air-to-air heat exchanger in 1997.

The effect of dimensionless parameters on the effectiveness of rotary heat exchangers was investigated by N. Ghodsipour and M. Sadrameli in 2003. The simulation and experimental

results both proved that hot and cold air velocity and their interactions area had significant effect on the efficiency of the regenerator and rotational speed had inferior influence.

L.A. Sphaier and W.M. Worek (2004) carried out a new dimensionless formulation research regarding the performance of porous wheels based on the previous experimental results and proved a possible optimization of wheel construction and compactness by reducing the felt thickness.

The disadvantages of the enthalpy wheel exchanger including overtaking air, low recovery effectiveness (about 70%) and high energy cost to drive the wheel make it inferior to the hydrophilic membranes exchanger and solid desiccant wheel.

2.2.3 Hydrophilic Membranes Exchanger

As the enthalpy wheels are usually expensive, and need additional power to keep them rotating and carry-over air between two streams, in recent years, hydrophilic membrane technologies have been developed to recover sensible heat as well as latent heat from exhaust air streams. It was called a heat/mass exchanger with hydrophilic membrane cores (L.Z. Zhang and Y. Jiang, 1999). The device is similar to an air-to-air sensible heat recovery, but the metal tube/plate of traditional exchangers is substituted by a hydrophilic membrane, through which both heat and moisture can be transferred simultaneously. Compared with the energy wheel, it has higher enthalpy efficiency and also prevents the carry-over happening (L. Zhang, 2007).

Some non-metal materials such as polymers, paper, cloth and ceramics have been used in place of metal foils (K.R. Kistler and E.L. Cussler, 2002; L.Z. Zhang and J.L. Niu, 2002). In this structure employing these materials, the liquid vapour can penetrate through from one air stream to another but the gas-state air cannot infiltrate.

L.Z. Zhang developed one type of heat and mass exchanger using vapour-permeable wall materials such as paper, polymer membrane, and ceramics, as shown in Figure 2-4 (L.Z. Zhang,

2008). This heat/mass exchanger is different from those previously introduced: no extra cooling fluid is utilized, and supply air recovers the sensible and latent heat from the exhaust air. Moisture in the humid side condenses on the membranes' surface and penetrates through the porous membranes. Sensible heat transfer mechanism is similar to the traditional air-to-air sensible exchanger, as shown in Figure 2-5, which is one type of metal air-to-air heat plate exchanger investigated by R.T. Ogulata and F. Doba in 1997. Numerical simulation and experimental results proved that this developed heat/mass transfer has sensible recovery effectiveness as low as 0.4, which is much lower than the traditional metal exchanger effectiveness 0.98~0.98. The mass transfer is also far away from the prospective value. Lower thermal conductivity of the vapor-permeable materials leads to low heat recovery and the smaller diffusion coefficient of moisture through the porous membranes results in the low mass transfer.

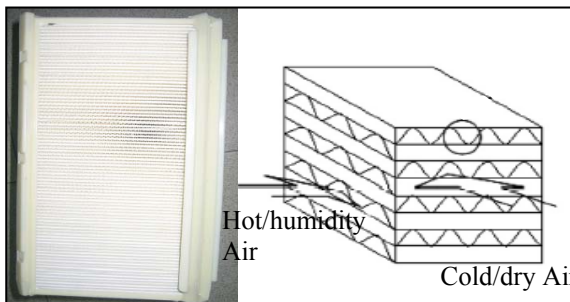


Figure 2-4 Plate-fine heat and mass exchanger

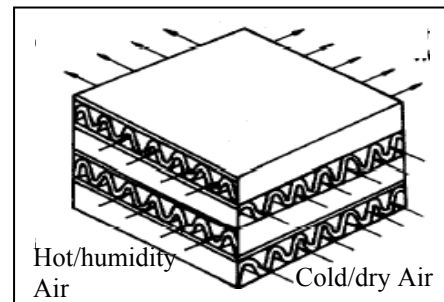


Figure 2-5 Cross-flow air-to-air heat exchanger

A plate enthalpy exchanger with hydrophilic membranes is researched in this thesis and its design and performance will be detailed in the following chapters. The enthalpy exchange efficiency will be 30% improved over the general enthalpy plates or wheels, which have low efficiencies at about 60% (J.L.A. Francey and P. Golding, 1981).

2.3 Adsorption

Desiccant cooling technologies utilize solar energy or other types of lower grade energies to regenerate the weak desiccant and use the concentrated desiccant to absorb moisture from the

air stream to achieve the dehumidification/cooling purpose. Currently available desiccant systems can be classified into solid, liquid and solid / liquid desiccants systems.

Solid desiccant dehumidification systems include desiccant wheel, desiccant pack or desiccant bed, which can adsorb moisture from the air flow but have difficulty in regenerating the saturated desiccant with no interfering the system's continuous operation. The commonly available solid desiccants include Silica Gels, Zeolites, Molecular Sieves, Activated Aluminas, and Carbons. These substances have relative lower adsorption capacity, for instance a typical molecular sieve attracts only 17% water of its dry mass when the air flow is at 21°C and 20% (Qun Cui, et al, 2005). Usually, the solid desiccants need higher regeneration temperature than liquid desiccant, saying above 80°C, which makes it difficult to utilize the solar energy and other low grade waste energies (Grossman G, 2002, Y. J. Dai, et al, 2002, and K. Daou, et al, 2004)

2.3.1 Categories of Solid Desiccant

Solid desiccant dehumidification employs the porous and strong hydrophilic materials to adsorb moisture from the air stream. The generally used solid desiccants include silica gel, natural and synthetic zeolites, activated alumina, titanium silicate, synthetic polymers, lithium chloride, etc (Y.J. Dai, et al, 2002; M. Kanoğlu et al, 2004; Qun Cui et al; 2005, J. Hirunlabh et al, 2005; C.X. Jia et al, 2006).

Y.J. Dai proved by experiments that the regeneration temperature of carbon-methanol was in the range of 80~100°C; DH-5* and DH-7* were about 100°C; and 13X*, alumina and silica gel need a higher regeneration temperature in the range of 200~300°C (Y.J. Dai, et al, 2002).

One type of clinoptilolite-type natural zeolite was tested as the adsorbent to carry dehumidification and cooling tasks by M. Kanoğlu in Turkey. Results indicated that natural zeolite has the potential to perform dehumidification, but its absorption capacity is not high like

13X, activated alumina, silica gel, charcoal etc (M. Kanoğlu, et al, 2004). J. Hirunlabh, et al (2005) reported a successful case using a silica gel bed combined with the traditional central HVAC to serve desired air to the office, which could save significant running costs.

Qun Cui et al preferred DH-5 and DH-7 as the adsorbents rather than silica gel and molecular sieve owing to their higher dehumidifying capability, which reaches 0.7kg/kg. The wide regeneration temperature and higher cooling capacity of DH-5/DH-7 were found to be superior to silica gel and molecular sieve (Qun Cui, et al, 2005).

Comparing investigations regarding the performance of activated alumina, silica gel, 13X and LCIX* were carried out by K. Daou, et al in 2006. It was concluded that the activated alumina and silica gel were ageing more severely after a large number of adsorption/desorption processes, but need a regeneration temperature as high as 200°C, which was very difficult to obtain from solar energy or other kinds of low degree waste heat. 13X molecular sieves served dehumidification more stably but at a lower capacity. LCIX had the longest durability for a large number of adsorption/desorption cycles but had the highest regenerator temperature at 250°C.

C.X. Jia, et al (2006) carried out experiments and simulations of lithium chloride assisted air cooling system with refrigerant R-22. Results indicated that COP of the lithium chloride assisted cooling system was 37.5% higher than the conventional vapour compression system. However the regeneration temperature of lithium chloride was lower than 100°C.

Absorption capacity, durability, stability and regenerator temperature are the main four factors to be considered in selection a solid desiccant. Table 2-2 lists the parameters of several commonly used solid desiccants, which are all concluded from experiments (Y.J. Dai, et al, 2002; M. Kanoğlu, et al, 2004; Q. Cui, et al, 2005; C.X. Jia, et al, 2006; K. Daou, et al, 2006). DH-5 and DH-7 is the preferred choice of adsorbent owing to its high dehumidification capacity

and low regeneration temperature. Silica gel is the second material to service high absorption capacity with lower regenerating temperature. Charcoal takes the following position owing to its higher absorption capacity as well as higher regeneration temperature. Activated alumina is the fourth with a lower adsorption capacity than Charcoal. Although 13X and 5A have high adsorption capacity, their high regeneration temperatures hold back their application.

Table 2.2 Comparisons of adsorbent–adsorbate pairs

Adsorbent–adsorbate	Max. adsorption Capacity (kg/kg)	Regenerator Temperature (°C) (approximate value)
4A– water	0.22	350
13X– water	0.3	350
5A – water	0.33	350
Clinoptilolite (natural zeolite) – water	0.12	240
Mordenite – water	0.11	250
Chabazite – water	0.17	250
Charcoal – water	0.4	250
Activated alumina – water	0.19	250
Silica gel – water ⁽¹⁾	0.37	150

2.3.2 Solid Desiccant Carriers

Desiccant Wheel

The desiccant wheel is the most popular solid desiccant carrier and has a similar shape to the enthalpy exchanger wheel. For the desiccant wheel, solid desiccants are attached on the wheel fins; it then absorbs moisture from the fresh air and hot regenerator air is required to recover the saturated adsorbents. But for the enthalpy exchanger wheel, it mainly carries the heat/mass exchanger between indoor and outdoor air streams and does not need extra regeneration energy.

Figure 2-3 is one type of desiccant wheel investigated by W. Tanthapanichakoon and A. Prawarnpit in 2002. Its working process is divided into two steps: firstly, the humid air flows through the up-part of the wheel and releases the moisture to the solid desiccant attached on the

honeycomb structure; and then the up-part with saturated adsorbents turns down where adsorbed moisture evaporates out to the hot and dry regenerator air. Experimental and modelling results proved that the regenerator's air temperature influenced the dehumidification efficiency greatly, and the air flow speed had insignificant effect on it.

Jae-Weon Jeong and Stanley A. Mumma carried out further investigations in 2005 to strengthen the desiccant wheel performance. Two of the most common desiccant materials, silica gel and molecular sieve attached on the aluminium substrate in Figure 2-6, were analyzed. It was found that when the fresh and exhaust air flow speeds were both 1.5 m/s, the total energy effectiveness could reach 93.4% and 84.9% respectively for silica gel and molecular sieve coated wheel. And the face velocity and air flow ratio showed a very high contribution to both sensible and latent effectiveness. The entering fresh air humid and exhaust air conditions showed relatively small contributions to sensible effectiveness, but they showed higher contribution to latent effectiveness.

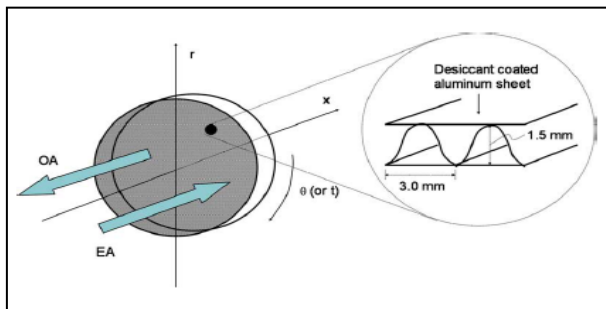


Figure 2-6 Silica gel and molecular sieve coated desiccant wheel

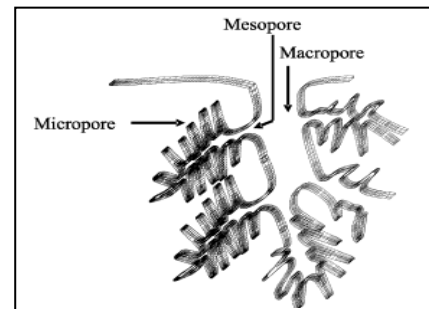


Figure 2-7 Activated carbons granular

An activated carbon fibre composed desiccant wheel was investigated by Y. Hamamoto, et al in 2005, as shown in Figure 2-7. Experimental results displayed that it performed good dehumidification results but low sensible heat recovery effectiveness caused by the following speciality of activated carbon fibre (ACF): 1) ACF surface is generally hydrophobic, especially in the vapor phase grades, which are activated at high temperatures; 2) ACF surface can be treated under air (oxidation) during its activation stage; 3) Surface oxides add a polar nature

(hydrophilicity and acidity) to ACF that will be suitable for water adsorption; 4) High porosity of ACF results in low thermal conductivity 0.0893 W/m/K (Y. Hamamoto, et al, 2006).

C.X. Jia, et al (2006) investigated another novel desiccant wheel to improve the dehumidification and regeneration effectiveness in 2006. This desiccant wheel consisted of a two-layered silica gel offering a host matrix of open pores and a hygroscopic substance, such as lithium chloride, penetrating into the micro-pores. Testing results indicated that the novel desiccant wheel removed 20~30% more moisture from the humid air compared to the normal silica gel wheel, and the COP reached 1.28, which was about 35% higher than the latter.

Solid Desiccant Bed

A solid desiccant bed and column are not commonly used like the desiccant wheel owing to their intermittent running characteristics. The desiccant bed cannot be employed in a continuous operation system because, when the solid desiccant bed is saturated, it needs to be regenerated and the dehumidification process has to be stopped. So it is usually used in the alternant working system as shown in Figure 2-8, which affords dehumidification in the night time and regeneration in the day time (S. Techajunt, et al, 1999).

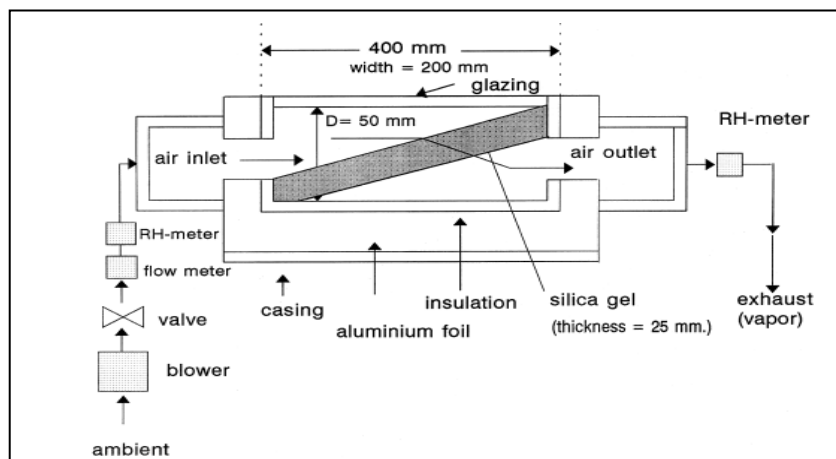


Figure 2-8 Experimental apparatus of silica gel bed

Comparing the desiccant wheel with desiccant bed, the first one is more conveniently cooperated with other traditional HVAC systems to service desired air into the room resulting in the following several advantages.

- Desiccant wheel is more convenient to be installed into the conventional HVAC system.
- Dehumidification and regeneration are carried out synchronously and the system keeps running continuously.
- Occupying a smaller space but offering more contact surface with air flow than the desiccant bed.
- Changing the rotate speed of the desiccant can control the dehumidification/regeneration capacity, which is difficult for a fixed desiccant bed/column.

2.3.3 Regeneration Energy Source

As studied in section 2.3.1, we can know that the regeneration temperature for most adsorbents is over 80°C. Hence the regenerating energy for the saturated adsorbents is a huge consumption of the dehumidification system. The commonly employed energies include electric, gas, solar energy and low degree waste energy.

Electric Energy

An electrical heater is the mostly popular energy used for regeneration due to its convenience as shown in figure 2-3. However, using electric power will improve the energy consumption and reduce the COP of the whole system. For systems utilizing electrical energy for regeneration, the COP can only be improved at a small degree than the traditional air dehumidification/cooling system (S. Ginestet, 2003; Melda Özdinç, 2005; C.X. Jia, 2006).

Gas Energy

Gas is another convenient energy used for regeneration, as shown in Figure 2-9 (J.R. Sand and J.C. Fischer, 2005). The burned hot air at a low humidity is supplied to the bottom of the desiccant wheel and carries moisture out. In this case, the burned air temperature will heat up the desiccant wheel and then induce the supply air temperature rising. Hence, to obtain a desired cooling air, this system has to cooperate with a traditional HVAC system and only part of the supply air is dehumidified. But the COP cannot be improved greatly, similar to the electrically-driven system.

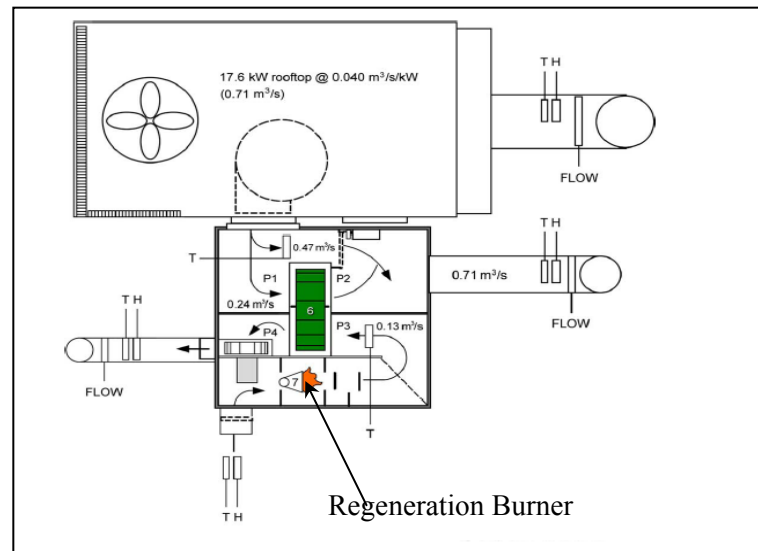


Figure 2-9 Schematic of desiccant dehumidification/rooftop cooling system

Solar Energy

Solar energy is a popular energy used for regenerating desiccants, and it can recover/store the weak desiccant during the day time and service the strong desiccant to the dehumidifier in both day and night time. For a big system, when the sun energy is plentiful, the desiccant regeneration and store system can even produce and save strong desiccants for a few days' running requirement, which is a great help for continuously cloudy/rainy days (Y.J. Dai, et al 2003). Methods to utilize solar energy as a desiccant regeneration source are classified into three kinds: solar desiccant, solar air and solar water.

A solar desiccant collector employs the saturated desiccant as an adsorbent to adsorb solar energy directly and evaporate out the moisture. As shown in figure 2-8, the solar collector bed recovers the weak solid desiccant during the day time and supplies a strong desiccant to dehumidify humid air at night time.

Environment or room air flows through the solar panel, is heated by the solar energy directly and is then supplied to the regenerator, as shown in Figure 2-10 (H-M.Henning, 2001). In this system, the regenerator air can reach a high temperature and the regenerator has a high efficiency, but a long air transfer route from collector to regenerator needs more channel space and insulation protection. So in a practical project, a solar water collector is the preferred way to collect and store solar energy.

A solar water collector supplying the hot water to heat up the regenerator air is the most acceptable method to utilize and storage solar energy. As shown in Figure 2-11, when the solar energy is plentiful, hot water carries heat exchange with the regenerator air and surplus energy is stored in the tank preparing for the shortage of solar energy (A. Kodama, 2005).

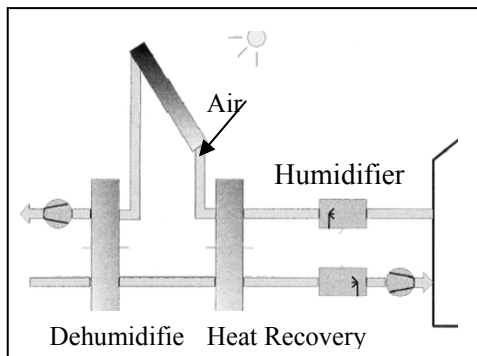


Figure 2-10 Schematic of solar air collector utilized for regenerator

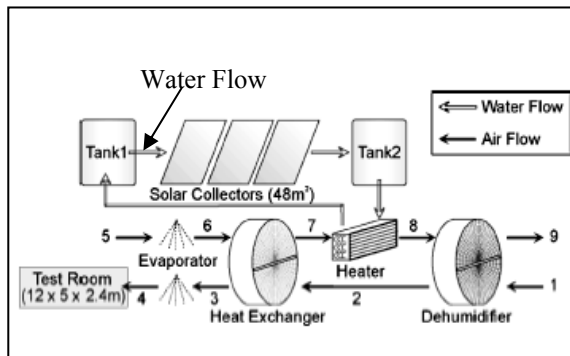


Figure 2-11 Schematic of solar water collector utilized for regenerator

Lower Degree Waste Energy

S.S. Elsayed, et al researched one kind of desiccant integrated air conditioning system, which employed the waste heat from an air cycle refrigerator to regenerate the weak desiccant, as presented in Figure 2-12. Results indicated that the coefficient of performance on the air

conditioning system was 80% higher than the conventional vapour compression system (S.S. Elsayed, et al, 2005).

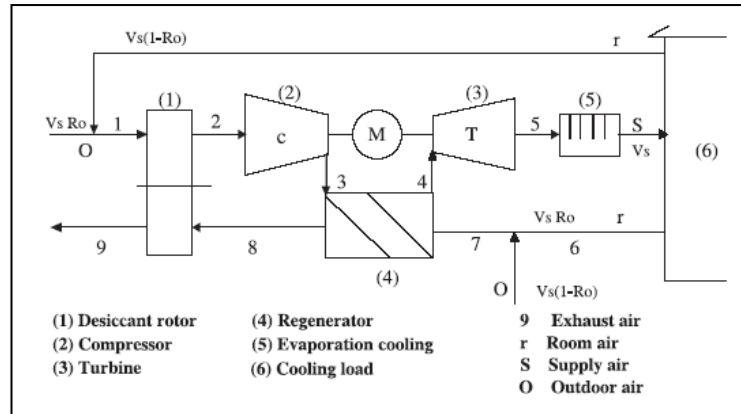


Figure 2-12 Desiccant air cycle refrigerator system

Advantages and disadvantages of utilizing solar energy compared with three other kinds of energies are expressed as the following:

- Solar energy is one type of renewable energy, saving energy and reducing air pollution.
- Solar energy is plentiful in the regions with a hot and humid climate.
- Solar water can service and store the solar energy more conveniently than solar desiccant and solar air.
- The capital costs of utilizing solar energy is high but running costs is less than electric and gas energies.
- Less convenient than electric and gas heaters.
- Cannot be used for a long time without solar radiation.
- Less regenerator efficiency compared with electrical and gas heaters.

2.3.4 Solid Desiccant Hybrid Cooling Systems

Solid Desiccant Associated Chilled–Ceiling Cooling System

In 2002, J.L. Niu, et al, carried out experiments regarding a chilled-ceiling combined with a desiccant cooling system in July, as shown in Figure 2-13. Results indicated that this system

could save up to 44% of primary energy consumption than a conventional constant volume all-air system (J.L. Niu, et al, 2002). Additionally, more than 70% of annual operating hours for desiccant regeneration could employ low-grade solar heat of less than 80°C in the city such as Hong Kong. In this case, the regeneration gas energy is substituted by renewable energy, and the COP of the system was improved greatly. In this system, the exhaust air from the room is first cooled by evaporative cooling and transfers sensible heat to the supplying air in the sensible heat wheel, and is then further heated by the gas heater. In this progress, the cooling energy is saved but more heating energy is required to heat up the humid exhaust air and the absorbed moisture in the evaporative cooler is adverse to regenerating moisture out of ambient air.

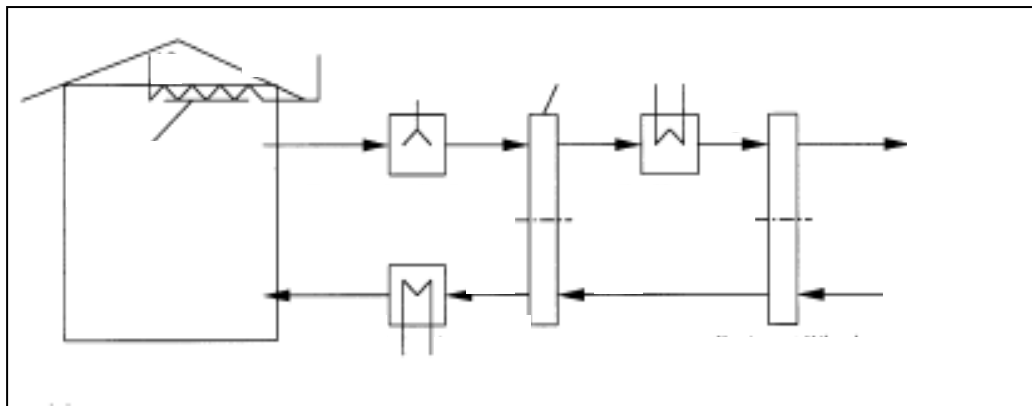


Figure 2-13 Chilled–ceiling with desiccant cooling

Solid Desiccant Integrated Rooftop HVAC System

Figure 2-9 shows an active solid desiccant integrated rooftop HVAC system, which employs the gas energy to regenerate the adsorbent. In this system, the adsorbent only dehumidifies a portion of incoming air after it is cooled and possibly dehumidified by the evaporator of the packaged unit (J.R. Sand and J.C. Fischer, 2005). Compared to the traditional desiccant based cooling system this new module can save \$1760 annual running costs as well as two-thirds of manufacturing costs, when they service the same cooling capacity. Although this system is more energy efficient, compact and cost-effective than the active desiccant preconditioning system,

the high regeneration temperature and over-carrying air stream with high concentrations of CO₂ and SO₂ in the servicing room are the emergent problems to be solved.

Solid Desiccant Integrated Direct/Indirect Evaporating Cooling System

One type of classical solid desiccant associated direct/indirect evaporative cooling system is shown in figure 2-11, which was investigated by A. Kodama in Japan in 2005. In this system, both direct and indirect evaporative cooling is employed to cool the supplying air. Solar energy is utilized as the main dehumidification/cooling energy except for electric energy consumed by fans and pumps, so the solar irradiation and solar collector effectiveness influence the COP heavily. The COP of the system was over 0.6 when the solar irradiation was 0.2kW/m² (A. Kodama in Japan, 2005). In this kind of solid desiccant regeneration system, the high temperature regeneration air increases the supply air temperature. Hence, low thermal capacity materials with high adsorption are suggested to produce the rotary wheel.

Solid Desiccant Integrated Air Cycle Refrigerator Driving Air Conditioning System

In the system shown in figure 2-12, the safe material air and water are used as the refrigerant, and the waste heat from the air cycle refrigerator acts as the regeneration energy to resume saturated absorbent. Waste heat at high temperature from the air cycle refrigerator is utilized for regenerating the desiccant rotor wheel, and an evaporative unit is controlled to adjust the supplying air humidity and temperature before going into the working space (S.S. Elsayed, et al, 2005). Testing results indicated that the coefficient of performance decreased with the regenerator temperature increasing, and it was over 3.0 when the regenerator was lower than 60°C. However, the regeneration temperature for most adsorbents is over 80°C, which will reduce the COP heavily. So this kind of system is better combined with the liquid desiccant, which needs a low regeneration temperature and offers a similar dehumidification capacity.

2.4 Absorption

Liquid desiccant dehumidification systems can operate continuously at a regeneration temperature below 80°C (K. Daou, et al, 2006; G. Mittelman, et al, 2007). Lithium Chloride, Lithium Bromide and Triethylene Glycol are usually used as a liquid desiccant owing to their high absorption capacity, for instance, Lithium Chloride can hold 130% of water of its mass under the same air flow condition (21 °C and 20%)(D.Pietruschka, et al, 2006). Liquid desiccant can remove the extra moisture from the air flow but cause the air temperature to increase due to the condensation of water vapour, which release heat to the air. Therefore, a pre-cooled liquid desiccant is needed to achieve both cooling and dehumidification of the passing air.

2.4.1 Categories of Liquid Desiccant

The liquid desiccants are competitive with solid desiccants due to their advantages such as: more flexibility, capability of absorbing pollutants and bacteria, relative lower regeneration temperature and lower air side pressure drop, etc (G. Grossman, 2002; K. Daou, 2004). Commonly used liquid desiccants involve LiCl, LiBr, CaCl₂, and KCOOH, LiCl+LiBr solution, etc (K. Gommed and G. Grossman, 2004; F.N. Ani, et al, 2005; G.A. Longo and A. Gasparella, 2005).

In 1937, hygroscopic salt solution such as LiCl+H₂O, LiBr+ H₂O, KCOOH+ H₂O etc, were used as absorbents replacing the commonly solid desiccants to deal with large latent loads. With the technological development of utilizing waste and renewable energy such as solar energy, more liquid desiccant systems constituted of a dehumidifier core and regeneration unit have been researched and employed with conventional HVAC system to service the desire air at a high COP (G.A. Longo and A. Gasparella, 2005).

Lithium bromide solution (LiBr+ H₂O) is the most stable desiccant with advantageously low vapour pressure, but its cost is slightly higher compared with others. The high cost, strong

causticity to metals and high regenerator temperature of Lithium bromide obstruct its development and application. LiCl solution is more used owing to its higher absorption ability and relatively lower regenerator temperature (60~65°C) although it is corrosive but not a toxic material and does not pose any health hazards (K. Gommed and G. Grossman, 2004; F.N. Ani, et al, 2005).

G.A. Longo carried out experimental and theoretical analysis of heat/mass transfer in a packed column dehumidifier/regenerator with salt solutions of LiCl+H₂O, LiBr+H₂O and KCOOH+H₂O. Theoretical analyses indicated that a transition concentration between regeneration and dehumidification around 25%, 42% and 57% of LiCl, KCOOH and LiBr solution respectively. The LiCl and LiBr solutions presented a better dehumidification performance than KCOOH solution, which performed better in regeneration. Although KCOOH+ H₂O was less corrective and more compatible with the environment, its high price obstructed its application (G.A. Longo and A. Gasparella, 2004).

R.M. Lazzarin (1999) compared the dehumidifier performance of LiBr and CaCl₂ solutions in 1999, and deduced that CaCl₂ performed less dehumidification capacity than LiBr solution when their mass concentrations had a similar crystallization temperature (the mass concentrations of LiBr and CaCl₂ were 60% and 40% respectively, and the similar crystallization temperatures were of 11~12°C). In the experimental and modelling researches carried out by D. Pietruschka (2006), it was proved that Calcium chloride solution offered significantly lower dehumidification potential than LiCl solution, although it had a cheaper price and no causticity to metal.

Glycols perform the dehumidification as absorbent very well and are less corrosive than hygroscopic salt solutions. However, glycols have low evaporative pressure and easily evaporate into the supplying and regenerator air, which will poison the breathing air. However,

desiccant salt has zero evaporative vapour pressure under the atmospheric pressure and no poison to the environment air (G.A. Longo and A. Gasparella, 2005; L. Mei and Y.J. Dai, 2006).

Table 2.3 Comparison of several aqueous solutions from seawater

Property	Unit	Aqueous solution of:					
		CaCl ₂	LiBr	LiCl	MgCl ₂	ZnCl ₂	NaCl
Concentration (mass solute/mass solution)		0.36	0.39	0.26	0.31	0.52	0.26
Hygroscopicity (equilibrium RH)	%	50	50	50	50	50	75
Cost	USD/m ³	560	7300	4600	450	1400	180
Abundance in seawater ^a	m ³ /m ³	0.0023	4×10 ⁻⁶	3×10 ⁻⁶	0.013	1×10 ⁻⁹	0.09
Density	kg/m ³	1.35	1.38	1.40	1.29	1.58	1.20
Viscosity	mPa s	4.6	1.8	2.5	6.0	4.7	1.8
Specific heat capacity	kJ/kg °C	2.6	2.6	3.0	2.1	2.3	3.4
Thermal conductivity	W/m °C	0.56	0.48	0.56	0.52	0.46	0.58
Diffusivity of water in the solution	10 ⁻⁹ m ² /s	0.54	1.17	0.90	0.91	0.80	1.86
Differential heat of dilution	kJ/kg	80	no data	65	65 ^d	no data	no data
Water absorption capacity ^b	kg/m ³	85	84	91	76	120	n.a.
Human toxicity ^c	L	0.14	0.23	0.10	0.49	0.03	0.66
Ecotoxicity (<i>Daphnia magna</i>)	ml/L	4.9 (2)	no data	0.06 (2)	4.3 (1)	0.001 (6)	20 (5)

Comparison of the properties of six liquid desiccants at 25°C, to allow a fair comparison, a concentration giving an equilibrium relative humidity of ERH=50% has been chosen in each case, with the exception of sodium chloride where ERH=75%, this being the minimum achievable.

a) Volume of desiccant solution that could theoretically be extracted from unit volume of seawater, assuming 100% recovery speed.

b) Mass of water that, on absorption in the solution, will cause a 10% relative increase in equilibrium relative humidity.

c) Estimated lethal dose in humans scaled from LD50 values for rats. d) At 50°C.

In 2008, A.A.M. Hassan and M. Salah Hassan tried to add 20% (in weight of water) calcium nitrate to 50% (in weight of water) CaCl₂ solution. The mixture solution CaCl₂ + Ca(NO₃) carried the dehumidification load under the same situation as the 50% CaCl₂ solution, and the depressed vapour pressure of the mixture solution was improved by 38.68%, 50.36%, 52.89% and 49.21% under the temperatures 30°C, 40°C, 50°C and 60°C respectively (A.A.M. Hassan and M. Salah, 2008). Their research also proved that, when the mixture scale of CaCl₂ to Ca(NO₃) was 0.4, it had a higher performance than the mixture solution of LiCl to CaCl₂ with the scale of 1.0.

P.A. Davies and P.R. Knowles (2006) researched the seawater biterms as a source of desiccant to be used in the solar green-house as shown in Table 2-3. It was found that the $ZnCl_2$ solution had the best water absorption capacity but it took the lowest content in seawater. LiBr, $CaCl_2$ and LiCl solution had the inferior water absorption capacity following $ZnCl_2$ solution gradually, and the $CaCl_2$ solution had the maximal mass concentration in seawater and also was the cheapest. Although the LiCl solution mass concentration was low in seawater (only $3 \times 10^{-6} \text{ m}^3/\text{m}^3$), it had the high water absorption capacity and low toxicity to humans as well as low causticity. Hence, $CaCl_2$ has economical advantages than LiCl solution, but lower applicable capability than LiCl

LiBr, LiCl and $CaCl_2$ are the main used desiccant solution in this project; the performance of these three solutions employed in the novel heat recovery/desiccant cooling system were researched based on experimental and modelling studies.

2.4.2 Liquid Desiccant Carriers

Both in the dehumidifier and regenerator, liquid desiccant need contact directly with the humid air and regenerator air to carry out the heat/moisture transfer. The commonly researched contacting surface includes a wet wall/falling film, a spray chamber or a packed tower, which can provide enough interface between solution and air flow. At the same time the solution carrier has to prevent the corrosive particulate being carried out by the air flow.

Wet Wall/Falling Film

In 1997 the salt solutions were investigated to using in the HVAC system. A.Y .Khan (1998) carried out a research to spray desiccant solution along a finned-tube heat exchanger. In this earlier stage desiccant carrier, the hygroscopic solution was sprayed directly from the top of the tube heat exchanger, in which cooling water flowed through the tubes in the cross direction. Warm and humid air was forced through the gaps between the tubes keeping a 90° angle with

flowing down solution film as well as cooling tube. In this dehumidifier core, the desiccant solution formed an intermittent film, which offered a small contacting surface with the air stream and lost particulates to the air stream.

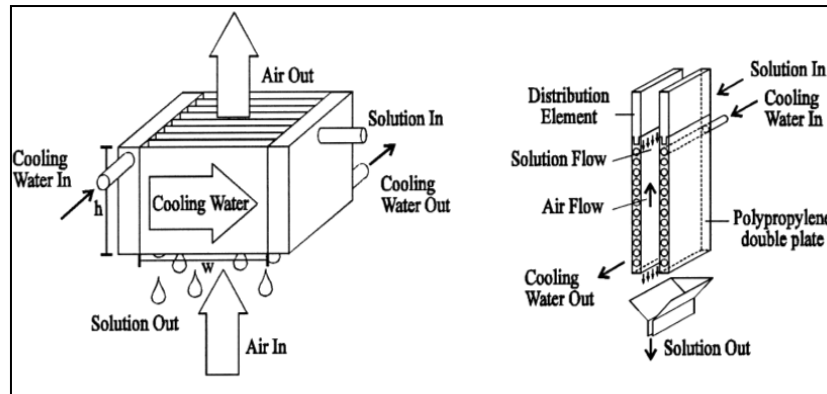


Figure 2-14 Polypropylene sandwich dehumidifier/regenerator cores

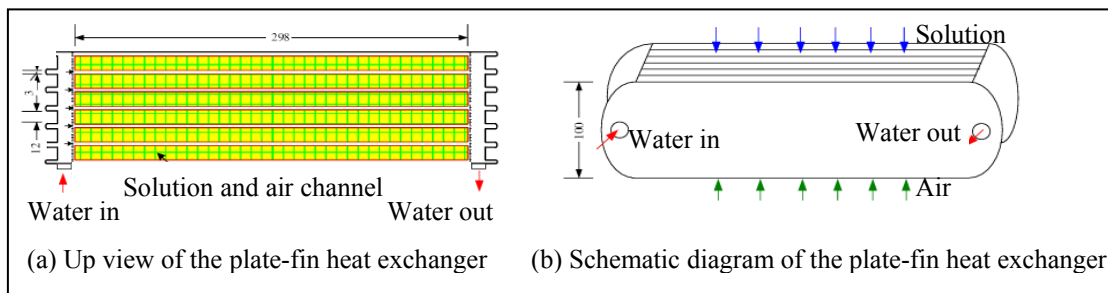


Figure 2-15 Stainless steel internal dehumidifier/regenerator cores

W. Kessling, et al (1998) researched a new dehumidifier/regenerator core to enhance interface and reduce the solution lost, which consisted of two layers of polypropylene with cooling pipe in the interlayer and a special distribution element was used, as shown in Figure 2-14. This dehumidifier core has the following advantages: cooling pipe covered in the interlining cools the hygroscopic solution sufficiently; no sprayer used; resisting hygroscopic solution corrosive forces; cheap materials and convenient to be manufactured. However, the disadvantages exist such as: solution cannot be distributed uniformly; particulates can hardly be held by the polypropylene layer; cooling pipe in the interlayer increases the dehumidifier/regenerator core size.

Y. Yin, et al (2007) undertook an experimental study on a new internally cooled/heated dehumidifier/regenerator core, as shown in Figure 2-15. Cooled strong solution was sprayed from the top of the unit and humid/hot air flowed up from the bottom. Between two pieces of stainless steel plates there was a cooling water tunnel, which brought the condensed latent heat and sensible heat out of the hot air. In this unit, the contacting surface between the solution and air stream is enhanced and the cooling effectiveness is improved. But the stainless plate still cannot catch the solution particulate as well as fibre, silica gel and activated alumina does.

S. Alizadeh and W.Y. Saman investigated the regenerator and collector effectiveness of a solar collector with CaCl_2 solution film covering the bottom of it and contacting with a forced in air stream. Testing results agree with the prediction made by A. Ali and L.C.S. Mesquita: that air flow speed, thick desiccant film and solar collector angle greatly affected the effectiveness of the whole system (A. Ali and K. Vafai, 2004; L.C.S. Mesquita, et al, 2006). P. Donggen (2007) further developed the desiccant solar collector and regenerator technologies by adding a regenerator tower after the desiccant flowing out from the solar collector. In the tower, hot strong solution was dehumidified again; with the moisture evaporate out, the solution temperature as well as moisture content was reduced.

M.D. Larson researched (2007) that polyethylene and polypropylene membranes employed to form wet wall/falling film could endure big pressure and temperature change with the air flow and solution condition varying and be cheaper than metal/stainless.

Packed Tower

Packed towers are classified into regular and random structure. Random packs have been used in researches such as ceramic saddles, sandy layer, plastic or polypropylene pall rings/spheres and polypropylene plant as shown in Figure 2-16 and 2-17 (W. Kessling, et al, 1998; A.M. Hamed, 2002; S. Alizadeh, 2007).

Regular structures include honeycomb paper, Kool-Cel pad and Celdek structure packs etc, as shown in Figures 2-18 and 2-19 (Y.J. Dai, et al, 2001; K. Gommed and G. Grossman, 2004; Y.J. Dai and H.F. Zhang, 2004; X.H. Liu, 2005, Web 1).

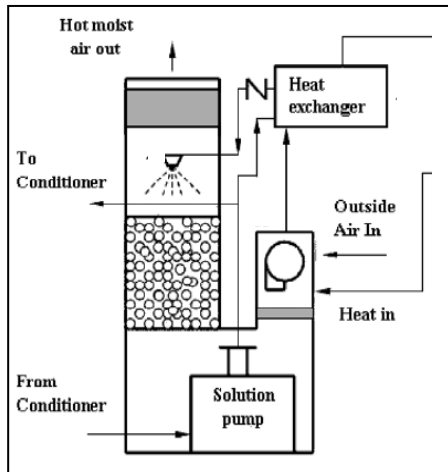


Figure 2-16 Polymer pall rings/ spheres carrier for regenerator

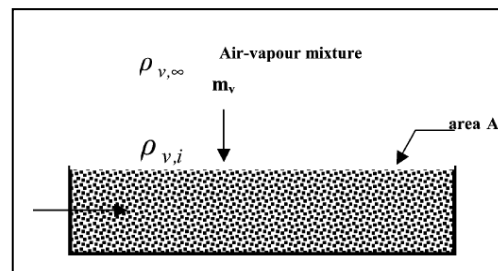


Figure 2-17 Sandy bed impregnated with Calcium Chloride

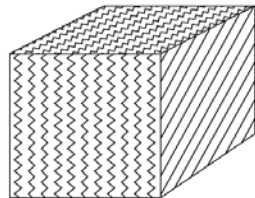


Figure 2-18 Honeycomb paper

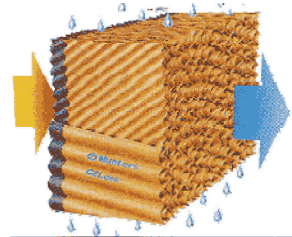


Figure 2-19 Celdek structure pack

Kool-Cel pad is constructed with two air flows at equal 45° angles, which allows air flow to enter from either side of the pad. And the Celdek structure is the development of Kool-Cel pad, in which one flute is steeply pitched and the other has less pitch so the air enters the pad from the side of the steep pitch, as shown in Figure 2-19 (Web 2.1). Compared with the Kool-Cel and fixed orientation of the mass transfer surfaces, the Celdek structure was proved to enhance the mass absorption capacity of the dehumidifier core but bring more air flow resistance (T.W. Chung, et al, 1995; G.A. Long and A. Gasparella, 2005).

In the honeycomb structure, the solution contacts with the air stream through the honeycomb structure and solution particulates are held very well by paper fibre (Y.J. Dai and H.F. Zhang).

F.N. Ani carried out the research on the effect of absorber packing tower height on the performance of a hybrid liquid desiccant system. It was found that, when the dehumidifier core height was changed from 200mm to 1,000mm, the performance coefficient improved 48.5% and the air pressure was accordingly reduced.

Spray Chamber

In recent researches, the spray chamber is seldom used separately to absorb/desorb moisture from the air flow, but is often used with different packed towers to improve the interface with the air flow. Tubular/plate absorber forming the falling film are two kinds of spray chambers which induce the air contacting directly with the falling solution film, but it leads to the solution particulates being carried away by the following air stream (S. Jain, et al, 2000).

The advantages and disadvantages of the three kinds of contacting methods are concluded as the following.

- Wet wall/falling film can offer a better contacting surface of solution and air flow, but the corrosive particulates are possibly carried out by the following air.
- Wet wall/falling film researched by A.Y. Khan, W. Kessling, et al and Y. Yin, et al were all associated with the cooling pipe, which carried the latent heat away quickly and improved the cooling capacity. The packed tower needs additional cooling/heating equipment outside the dehumidifier/regenerator.
- Compared with the wet wall/falling film, packed tower can avoid particulates being carried out and improve the contacting surface; however, the air flow resistance is aggravated synchronously.
- Random packs such as ceramic saddles, sandy layer, plastic or polypropylene pall rings/spheres and polypropylene plant can afford more contacting surface than a regular structure, and are convenient to be obtained, replaced and manufactured as well as the lower cost compared to the regular ones.

- In regular packed structures, the air temperature, desiccant solution flow speed, temperature and concentration influence the dehumidification effectiveness greatly, but the effects are slight in the random structure (V. Oberg. and D.Y. Goswami, 1998; Y.H. Zurigat, et al, 2004).
- The Celdek structure pack provides more contacting surface compared with the Honeycomb, but also brings higher flow resistance (A.M. Hamed, 2002 and S. Alizadeh, 2007).

The aims of our project is to designed and install a heat/mass exchanger and dehumidifier into a windcowl/catcher's air channel, which will offer a zero cost ventilation. Hence, lower air flow resistance, higher contacting surface and no schlepping out solution as well as low cost are the conditions to build up the dehumidifier core. Simple plate membranes made of cellulose fibre constitute the dehumidifier core, in which the cellulose fibre material can absorb and hold the solution very well, and two pieces of the parallel membranes build up a low resistance air tunnel.

For the regenerator, because it is not installed into the windcatcher/cowl, the core is made into a honeycomb structure using the same fibre paper to enlarge the contacting surface and regeneration effectiveness. Fibre paper is employed as the dehumidifier/regenerator materials in this project due to its low cost, convenience to be shaped, manufactured, installed, and replaced, as well as having a high hydrophilic characteristic.

2.4.3 Regenerator Energy Source

The generally used heating energies for regenerating the weak solution include: electric, gas, solar, waste heat and solar energy, etc. Solar energy is popularly used as liquid desiccant regeneration temperature is usually under 80°C, which can be conveniently collected from the sun energy (K. Daou, et al, 2006; G. Mittelman, et al, 2007).

There are mainly three methods to employ solar energy to regenerate the weak desiccant solution: solar water collector, solar air collector and solar desiccant collector. The first one is described in the section 2.3.3, and the second one is similar to regenerating the solid desiccant by solar air (hot air from the solar collector is forced through the regenerator pack and absorbs the moisture out from the weak desiccant). For the third method, the weak desiccant is pumped to the top of the solar collector and sprayed down along the collector layer, then influxes into the solution tank. Usually, the layer at the bottom of the solar collector is made of porous materials to hold the following desiccant for a long time and enlarge the contacting time with the air stream. The air steam can be forced into the parallel-flow or counter-flow direction with the desiccant solution, as shown in Figure 2-20 (S. Alizadeh and W.Y. Saman, 2002) and Figure 2-21 (P. Donggen, et al, 2007) respectively.

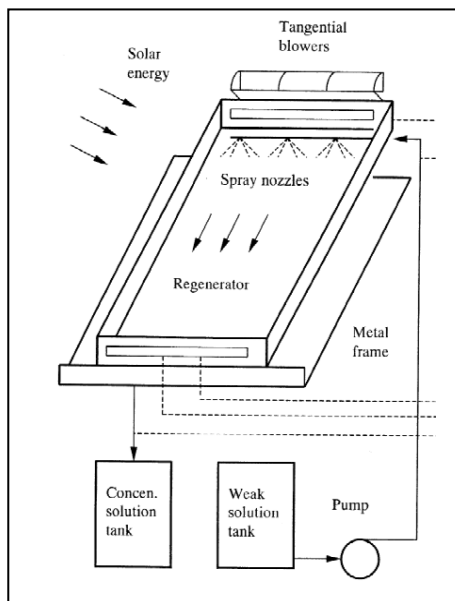


Figure 2-20 Parallel-flow desiccant-solar regenerator

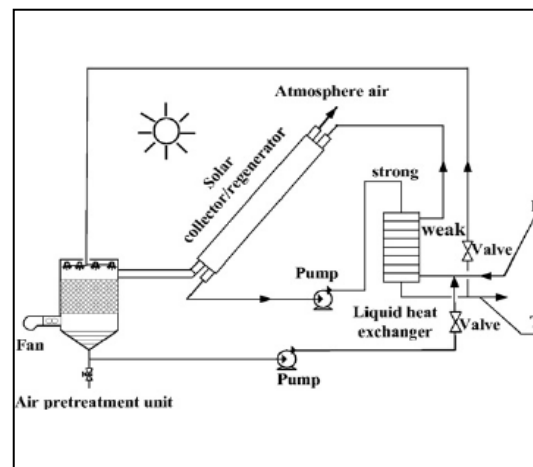


Figure 2-21 Counter-flow desiccant-solar regenerator

A.E. Kabeel researched the performance of a solar regenerator, in which the black cloth layer was used to improve the solar collector effectiveness and decline the desiccant flowing down rate. Results indicated that regenerator ratio increases with the air flow speed and solar collector efficiency interface increasing and decreases with the desiccant flow rate and air relative

humidity increasing (S. Alizadeh and W.Y. Saman, 2002; A.E. Kabeel, 2005; P. Donggen, et al in 2007).

Solar water is more popularly used to heat up the desiccant through a heat exchanger than a direct solar–desiccant regenerator. This is because of the following reasons:

- Solar water is more convenient to be transported than a desiccant solution.
- Most solutions are corrosive and toxic to humans. Leaking of the solutions is dangerous.
- Many more solutions are required if employing the solar-desiccant regenerator.
- Effectiveness of a solar water regenerator is lower than a solar–desiccant regenerator.
- Solar energy can be stored in the desiccant solution as well as in a water tank.

A water solar collector is the safest, handiest and most effective method to collect, transfer and storage the solar energy for regenerating a weak desiccant.

2.4.4 Cooling Energy

When the regenerator energy is substituted by solar/waste energy, the cooling energy cost is the main input energy for desiccant dehumidification and cooling system. Hence, the COP of the system is heavily influenced by cooling energy in this case.

A cooling tower is widely used to deal with the over heating of the regenerator; however, the cooling tower temperature and cooling water flow rate are seldom researched in estimating the COP (S. Jain, et al, 2000; K. Gommed, 2007; P. Donggen, 2007). Hence, the relationships between the cooling water temperature/flow rate and dehumidification effectiveness/COP are investigated in this thesis. The starting evaporative cooling temperatures to cool the dehumidifier and optimal COP will be found when the desiccant solution and air conditions are defined.

Groundwater was used in some cases to cool the hot and strong desiccant. But this technology is limited by its high primal investment and running cost. When the desiccant system cooperates with groundwater cooling, it will be convenient to utilize ground energy to cool desiccant solution, such as the case studied by W. Casas and G. Schmitz — Gas-driven desiccant assisted air conditioning system with geothermal energy of an office building — in 2005 (W. Casas and G. Schmitz, 2005).

2.4.5 Solution Flowing Direction to Air Flow

The desiccant solution can contact with the flowing air in the following three ways: counter-flow, parallel-flow and cross-flow. The most-used flowing way in the dehumidifier and regenerator is counter-flow, which is considered as having the highest heat/mass transfer effectiveness (K. Gommed and G. Grossman, 2004; X.H. Liu, 2005; K. Daou, et al, 2006; L.C.S. Mesquita, 2006).

Cross-flow dehumidifier performance was studied in experiments by X.H. Liu in 2005. Comparing the results with other literatures about counter-flow, it was found that: moisture removal rate from air varied less with the air temperature changing in cross-flow but in the counter-flow it would decrease/increase greatly with the air temperature increasing for the same solution. Other inlet parameters, such as air flow speed, desiccant flow rate and temperature, etc, also affected the dehumidifier effectiveness and moisture removal rate similar to the counter-flow (X.H. Liu, et al, 2005; X.H. Liu, et al, 2006).

X.H. Liu, et al again developed a simplified model to predict the performance of a dehumidifier using cross-flow and counter-flow respectively (X.H. Liu, et al, 2006). There was a big difference of about $\pm 20\%$ between the simulation and experimental results of the moisture effectiveness. This is caused by the calculation methods, in this model; the enthalpy was considered as the basic calculating parameter of the heat and mass transfer between air stream and solution. However, in the practical processes, the temperature and vapour pressure

difference between the air flow and solution induce the heat and moisture moving from the humid air to the hydrophilic solution respectively. Hence, in this thesis, numerical models are approached to estimate the processing characteristics of the heat/mass exchanger, dehumidifier and regenerator as well as the whole system based on the parameters of the temperature and vapour pressure.

2.4.6 Liquid Desiccant Hybrid Cooling Systems

Owing to the special characteristics of the liquid desiccant, the working methods with other types of air cooling systems are different from the solid desiccant. Solar and ground energy, waste energy, and direct/indirect evaporative cooling technologies are mostly employed to carry the dehumidification and cooling. These renewable dehumidification/cooling systems save energy and reduce pollution greatly.

Desiccant Combined with Direct/Indirect Evaporative Cooling Systems

Figure 2-22 is one typical dehumidification/indirect evaporative cooling unit (W.Y. Saman and S. Alizadeh, 2002). Two tunnels constitute one heat exchanger group. In the primary air stream tunnel, water is sprayed from the top of the unit and evaporation latent heat is absorbed from both air streams. In the secondary air stream, solution is sprayed from the top and condensation latent heat is released into the primary air stream. Experiments carried out by W.Y. Saman and S. Alizadeh revealed that, when the heat exchanger angle is 45° and air mass flow rate is 0.3 kg/s, the effectiveness of the dehumidification/cooling unit could reach about 75%.

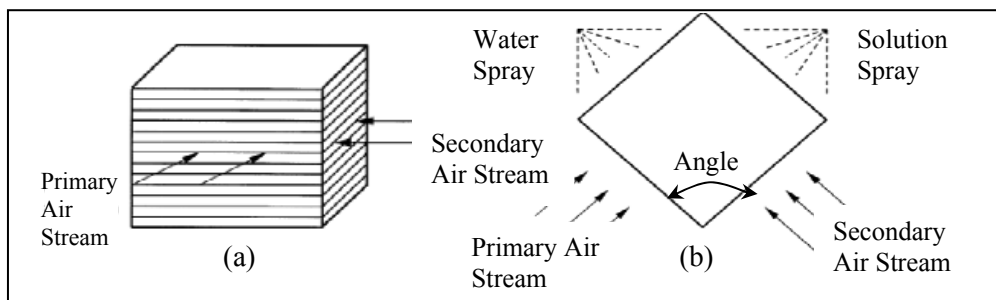


Figure 2-22 Cross-flow dehumidification/indirect evaporative cooling unit

D. Pietruschka, et al investigated the solid/liquid desiccant assisted indirect evaporative cooling. Their results indicated that: 1) liquid desiccant & evaporative cooling system could perform 50% higher dehumidification than solid desiccant; 2) no big air temperature increased when liquid desiccant absorbs moisture, which was contrary to the solid wheel; 3) 30% more cooling power was gained than when only employing the evaporative cooling in solid desiccant wheel; 4) LiCl solution performed 40~50% higher dehumidification rates than CaCl₂ solution (D. Pietruschka, et al, 2006).

In 2007, S. Alizadeh carried out further investigating on utilizing solar energy with a liquid desiccant/indirect evaporative cooling system in Australia. The experimental results indicated that: the polymer plate heat exchanger/dehumidifier unit effectiveness could reach 82%, the COP of the polymer pall ring/spheres packed-bed regenerator raised from 0.65 to 1.25, and the electrical coefficient of the whole liquid desiccant system approached 6.0 (S. Alizadeh, 2007).

Desiccant Combined with Vapor Compression Air Conditioning System

A hybrid air conditioning system, which consisted of dehumidification, evaporative cooling and vapour compression air conditioning, had been investigated in 2001 by Y.J. Dai, et al, as shown in Figure 2-23. The reasons for the hybrid system being superior in performance to conventional systems result from the fact that desiccant dehumidification and evaporative cooling changed the inlet states of the air entering into the vapour compression system and the rejected air energy was recycled and used in the regenerator to recover the weak desiccant.

This system reduced the electricity consumption of the compressor, flow rate of condensation air, the size of the vapor compression system, and improved COP of the system. COP of the hybrid system with desiccant/evaporative cooling increased 40.53% than the vapor compression air conditioning and ECOP increased 76.00%. Without the evaporative cooling system, the COP and ECOP were improved by 26.21% and 38.80% respectively (Y.J. Dai, et al, 2001).

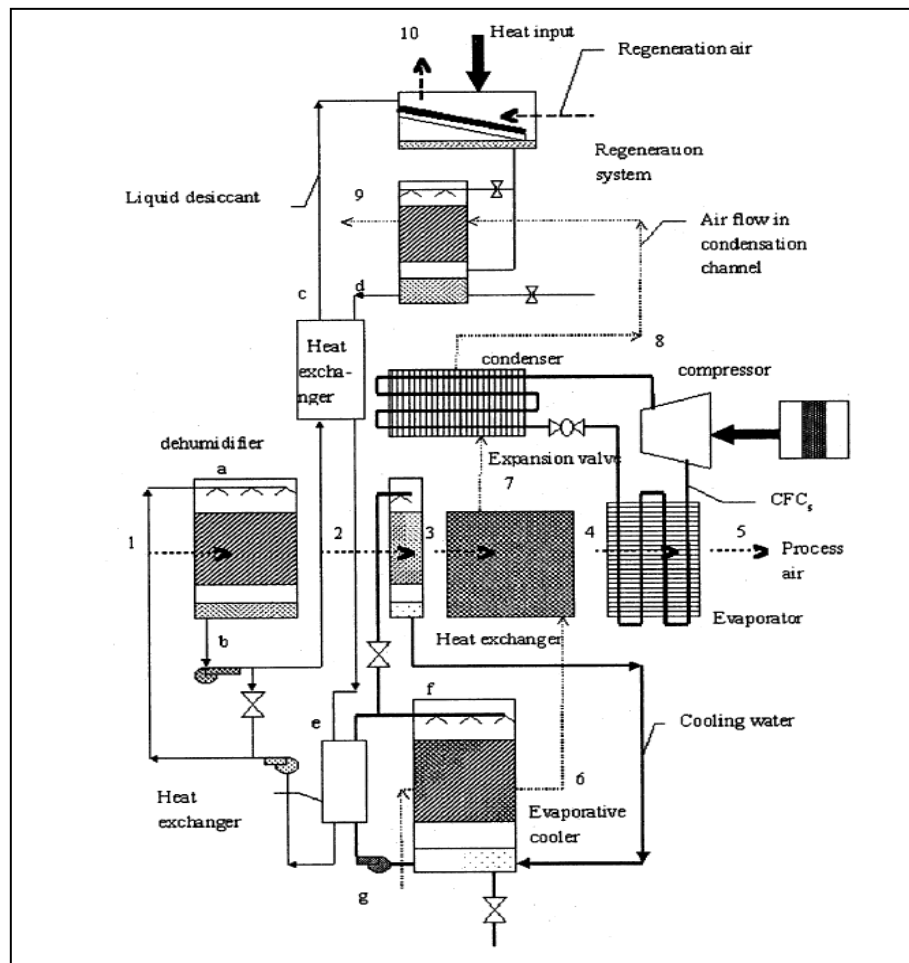


Figure 2-23 Hybrid desiccant and air vapour compression cooling

Evaporative Cooling and Desiccant Dehumidifier Applied in Greenhouse

A liquid desiccant assisted evaporative cooling system for the greenhouse was investigated by P.A. Davies who researched it to promote the cultivating crops in very hot countries (P.A. Davies, 2005). As shown in Figure 2-24, the solar collector is designed on the roof of the greenhouse to reduce the entering solar energy as well as absorbing energy to regenerate the weak desiccant. Inside, hot and humid air flow was dehumidified by a desiccant pad first and then cooled by the evaporator. Outside, exhaust air evaporated water and produced cooling energy on the wall to cool the whole house. The maximum reduced temperature in summer was 15°C by this system, which was 5°C lower than conventional evaporative cooling. Results indicated that this kind of greenhouse had the potential to be utilised in a hot country to increase

the crop productions. And if the evaporator pad is substituted by an indirect evaporator cooler, this system is more powerful to service low temperature and low humidity air to keep fruits fresh.

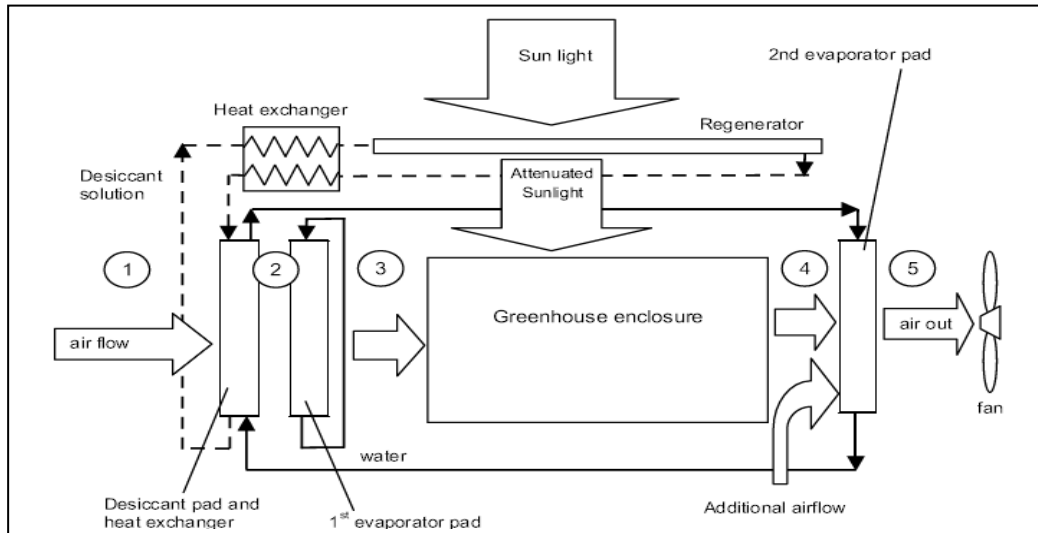


Figure 2-24 Evaporative-cool greenhouse assisted by liquid desiccant and solar energy

Heat Pump Combined with Desiccant Dehumidification/Cooling System

Heat pump technology is employed with the desiccant dehumidification/regeneration system as shown in Figure 2-25. In this system, the working refrigerant such as R22, R407c, R417a etc, flowing out from the compressor, firstly cools the diluted solution and the regenerator air in two condensers respectively, and, with it flowing forward, it heats up the concentrated solution in the evaporator again. It is a self-regenerating liquid desiccant cooling system to dehumidify, heat/cool the ambient air by an electric heat pump. In the design, for demand of cooling only, the COP of the system was 4.0, for a demand of both cooling and dehumidification, the COP was 3.0 (R.M. Lazzarin and F. Castellotti, 2007). In this project, the evaporator and condenser were the two parts to offer heating and cooling energy by the refrigerant such as R22, R407 or R417a. In our project, for saving the electrical/gas energy, solar energy is purposed for the regeneration, and evaporative cooling water offers cooling energy.

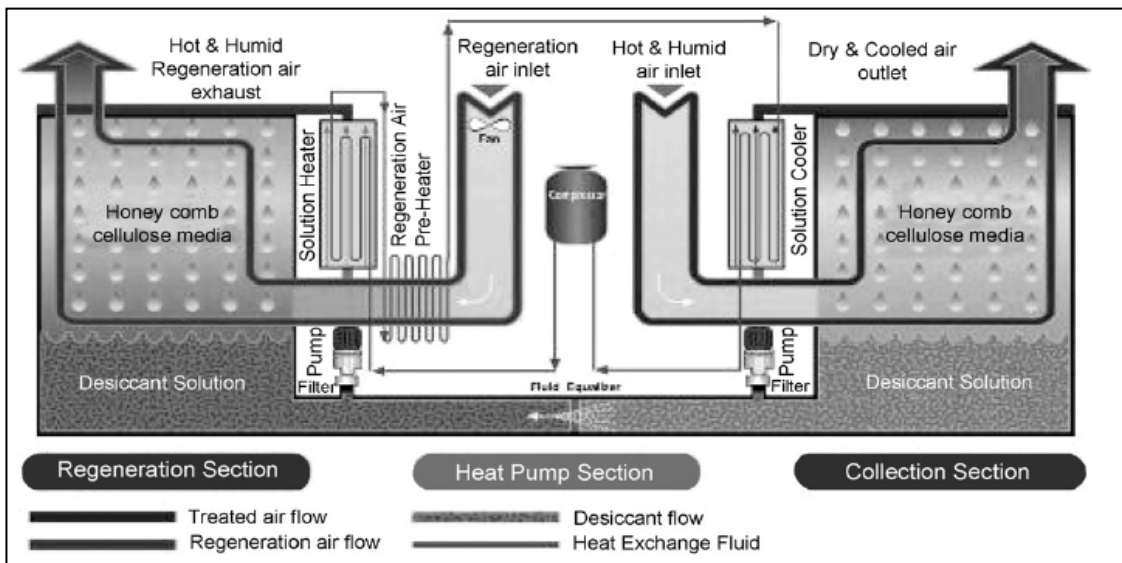


Figure 2-25 Heat pump desiccant cooling system

Reverse Osmosis Technologies Integrated Desiccant/Evaporative Cooling System

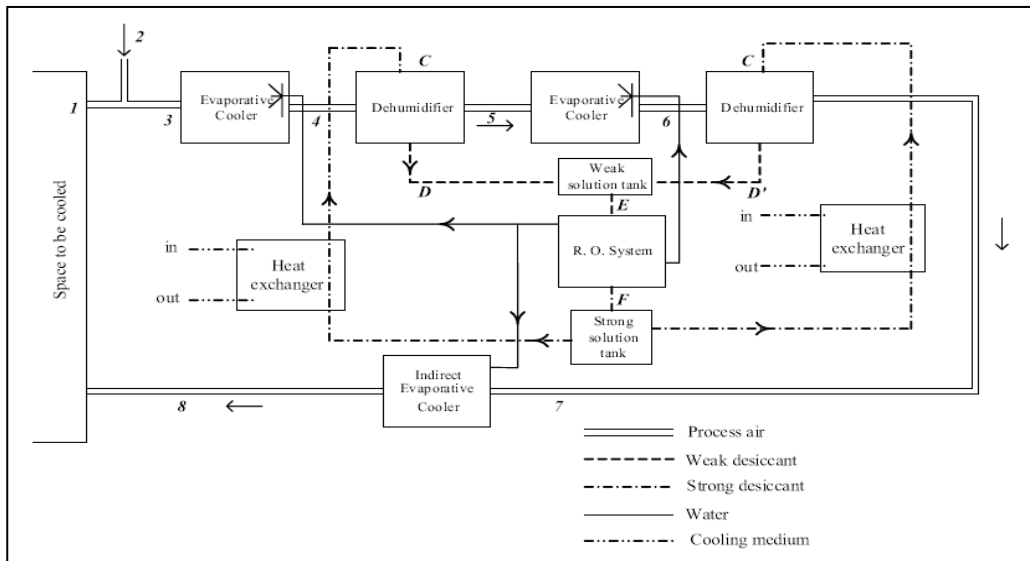


Figure 2-26 Schematic of the reverse osmosis dehumidification/cooling system

Utilizing repetitious evaporative, dehumidification technologies, and reverse osmosis process as the mechanical energy to cool and dehumidify hot/humid air was tried by F.A. Al-Sulaiman, et al in 2007. The reverse osmosis process regenerates the weak desiccant as well as offering cooling water to the evaporative chamber for cooling the supplying air, as shown in Figure 2-26. The COP of this system was found to be 1.2 based on the reverse osmosis process with 3%

recovery (F.A. Al-Sulaiman, et al, 2007). The recovery effectiveness of the reverse osmosis process influenced the COP heavily, but it was still very low at present. Hence, the proper membrane with satisfied porous and pore size as well as effective method to produce high pressure by mechanical energy are the keys to improving the low COP.

2.5 Summary

A thorough review of the related knowledge regarding the heat/mass exchanger, solid and liquid desiccant dehumidification/regeneration technologies and hybrid absorbent/adsorbent cooperated cooling systems, was carried out. These subjects are related to the project researched in this thesis and the pre-reading and understanding of these technologies are necessary to progress the proposed research work.

In section 2.1, the purposes utilizing the enthalpy exchanger and desiccant cooling and the regions suitable for using these technologies were summarised. The intention of utilizing the enthalpy exchanger is to save energy and reduce air pollution. Besides the common use of adsorbents/absorbents in paper factories, spinning mills, food factories, storage, etc, treating environment air to a desired living condition for residential/working buildings by dehumidification/cooling technologies is a hot topic at present. Humid regions such as Europe, South America and South Asia, etc are all suitable areas to apply desiccant cooling technologies.

In section 2.2, enthalpy exchangers including the enthalpy plate, wheel and hydrophilic membranes exchangers were reviewed. Different technologies of the enthalpy plate and wheel, and their advantages and disadvantages, were discussed and it was pointed out that the hydrophilic membranes exchanger is the new developing technology to carry the mass/heat exchanger effectively without a carry-over problem.

In section 2.3, solid desiccant categories and their carriers, regeneration source and technologies, as well as their integration with other air conditioning systems were summarised. (1) Various

adsorbents and their dehumidification/regeneration characteristics were studied widely and it was found that most solid desiccants with higher absorption capacity had a high regeneration temperature over 80°C. (2) Desiccant wheel technologies were investigated to improve the dehumidification/regeneration efficiency and the main researches focus on wheel structure, rotation speed, wheel fin size, air flow speed and the attached adsorbents, etc. (3) Gas, electric, solar and waste energy-driven regenerators were reviewed, and it was found that solar water was the most convenient method for using renewable energy as well as keeping a high regenerator speed. (4) A series of solid desiccant integrated cooling systems and their performance were studied. It was indicated that these hybrid systems could produce good air conditions, save energy and reduce pollution simultaneously, but the COP still needs to be improved.

In section 2.4, liquid desiccant categories and their carriers, regeneration source and technologies, and the hybrid dehumidification/cooling systems were reviewed. (1) Investigations of many hygroscopic solutions utilized as absorbent were introduced, and it was found that most absorbents could afford good dehumidification performance with a lower regeneration temperature than adsorbents. However, the causticity characteristic of absorbents needs to be solved in further technologies. (2) Technologies on improving the interface between liquid solution and air stream were reviewed; structure and materials of the wet wall/falling film or packed tower were the mainly researched objects to improve the dehumidification/regeneration efficiency. (3) Technologies of utilizing renewable energy for regeneration and cooling hot strong solutions were introduced. (4) Three kinds of flowing direction between solution and air flow were introduced, and the influences of air and solution parameters on dehumidification/regeneration effectiveness were analyzed (5) Liquid desiccant combined with cooling systems were displayed and the results indicated that liquid desiccant assisted cooling systems had higher COP than the solid desiccant.

Chapter 3. Optimal Study of Heat/Mass Recovery Materials

3.1 Introduction

This chapter investigates several types of materials, namely metals, fibres, ceramics, zeolite and carbon, which have potential to be used as the heat and mass transfer medium for the heat/mass (enthalpy) recovery and desiccant cooling systems, and from the investigation, the most favourite material and structure are identified.

As analyzed in chapter 2 the traditional enthalpy plate exchangers such as activated carbon-methanol, zeolite-water, and $\text{CaCl}_2\text{-NH}_3$ covered shell, tube, flat pipe, and flat plate, plate-fin heat exchanger have huge heat and mass transfer resistance (R.Z.Wang, et al, 1998 and A.Hachemi, 1999). Air to air enthalpy exchanger wheels can carry the heat/mass transfer synchronously, but have the disadvantages such as over-take and consuming driven power, etc (S. Nair, et al 1995; J.Frauhammer, et al 1997, and L.A. Sphaier and W.M. Worek 2004). Recently, one type of hydrophilic membrane exchanger is developed to carry the heat/mass transfer and avoid the over-take problem. High capillary force and proper porosity and pore size are the key parameters for these kind membranes, and other factors such as thermal conductivity, durability, rigidity, et al are all need to be considered.

These properties of the proposed heat/mass medium (wall material) are important to determine the heat/mass transfer performance of the recovery and dehumidifier, regenerator. Wide range of materials can be used for this purpose, and may be classified as metal, fibre, ceramics, zeolite and carbon type. Metal type includes metal forms, metal wools, sintered metals and wicked metal plates/tubes with holes; Fibre type includes paperboard, cloth (wood or glass) fibres; Ceramic type involves SiC/SiC composites, Zirconia Ceramic, Zirconia toughened aluminium, ZrO_2 , Al_2O_3 , and Aluminum nitride and polystyrene composites; Zeolite type includes porous

ceramics, molecule sieves and synthetic polymers; and carbon fibre refers to carbon-carbon composites and activated carbon.

In general, a good heat/mass transfer material should have the characteristics of high thermal conductivity, high mass diffusivity and large capillary force, which allow a large amount of heat and mass to be conducted from the one side of the wall to the another side, and adequate amount of desiccant to be retained on the wall for dehumidification and regeneration. Also the material should have the advantages of being cheap and suitable for being shaped into various geometries. Furthermore, it should be ease of cleaning and replacement.

3.2 Theoretical Analyses of the Heat/mass Transfer

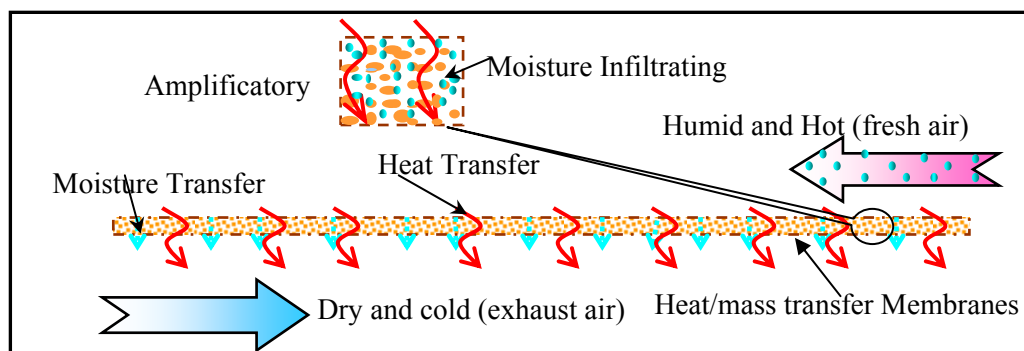


Figure 3-1 Schematic diagram showing the principle of the heat/mass transfer

Figure 3-1 indicates the heat and mass transfer through the heat/mass membrane. When the humid and hot air flows through the humid air channel, it loses heat through the membrane due to the temperature difference between the hot and cold air flows. As a result, the temperature of the hot air falls by some degrees and the relative humidity is increased. In the meantime, the moisture content difference between the humid and dry air induces the gaseous water condensed on the wet air side, and then infiltrates through to the dry air side. In the dry and cold air side, owing to the heat transferred from the hot side, the vapour pressure decreases to a lower level, which evaporates the abundant moisture transferred from the humid side. To achieve the mass transfer target, there must be a proper filtration interspaces allow liquid water to penetrate and avoid air to across.

The sensible heat transfer capability is defined as:

$$q = (t_f - t_e) / \left(\frac{1}{k_f^s} + \frac{\delta}{k} + \frac{1}{k_e^s} \right) \quad (3-1)$$

In this study, it's assumed that the heat and mass transfer is processed in the Laminar Flow (it will be proved in the section 3.2.1). From an industrial point of views the correctional convective heat-transfer Nusselt Number can be calculated by the following equations (J.R. Welty et al, 2000):

$$k^s = \frac{k_b^{air} Nu}{D} \quad (3-2)$$

$$Nu = 1.86 \left(Pe \frac{D}{L} \right)^{1/3} \left(\frac{\mu_b}{\mu_w} \right)^{0.14} \quad (3-3)$$

$$Pe = Re \cdot Pr \quad (3-4)$$

$$Re = \frac{uD}{\nu_b} \quad (3-5)$$

$$Pr = \frac{\nu_b}{\alpha_b} = \frac{\mu_b c_b}{k_b^{air}} \quad (3-6)$$

While the convective heat-transfer coefficient could be written as follows:

$$k^s = 1.86 \left(\frac{uD}{\nu_b} \cdot \frac{\mu_b c_b}{k_b^{air}} \cdot \frac{D}{L} \right)^{1/3} \left(\frac{\mu_b}{\mu_w} \right)^{0.14} \frac{k_b^{air}}{D} \quad (3-7)$$

The moisture transfer capability is defined as:

$$m = \frac{(p_f - p_e) / RT}{\left(\frac{1}{k_f^l} + \frac{\delta}{k_{mass}} + \frac{1}{k_e^l} \right)} \quad (3-8)$$

Schmidt and Lewis number are used to indicate the similarity between moisture transfer, momentum diffusivity and thermal diffusivity, which can be expressed as:

$$Sc = \frac{\mu_b}{\rho_b D_{AB}} \quad (3-9)$$

$$Le = \frac{k_b^{air}}{\rho_b c_{bp} D_{AB}} = \frac{\alpha_b}{D_{AB}} = \frac{Sc}{Pr} \quad (3-10)$$

Based on the Chilton-Colburn relation, the convective mass-transfer coefficient is written as:

$$k^s = k^l \rho_b c_{bp} (Le)^{2/3} \quad (3-11)$$

$$\text{Then } k^l = k^s (\rho_b c_{bp})^{-1} \left(\frac{\alpha_b}{D_{AB}} \right)^{-2/3} \quad (3-12)$$

The mass diffusion coefficient, D_{AB} is a function of air temperature and pressure, and can be calculated using the following equation (James R. Welty et al, 2000):

$$D_{AB} = D_0 \frac{P_0}{P} \left(\frac{t_b + 273.15}{T_0} \right)^{3/2} \quad (3-13)$$

For the air application under the atmospheric pressure, P_0 / P is 1 and T_0 is 273.15K. In this case, D_0 is $2.2 \times 10^{-5} \text{ m}^2/\text{s}$.

The thickness of the wall δ is in the range of 0.1 to 0.5mm, while thermal conductivity k takes the average of the k values of the materials and the filling water, owing to its porous structure.

In that case, k value can be written as (Parrott J.E. and Stuckes A. D., 1975):

$$k = \mathcal{G}k_{water} + (1 - \mathcal{G})k_{materials} \quad (3-14)$$

Where k value of the filling water is about 0.6W/mK, and k value of the wall material ranges from 0.3 to 400W/m.K, and porosity \mathcal{G} of the material varies from 20% to 90%.

3.2.1 Sensible Heat Transfer Analyses

Assumed the air channel length L and equivalent diameter D of the fixed air-to-air recovery is 0.5m and 5mm, and the thickness δ of the membranes is 0.5mm. The humid/hot air and cold/dry air conditions and the calculated convective heat/mass-transfer coefficient are listed in Table 3.1.

Table 3.1 Air parameters and calculated Re

	Temperature (°C)	Relative humidity (%)	Moisture content (kg/kg dry air)	Air flow speed (m/s)	Convective heat-transfer coefficient (W/m ² K)	Convective mass-transfer coefficient (m ² /s)	Reynolds Number (Re)
Hot/humid Air	35	70	0.02516	0.5~5	10.2430~22.067	0.0089~0.0191	148~1480
Cold/dry Air	25	50	0.00988	0.5~5	10.3215~22.237	0.0086~0.0186	157~1565

Calculated Reynolds number Re are all smaller than 2300, hence, the heat and mass transfer all occur in the Laminar Flow and equations 3-7 and 3-11 are suitable to be used in this heat/mass transfer progress through the membrane wall.

From the table 3.1, we can calculate that $\frac{1}{k_f^s} + \frac{1}{k_e^s}$ value is about 0.1945~0.09029, which is at least 60 times of $\frac{\delta}{k}$ ($\delta = 5 \times 10^{-4} \text{m}$, $k = 0.3 \sim 400 \text{W/mK}$). Hence, the thermal conductivity acts slight influence on the sensible heat transfer.

3.2.2 Latent Heat Transfer Analyses

For the term of mass transfer, $\frac{\delta}{k_{mass}}$ is determined by the membrane's thickness and the water diffusion coefficient k_{mass} across the membrane. Vapour pressure difference induces the moisture condensed on the wet porous membrane side and then it crosses to the dry side. In this process, two important factors should be considered that the porous membranes must offer enough porosity and proper pore size. The sufficient vacancy in the membrane surface is required to contain the condensed moisture effectively. And the right pore size is to permit the liquid water across as well as prevent the gaseous air penetration. Therefore, the lowest porosity on the membrane surface and the proper pore size is calculated.

As the assumed humid/hot and dry/cold airstreams' parameters shown in Table 1, the maximal moisture content difference is 0.01528kg/kg (dry air). It is supposed that all this moisture is

condensed on the membranes surface. Hence, the required vacancy to contain the liquid moisture is calculated by the following equation:

$$V'_{moisture} = \frac{|d_f - d_e| \pi D^2 u}{4 \rho_{moisture}} \quad (3-15)$$

Where the equivalent diameter D is 0.005m, maximal air flow rate is 5m/s and moisture density is $1 \times 10^3 \text{kg/m}^3$.

In the wet channel, the humid air contact with the two sides of the channel and the transfer wall volume is calculated by the following equation:

$$V'_{wall} = \delta \pi DL \quad (3-16)$$

Where the channel length is 0.5m. Therefore, the minimum porosity of the recovery membrane is as the following:

$$\rho \% \geq 100 \frac{V'_{moisture}}{V'_{wall}} \quad (3-17)$$

So the calculated minimal porosity of the heat/mass transfer wall is $3.82 \times 10^{-2} \%$. It is easy to be gained for most of the materials.

Knudsen Diffusion is quoted to find the optimal pore size of the porous membranes, which considers the diffusion of gas molecules through very small capillary pores. When the pore diameter is smaller than the mean free path of the diffusing gas molecules, and the density of the gas is low, the gas molecules will collide with the pore walls more frequently than with each other. This Knudsen number Kn is expressed by the following equation (Welty J. R., et al, 2001):

$$Kn = \frac{\lambda}{d_{pore}} \quad (3-18)$$

λ means the free path length of the diffusing species, and d_{pore} is the pore diameter of the porous membrane. In practical, free path length for molecules in the liquid state is very small, typically near to the molecular diameter of the molecular. Hence, free path length of the diffusing gaseous species need to be calculated by the following equation:

$$\lambda = \frac{\kappa T}{\sqrt{2} \pi \gamma^2 P} \quad (3-19)$$

κ is the Boltzmann's constant (1.38×10^{-16} ergs/K), T is the absolute temperature (290~350K), γ is the Lennard-Jones diameter of the spherical molecule (for air it is 3.617×10^{-8} cm), P is the system pressure (101.325kPa). The free path length of air molecular is about 9×10^{-4} cm.

When the Kn is greater than 1 meaning pore diameter smaller than free path length of air molecular, the Knudsen diffusion control the molecular diffusion cross the membranes. Under this situation, the Knudsen diffusivity of the air is calculates by the equation as expressed:

$$k_{mass} = 48.5 d_{pore} \sqrt{T / M_A} \quad (3-20)$$

M_A is the Molecular weight of passing Molecular. Water molecular diameter in liquid state is about 2.75×10^{-8} cm, and average air molecular diameter in gas state is about 3.617×10^{-8} cm (Web3.1, Web3.2).

For the air-to-air heat/mass transfer membranes, to permit the water molecular across and avoid the air molecular penetration, the pore diameter of the porous membrane should be bigger than the water molecular diameter (2.75×10^{-8} cm in liquid state) and smaller than the free part length of air molecular (9×10^{-4} cm). However, it can be known from equation 6 that although the pore diameter is smaller than the gaseous free part length, there is still a few molecular passing through. But when the Knudsen diffusion k_{mass} of the air through the pore is 1×10^{-2} times smaller than the convective air flow rate u (0.5m/s) in the tunnel, the air mass transfer through

the porous membrane can be ignored. In this case the equation 3-21 could be inducted as the following:

$$d_{pore} \leq \frac{u}{1 \times 100 \times 48.50 \sqrt{T / M_A}} \quad (3-21)$$

Figure 3-2 shows the reasonable pore diameter size range ($2.75 \times 10^{-10} \text{m} < d_{pore} < 3.2 \times 10^{-7} \text{m}$) to allow the moisture penetration and the air infiltration is ignored, and the air diffusivity through the capillary pores. In the shadow area from the pore size $2.75 \times 10^{-10} \text{m}$ to $3.2 \times 10^{-7} \text{m}$ can carry out the heat/mass transfer with the conditions that the moisture penetration is available and the air infiltration is ignorable. And it is also been found that the air temperature slightly influence air diffusivity.

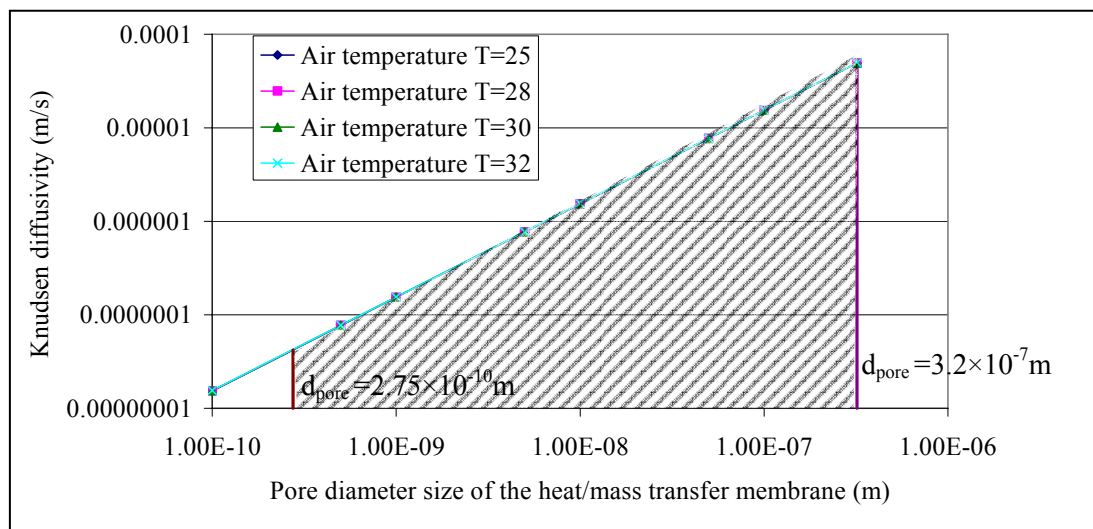


Figure 3-2 Pore diameter size of the heat/mass transfer membrane

3.3 Characteristics Considered in Selecting the Heat/mass Recovery Materials

As analyzed previously, materials' thermal conductivity slightly affects the heat transfer from one side to another side in the heat/mass recovery. Hence, thermal conductivity is considered as an inferior factor in selecting the optimal material for heat/mass exchanger.

Moisture penetrates across the material layer from the wet to dry side as shown in Figure 1. In this process, capillary forces of the material and pore diameter play significant roles. Porosity usually is defined to describe the capillary force of material's absorb ability. Higher porosity can hold more moisture in the interspaces and bigger pore diameter has lower mass flow resistance. However, as mentioned previously, pore diameter should be in the range of $2.75 \times 10^{-10} \text{ m} < d_{\text{pore}} < 3.2 \times 10^{-7} \text{ m}$ to enable the moisture penetration and avoid the gaseous air across.

Besides these two factors, the thickness of the recovery membrane heavily affects the heat and mass transfer resistance. As we know the stiff material is hard to be shaped into thin membrane, and soft material is easy to be made into filmy membrane but difficult to sustain. Hence, moderately hard of the material is another selection factor following porosity and pore diameter. Young's modulus is normally used to describe the hard of materials, and is defined as the ratio of the tensile stress to strain produced (M. Piggott, 2002). In addition, the adsorption water filling in the hydrophilic membranes damages the Yong's modulus. For instance as the celluloses fibres, wood, paperboard and others low fibre content, present lower Young's modulus and stress when it's saturated by water (A. Espert. et al, 2004).

Durability of the material is required for the optimal hydrophilic membrane. Commonly, this factor is decided by the material's properties. However when the membranes is filled with water or aqueous liquid, the durability will be reduced, for instance, the steel will be rusted, the paperboard exchanger shape will be changed, the oxidation of activated alumina will be accelerated, and the frangibility of synthetic polymers exchanger under a high running temperature will be increased. Hence, durability is an important part to evaluate the optimization and economic performance of the heat/mass recovery.

Economic analysis is the last step to estimate the optimal heat/mass transfer material. Based on the structure requirement, the cost should include two parts: one is the material cost and the other is the manufacture cost. Materials such as, copper and aluminium is more expensive to be

shaped into thin membranes than cellulose fibre. Cost is a criterion which depends very greatly on the end use of the structure containing the materials (M. Piggott, 2002).

3.4 Comparative Analyses of Potential Heat/mass Transfer Materials

3.4.1 Metal Type

The traditional metal heat exchanger is mainly made of aluminium, copper and their alloys, which can be shaped into a surface such as plate or tube. This kind of surface has much less capillary force to retain the condensed moisture from the humid/hot side. To increase surface capillary force, porous structure is considered to replace the smooth surface of the sheet or tube (L.Tadrist et al, 2004). Several metal porous structures, namely, wicked metal, metal foams or wools, will be studied in this paper. Porous metals have the thermal conductivity from 29.43 to 400W/mK, which is mainly determined by the porosity and characteristic of the metal (X. Zhao, et al, 2008). As we proved the thermal conductivity of materials slightly affect the heat/mass transfer, Table 3-2 gives the most important three factors including the porosities, pores size and membrane thicknesses of the selected metals (A. Schulz, et al, 2005, Z. Y. Zhao, et al, 2005, Kenneth L. Rubow, 2005, W. Jinhu and W. Yang, 2004, K. Boomsma, et al, 2003, L. Gu, 2002)

Wick may be one of the following structures, i.e., sintered particles, microcosmic holes, meshes, grooves or whiskers, and is attained to the tube/sheet to hold water for transfer. As shown in Table 3.2, the porosities of wicked metal vary in a wide range, from 39% to 98%, depending upon their construction, density, pore size and configuration. Although the wicks porosities are enough to contain the condensed moisture, the microcosmic holes size, from 15 to 90 μ m, can't match the pore diameter requirement ($2.75 \times 10^{-10} \text{m} < d_{pore} < 3.2 \times 10^{-7} \text{m}$) of the hydrophilic membrane. Figure 3-3 presents a whisker-attained tube heat exchanger, which has microcosmic cylindrical pores 5 μ m in diameter with porosity about 40% on the external surface of the tube (Schulz A. et al, 2005).

Table 3.2 Porosities, pores size and membranes thicknesses of wicked metal, metal foams and wools

Porous metal	Pore size ($\times 10^{-6}m$)	Porosity	Membranes thickness (mm)
Open Cell metal foam	2300	92%	2.0
Al metal foam	2000	Up to 90%	550
Whisker-attained tube	3	40%	1.0
Metal bronze sintered (wicked)	30~90	80~98%	0.1~10
Sintered (wicked) metal	15~30	39%	1.6
Amorphous metal foams	20 ~3000	<90%	2~10
Bulk metallic glasses metal foam	25~250	15~22%	7~10
Metal fibre (wool) in foam	>5.5	>50%	2.0
Metal wool	0.1~10	85%	3.2
Sintered Power	< 20	Average 31.5%	0.7
Sintered metal wool	3~59	65~87%	0.17~0.82

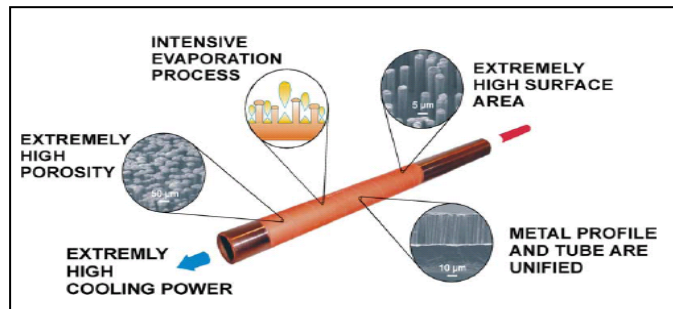


Figure 3-3 Heat exchange copper tube with the micro-structured surface

In recent years, highly conductive foams based on copper or aluminium was used to make heat/mass exchanger membranes. These open cell structures allow moisture/heat to be removed from the humid/hot side and added to the dry/cold side (John Banhart, 2001). The foams can be produced in different methods, such as melts, powders, sputtering and deposition (T.W.Clyne and F.Simancik, 2000). Each method covers a characteristic range of density, cell size and cell topology, thus resulting in the porosity up to 90% (W. Azzi, et al, 2005). At present, the pore sizes ranging from $5.5\mu m \sim 3mm$ with a varying porosity from 10% to 90% have been achievable, thereby the porosity, shape information and construction expense are related to each other (J.F. Despois, 2007; A.H. Brothers and D.C. Dunand, 2006; A.H. Brothers, 2005; E.J. Minaya, 2004; T.W.Clyne and F.Simancik, 2000). Similar to the wicked metal, the metal foam

can satisfy the porosity requirement but can't meet the demand of pore size and membrane thickness. Figure 3-4 presents the configuration of the commonly available metal foams (Web3.3).



Figure 3-4 Metal foams



Figure 3-5 Metal wools

Metal wools are another type of porous metal mainly made from copper, aluminium and steel. The porosities are various based on the metal fibre length, fibre diameter, and the density, in the range of 30% to 70% (E.J. Minaya, 2004). It's found that the porosity of one kind of copper wools was 0.95 and the thermal conductivity of the copper reduced to 1.0~2.7W/mK (C. Lacroix. et al, 1999). J. P. Mass et al (2006) pointed out that the porosity reduced with the pore size decreasing and presented that when the pore size is 0.1~59 μ m, the average fibre volume fraction is approximate 2%. One kind of metal wool membrane could meet the porosity and pores size demand but its thickness induces high resistance to the heat/mass transfer. Hence, this is a challenge to develop a thin metal wool membrane with high porosity and proper pore size in the future. Figure 3-5 presents the configuration of the commonly available metal wools (Web3.4).

Analyses results indicate that all types of metal have high thermal conductivity to carry on heat transfer and also have enough porosity to obtain enough moisture. However, the pore size of metal wick, metal foam and metal wool can't meet the requirement of the porous membranes.

In terms of hardness, both copper and aluminium are suitable for use as the exchanger plate, as they got adequate Young's Modulus ranging from 70 to 140GPa which is suitable for shaping and shape-remaining (M.Piggott,2002 and Pelletier H,2006). Both copper and aluminium have

long time durability in any shape of wick, foam and metal. In term of cost, aluminium is a better choice over the copper, as it is much cheaper compared to copper. And based on the manufacture cost of micro-holes in the wick, the metal wool and foam are favourable than wick.

3.4.2 Fibre Type

It has been found that fibre materials, including paperboard, cloth, wood or glass fibre, natural fibre, all have relatively high hydrophile and lower thermal conductivity and hardness. It is found that the fibres have much lower thermal conductivity than metals, ranging from 0.01 to 0.3W/mK (X. Zhao, et al, 2008 and James R. Gaier, et al, 2003). Figure 3-6 shows the structures of soft and hardwood fibre, and Table 3.3 presents the porosities, pores size and membrane thicknesses of various fibre materials (Chang Seok Ki, et al, 2007; Kiyoshi Itatani, ET AL, 2006; Li-Wu Fan, et al, 2006; Thomas Schuman, et al, 2005; Mitsuhiro Murayama, et al. 2005; James R. Gaier, et al, 2003; Yun M. Chung, ET AL, 2003; N. C. Gallego and D. D. Edie, 2001)

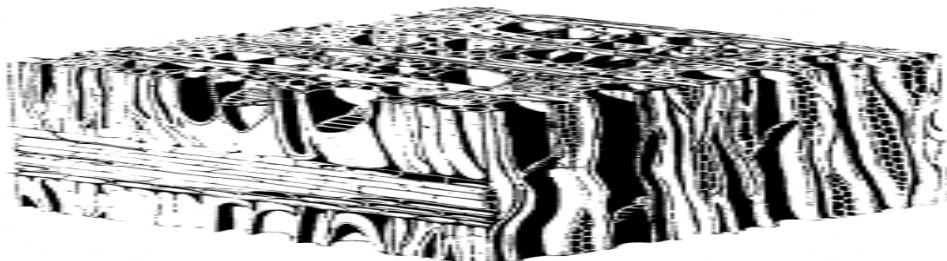


Figure 3-6 Fibre structure of hardwood

It is seen from Table 3.3 that woven fibre, natural random fibre and carbons fibre have the abundant level of porosity which ranges from 10% to 95%; the pore size of the various fibres change from 1.37Å to 5µm, which is in the range of the required membranes pore value; and most of the membranes made of fibre are thin enough to carry the heat/mass transfer with less resistance. The natural fibre general has a fibre diameter from 0.1 to 205µm with a micro lumen (less than 5µm) and fibrillar angle (<20°), this character allow the fibre materials has strong absorption ability (M. Idicula, el al, 2006) and C. J. Tsenoglou (2006)

experimented that the clean fibre had the water penetration value of $5.35 \times 10^{-12} \text{m}^2/\text{s}$ under normal temperature and could be improved by coated by hydrophilic materials.

Table 3.3 Porosities, pores size and membranes thicknesses of various fibres

Fibres	<i>Pore size</i> <i>($\times 10^{-6} \text{m}$)</i>	<i>Porosity</i>	<i>Membrane thickness</i> <i>(mm)</i>
Woven fibre	0.3~2.5	>50%	0.86
Randomly oriented ultra-fine fiber	0.2~0.4	52~83%	0.15~0.3
Carbons fibres	> 0.000137	0~95%	1.6
Hardwood fibre	2~5	63~71%	<15
Si-Al-C fibres	0.1	>10%	0.394~0.706
Porous paper	0.05~0.1	<90%	$0.2 \sim 2.0 \times 10^{-3}$
Pigment-filled polymer coated paperboard	0.08~0.14	>70%	0.3
Paper board	0.01~0.06	30~95%	0.012~0.5
Natural fibre (Banana, Pineapple, Sisal, etc.)	0.1~5	<50%	0.015~0.5

The effective thermal conductivity of a fibrous material increases with the fibre length and it approaches a stable level when the fibre length is sufficiently long. The effective thermal conductivity decreases with porosity increasing (Moran Wang, et al, 2006). Although thermal conductivities of the fibres are lower than that of metals, porosities of most fibres listed in Table 3.3 are enough to absorb moisture from the humid air, and the pores size of fibre are bigger than the liquid water molecular diameter $2.75 \times 10^{-10} \text{m}$ and smaller than $3.2 \times 10^{-7} \text{m}$. Hence, the fibers membranes have the ability to achieve the heat/mass transfer synchronously, and avoid the gaseous air penetration across.

In terms of hardness, most fibre materials are not strong enough for use as exchanger plates. However, flax or wooden fibres are the exception and have Yong's Modulus as high as 70 to 110Gpa (Chang Seok Ki, et al, 2007; Thomas Schuman, et al, 2005; Mitsuhiro Murayama, et al. 2005; Yun M. Chung, ET AL, 2003; N. C. Gallego and D. D. Edie, 2001). The life span of the fibre exchanger is short as it is easy to be deformed or damaged when being soaked by water,

except for flax or wooden fibre. In term of cost, the fibres are extremely cheap, and so frequent replacement is affordable that could overcome the disadvantages of short life span.

3.4.3 Ceramics Type

Porous ceramics could be one of the potential materials used for hydrophilic membrane exchanger due to its advanced properties, i.e., high porosity, high thermal conductivity and durability. One way making porous ceramics is mixing ground vermiculite and allophone at heated condition of 600-800°C (K. Okada, et al, 2008). Porous solids, such as extrude monoliths with parallel channels and thin walls, are made of various oxide and non-oxide ceramics, ceramics foams and metal structure, which can perform both moisture and heat exchanging. Figure 3-7 presents the porous ceramics structure made by Fend (Fend T. et al, 2004)



Figure 3-7 Structure overviews of ceramics

The thermal conductivity of the porous ceramics depends upon elements contained, the pore size and distribution, the porosity of the ceramics and the manufacturing processes. Thermal conductivities of the ceramics are higher than that of fibres, but lower than that of metal. It varies from 0.1 to 240W/m.K. Generally the thermal conductivity decreases with the porosity increasing (X. Zhao, et al, 2008 and B.Nait-Ali, et al, 2006). Table 3.4 shows the porosities, pores size and membrane thicknesses of a range of different ceramics (B. Nait-Ali, et al, 2007; M. Iuga, and F. Raether, 2007; Toshihiro Isobe, et al, 2007; Kiyoshi Okada, et al, 2006; Yan Ma, et al, 2006; T. Taguchi, et al, 2005;G. Krauß, et al 2002)

All porosities of the ceramics are sufficient to retain water needed for moisture transfer. Ceramics made of different materials generally constitutes the pore size form 0.005 μm to 38 μm , hence, part of ceramics such as 8-YSZ ceramics, foamed glass ceramics and Zirconia toughened alumina, etc, can meet pore size requirement of the hydrophilic membrane. (B. Nait-Ali, et al, 2007; M. Iuga, and F. Raether, 2007; Toshihiro Isobe, et al, 2007; Kiyoshi Okada, et al, 2006; Yan Ma, et al, 2006; T. Taguchi, et al, 2005;G. Krauß, et al 2002). A ceramics with higher porosity would be perfect, as it has higher moisture contain and infiltration capacity that would enable moisture infiltration and prevent air across. Water permeability of the ceramics increases with increasing of porosity and pore size. Hence, most ceramics could be shaped in to thin membranes and carry out the heat/mass transfer.

Table 3.4 Porosities, pores size and membranes thicknesses of porous ceramics

Porous ceramics	Pore size ($\times 10^{-6}m$)	Porosity	Membrane thickness (mm)
Zirconia toughened alumina	0.25	60~80%	—
Porous alumina ceramics	8.5 to 38	39~43%	0.5~3
Porous SiC ceramics	0.31~1.39	45.7~49.8%	<3
AlN ceramics	21~38	40	0.2~0.24
8-YSZ ceramics	0.01~0.05	45~75%	0.08
Alumina ceramics	0.5	45~70%	0.08
Foamed glass ceramics	0.005~0.01	37~90%	5
MgO–ZrO₂ ceramic	10~20	37~60%	1~2
SiC/SiC composites	0.7~3.2	<90%	0.03

In terms of hardness, most porous ceramics are suitable as exchanger plate, which has Young's Modulus ranging from 50 to 400 Gpa (Pabst W., et al, 2006; Douglas E.Burkes, et al, 2006; Krauß G., et al, 2002; Hyunjo Jeong and David K.Hsu, 1996). Porous ceramics are durable in use at the wetted condition. In term of the cost, it's more expensive than fibre and metal (Web3.5).

3.4.4 Zeolite Type

Zeolites include natural and synthetic crystalline zeolites. The crystalline zeolites can be used for a wide variety of purposes include static, dynamic drying, iron exchange, selective separations involving gases and liquids. The industrial applications involve primarily “Linde Molecular Sieves” called LMS and Davison “Microtraps” for the obvious reasons of availability in quality and cost. The synthetic zeolites are attractive for drying and separation owing to their affinity for water and other small diameter molecules and also their ability to reject large diameter molecules (Hersh C. K., 1961). The porosities, pores size and membrane thicknesses of kinds of zeolite are listed in Table 3.5 (Mark Johnson, et al, 2006; Honglei Sun, et al, 2006; X. Py, et al, 2002; Robert F.Gould, 1971; Hersh C. K., 1961).

Table 3.5 Porosities, pores size and membranes thicknesses of porous zeolite

<i>Porous zeolite</i>	<i>Pore size ($\times 10^{-6}m$)</i>	<i>Porosity</i>	<i>Membrane thickness (mm)</i>
Zeolite P-C, P-W, P-R	0.0003	1~4%	<0.5
Gram activated zeolite	0.0006~0.001	50%	<0.5
ZSM-3	0.00143	38.1%	<0.5
Natural zeolite	About 0.00044	20~60%	<0.5
LMS-Type 4A	0.00042~0.0011	14%	<0.5
PSZ MEL zeolite	0.002~0.05	20.3~64.8%	<0.5
Molecular sieve filled vinyl alcohol	0.00053~0.001	20~80%	0.08
Sodium ion zeolite	0.000098	<50%	<0.5

The thermal conductivity of Linde molecular sieves is around 0.59 W/m· K, which is much smaller than that of metals and porous ceramics (Hersh C. K., 1961). However, the value is similar to the thermal conductivity of fibre.

Linde Molecular Sieves (LMS) have a high sorption capacity at low water vapour concentrations, and maintain the high sorption capacity at fixed relative humidity, which is a direct contrast to silica gel and activated alumina (Jeong J. and Mumma S. A., 2005). LMS has porosity of 4% to 80%, and its absorption capacity is even higher due to its characteristics of water affinity. LMS as the popular molecules sieving and separation materials, it has pore

diameter as low as 1×10^{-10} m (C.K.Hersh. 1961). And the zeolite membrane is easy to be manufactured into thin films as shown in table 3.5. Hence it has the ability to service as the thin heat/mass recovery membranes with the proper pore size ($2.75 \times 10^{-10} \text{ m} < d_{pore} < 3.2 \times 10^{-7} \text{ m}$) and high absorption capacity.

In terms of hardness, most zeolites are adequately strong for use as exchanger plates, which have Young's Modulus ranging from 1 to 20Gpa (J. Lin, et al, 2005; D. Metin, et al, 2004,). The durability of zeolites is decided by the composites. In term of the cost, they have similar prices as the ceramics.

3.4.5 Carbon Type

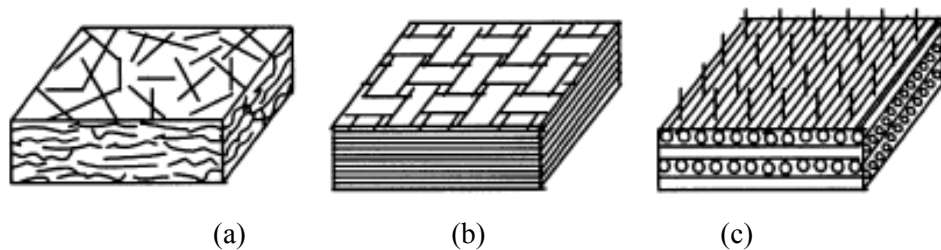


Figure 3-8 Performs structure of three kinds of carbon fibre: (a) laminated short fibre felt (b) laminated carbon cloth felt (c) needle picked long fibre felt

Carbon fibres have become an important reinforcement material in composite materials because of its low density, high strength (up to 7 GPa) and tensile modulus up to 600 GPa. In addition, high electrical and thermal conductivity of carbon fibre makes it useful in a wide variety of products (A. Hoque. et al, 2001). Such as activated carbons are often used for desiccant, Carbon-carbon composites are used mostly in aerospace, Mesophase pitch-based carbon fibers with high preferred orientation have low density and high thermal conductivity (TC), with a TC at room temperature up to 1120 W /m K, etc,(Zhaokun Ma, et al,2006 and Zhenyi Liu, et al, 2005). Table 3.6 presents the porosities, pores size and membrane thicknesses of porous carbons and its composite (Ramasamy Sivakumar,, ET AL, 2007; Zhaokun Ma, et al,2006; X.L. Wang, et al, 2006; Tae Jin Kang , et al, 2006; A.G. Straatman , 2006; Zhenyi Liu., et al, 2005;

Yanxiang Wang , et al, 2004; X.Py, et al, 2002). Figure 3-8 shows three types of carbon fibre structure (Manocha L. M., et al, 2006; Ma Z., et al, 2006; Liu Z., et al, 2005).

AC-ENG composite, acetylene black carbon, porous carbon (SiC) and carbon foam have high porosities to contain the condensed moisture from the humid air size. Besides carbon foam, all the carbons and its composites listed in Table 3.6 can offer the proper pore size in the range of $2.75 \times 10^{-10} \text{ m} < d_{pore} < 3.2 \times 10^{-7} \text{ m}$. Pore diameter between carbon fibres can be as small as $6 \times 10^{-9} \text{ m}$, which can offer the moisture transfer and prevent air penetration (N.A. Eltekova, et al, 2000; Y.Wang, et al, 2004 and Z Ma, et al, 2006). Considering the membranes thickness as well as porosity and pore size, the AC-ENG composite, CM-260, acetylene black carbon all can carry as the hydrophilic heat/mass transfer membranes.

Table 3.6 Porosities, pores size and membranes thicknesses of porous carbons

Porous carbons	Pore size ($\times 10^{-6} \text{ m}$)	Porosity	Membrane thickness (mm)
C-C/Al composites.	0.1~4	31.4~33.8%	3
CM-260	0.02~5	2~30%	0.0057
spun hybrid carbon composites	0.1~5	<40.7%	5
AC-ENG composite	0.0006~0.0026	80%	<0.5
Carbon nanotube/silica	0.018~0.02	10~45%	<1
Acetylene Black carbon	0.001	70%	<0.1
Carbon foam	310~643	67~89%	<1
Porous carbon (SiC)	0.03~2.58	35~67%	3

Carbons materials have stronger capillary force than metals and better thermal conductivity than fibres, which are enough for the heat/mass heat transfer between two airstreams. A carbon material with high porosity and adequacy thermal conductivity is a preferable for the heat/mass transfer purpose.

In terms of hardness, carbon fibres are strong enough for making heat/mass transfer element, which have Young's Modulus ranging from 1 to 220 Gpa (Metin D., et al, 2004).it's cheaper than metal, ceramic and zeolite but more expensive than cellulose fibre.

3.5 Comparison of the Material Types and Results Discussion

Table 3.7 summaries level of performance of the above mentioned materials, in terms of thermal conductivity, porosity, pore size, hardness, durability and cost.

Table 3.7 Properties summaries of the selected material types

Materials	Thermal conductivity (W/m K)	Porosity (%)	Pore size (μm) (approximate)	Hardness (shaping ability)	Durability	Cost (£)*
Metal	High	20-90	$15\sim 3\times 10^3$	High	Long time	30 to 100
Fibre	Low	1 - 60	$1.3\times 10^{-4}\sim 5$	Low	Short time	< 5
Ceramic	Variable	1 - 80	$5\times 10^{-3}\sim 38$	High	Long time	150 to 250
Zeolite	Low	40 - 80	$9.5\times 10^{-5}\sim 5\times 10^{-2}$	Medium	Medium	150 to 250
Carbon	Variable	Variable	$6\times 10^{-4}\sim 643$	Medium	Medium	30 to 80

Cost per sheet 100 x 100 x 0.5 (mm x mm x mm)

From the Table 3.7, the analyses are listed in the followings:

- Metal has high thermal conductivity and porosity however it's very difficult to prevent the air penetration when moisture is transferring through the thin membranes. So it is not the suitable material for heat/mass transfer membranes.
- Fibre can carry on heat/mass transfer synchronously without air penetration. However its thermal conductivity is very low, which is proved affecting the sensible recovery slight. And it is the cheapest materials and can be shaped and installed conveniently, these peculiarities can cover the shortage of less durability.
- Ceramic and Zeolite are the perfect materials as the heat/mass transfer membranes with a proper pore size and high absorption. However, they are all harder and more expensive than the fibre membranes.

- Carbon is the best selection to product heat/mass recovery membranes, which can offer heat/mass transfer and be easily shaped into different structures at a moderate price. However, its price is still 16 times higher than the fibre membrane per unit.

From the analyses it can be concluded that carbon membranes and cellulose fibre both can carry on heat/mass transfer synchronously. Although a carbon membrane is superior to fibre membrane in the hardness, fibre cellulose is 16 times cheaper than carbon membranes. This allows the reshaped/damaged fibre membrane to be replaced frequently. Hence, based on the economical reasons, fibre materials are selected as the investigation materials in this project.

3.6 Summary

Five major porous materials named metal, fibre, zeolite, ceramic or carbon are introduced in this chapter. Each type has its own favourite configuration when being used as the heat/mass transfer medium.

Since conductive heat transfer imposes very little impact on the sensible heat transfer comparing with convective heat transfer, the thermal conductivity of materials is an ignorable parameter in material selection. Porosity and pore diameter are the most two important parameters to judge the feasibility of heat/mass transfer. Higher porosity has strong capillary to absorb moisture from the humid air and proper pore size in the range of $2.75 \times 10^{-10} \text{m} < d_{pore} < 3.2 \times 10^{-7} \text{m}$ can allow moisture across and prevent air penetrating.

Considering the porosity and pore diameter, fibres, ceramics, zeolites and carbons all can meet the heat/mass transfer demand. However, because the ceamics and zeolite are two hard to be shaped as well as expensive, they are not preferred for the heat/mass recovery membranes. Carbon and fibres are the preferred materials with the moderate pore size, porosity. Fibre takes the predominant place owing to its low price. Owing to the economical view, fibre is more superior in saving testing consumption and application extending of the investigated product.

Chapter 4. Performance Investigations of Fibre Heat/Mass Exchanger

4.1 Introduction

As indicated in Chapter 3, fibre cellulose is the optimal material for heat/mass transfer. It is cheap and carries out the heat/mass transfer with a high capillary. Theoretical analyses have proved that the clean fibre paper exchanger membrane (FPEM) had low mass transfer efficiency due to its low moisture diffusion coefficient. Solid desiccant-coated fibre membrane and liquid desiccant-soaked desiccant have a higher mass transfer efficiency. Solid desiccant coated on the FPEM could improve the fibre adsorption capacity, but couldn't increase the moisture diffusion coefficient, but liquid desiccant soaked into FPEM could enhance both the fibre adsorption capacity and moisture diffusion owing to the changed transfer mechanisms.

Numerical simulations were carried out based on the basic heat/mass transfer mechanisms of clean fibre membranes, and results indicated that the heat/mass recovery was low. Comparing the performances of solid desiccant-coated and liquid desiccant-soaked FPEM, it was clear that the latter performed more effectively. Afterwards the heat/mass transfer coefficients used in clean fibre modelling were corrected according to the experimental results of liquid desiccant soaked FPEM and the correction coefficients were employed in the exchanger numerical simulation in order to investigate the relationship between the air parameters, and exchanger structure and size with the exchanger performance. The difference between the numerical simulation and experimental results was in an acceptable range, hence, the correction heat/mass transfer coefficients used in numerical simulation were proved to be correct.

4.2 Theoretical Analyses of Cellulose Fibre Membranes

4.2.1 Description of the Selected Heat/Mass Transfer Membranes

Three types of fibre heat/mass transfer membranes (FPEM) were investigated namely clean fibre membrane (FPEM), solid desiccant-coated fibre paper membrane, and liquid desiccant-

soaked fibre paper membrane (FPEM) as shown in Figure4-1 (a), (b) and (c) respectively. It is assumed that the fresh air is humid /hot, and the exhaust air is dry /cold in Figure 4-1.

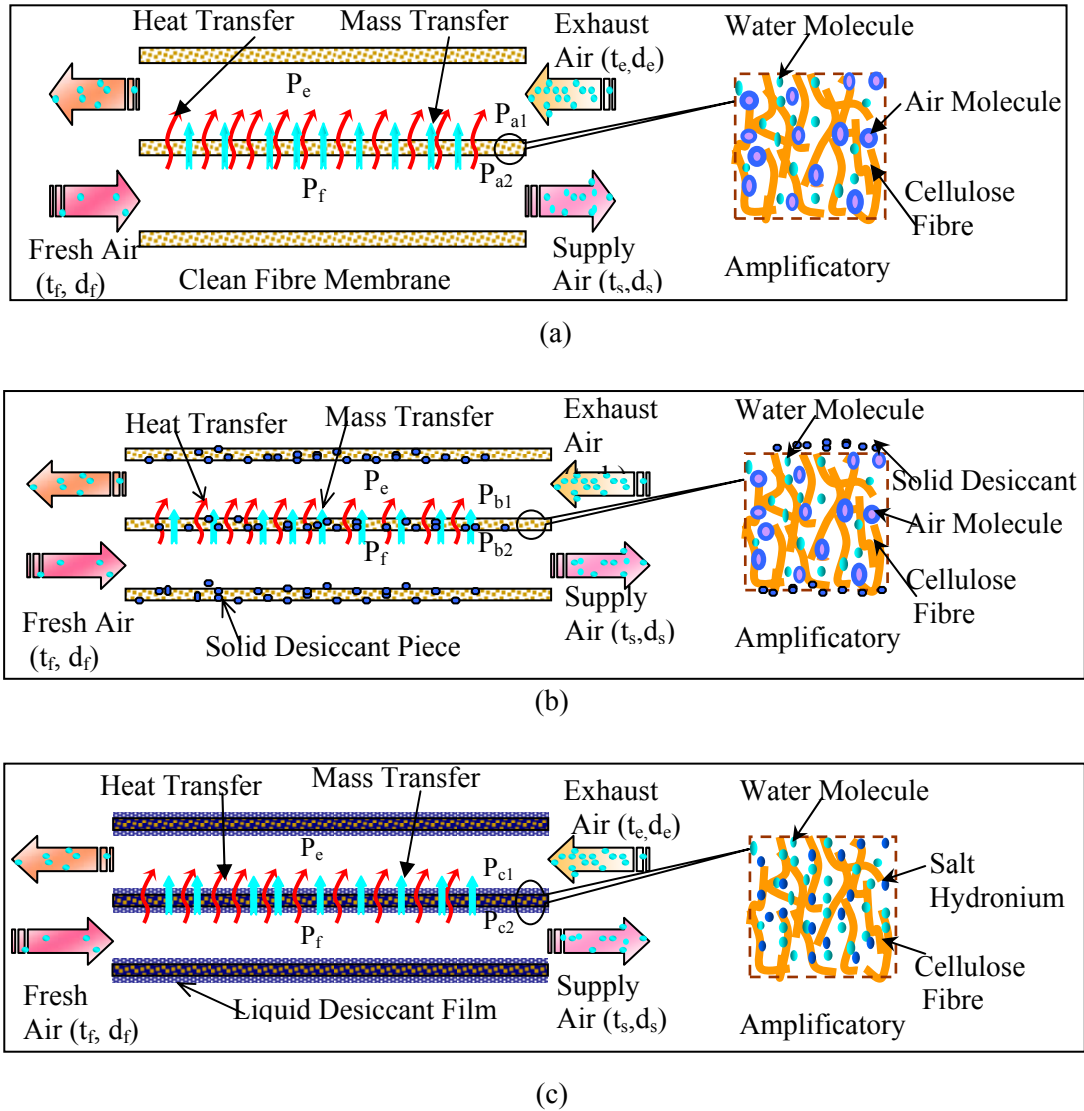


Figure 4-1 Schematic diagram of three types of cellulose fibre membranes: (a) Clean fibre membrane (b) Solid desiccant-coated fibre membrane (c) Liquid desiccant-soaking fibre membrane

Clean Fibre Membrane

Thousands of long fibre cellulose is structured into the normal fibre membrane (FPEM), where the voids between the fibres afford the feasibility of heat/mass transfer, as presented in Figure4-1 (a). A large quantity of long cellulose fibre is squeezed into a 0.1~0.5mm thickness membranes, which produces a strong moisture affinity and penetration capacity, owing to the

hydrophilic characteristic of long fibre. The temperature difference between fresh and exhaust air induces sensible heat transfer. Vapour pressure P_{a2} at the wet and cold side surface of the membranes is higher than P_{a1} at the hot and dry side, and this leads to the moisture moving from the humid side to the dry side. In the humid air side channel, with the condensed moisture on the membrane surface diffusing to the dry channel, the surface vapour pressure P_{a1} is lower than the bulk vapour pressure P_f of fresh air, this result in more moisture condensed on the membranes' surface. In the dry air channel, with the moisture infiltrating through the fibre membranes, the deposited moisture leads the surface vapour pressure P_{a1} being higher than P_e , resulting in moisture evaporating into the dry exhaust air.

Solid Desiccant Coated Fibre Membranes

As presented in Figure 4-1(b), both sides of the cellulose fibre membrane surface are coated with desiccant powder (CaCl_2 particulates), which help to enhance its absorption/desorption capability. Sensible heat transfer mechanism through the CaCl_2 coated fibre membrane is same as the clean FPEM, but the mass transfer is different. The strong CaCl_2 on the fibre membrane surface increases the hydrophilic of the fibre and enlarges the vapour pressure difference between the membrane surface and the humid air channel. Moisture is adsorbed from the humid air and deposited on the membrane's surface, then crosses to the dry side and adsorbed by the solid CaCl_2 particulates. In the dry side, CaCl_2 particulate absorbs moisture moving over, and when it approaches to the saturation it releases moisture into the dry air.

Liquid Desiccant Soaked Fibre Membrane

In Figure4-1 (c) the cellulose fibre membrane is filled with liquid desiccant (LiCl solution), which changes the fibre membrane into a solution film. Vapour pressure P_f of humid air is higher than the vapour pressure P_{c2} of the desiccant solution, and moisture is absorbed. During the process, the moisture from humid air is condensed into the solution film, the Li^+ , Cl^- ions

moves to the humid air channel and H₂O moves contrarily. Therefore, the moisture is brought to the dry air side and evaporated out with the exhaust dry air.

4.2.2 Heat/mass Transfer Mechanisms

The heat exchange process through the cellulose fibre membranes is described in Chapter 3, in which the equations from 3-1 to 3-7 express the transfer mechanisms (the heat/mass transfer in the laminar flow layer has been proved in chapter 3).

It is the same with sensible heat transfer the mass transfer mechanism has been presented in chapter 3 by equations 3-8 to 3-12. Liquid -Mass diffusivity efficiency is expressed by Stokes-Einstein equation as follows (J. R. Welty et al, 2000):

$$k'_{mass} = \frac{\kappa T}{600 \pi r \mu} \quad (4-1)$$

For this case, the hindered solution (moisture) diffusion in solvent-filled pores (liquid desiccant filled fibre pore) is expressed by the following equation:

$$k_{mass} = k'_{mass} F_1(\xi) F_2(\xi) \quad (4-2)$$

$$\xi = \frac{d_{solute}}{d_{pore}} = \frac{solute \quad molecular \quad diameter}{pore \quad diameter} \quad (4-3)$$

$$F_1(\xi) = \frac{\pi (d_{pore} - d_{solute})^2}{\pi d_{pore}^2} = (1 - \xi)^2 \quad (4-4)$$

The correction factor $F_2(\xi)$, the hydrodynamic hindrance factor, is based on complicated hydrodynamic calculations involving the hindered Brownian motion of the solute within the solvent-filled pore. The most common equation, developed by Renkin is reasonable for the $0 \leq \xi \leq 0.6$ (J. R. Welty et al, 2000). Combined with the pore size range analyzed in Chapter 3, the optimal pore size of the fibre heat/mass membrane is $4.5 \times 10^{-8} \text{ m} \leq d_{pore} < 3.2 \times 10^{-7} \text{ m}$

$$F_2(\xi) = 1 - 2.104 \xi + 2.09 \xi^3 - 0.95 \xi^5 \quad (4-5)$$

4.2.3 Analyses of Heat/Mass Transfer

Analyses in section 3.2.1 indicate that thermal conductivity slightly affects the sensible heat recovery. Therefore, convective heat transfer efficiency determines the sensible heat recovery and also relates to the air stream parameters as well as the exchanger structure and size. Hence, the sensible heat recovery of three types of membranes is similar.

It can be known from equation 3-8 in chapter 3 that the mass transfer is impacted by three parts: fresh and exhaust air side convective mass transfer efficiency k_f^l and k_e^l respectively, and mass diffusion efficiency k_{mass} . The first two are fixed to the same air stream parameters and exchanger structure and size. The mass diffusion efficiency k_{mass} is related to the fibre membranes' characteristics.

When the membrane thickness δ is 0.5mm, and the water diffusion efficiency across the clean fibre is $5.35 \times 10^{-12} \text{m}^2/\text{s}$ (Christos J. Tsenoglou, et al, 2006), the water diffusion resistance

$\frac{\delta}{k_{mass}}$ value is $9.3 \times 10^7 \text{s}/\text{m}^2$, which is 2.8×10^5 times the convective mass transfer resistance

$\frac{1}{k_f^l} + \frac{1}{k_e^l}$ (values are gained from Table3.1). Therefore, the water diffusion across the fibre

membranes plays the leading role of latent heat transfer.

Clean Fibre Membrane

Heat transfers through the three types of fibre membranes are similar to each other, so the mass transfers are mainly investigated. Because of the strong hydrophilic of cellulose fibre, the vapour pressure at the fibre membrane surface is a bit lower than that of the humid air, and a small quantity of moisture is adsorbed and transferred to the dry air side. As we know, capillary force induces the moisture transfer through the fibre pores, but it is hedged by the air molecules.

As shown in the amplificatory diagram in Figure 4-1 (a), during the moisture diffusion across the voids of the fibres, it is hindered by the air molecules which have the same molecule diameters as the H₂O molecules, but a bigger free path length (9×10^{-6} m). As mentioned in Chapter 3, the fibre pore size is in the range of $4.5 \times 10^{-8} \text{m} \leq d_{\text{pore}} < 3.2 \times 10^{-7} \text{m}$ to allow H₂O molecules across and to prevent air molecules penetration, but still a few number of air molecules enter into the fibres' interspaces, and move irregularly inside the pore and block the path. Hence, the moisture diffusion efficiency across fibre membranes is very small and needs to be improved.

Solid Desiccant-Coated Fibre Membrane

Solid CaCl₂ attached onto the fibre membrane enhances the adsorption ability of the fibre and congregates more moisture to diffuse through the fibre membranes as shown in Figure 4-1 (b). However, it can't reduce the diffusion resistance of the fibre membranes, and the voids of the fibres air are still permeated with air particulates, as presented in the amplificatory diagram. Hence, coated solid desiccant only enlarges the vapour pressure difference $\Delta P = P_{b2} - P_{b1}$, and increases the water diffusion speed by some degree but can't change the transfer mechanism. With the moisture condensing on the membranes' surface of the humid air side, latent heat is released to the cold air stream, in the same way evaporation heat is adsorbed from the hot stream when the moisture evaporates into the dry air stream. Therefore, more sensible heat is transferred through this kind membrane than clean fibre membrane when the mass transfer is improved by some degree.

Liquid Desiccant-Soaked Fibre Membrane

When the fibres voids are filled with liquid desiccant solution (LiCl solution), the mass transfer process is different from the first two types of fibre membranes. Firstly, the absorption ability of fibre membranes is improved by the hydrophilic solution, and secondly the mass transfer

process is different from the first two fibre membranes. Concentration differences of the electrolyte solution induce the moisture transfer, and not the capillary force of the fibre membrane's tiny pore. And in the Figure 4-1 (c) amplificatory diagram, it is obvious that the voids of the fibres are filled with Li^+ , Cl^- ions, H_2O molecules and their hydrate. Li^+ , Cl^- ions have diameters of about 2×10^{-10} m, which is equal to the H_2O molecules, and 1000 times smaller than the air molecule and its free path (D. P. Chen, et al, 1999). Hence, the hindrance of Li^+ , Cl^- ions to the moving of H_2O molecules is smaller than the air molecules, and in addition, the Li^+ , Cl^- ions hydrate strengthen the H_2O molecules movement. Therefore, the moisture transfer in the LiCl solution filled fibre membrane is improved greatly, and the sensible heat transfer is also incidentally enhanced.

4.3 Numerical Simulation of Cellulose Fibre Membrane

From the previous analyses, the heat and mass transfers through the liquid desiccant filled membranes should be greatly improved by the desiccant film. However, the increased percentage of the recovery effectiveness is undefined. Numerical simulation and experiments were carried out to confirm the values of heat and mass transfer efficiency of the solid desiccant coated FPEM and liquid desiccant soaked FPEM.

4.3.1 Description of the Fibre Exchanger Configuration

Three types of fibre membranes are all constructed into the configuration as shown in Figure 4-2. For the clean fibre membrane and solid desiccant coated one, the sprayer is closed, and for the hydrochloric solution, the sprayer is working, and controlled by the supplying pump. So the designed feasible exchanger core includes three parts: porous cellulose fibre membrane, waveform stand, and a liquid desiccant supply system as shown in Figure 4-2.

Waveform stand is strong enough to support two sides of cellulose fibre membranes and overcomes the short durability of fibre paper, which is described in Chapter 3. Two fibre paper

membranes and one Waveform stand constitutes an air passage, which is divided into a large number of small channels by the stand synchronously. To compare the performance of FPEM filled with liquid desiccant with the clean and solid desiccant coated FPEM a liquid desiccant supplying system is employed in this heat/mass exchanger stack to offer adequate soaking solution. To avoid the collection tank blocking the air flow, the desiccant tank is designed as small as possible, and to spray liquid desiccant effectively and collect it by gravitation, as well as reducing the blockage caused by the pipes, sprayers, and tank, to the air channel, the fibre paper stack is designed into an octahedron with two hexagon surface as shown in Figure 4-2.

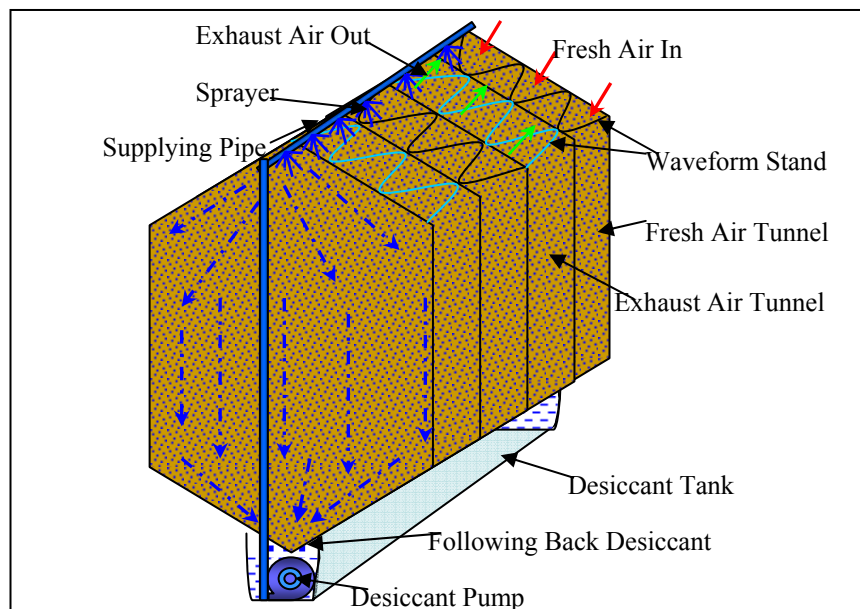


Figure 4-2 Schematic diagram of cellulose fibre stack exchanger

Liquid desiccant is pumped from the collecting tank at the bottom of the stack to the top point of the fibre paper core, and then fills into the voids of the paper by fibre strong absorption ability. Over-flow liquid desiccant follows down by gravitation and is collected by the tank. The main task of the salt solution is to enhance the energy recovery efficiency, and not to dehumidify the fresh and exhaust air, so the desiccant is only sprayed intermittently to keep the cellulose fibre membranes wet. Fresh air flows down along the channel carrying heat/mass exchanger with the counter flowing exhaust air. Moisture absorbed by the liquid desiccant from

the humid air side is transferred to the dry side and evaporated by the dry airflow. In this process, large numbers of micro-circles of heat/mass transfer occur through the membranes.

Preliminary numerical simulation was carried out to investigate the performance of the clean fibre membranes exchanger based on the basic heat and mass transfer mechanism, which are expressed in equations 3-1 to 3-12 and 4-1 to 4-5, and do not include the mutual effect of the heat and mass transfer.

4.3.2 Grids Distribution and Assumptions

As analyzed in paragraph 4.3.1, the two triangles at the top and bottom of the cellulose fibre membranes mainly practice as desiccant distributor and air passage, and the rectangle part is the main part of the heat/mass exchange stack. So, in the numerical simulation, only this part is considered. Then the grid on the cross section of the rectangle is shown in Figure 4-3. The numbers of fresh and exhaust air layers is 'K', which is determined by the height of each triangle channel H_1 and the height of the cellulose fibre exchanger stack L_3 . The number of the channels constituting each layer is 'm', determined by the width of the fibre paper exchanger L_1 and the side length of the channel triangle.

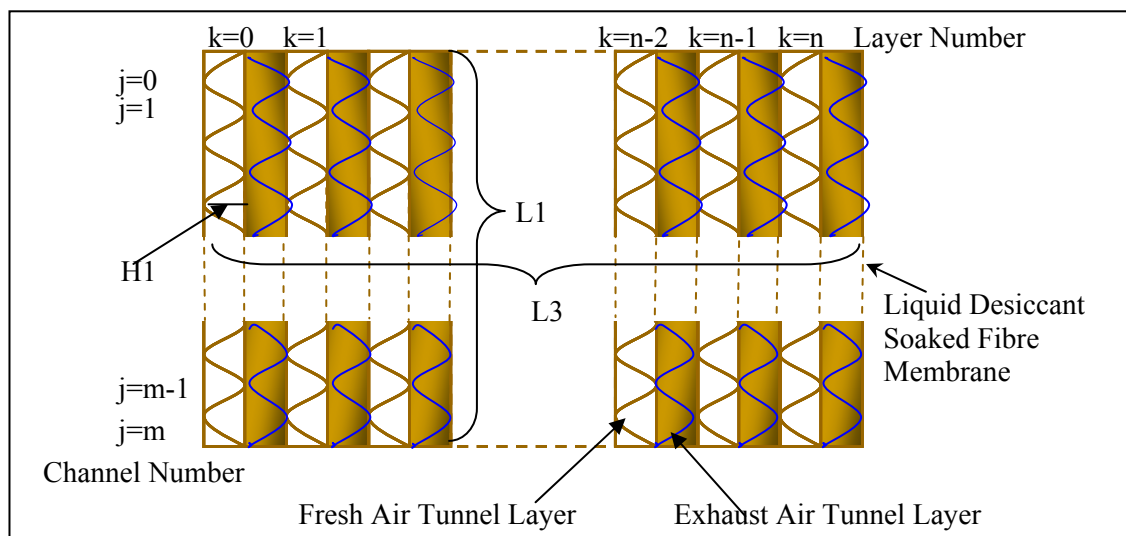


Figure 4-3 Air flow layers and channels

Assumptions made to simplify the numerical simulation are as follows:

- Air flow speed, temperature and moisture content across each fresh/exhaust layer were assumed to be the same.
- Heat/mass transfer occurred vertically through the fibre paper membranes, and there was no heat/mass transfer along the air flowing direction as shown in Figure 4-4.
- Plenty of liquid desiccants were supplied to keep the cellulose fibre membranes wet and no superfluous desiccant was sprayed.
- Latent heat released from the condensation moisture on humid side of the membrane equalled the evaporation heat demanded on the other dry side.
- No heat/mass transfers occurred through the waveform stand.

4.3.3 Heat/Mass Transfer Balance and Efficiencies

Sensible energy balance through the fibre paper membranes in each cell can be written as follows:

$$dq = (t_f - t_{w1}) / \left(\frac{1}{k_f^s}\right) dA = (t_{w1} - t_e) / \left(\frac{1}{k_e^s}\right) dA = (t_{w2} - t_{w1}) / \left(\frac{1}{\delta}\right) dA \quad (4-6)$$

k_f^s , k_e^s can be calculated by the equations from 3-2 to 3-7 in Chapter 3 (it has been proved that the heat/mass transfer occurring in the Laminar Flow layer), and k is determined by the cellulose fibre and liquid desiccant, which can be calculated by equation 3-14.

Mass energy balance through the fibre paper membranes in each cell can be written as follows:

$$dm = (p_f - p_{w1}) / \left(RT \frac{1}{k_f^l}\right) dA = (p_{w2} - p_e) / \left(RT \frac{1}{k_e^l}\right) dA = (p_{w2} - p_{w1}) / \left(RT \frac{1}{\delta}\right) dA \quad (4-7)$$

k_f^l , k_e^l can be calculated by the equations from 3-9 to 3-13 in chapter 3.

Total energy balance in each cell

$$\Delta h_f = \Delta h_e \quad (4-8)$$

The heat, mass and enthalpy (total energy) recovery effectiveness are expressed in the Ref. (ASHRAE, 2004):

$$\varepsilon_{Ex}^{Se} = m_f c_f (t_f - t_s) / C_{\min} (t_f - t_e) \quad (4-9)$$

$$\varepsilon_{Ex}^{la} = m_f (d_f - d_s) / m_{\min} (d_f - d_e) \quad (4-10)$$

$$\varepsilon_{Exc}^{En} = m_f (h_f - h_s) / m_{\min} (h_f - h_e) \quad (4-11)$$

$$C_{\min} = \min\{\rho_f V_f c_f, \rho_e V_e c_e\}$$

$$m_{\min} = \min\{\rho_f V_f, \rho_e V_e\}$$

In this model, the air parameters such as enthalpy h , specific heat c , thermal diffusivity α , and density ρ , dynamical viscosity μ , thermal conductivity k , etc. are all gained from Appendix I.

4.3.4 Calculation Method and Cell Element

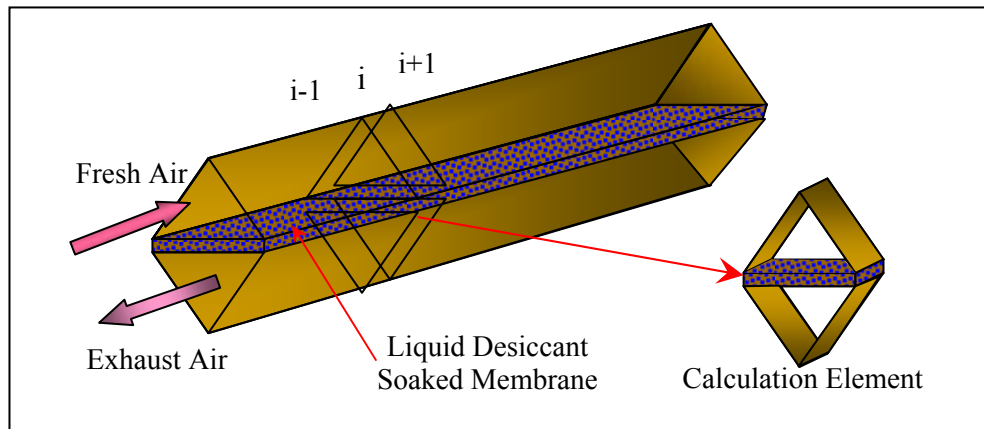


Figure 4-4 Simplified fresh and exhaust air channels and calculation cell

Finite-element approach was applied in this numerical simulation. As shown in Figure 4-4, each element involves a fresh air section, an exhaust air section, and a heat/mass transfer membrane. For calculating the energy and mass balance of each cell, I made the following assumptions: (1) each cell had a uniform membrane surface temperature; (2) in the fresh/exhaust air channel section of each cell, the air had uniform temperature and moisture content; (3) liquid desiccant temperature was the same as the temperature of the cellulose fibre membrane.

Each cell length was selected at 0.01mm and the width was decided by the channel size, which could be varied based on the exchanger requirement. Then there are $n = \frac{L_2}{0.01}$ cells in each channel and $m = \frac{L_1}{0.866H_1}$ channels in each layer. The cell and channel numbers will change when the sizes of channel height and length varying.

4.3.5 Base conditions for Numerical Simulation

The base conditions for carrying out the simulation are listed below:

- The length and height of each channel were 800mm and 6.5mm respectively.
- The thickness of the cellulose fibre was 0.3mm, thermal conductivity of this kind of fibre and LiCl solution were both 0.5W/mK (M. R. Conde, 2004) and moisture infiltration coefficient through fibre membranes was $5.35 \times 10^{-12} \text{m}^2/\text{s}$ (C. J. Tsenoglou, et al, 2006).
- The fresh and exhaust air flow speed was 0.7m/s respectively.
- The fresh air temperature was 35°C and the relative humidity was 70%.
- The exhaust air temperature was 24°C, and the relative humidity was 50%.

The heat, mass and total energy recovery effectiveness were the main topics investigated in this simulation.

4.3.6 Numerical Simulation Results

Figure 4-5 presents the simulation results of the clean fibre membrane exchanger. It is obvious that heat and mass recovery efficiency changes little with the air temperature increasing. The average heat recovery efficiency is about 58.99%, and there is only 0.1% increasing with the temperature rising one degree. The mass recovery efficiency average value is as low as 54.47%. These numerical simulations were carried out based on the basic heat/mass transfer mechanism expressed by equations 3-1 to 3-14 in Chapter 3. The thermal conductivity and mass diffusion coefficient was 0.5W/mK and $5.35 \times 10^{-12} \text{m}^2/\text{s}$ respectively. However, the mass diffusion coefficient of the solid desiccant-coated FPPEM and the liquid desiccant-soaked FPPEM were all

improved, and the increasing percentage values were gained from the experimental results. Additionally, the sensible heat transfer benefited from the mass transfer process and the improved percentages will be concluded from the test results.

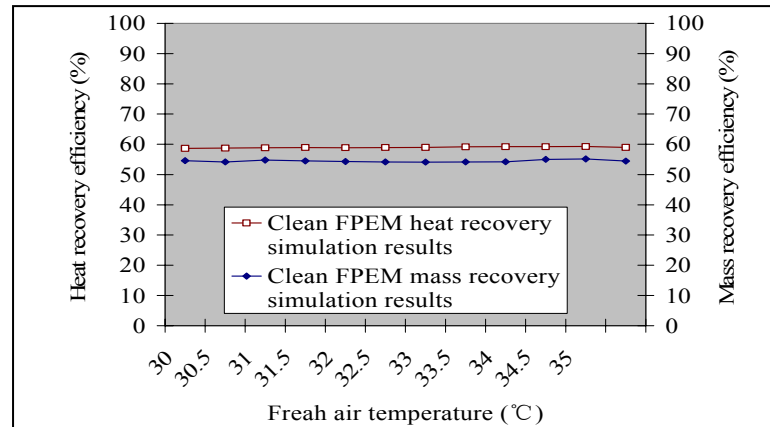


Figure 4-5 Heat/mass recovery efficiency vs. fresh air temperature

4.4 Experimental Testing of the Fiber Membrane Exchanger

4.4.1 Prototype of the Fibre Membrane Exchanger

Figure 4-6 shows the prototype of the solid CaCl_2 particulates coated and LiCl solution filled heat/mass recovery membranes, which were produced into the pre-designed shape as displayed in Figure 4-7 (a).

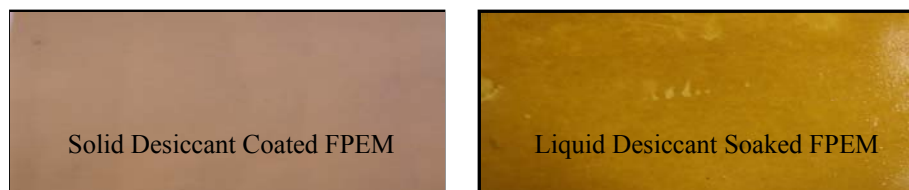


Figure 4-6 Prototypes of solid desiccant coated and liquid desiccant soaked FPEM

The cellulose fibre energy exchanger prototype presented in Figure 4-7 (a) is composed of two exchanger packs. In each pack, there are 50 fresh air layers and 50 exhaust air layers combined together as shown in Figure 4-7 (c). The Waveform stand supports two pieces of fibre paper membranes to divide each air tunnel into a large number of small triangular channels. In each channel, fresh air flows along the channel carrying heat and mass exchange, with the adjoining contrary flowing exhaust air through the cellulose fibre as shown in Figure 4-7 (b). In the layer

of fresh air, the entrance and exit of exhaust air and the vertical sides are all sealed as shown in Figure 4-7 (b). Fresh air has cross-flow heat/mass exchange with the exhaust air first, and then contrary-flow exchange and cross-flow again. In this design, the contrary-flow exchange takes the primary energy exchange task, and that the equilateral triangle parts at the top and bottom of the exchanger mainly act as the air passage, thus the cross-flow exchange was ignored in the numerical simulation.

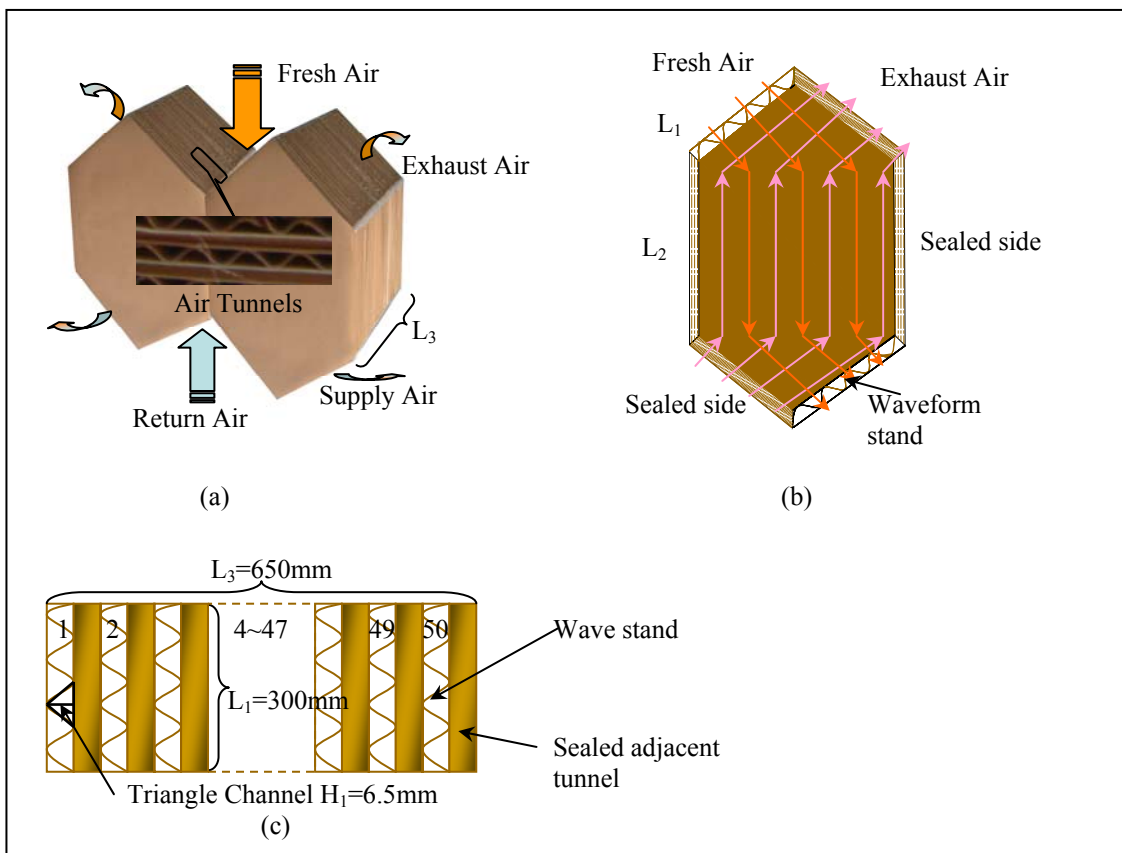


Figure 4-7 (a) Prototype of cellulose fibre exchanger (b) Schematic diagram of one layer of the fresh air tunnel (c) Schematic diagram of C side

In the prototype fibre paper exchanger, the length L_2 of each channel is 500mm, the width L_1 of each layer is 300mm and the height L_3 of each exchanger stack is 650mm. In each small triangular channel, the height of the triangle is 6.5mm, and then each side length of the small equilateral triangle is 7.51mm. The calculated equivalent diameter is 4.33mm. The thickness δ

of the fibre paper membrane is generally about 0.1~0.5mm, in this experiment, the fibre paper membrane thickness is 0.3mm.

4.4.2 Air Environment Control System

The cellulose fibre exchanger test rig was set up in the University of Nottingham, where the temperature in spring is low and unsteady to carry out the experimental testing. To obtain the accurate testing results, and investigate the relationship between the air temperature, humidity, and flow speed, with the energy recovery effectiveness, two air condition control systems were set up in this test rig to obtain the steady and appropriate indoor/outdoor air streams. One was controlled to supply the fresh air with the temperature and relative humidity varying from 29 to 35°C and 30 to 70% respectively. The other was for the return air from indoors, where the air temperature was controlled in at about 24~25°C and the humidity was about 50%.

The schematic diagram of the fresh air control system is shown in Figure 4-8. Environment air is forced in to the electrical heater by the 2kW centrifugal fan, which is controlled by the voltage transfer to vary the airflow speed from 0 to 1000m³/h. Along the process, the forced in air flows through an electrical heater, which is a combination of two 2kW electrical heaters presented in the prototype Figure 4-9. Overheated air progresses into the next humidifier unit, where the high temperature airflow contacts with the wet cellulose fibre membranes to evaporate the moisture. In the humidifier unit, the water is pumped from the water tank to the top of a fibre paper stack, which has strong water absorption ability, and then overflows back to the tank. Voltage transfers are connected with the electrical heaters to alter the air temperature, and a regulating valve is installed in the supplying water pipe to control the feeding water flux, and then control the air humidifying quantity. Thermal insulations were used to prevent heat loss and keep the air temperature steady, as shown in Figure 4-9. Hence, this airflow control system can present a suitable air temperature, humidity, and flow speed, according to the experiments' requirements.

Another return air control system is also designed to product the steady air temperature and humidity from the serving room. Based on the humid and cold environment in the UK, one 2 kW electrical heater and a small humidifier unit are utilized in this control system. The airflow speed control is similar to the fresh air.

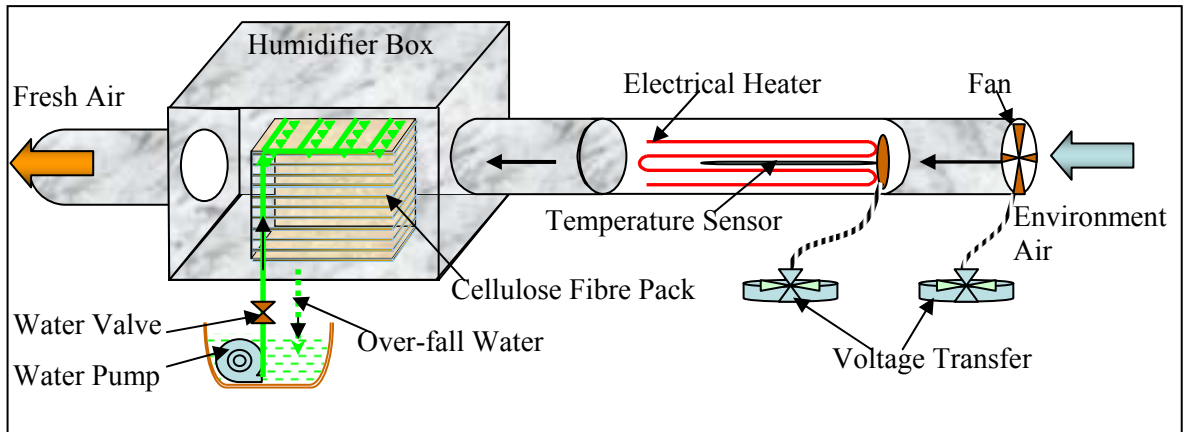


Figure 4-8 Schematic diagram of the airflow control system

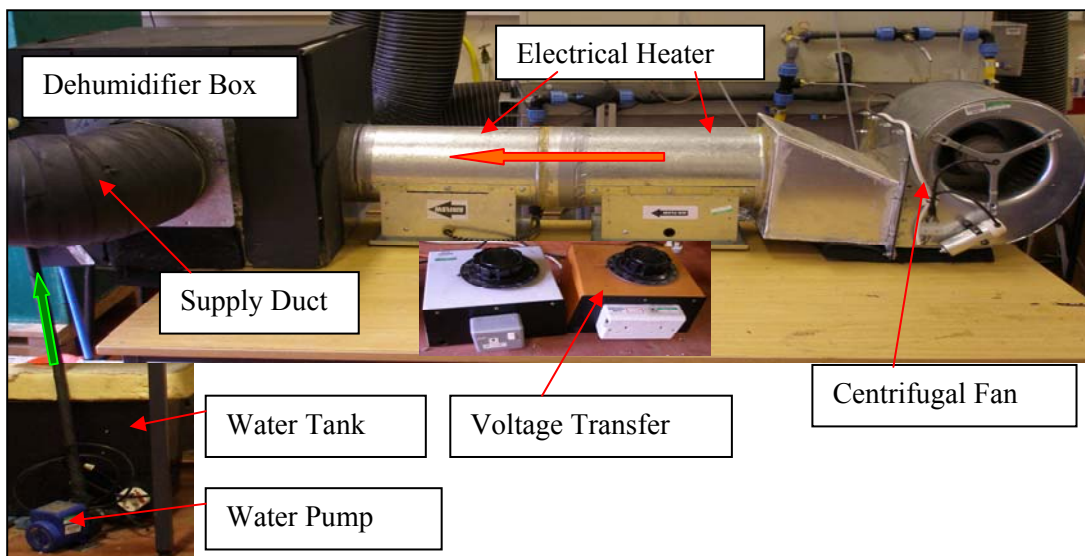


Figure 4-9 Prototype of the airflow control system

4.4.3 Fibre Exchanger Test Rig

A prototype heat/mass transfer test rig was build up in the laboratory at the University of Nottingham as shown in Figure 4-10. The heat/mass transfer unit was sealed by two wooden boxes from the top to the bottom, and the fresh air tunnel and exhaust air tunnel were separated

by interlayer inside boxes. Fresh/return air from the air control systems was supplied to the entrance/exit of the heat/mass transfer unit by black air ducts. Insulations were attached on the boxes' inside surfaces to keep the temperature and humidity uniform and steady. HMP45A-type (Figure 4-11) humidity sensors and T-type (Figure 4-12) thermocouple probes were installed into the fresh air, return air, supplying air and exhaust air tunnels to measure the air temperature and humidity. Each measuring apparatus was connected to a DT500 Data-taker, which acquired data from the measure points, and transferred them to a computer.

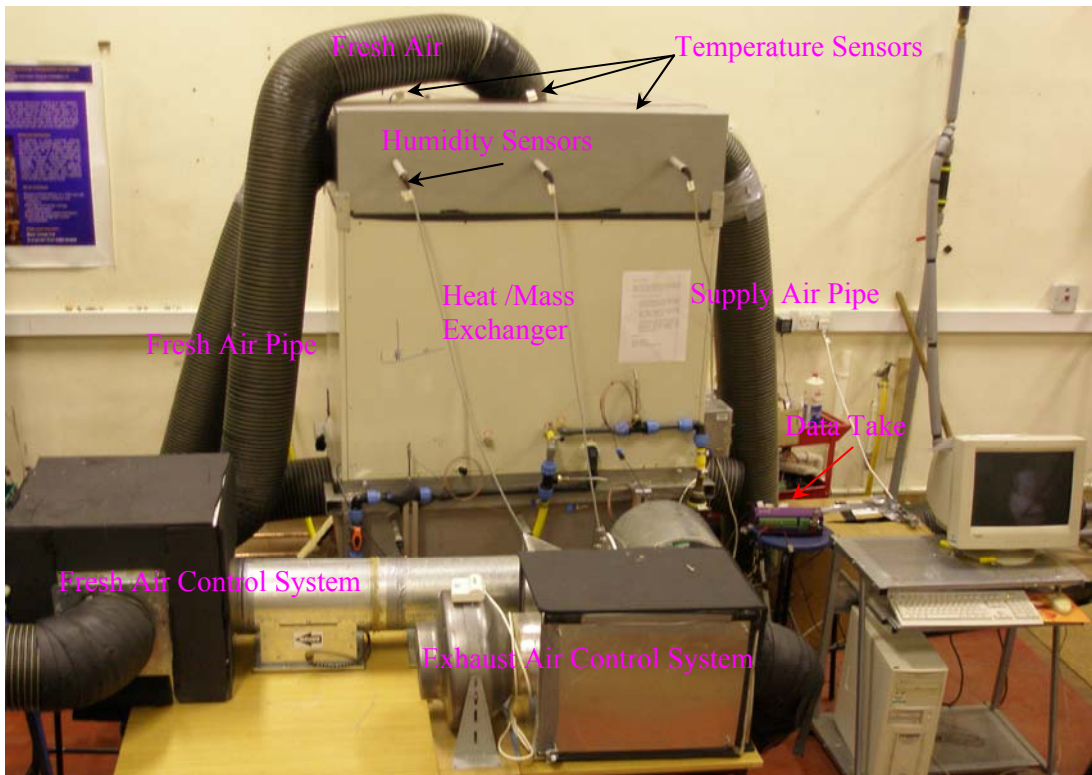


Figure 4-10 Heat/mass exchanger testing rig

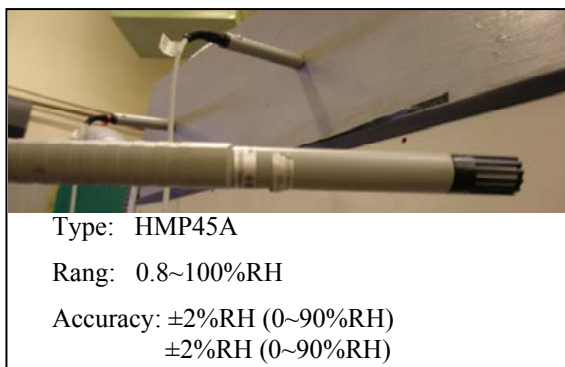


Figure 4-11 Humidity sensors

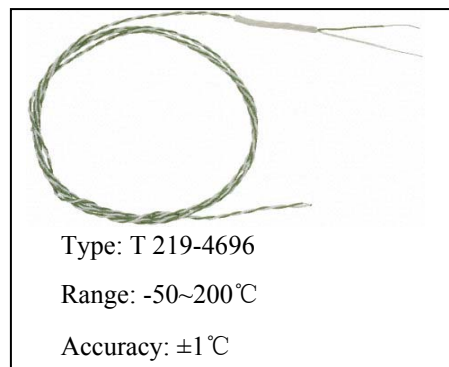


Figure 4-12 Thermocouples

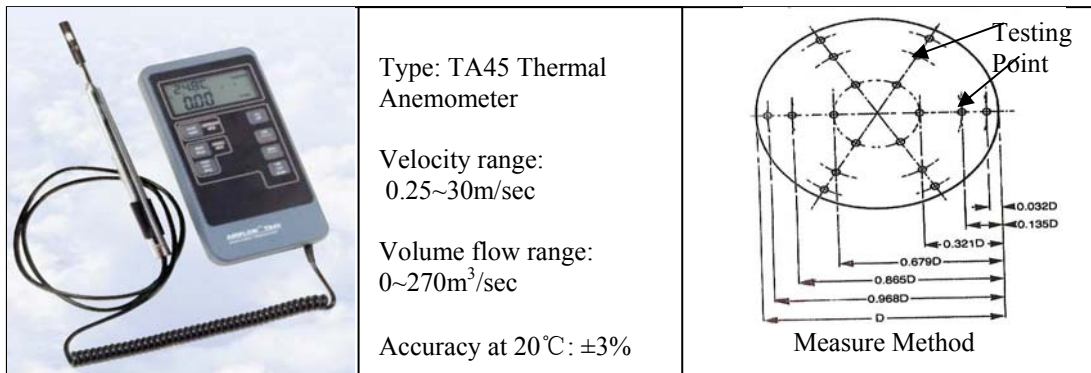


Figure 4-13 TA 45 thermal anemometer and measure method

Figure 4-13 shows the air flow speed measuring equipment—thermal anemometer and its measuring method, which is suitable for testing the air flow speed in duct.

To obtain steady fresh air and exhaust air streams, with the air temperature and relative humidity varying in a small range, took at least 30 minutes to adjust the electrical heater and humidifier in the air control system. After the system remained steady, testing results were recorded and transferred into the computer by the data-taker each minute. The average result values of each testing progress (about 30 minutes) were used into the results analysis. The heat, mass and total energy recovery effectiveness are calculated through the equations 4-9, 4-10 and 4-11 respectively and the testing errors are 6.7 %, 6.24 % and 7.55 % respectively (Law of Error Propagation) (A.A.Clifford, 1973)

4.4.4 Comparison of Solid Desiccant-Coated and Liquid Desiccant-Soaked FPEM

The testing results of CaCl₂ particulates-coated, and LiCl solution-soaked FPEM recovery are shown in Figure 4-14. It can be seen that the heat recovery performance of the CaCl₂ particulates-coated FPEM is only 1.9% lower than the LiCl solution-soaked FPEM, and these two kinds of FPEMS perform a similar changing trend with the fresh air temperature varying. However, the mass transfer of the LiCl solution-soaked FPEM is obviously effective compared to the CaCl₂ particulates-coated FPEM. The efficiency of the former reaches 90.7 %, which is 6.4% higher than the latter. Mass transfer changed little with the fresh air temperature increasing. As analyzed in the section 4.2 that the force driving the moisture transfer through the liquid

desiccant soaked fibre membrane changed from the vapour pressure difference to the concentration difference, which avoided the air molecule blocking and then improved the moisture transfer rate. Synchronously, the enhanced moisture transfer promotes the heat transfer coefficient at some degree. Hence, desiccant soaked fibre paper membranes produce a better heat and mass transfer performance, especially for the humid climate. Therefore, the liquid desiccant soaked fibre membrane is going to be utilized as the heat/mass exchanger membrane in the further numerical and experimental studies in this project.

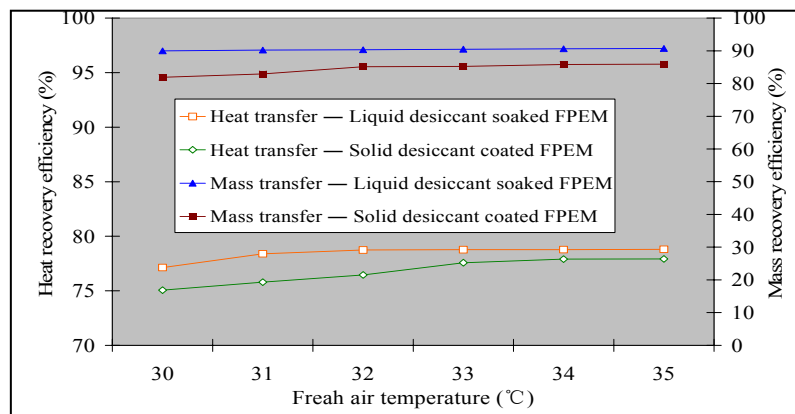


Figure 4-14 Energy recovery performances vs. fresh air temperature

4.4.5 Comparison of Simulation and Experimental Results

As the comparison results of the testing and experimental shown in Figure 4-15, it is obvious that the numerical and experimental results have the same changing trend when the air temperature increases. However, the experimental results of the liquid desiccant-soaked FPEM are better than the modelling. This is because that the simulation is set-up based on the heat and mass transfer mechanism of the clean fibre membrane, in which the vapour pressure difference induces the moisture transfer and is very small. But in the practical tested liquid desiccant-soaked FPEM, concentration difference produces the moisture transfer between the FPEM's two sides. This enhanced the moisture transfer as well as heat transfer.

Hence the liquid desiccant-soaked FPEM has higher heat/mass transfer efficiency, and it was selected as the working membrane in the next experiments and numerical simulations, and its

heat and mass transfer coefficient was corrected by the experimental results based on the basic heat/mass transfer coefficients.

It was proved in Chapter 3 that the thermal conductivity of fibre membrane slightly impact the heat transfer, and the convective heat transfer for three kinds of fibre membranes were similar to each. However, the mass transfer test results of CaCl₂-coated and LiCl-soaked FPEM is about 35% higher than the simulation results. It is caused by the improved mass transfer, which enhances the heat transfer by about 20% during the moisture condensation/evaporation processes.

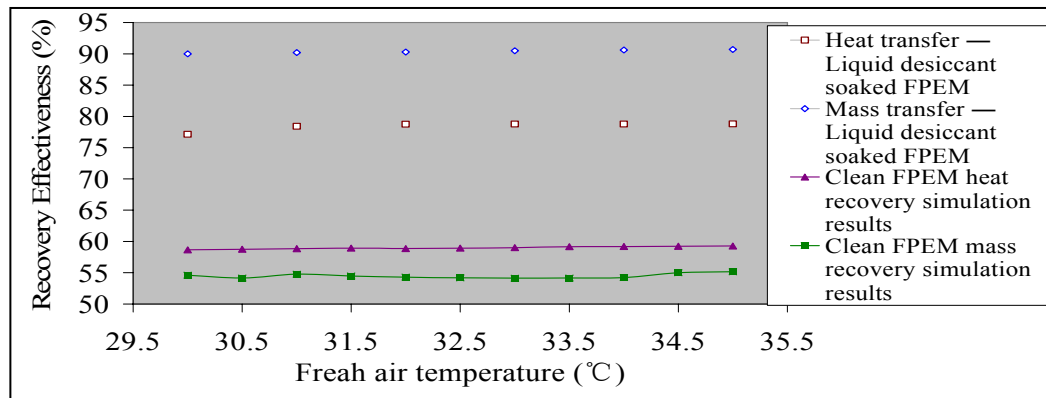


Figure 4-15 Comparison of experimental and simulation results of FPEM recovery

Experimental results of the mass transfer through liquid desiccant-soaked FPEM are about 35% higher than the simulation results. This is because the mass transfer across the LiCl-soaked FPEM is driven by the concentration difference in the solution film, which is different from the capillary force of the clean fibre membranes. This is explained by details in Chapter 3.

From Chapter 3, it is known that heat transfer is determined by the convective heat-transfer efficiency, and mass transfer relies on the moisture diffusion coefficient. Comparing the testing and simulation results, the heat and mass transfer resistances employed in the next numerical modelling are corrected as follows: for the heat transfer, the convective heat-transfer resistance ($\frac{1}{k_f} + \frac{1}{k_e}$) is reduced by 50%, and for the mass transfer, the moisture diffusion coefficient is

improved to $5 \times 10^{-5} \text{ m}^2/\text{s}$.

4.5 Modelling Based on the Corrected Heat/mass Transfer Coefficients

Further numerical simulation was carried out to investigate the optimal size of the counter-flow exchanger and its best operating conditions. These include the geometric size of the airflow channel, the airflow speed, the fresh air to exhaust airflow speed ratio, and the fresh air and exhaust air parameters. The heat, mass, and enthalpy recovery effectiveness, and the supply air temperature and humidity, were estimated by the computer modelling. Except for the heat and mass transfer resistances being replaced by the correction values, the pre-set conditions and calculating methods were kept the same as the original numerical modelling.

4.5.1 Modelling Results

I. Impact of Channel Length on Energy Recovery Effectiveness

Varying the channel length from 0.4 to 2 m, and keeping the other parameters unchanged, simulations were carried out to investigate the effect of the channel length on the heat, mass and total energy recovery effectiveness.

It can be seen that heat, mass and enthalpy recovery effectiveness increase as the channel length increases, and the heat recovery effectiveness is relatively low. Enthalpy recovery effectiveness is a function of heat and mass recovery effectiveness, and its values are more heavily influenced by mass recovery, as shown in Figure 4-16.

Heat, mass and enthalpy recovery effectiveness rise considerably as the channel length increases from 0.1m to 1m, and when the channel length is over 1m, the mass and heat energy recovery effectiveness is as high as 89.59% and 78.09% respectively. The increasing trend of mass and enthalpy recovery effectiveness becomes slower when the channel is longer than 1m, but heat recovery effectiveness still maintains a sharp increase until the channel length over 1.4 m. When the channel length is more than 1.4 m, mass, heat and enthalpy recovery effectiveness reach the highest value and then the increase speed is negligible, with the channel length rising. So the

channel length between 0.8~1m is the optimal length to save space, materials, and energy with high recover effectiveness.

II. Impact of Channel Height on Energy Recovery Effectiveness

Simulations were carried out to investigate the influence of channel height on the energy recovery effectiveness. The heights of the channel varied from 1.5 to 8mm, while keeping other parameters unchanged, i.e. fresh and exhaust air flow speed 0.7m/s, air channel length 1m, and the pre-set fresh/exhaust air condition (fresh air 35°C, 70% & exhaust air 24°C, 50%).

The Figure 4-17 shows that the heat, mass and enthalpy recovery effectiveness decreases with the air channel height increasing. In the channel height range of 1.5 to 6.5mm, the recovery effectiveness decline is slower than that when the height is over 6.5mm. When the channel height is as low as 1.5mm, the mass and heat recovery efficiencies reach 98.71% and 90.9% respectively, leading the enthalpy recovery efficiency to more than 97.01%.

A lower channel height results in higher energy recovery effectiveness, however, the frictional kinetic resistance caused by a lower channel height is aggravated, as the manufacturing difficulty is improved. A channel height of 4.5~6.5mm gives an effective energy recovery , has less frictional kinetic resistance, and is also more conveniently shaped.

III. Impact of Air Temperature on Energy Recovery Effectiveness

Simulations were carried out to research the influence of fresh air temperature on the energy recovery effectiveness by keeping the relative humidity of the fresh air unchanged at 70%, but changing the temperature from 29°C to 37°C, while keeping other parameters unchanged, i.e. 0.7m/s fresh and exhaust airflow, 1m air channel length, and 6.5mm channel height.

Figure 4-18 shows that the air temperature difference slightly affects the heat, mass and enthalpy recovery effectiveness. There is only 1% increase in heat recovery effectiveness per

degree. The mass recovery effectiveness remains at the similar level of 89.58%. The enthalpy recovery effectiveness is the function of the sensible and latent heat recovery effectiveness, which stays at 86.96%.

IV. Impact of Air Flow Speed on Energy Recovery Effectiveness

Simulations were carried out to investigate the effect of the airflow speed on the energy recovery effectiveness, with the pre-set air conditions unchanged, i.e. 1m air channel length and 6.5mm channel height, the pre-set exhaust air 24°C, 50%, and fresh air 35°C, 70%. The fresh and exhaust air flow speeds through each channel were changed from 0.1 to 15m/s synchronously. The simulation results are presented in Figure 4-19.

In figure 4-19, heat, mass and enthalpy recovery effectiveness decrease with the air flow speed increasing. When the air flow speed is 0.1m/s, the heat and mass exchange effectiveness are 89.46 % and 96.67 respectively. The declining trend of the energy recovery effectiveness becomes slower when the air flow speed is over 4m/s. As proved in Chapter 3, the heat transfer across the fibre membranes is decided by the convective heat transfer, which is a function of the air flow speed u to the power $(-\frac{2}{3})$, expressed in equation 3-7. Hence, for the heat transfer, the energy recovery effectiveness decreases with the air flow speed increasing. For the mass transfer, it is mainly determined by the moisture diffusion coefficient of the fibre membranes. When the airflow speed is increased the moisture across the membranes is aggravated, hence the recovery effectiveness is reduced.

V. Impact of Air Moisture Content Difference on Energy Recovery Effectiveness

Simulations were carried out to research the influence of the air moisture content difference on the energy recovery effectiveness, changing the fresh air relative humidity from 10% to 70% at the temperature of 35°C, while keeping the other parameters unchanged, i.e. 0.7m/s of fresh and

exhaust air flow speed, 1m of air channel length, and 6.5mm of channel height, and the pre-set exhaust air at 24°C and 50%.

From Figure 4-20 it can be seen that the heat recovery effectiveness keeps few change but mass recovery effectiveness increases with the moisture content difference increasing. When the heat recovery effectiveness is higher than the mass, the enthalpy recovery effectiveness is close to the first. This is because the moisture content difference between the fresh and return air is small, then the moisture transfer quantity is light, therefore the heat recovery heavily affects the enthalpy recovery. With the moisture content difference increasing, the influence of mass recovery to the total energy is enhanced and the enthalpy recovery effectiveness curve approaches to the mass recovery effectiveness gradually.

Although the mass and enthalpy transfer effectiveness vary in wider range when the moisture content differences between the fresh and exhaust air are changed from 1.233 to 23.397 g/kg(dry· air), the supply air moisture content almost increases linearly, as shown in Figure 4-21.

VI. Impact of Air Flow Speed Ratio on Energy Recovery Effectiveness

Keeping the pre-set conditions unchanged, i.e. 1m of air channel length and 6.5mm of channel height, pre-set exhaust air at 24°C, 50% and fresh air 35°C, 70%, the airflow speed ratio of fresh air to exhaust air changed from 0.25 to 2.0, which kept the fresh air flow speed unchanged at 1.2 m/s, but changed the exhaust air from 0.6 to 4.8m/s. The simulation results are presented in Figures 4-22 and 4-23.

Figure 4-22 expresses that when the airflow speed ratio is 1.0, the energy recovery effectiveness reaches its' lowest point and increasing or decreasing the airflow speed ratio both enhances the recovery performance. This is because when the fresh and exhaust air parameters is unvaried, it means that the value of $(t_f - t_s)/(t_f - t_e)$, $(d_f - d_s)/(d_f - d_e)$ and $(h_f - h_s)/(h_f - h_e)$ are unchanged in equations 4-9, 4-10 and 4-11. When the exhaust air flow speed is decreased, the

value of m_{\min} and C_{\min} is reduced, which induces the recovery effectiveness increasing. When the exhaust airflow speed is increased, the convective heat and mass transfer coefficient of exhaust air side in equations 3-1 and 3-8 are all increased, which results in the recovery effectiveness increasing. Hence, the energy recovery effectiveness increases considerably with the exhaust air increasing/decreasing. Although the recovery effectiveness decreases first and then increases with the airflow speed ratio rise, the supply air temperature and moisture content gradually approaches the fresh air, as shown in Figure 4-23. Although a lower airflow speed ratio results in a better supply air temperature and moisture content, it could not make the best use of the exhaust air energy. When the airflow ratio was 1.0, the energy recovery effectiveness was over 86%, which is acceptable for a heat/mass air-to-air exchanger. To save more energy from exiting energy, and treat the supply air close to the desired air condition, the airflow ratio 1.0 is an optimal selection

4.5.2 Summary of Simulation Results

From Figures 4-16 to 4-23, it can be seen that the energy recovery effectiveness is mostly influenced by the moisture content difference, the airflow speed, and channel size, and less affected by the air temperature. For the fresh and exhaust air conditions that: fresh air temperature is 35°C and the relative humidity is 70%; exhaust air temperature is 24°C, and the relative humidity is 50%, the best air-to-air exchanger size and running conditions are concluded as follows:

- For a compact exchanger size with high recovery effectiveness, the preferred channel length same with the exchanger length is 0.8~1m
- For a compact exchanger size with high recovery effectiveness and less air flow resistance and manufacturing difficulty, the selected channel height is 4.5~6.5mm
- For a high recovery effectiveness and recovery the exhaust energy as possible, the fresh air to exhaust air flow speed ratio is 1.0 and the flow speeds are 0.5m/s.

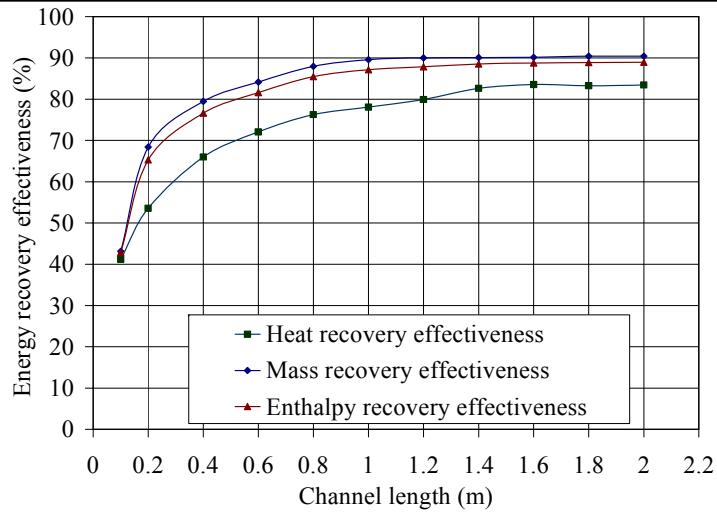


Figure 4-16 Energy recovery effectiveness vs. channel length

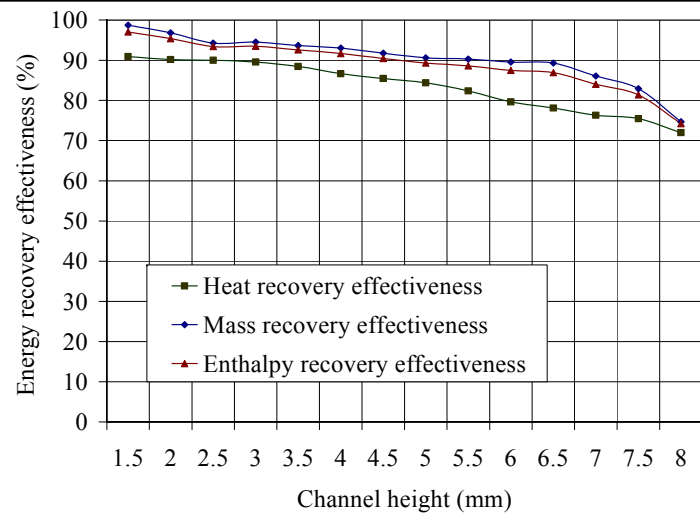


Figure 4-17 Energy recovery effectiveness vs. channel height

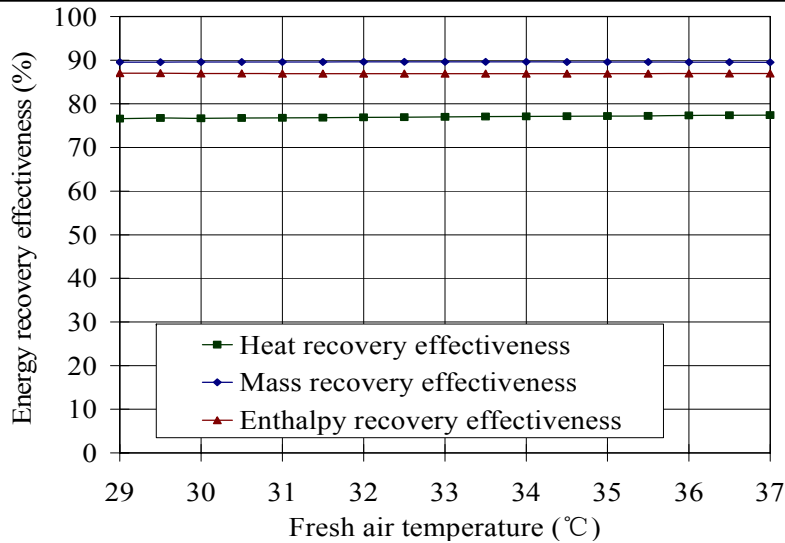


Figure 4-18 Energy recovery effectiveness vs. fresh air temperature

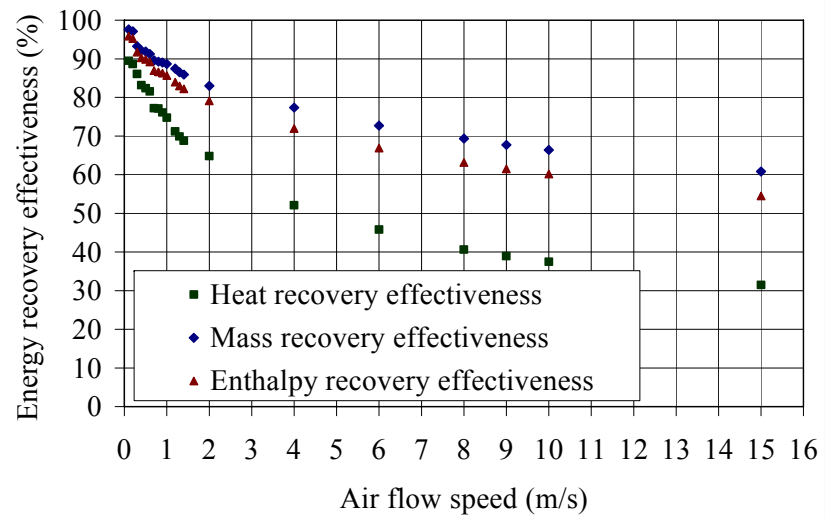


Figure 4-19 Energy recovery effectiveness vs. fresh air flow speed

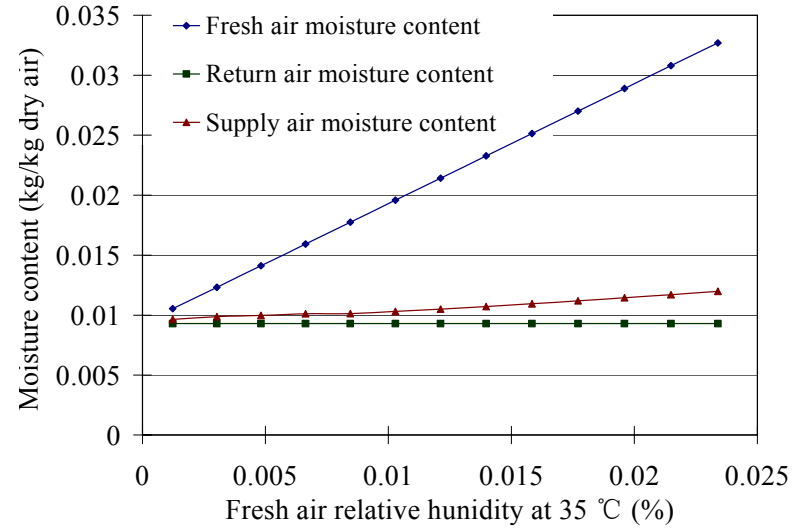
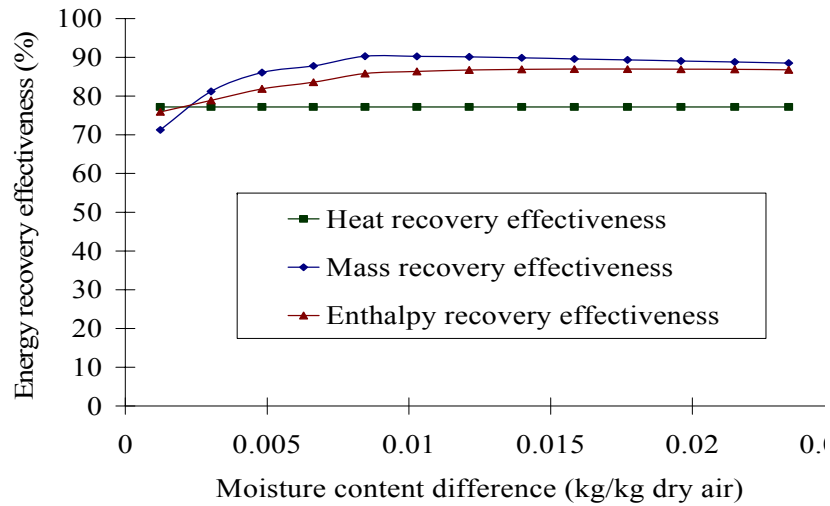


Figure 4-20 Energy recovery effectiveness vs. moisture content difference

Figure 4-21 Moisture content vs. fresh air relative humidity

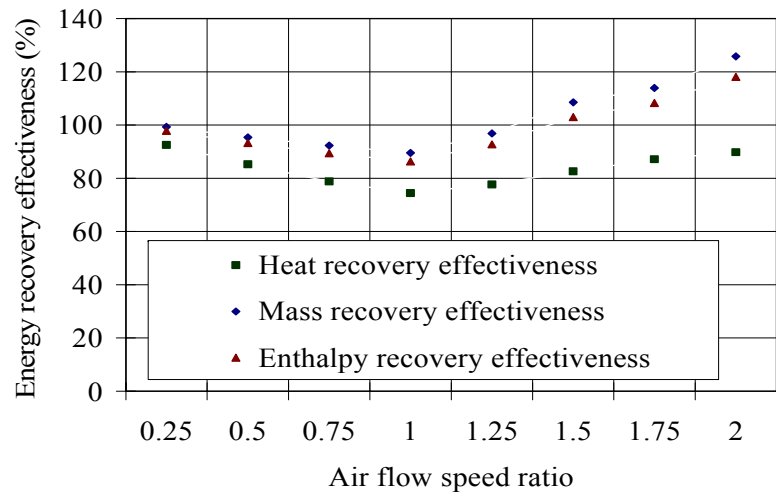


Figure 4-22 Energy recovery effectiveness vs. air flow speed ratio

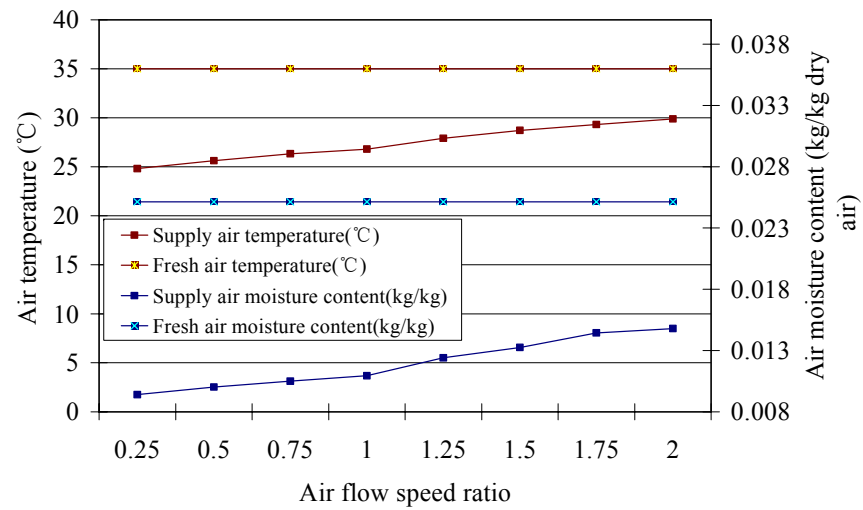


Figure 4-23 Supply air parameters vs. air flow speed ratio

4.6 Comparison between the Experimental and Correction Modelling Results

For the fixed test rig shown in figure 4-10, the size and structure of the exchanger is settled, and only the moisture content and airflow speed influence the energy recovery effectiveness. The test results are presented in Figures 4-24 and 4-25, and the comparisons with the numerical modelling results are analysed synchronously.

4.6.1 Airflow Speed Influencing the Energy Recovery Effectiveness

Keeping the fresh and exhaust air temperature and relative humidity at 32.5°C, 50.4% and 24.6°C, 59.4% respectively, and then changing the air flow rate from 500 to 800m³/h, numerical simulations under these conditions were carried out, and the simulation and experimental results are both displayed in figure 4-24.

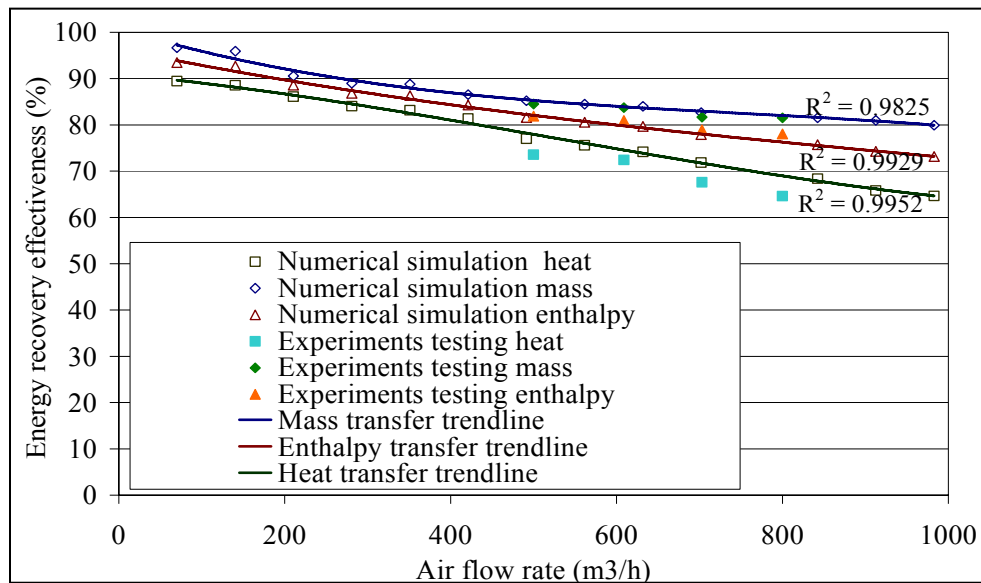


Figure 4-24 Experimental and modelling energy recovery effectiveness vs. air flow rate

Heat, mass and enthalpy recovery effectiveness decreased with the air flow rate increasing in the experimental testing. Comparing the test and simulation results, we found that for the term of heat recovery effectiveness, the simulation results were 3% higher than the experimental results, and the errors increased with the air flow rate increasing; for the term of mass recovery effectiveness, simulation results were 99% closer to the experiments results; for the term of

enthalpy recovery effectiveness, the simulation results were 1% lower than the experiments results.

4.6.2 Moisture Content Difference Influencing the Energy Recovery Effectiveness

Keeping the exhaust air at about 24.5°C and 55%, and changing the fresh air temperature and moisture content in the range of 34.7~35.6°C and 16.6~13.4g/kg (dry· air) respectively, fresh and exhaust air had the same airflow rate 500m³/h. The simulation and test results are shown in figure 4-25.

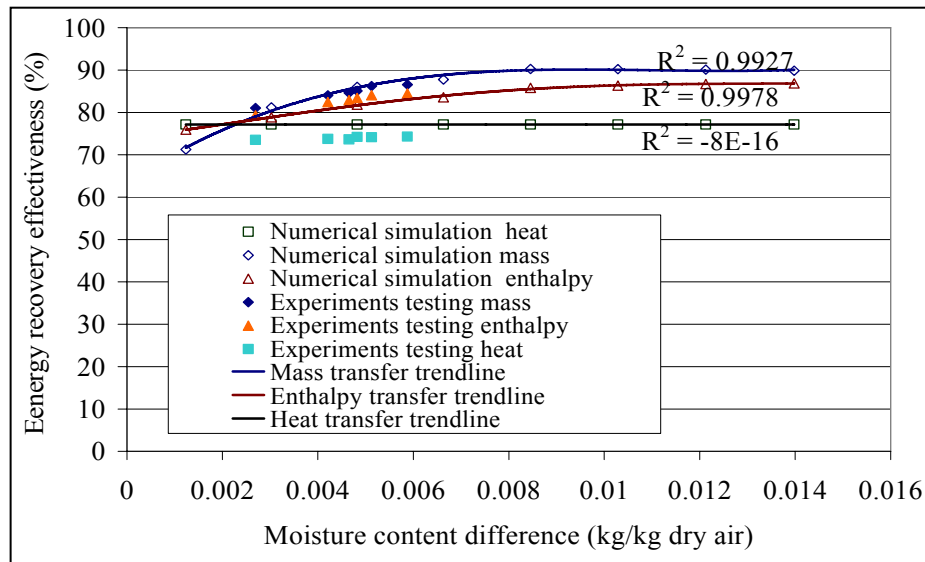


Figure 4-25 Experimental and modelling energy recovery effectiveness vs. air moisture content difference

The experimental results presented in figure 4-25 indicate that the heat transfer effectiveness changed slightly, however, the mass and enthalpy recovery effectiveness increased with the moisture content difference increasing. The average heat, mass, and enthalpy recovery effectiveness is about 73.93%, 84.61% and 82.78% respectively for the airflow rate of 500m³/h.

Contrasting the simulation and experimental results, it can be seen that the mass transfer results of the simulation approach to the experiments results in an error of 1%, however, the heat

transfer is about 3.25% higher than the experiments results. The enthalpy recovery effectiveness of the modelling results is 2.4% lower than the experiments.

4.6.3 Reasons Causing the Differences between Simulations and Testing Results

The reasons causing the differences between the test and experimental results are as follows: (1) the simulations' pre-set conditions were the average values of the practical test conditions, which varied in a small range, and this could cause errors between the experimental and simulation results; (2) the influence of the sensible heat transfer to mass transfer considered in the simulation is not accuracy. (3) mass transfer through the liquid desiccant soaked-fibre membrane is the correction based on the clean fibre membrane, this assumption arouses errors to simulation; (4) the simulation limit accuracy could brings errors; (5) the experimental tests were carried out in the winter in the University of Nottingham, where the weather was cold and humid, and although the air ducts and boxes all had heat preservation, the weather still affected the sensor probes to some degree; (6) the air flow rates of fresh and exhaust air were measured by the thermal anemoscope, and the average values of 12 measuring points distributed at the cross section of the duct were used in calculating the recovery effectiveness, hence, there is potential to bring errors into the test results.

The first three reasons mainly impact the simulation results and cause the difference. Although there are differences between the numerical and testing results, as shown in figures 4-24 and 4-25, the differences are lower than 4%, which is acceptable to our research. Hence the corrected heat/mass fibre exchanger modelling could be imported into the whole system modelling in Chapter 7.

4.7 Summary

Based on the research results in Chapter 3, three types of fibre membranes performance were described and investigated. It was concluded from the theoretical analysis that the liquid

desiccant-soaked fibre should perform better than the clean and solid desiccant-coated FPEM. Experimental results proved that the first type fibre membranes were more effective than the last two types. Heat and mass transfer coefficient corrections for liquid desiccant-soaked FPEM were made, based on the comparison of the numerical simulation results of clean fibre membranes, and the experimental results of liquid desiccant-soaked FPEM. A further numerical model was developed, based on the corrected heat/mass transfer coefficient, and was proved to give reasonable accuracy in predicting heat/mass exchanger operation characteristics. The relationship between the performances of the liquid desiccant-soaked FPEM with the exchanger structure and size, and fresh/exhaust air parameters were studied. It was found that:

- Enthalpy recovery effectiveness is a function of heat and mass transfer, and is heavily influenced by the latter.
- Exchanger channel length greatly affects the heat/mass recovery effectiveness, however, the influence declines when the length is over 1m. When the channel length is 1m, the heat, mass, and enthalpy recovery efficiencies reach 78.09%, 89.59%, and 87.13% respectively. Hence the preferred channel size is 0.8~1m for the pre-set conditions.
- A lower exchanger channel height results in better energy recovery effectiveness, but leads to friction force, manufacturing difficulty, and costs increasing. The preferred channel height is in the range of 4.5~6.5mm, which can offer excellent recovery results, and reduce the exchanger size as well as friction force and manufacturing difficulty.
- The air temperature difference between fresh and exhaust air slightly affects the heat, mass and enthalpy recovery effectiveness. The average mass transfer efficiency of the fixed exchanger size, shown in figure 4-18, is as high as 89.58% under the pre-set condition.
- Heat transfer is slightly influenced by the moisture content difference, but the mass transfer effectiveness strongly depends on it. The enthalpy recovery is a function of the

heat/mass transfer, and is determined by the heat/mass transfer direction. Mass transfer increases with the value of the moisture content difference increase.

- Energy recovery effectiveness decreases heavily with the air flow speed increasing, but the decline trend slows down when the air flow speed is over 4m/s.
- When the air flow speed ratio of fresh air to exhaust air is 1.0, the energy recovery effectiveness is at the lowest. When the fresh airflow speed is higher than the exhaust air (ratio > 1.0), the recovery effectiveness is high, but the supply air temperature/humidity approaches the fresh air conditions. When the fresh airflow speed is lower than the exhaust air (ratio < 1.0), the recovery effectiveness is high, and the supply air is close to the exhaust air condition, but can't recover the exhaust energy as possible. Hence, when the fresh airflow speed equals the exhaust air (ratio=1.0) the enthalpy recovery is as high as 86.34%, with an acceptable supply air condition, and most of the exhaust air energy is saved.

Experimental tests were carried out to prove the accuracy of the further model set up on the correction heat/mass transfer coefficient. Comparisons between the experimental and modelling results were carried out, and it was found that the errors of energy recovery effectiveness between them were less than 4%, which was possibly caused by the simulated pre-set conditions, corrected mass transfer coefficient, measuring methods, test conditions (air temperature/relative humidity varying in a small range), etc. Hence, the numerical modelling of the heat/mass exchanger is qualified to be imported into the whole system modelling, in Chapter 7.

The moisture content and air temperature after the heat/mass exchanger is still higher than the desired air conditions, and so it needs further treatment in the dehumidifier core, which will be investigated in Chapter 5.

Chapter 5. Performance Investigations of Desiccant Dehumidifier

5.1 Introduction

From Chapters 3 and 4, it is concluded that the cellulose fibre paper has strong absorption to hold the liquid desiccant particulates very well, and prevent the desiccant particulates from being taken away by flowing air. Besides the high absorption ability, cellulose fibre paper is the cheapest material and easiest to be shaped into various structures. Therefore, the cellulose fibre was employed to make the dehumidifier core in this project. Correlative work involving experimental testing and numerical modelling was carried out to display the performance of paper dehumidifier.

Both the heat/mass exchanger and dehumidifier are intended to be installed into a windcatcher/cowl, which can provide low cost ventilation. Therefore, the heat/mass exchanger and dehumidifier are shaped into a polygonal structure as shown in figure 1-6 to fit the air duct connecting to the windcatcher/cowl.

As analyzed in Chapter 2, liquid desiccant can perform better dehumidification and regeneration as well as flexible application. LiCl, LiBr and CaCl₂ solution were selected in this research and their performances were investigated on numerical simulation. Results indicate that LiCl solution performs the best dehumidification, but worst heat recovery. However, absorbing moisture is the primary task of the dehumidifier, LiCl solution was used in the experiments and performance characteristics were studied. The air control system described in Chapter 4 was utilized in this dehumidification testing again to offer various air conditions according to the research demands.

5.2 Description of the Dehumidifier Core Operation

Figure 5-1 (a) shows the structure of the desiccant dehumidifier pack, which is constituted of cellulose fibre membranes, solution tank, pump and sprayer, and supplying pipe. Two pieces of

fibres membranes are attached onto one piece of very thin polyethylene clapboard, and compose one complex membrane, two of which make one air channel as shown in Figure 5-1 (b) . The desiccant core is designed to be vertical allowing the liquid desiccant to flow down to the tank at the bottom of the core by gravitation. According to the whole project sketch diagram presented in figure 1-6, the air steam flows though the channel along the parallel direction at a fixed angle with the desiccant falling direction..

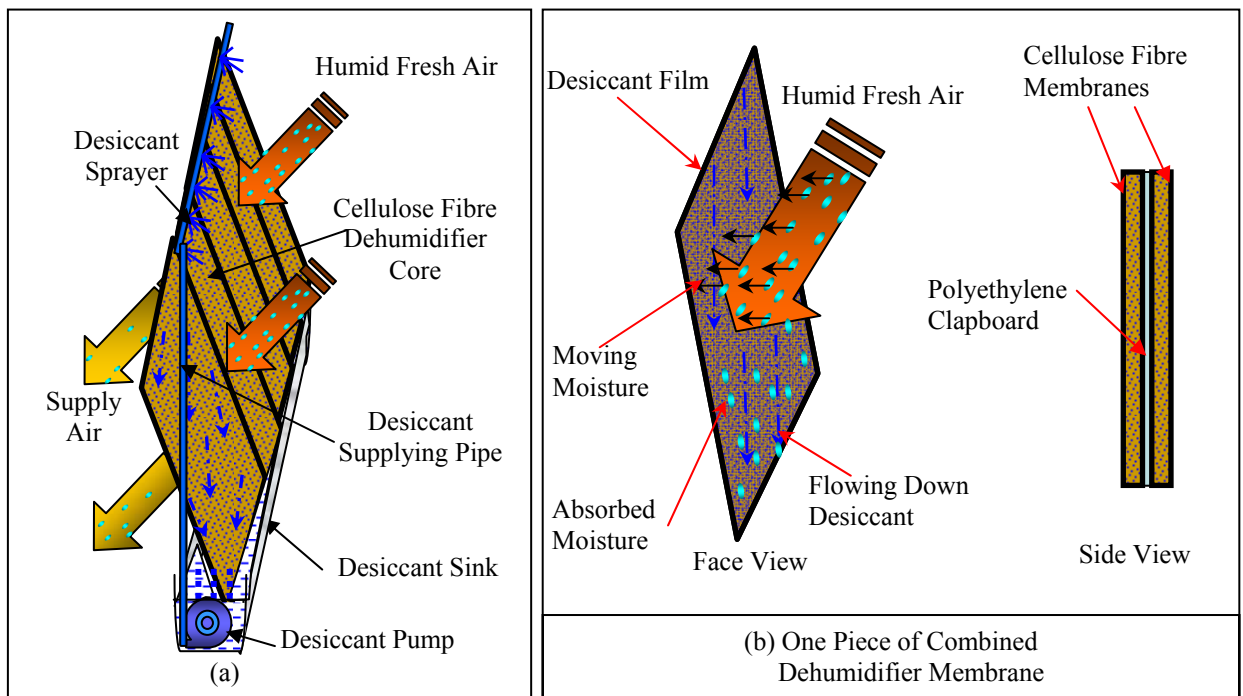


Figure 5-1 Sketch diagram of desiccant dehumidifier pack and desiccant film

Strong desiccant at lower temperature is sprayed from the top of the dehumidifier core and flows down along the fibre paper membranes. Because of the strong absorbability of the fibre paper, the liquid desiccant particles are firmly hold by the long fibre of the cellulose and superfluous desiccant flows down to the tank. Therefore, humid airflow flowing through the channel contacts directly with the liquid desiccant as well as does not bring the desiccant particles into the supplying room. When the humid air contacts with the strong and cold desiccant, higher vapour pressure at the air side forces the moisture to move to the strong solution film. At the same time, sensible heat, and condensation latent heat released by the moisture from air side are both transferred to the cold desiccant solution. In this research,

cooling tower or ground cold water as optimal cooling source is designed to cool the condensed hot solution from the regenerator. Hence, the solution is cooled under the fresh air and near to its dew point temperature.

5.3 Mathematical Theory

5.3.1 Heat Transfer between Air and Desiccant Solution

Heat transfer is induced by the temperature difference between the air stream and desiccant filled fibre paper membrane, which is similar to the strong desiccant solution. According to the calculation theory of forced convection heat exchanger inside a closed conduit, the heat transfer rate can be expressed as (James R. Welty, 2000):

$$q_d = (t_f - t_d) / \left(\frac{1}{k_f^s} + \frac{1}{k_d^s} \right) \quad (5-1)$$

$$\text{Re} = \frac{uD}{\nu_b} \quad (5-2)$$

When the air flow speed u is in the range of 0.1~ 3m/s, air temperature and humidity is about 35°C and 70%, and equivalent diameter D is about 5 mm, Reynolds number Re is 372 lower than 2000. The same theory is used for the desiccant solution side, the Reynolds number is also lower than 2000. The heat and mass transfer therefore happens in the Laminar Flow Layer.

k_f^s is the air steam convective heat transfer efficiency, which is calculated by the equations 3-2 to 3-7 in Chapter 3. k_d^s is the liquid desiccant convective heat transfer, which is determined by the liquid desiccant parameters involving specific heat c_b , thermal diffusivity α , density ρ , and dynamical viscosity μ , thermal conductivity k , which are expressed by the equations in Appendix II.

5.3.2 Mass Transfer between Air and Desiccant Solution

Mass transfer between the air stream and the liquid desiccant film occurs due to the vapour pressure difference between these two phases. It can be calculated employing the following equation (James R. Welty et al, 2000):

$$m_d = \frac{(p_f - p_d)}{R_m T \left(\frac{1}{k_f^l} + \frac{H}{k_d^l} \right)} \quad (5-3)$$

p_d and d_d are the equivalent vapour pressure and moisture content of the liquid desiccant under environmental pressure, which are calculated through the equations expressed in Appendix II. R is the molar gas constant for water (=461Jkg/K). H is Henry's law constant usually gained from the experiments and it increases with the solution temperature increasing under the atmospheric pressure 101.325kPa (James R. Welty et al, 2000).

For the air stream, the mass transfer efficiency is calculated through the equation 3-11

$k_f^l = k_f^s \rho_f^b c_f^b (Le)^{2/3}$ presented in Chapter 3. Generally, moisture transfer for the gas Le is assumed to be 1 (James R. Welty et al, 2000). For the liquid desiccant, the following equations are used to calculate the mass transfer effectiveness k_d^l :

$$k_d^l = k_d^s (\rho_d^b c_d^b)^{-1} \left(\frac{\alpha_d^b}{D_{AB}} \right)^{-2/3} \quad (5-4)$$

D_{AB} is the diffusion coefficient of water into the solution expressed in appendix II.

5.3.3 Heat and Mass Transfer Performance

Heat transfer effectiveness

$$\epsilon_{De}^{He} = m_f c_f (t_f - t_s) / C_{\min} (t_f - t_d) \quad (5-5)$$

The moisture absorption capacity per litre solution per second is defined as the dehumidification capability of this sort of solution as shown in the following equation:

$$\varepsilon_{De}^{moisture} = m_{absorb}^{moisture} / V_d = m_f (d_f - d_s) / V_d \quad (5-6)$$

5.4 Numerical Modelling

5.4.1 Channels Distribution and Assumptions

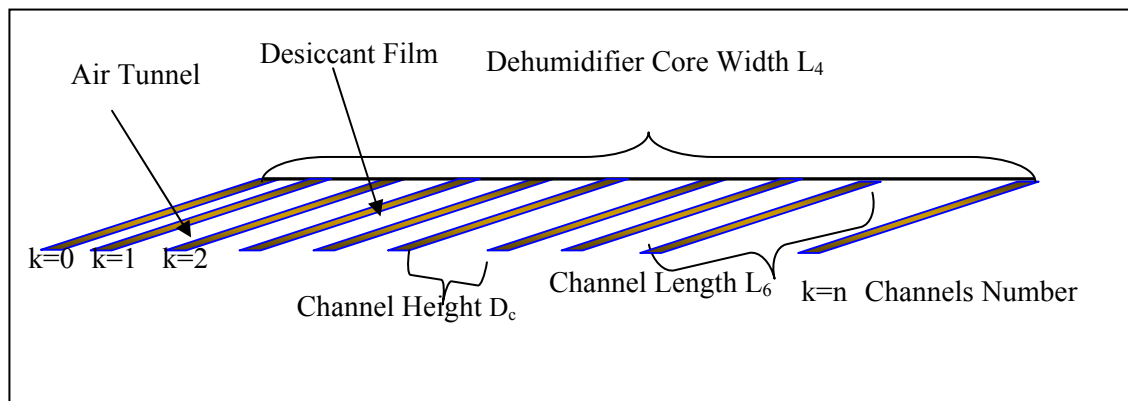


Figure 5-2 Calculate channel sketch diagram of the dehumidifier core

As described in the figure 5-1, the humid fresh air flow down through the channel constituted of two complex membranes combined of cellulose fibre and polyethylene clapboard. From the face view of the dehumidifier core in Figure 5-2, it can be known that the air channel is rectangle. In this model, the air flow direction is treated parallel with the solution flow. Channel number n is determined by the channel height D_c and dehumidifier width L_4 .

To simplify the numerical simulation, the following assumptions were made:

- Air flow speed, temperature and moisture content across each channel were the same.
- Desiccant solution temperature and concentration sprayed on each cellulose fibre membrane were the same.
- Fibre membranes were assumed as the desiccant film and had the same temperature with the desiccant solution.

- Heat/mass transfer occur vertically between the fibre paper membranes and air stream and no heat/mass transfer along the air flow direction as shown in figure 5-1 (b).
- Superfluous solution flowed down to the tank by gravitation.
- No desiccant particulates were carried out by the supplying air.
- Latent heat released from the condensate moisture was absorbed by the cold desiccant solution.

5.4.2 Calculation Method and Cell Element

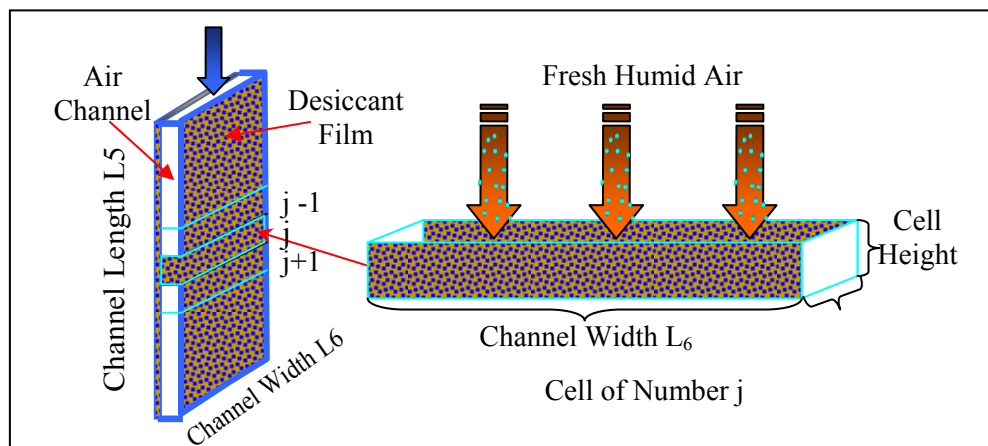


Figure 5-3 Calculate cell sketch diagram of one air channel

Finite-element approach was applied in this numerical simulation. As shown in Figure 5-3, each element involves a fresh air section and two desiccant filled cellulose fibre membranes. For calculating the heat and mass balance of each cell, the assumptions were made as the followings:

- (1) in the solution section, each cell has a uniform membrane surface temperature and vapour pressure;
- (2) in humid air section, each cell has a uniform air temperature and moisture content.

Cell number $m = L_5 / h$ of each channel is determined by the cell length h and the channel length L_5 same with dehumidifier length. In the numerical simulation, each calculating cell length was 1mm.

5.4.3 Heat and Mass Transfer

Mass Balance of Each Cell

For each cell, the moisture condensed from the humid air is absorbed by the strong desiccant solution as expressed in the following equation:

$$dm = (p_f - p_w) / (RT \frac{1}{k_f'}) dA = (c_w - c_d) / (\frac{1}{k_d'}) dA = (p_f - p_s) / (RT (\frac{1}{k_f'} + \frac{H}{k_d'})) dA \quad (5-7)$$

Heat Balance of Each Cell

For the air flow, heat is transferred from the hot desiccant solution and the transferred energy is expressed as:

$$dq = (t_f - t_d) / \frac{1}{k_f^s} dA \quad (5-8)$$

For the desiccant solution, the heat balance includes two parts: sensible heat transferred from the hot fresh air and latent heat released by the condensed moisture as expressed in the following:

$$dq = (t_f - t_d) / (\frac{1}{k_e^s} + \frac{1}{k_e^s}) dA + (2500 - 2.35t_d) dm \quad (5-9)$$

Henry's law constant H varies for different solution under the changing environment pressure, for this case, the environment pressure is Atmospheric pressure. And the accurate H values of different solution are listed in the table Appendix III.

5.4.4 Base Conditions for Numerical Simulation

The pre-set conditions for carrying numerical simulation are presented as the followings:

- Channel length L_5 was 0.25m and cell length and height was 1mm and 8mm respectively.
- Fresh air flow speed was 0.4m/s.

- Fresh air temperature was 35°C and relative humidity was 70%.
- Desiccant temperature for LiCl, LiBr and CaCl₂ solution was 29°C, which was higher than the fresh air dew point temperature and conveniently gained from the cooling tower /ground water.
- Table 5-1 lists the solutions' flow speed, concentration and temperature, Henry's law constant set for simulations.

According to the assumed fresh air temperature and relative humidity (35°C and 70%) the vapour pressure of this air stream is 3.94Pa. To absorb the moisture from the humid air, the vapour pressure of the working solution at 29°C (dew point of the air environment) should lower than 3.94Pa. From the Duhring diagram of the LiCl, LiBr and CaCl₂ solution in Appendix II, the working solution parameters is selected as listed in Table 5.1.

Table 5.1 Parameters of three kinds of desiccant solution

Desiccant solution	Temperature (°C)	Weight Concentration (%)	Desiccant flow Rate× 10 ⁻³ (l/s)	Henry's law constant (Appendix III)
LiCl+H ₂ O	29	35	1	$-0.00256t^2 + 0.86125t + 67$
LiBr+H ₂ O	29	55	1	$-6.25 \times 10^{-4}t^2 + 0.2125t + 58$
CaCl+H ₂ O	29	45	1	$0.995t + 59.5$

5.4.5 Modelling Results

I . Impact of Solution Mass Concentration on Dehumidifier Performance

The desiccant solution concentration varied from 0.2 to 0.8 and other parameters were kept unchanged. Simulations were carried out to investigate the performances of LiCl, LiBr and CaCl₂ solutions regarding the sensible heat recovery effectiveness and moisture absorption capacity.

Figure 5-4 shows the heat recovery effectiveness and moisture absorption capacity of three sorts of desiccant solutions. It is obvious that the LiCl has the highest absorption capacity and CaCl₂

has the lowest, and all three solutions display gradually better heat/mass transfer performance with the concentration increasing. For LiBr solution, moisture starts to transfer from humid air to desiccant solution when the concentration is over 40%, but for the other two solutions, the starting concentration is no lower than 20%. For the same absorption capacity $\varepsilon_{De}^{moisture} = 0.0125 \text{ g/L}$, at 29°C , LiCl solution concentration is 30%, LiBr solution is 50% and CaCl_2 is over 55%.

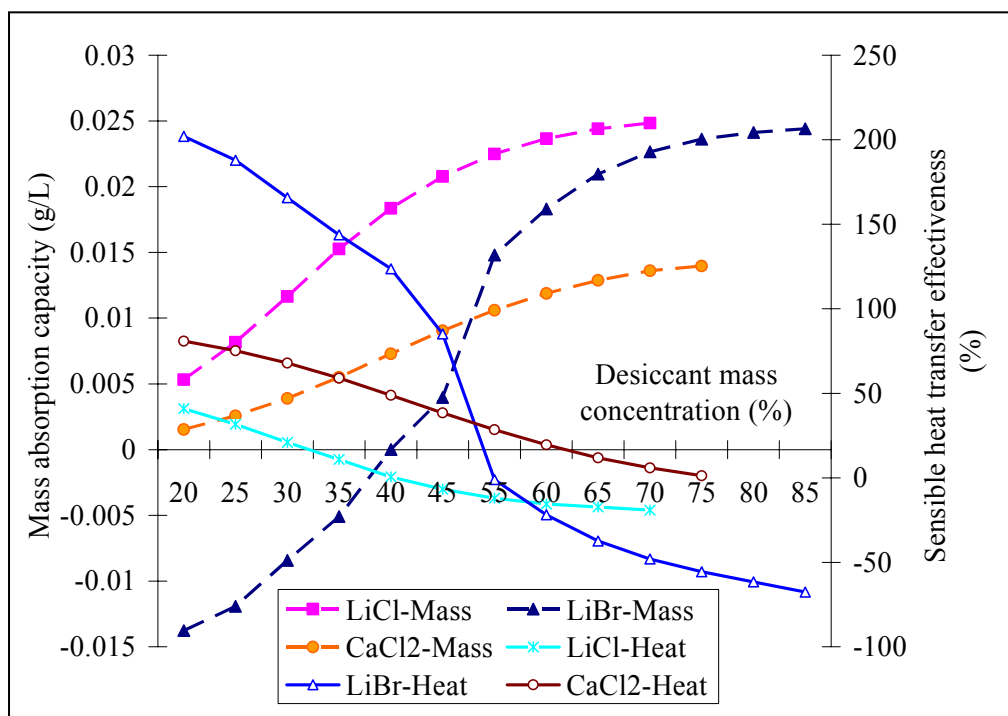


Figure 5-4 Dehumidifier performances vs. desiccant solution mass concentration

The heat recovery effectiveness declines with solution concentration increasing. With the concentration decreasing, LiBr solution has the biggest heat recovery effectiveness drop from 201.98% to -67.64%. This is because, when the LiBr concentration is lower than 40%, moisture is evaporated from the solution to air, and latent heat is absorbed from the air flow and solution. This causes the air temperature declining greatly. However, latent heat is released to air flow and solution when moisture is condensed out of humid air into desiccant solution. If the cooling capacity of cold solution can not cover the released latent heat to air flow, the air temperature rise and heat recovery effectiveness becomes negative as shown in figure 5-4.

Dehumidification is the main purpose, and heat recovery takes the inferior position compared to moisture absorption capacity. Hence, LiCl solution was investigated in the next modelling simulation due to its best dehumidification performance although its heat recovery ability is the lowest.

II. Impact of Channel Height on Dehumidifier Performance

Keeping the pre-set humid air and LiCl solution parameters unchanged and varying the dehumidifier channel height from 5 to 45 mm. Simulation results are displayed in Figures 5-5 and 5-6.

From the figure 5-5, it can be seen that the desiccant absorption capacity reaches the highest value of 0.0272g/L when the channel height is 35mm. Heat recovery effectiveness increases to 47.22% with the channel height reaching 25mm, and then declines after the channel height passes 25mm. Although the moisture absorption capacity and heat recovery effectiveness have the highest value with channel height increasing, the supply air moisture content is approaching to the humid air gradually as displayed in figure 5-6. This is because when the air flows speed is constant, increasing channel height results in enlarging the mass volume, which aggravates the moisture load to the fixed desiccant solution. Although the moisture absorbed by per litre of solution is increased, the moisture content drop of air is reduced and supply air is close to the fresh air. Channel heights of 10~15mm are the preferential range to gain higher moisture absorption capacity and heat recovery effectiveness and desire air temperature and humidity.

III. Impact of Channel Length on the Dehumidifier Performance

Keeping the pre-set humid air and LiCl solution parameters unchanged and varying the dehumidifier channel length from 0.1 to 0.9m. Simulation results are displayed in Figure 5-7.

As shown in figure 5-7, mass absorption capacity increases and heat recovery effectiveness decreases with the dehumidifier channel length increasing. When the channel length increases,

more moisture is absorbed by desiccant solution resulting in more condensed latent heat released to the air flow, so the supply air temperature rises and recovery effectiveness declines. The increasing trend of absorption capacity and declining trend of heat recovery effectiveness slows down when the channel length is over 0.4m. Hence, considering both the heat and mass transfer and moisture absorption taking the mainly role, 0.2 to 0.3m is the preferred dehumidifier channel length.

IV. Impact of Desiccant Temperature on Dehumidifier Performance

Varying the solution temperature from 14°C to 31°C and keeping the pre-set humid air and LiCl solution parameters unchanged. Simulation results are shown in Figure 5-8.

Increasing the desiccant temperature from 14°C to 31°C, there is 28.55% decrease in moisture absorption capacity from 0.0200 to 0.0143g/L. But heat recovery effectiveness varies from 71.94% to -10.78% indicating that desiccant temperature affects the heat transfer more heavily than mass. Especially when the desiccant temperature (29~30°C) is higher than the hot/humid air dew point temperature (28.69°C), moisture absorption keeps at an acceptable level of 0.0152 g/L and air temperature is reduced. Hence, for saving the energy, cooling tower or ground source both can be used as the cooling source to cool down the hot desiccant from the regenerator. However, to largely reduce the air temperature and carry out more latent heat, lower desiccant temperature than 25°C is preferred under the condition of renewable energy available.

V. Impact of Desiccant Flow Rate on Dehumidifier Performance

Varying the solution flow rate from 0.0025 to 100L/s, and keeping the pre-set humid air and LiCl solution other parameters unchanged. Figure 5-9 and 5-10 shows the dehumidification and cooling performance, and supply air parameters respectively.

Mass absorption capacity decreases and heat recovery effectiveness increases sharply with desiccant solution flow rate increasing to 4.8L/s. When the desiccant flow rate is over 4.8L/s, the decreasing and increasing trend is slowed down. For a steady humid air stream, the moisture load needed to be removed is fixed when the desiccant solution and temperature is unchanged. In this case, increasing the desiccant flow rate can enhance the convective mass-transfer coefficient to some degree, but also results in a big desiccant flow rate. As shown in equation 5-6 ($\varepsilon_{De}^{moisture} = m_f(d_f - d_s)/V_d$), when the moisture need to be absorbed is invariable, the increasing mass flow rate of solution induces the moisture absorbed by one litre of solution to decline.

Heat recovery effectiveness increases when the desiccant solution flow rate is improved. In figure 5-10, there are few changes in the air temperature and moisture content, when the desiccant flow rate is over 4.8L/s. And in our research, lower supply air temperature and moisture content with high absorption capacity is the main aim, so desiccant flow rate at about 3 L/s and temperature lower than 29 °C is the suggested running conditions.

VI. Impact of Air Flow Speed on Dehumidifier Performance

Varying the humid air flow speed in the range of 0.025 to 2.4m/s and keeping others pre-set humid/hot air and LiCl solution parameters unchanged. Figure 5-11 shows the dehumidification and cooling performance.

Moisture absorption capacity increases and heat recovery effectiveness decreases with the air flow speed increasing. When the air flow speed is over 0.6m/s, the absorption capacity and heat recovery obtusely increase and declines respectively. For a fixed desiccant flow rate, increasing the air flow speed enhances the moisture load to the solution leading the more moisture is condensed into one litre solution. However when the solution gradually approaches to the saturated state, the absorption capacity keeps at a similar level when the air flow speed is over

2.0m/s shown in figure 5-12.. Considering the mass transfer affecting the total energy recovery effectiveness heavily and being the main purpose of dehumidifier, the air flow speed of 0.15~0.2m/s is the preferred value.

VII. Influence of Air Temperature on Dehumidifier Performance

Changing the humid air temperature from 24 °C to 40 °C, and keeping the pre-set humid air relative humidity at 70% and LiCl solution parameters unvaried. Figure 5-12 shows the dehumidification and cooling performance.

Heat recovery effectiveness and moisture absorption capacity of the solution both increase with humid air temperature rising. When the air temperature is lower than the desiccant temperature 29°C, air temperature is heated up by solution and condensed latent heat (heat recovery effectiveness is positive as shown in figure 5-12). Air temperature from 29°C to 33.5°C, sensible heat is transferred from air flow to desiccant solution but can not fetch up the latent heat released to air flow, so the heat recovery effectiveness is negative. If air temperature is over 33.5°C, latent heat is carried out by desiccant solution and the heat recovery effectiveness is positive. Higher air temperature results in higher absorption capacity and heat recovery effectiveness. For a fixed desiccant solution, it is better to be employed as an air conditioning system in a place, where the dew point temperature of the fresh air is higher than the desiccant temperature.

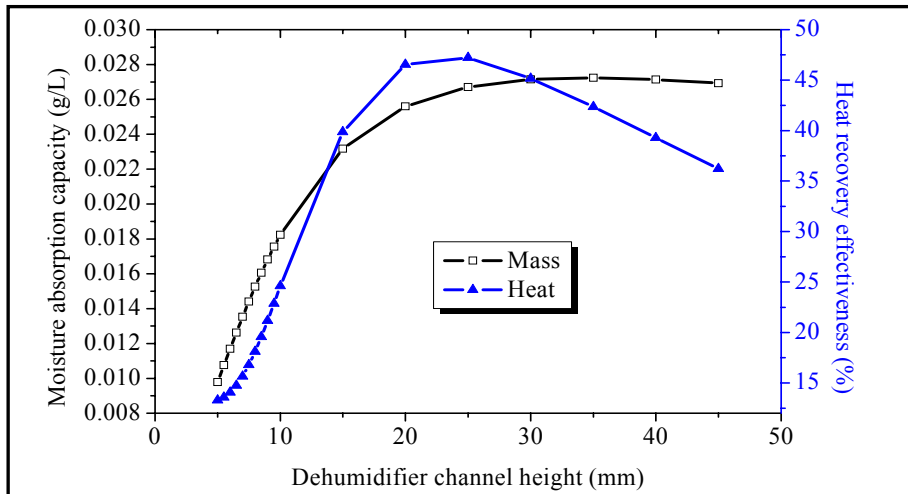


Figure 5-5 Dehumidifier performances vs. dehumidifier channel height

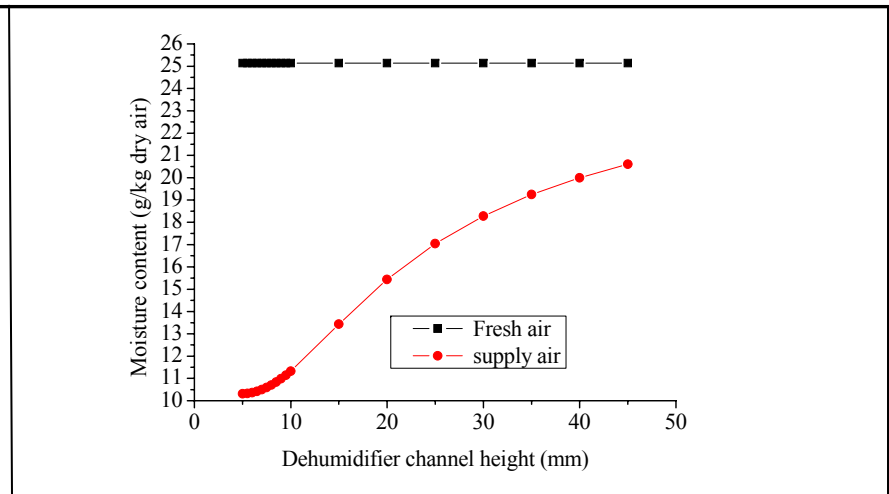


Figure 5-6 Air moisture content vs. dehumidifier channel height

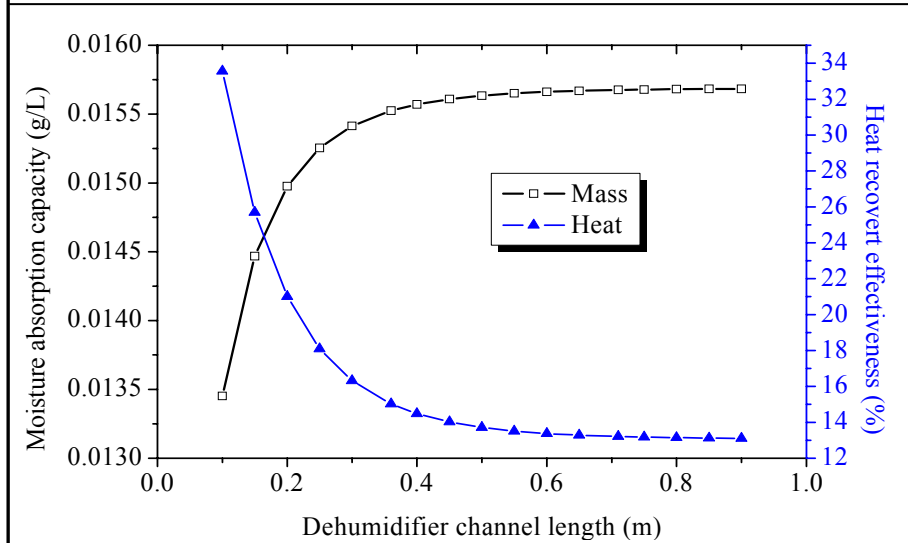


Figure 5-7 Dehumidifier performances vs. dehumidifier channel length

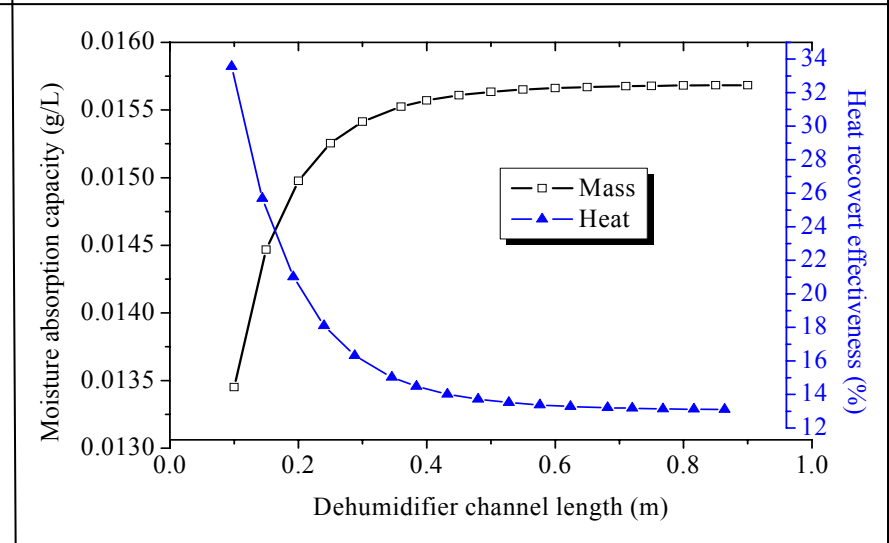


Figure 5-8 Dehumidifier performances vs. solution temperature

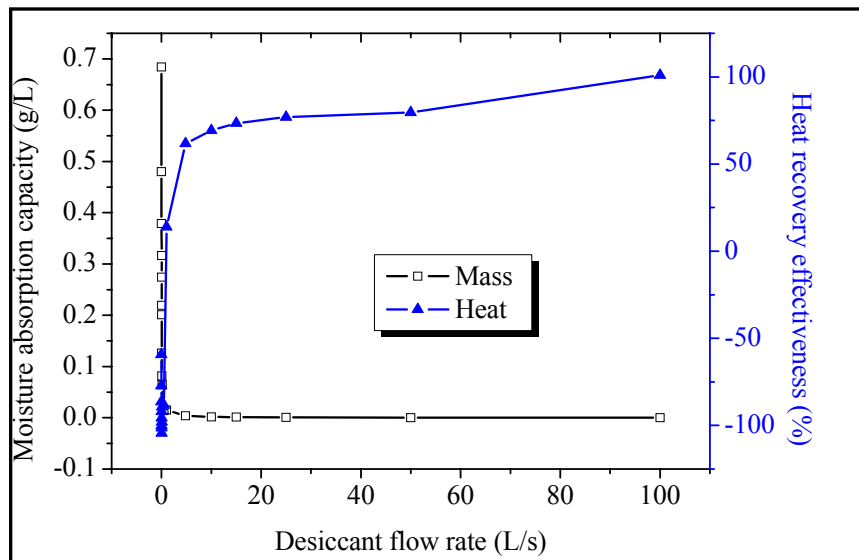


Figure 5-9 Dehumidifier performances vs. solution flow rate

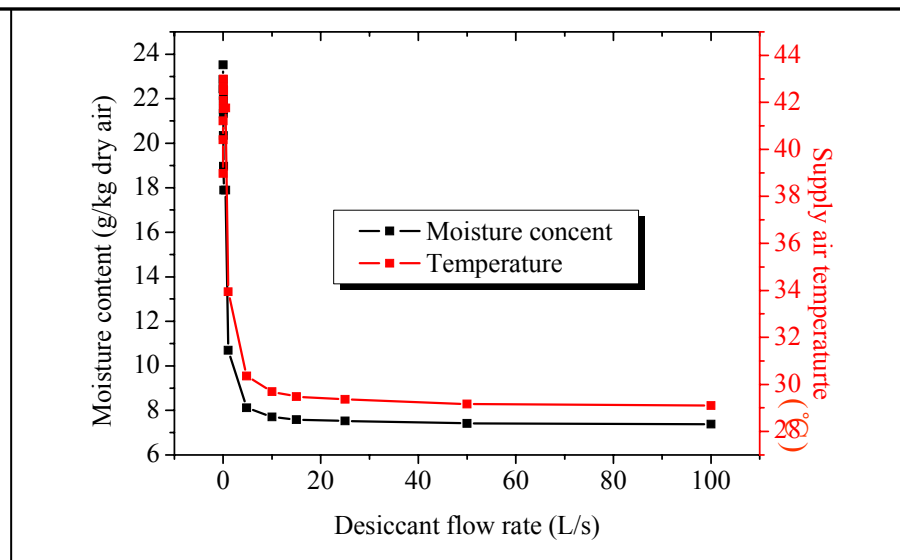


Figure 5-10 Supply air parameters vs. solution flow rate

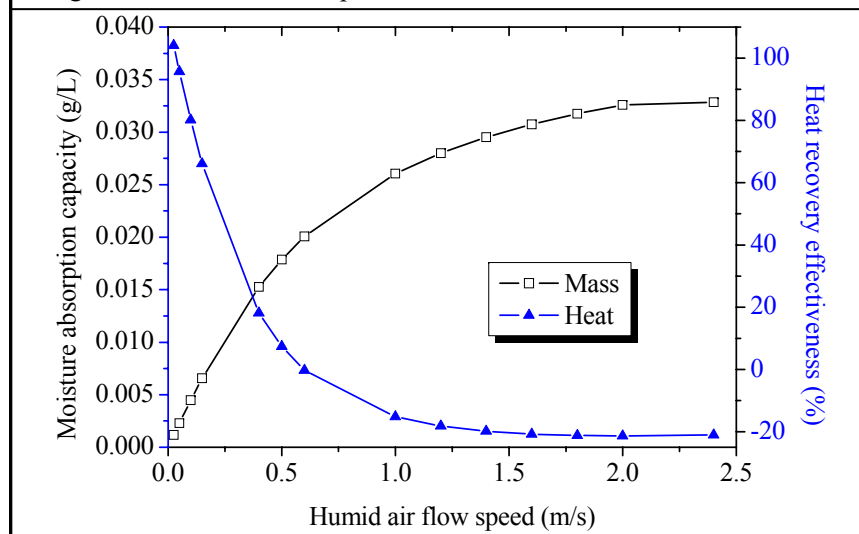


Figure 5-11 Dehumidifier performances vs. humid air flow speed

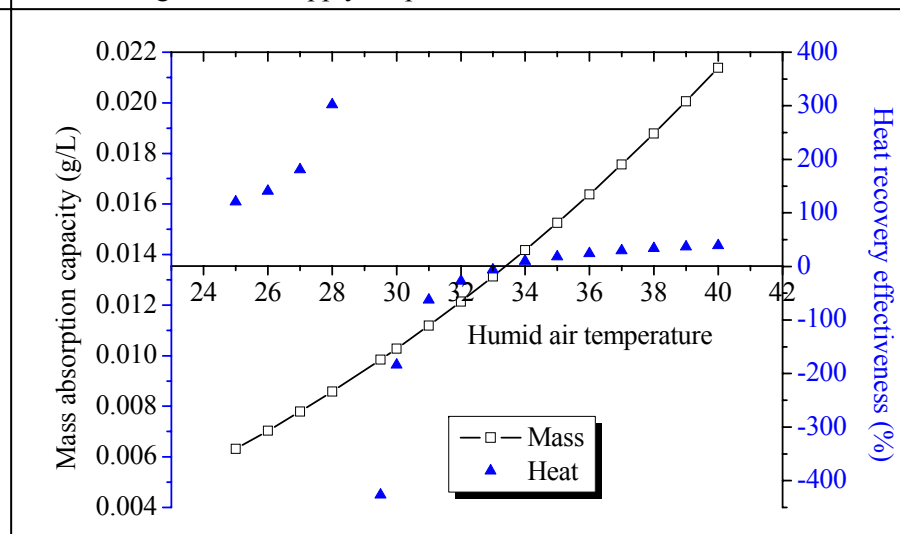


Figure 5-12 Dehumidifier performances vs. humid air temperature

VIII. Impact of Air Humidity on Dehumidifier Performance

Changing humid air relative humidity in the range of 10 ~ 95% (moisture content from 3.470272 to 34.60885g/kg (dry air)), and keeping the pre-set humid air temperature and LiCl solution parameters unchanged.

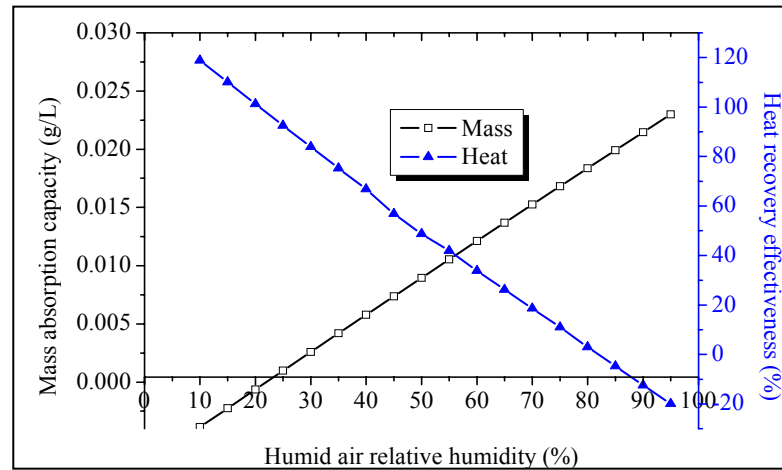


Figure 5-13 Dehumidifier performances vs. humid air relative humidity

Figure 5-13 shows the dehumidification and cooling performance of the dehumidifier under the same air temperature and varied humidity. The moisture absorption capacity increases and heat recovery effectiveness decreases with the air relative humidity increasing. This is because the higher moisture content of fresh air will enlarge the moisture condensed into the solution, which releases more latent heat heating up the air temperature. Hence, when the air temperature is about 35°C, the settled dehumidifier and desiccant solution can deal with the humid air with the relative humidity at about 65%.

IX. Summary of Simulation Results

From table 5-2, we can know that the channel size (height and length) and desiccant temperature affect the dehumidifier absorption capacity slightly. Humidity air flow speed is the main factor influencing the desiccant absorption ability, and air humidity takes the second influences. Desiccant mass concentration determines the dehumidification efficiency when the fixed

dehumidifier is employed for a definite climate. Even cooling load takes the inferiority roles comparing with the dehumidification purpose, desiccant flow rate and channel height are the leading factors impacting the cooling efficiency, and desiccant mass concentration, humid air flow speed, and humid air humidity, desiccant temperature are the second affecting factors.

Table 5.2 Factors and their influence on dehumidifier thermal performance

Influence factors	Changing range	Moisture absorption capacity (g/L)	Heat recovery effectiveness (%)
Channel height (mm)	5~45	0.009793~0.026935 (63.64%) ↑	13.30~47.22~36.22 (255.07%) ↑
Channel length (m)	0.1~0.9	0.013453~0.015684 (60.95%) ↑	33.554~13.102 (-16.59%) ↓
Desiccant mass concentration (%)	0.2~0.65	0.005326~0.024838 (366.32%) ↑	40.93~ -19.07 (-146.596%) ↓
Desiccant temperature (°C)	15~31	0.020044~0.014321 (-28.55%) ↓	71.94~-10.75 (-114.94%) ↓
Desiccant Flow rate (L/s)	0.0025~100	0.684~0.000188 (-99.97%) ↓	-59.36~100.91 (-270.0%) ↓
Humid air flow speed (m/s)	0.025~2.4	0.001161~0.032843 (2728.70%) ↑	104.04~-21.075 (120.257%) ↑
Humid air temperature (°C)	25~40	0.006314~0.02138 (238.65) ↑	120.63~-426.84~39.09 (-67.594%) ↓
Humid air relative humidity (%)	10~95	-0.00386~0.022996 (-695.098%) ↓	118.88~-19.96 (116.792%) ↑

5.5 Experimental Testing

5.5.1 Test Rig and Dehumidifier Core

A test rig was set up to test the operation performance of the liquid desiccant dehumidifier employing the cellulose fibre pack as the carrier. Figure 5-14 is the schematic diagram showing the principle and layout of the test rig, and a view of the prototype test rig is presented in Figure 5-15. Temperature, humidity sensors and air flow meter are the same with equipments described in chapter 4. All sensors are distributed in the test rig as shown in figures 5-14 and 5-16. The environment air was treated in the temperature and humid air controller shown in figure 4-15 in Chapter 4, and required testing air stream was supplied to the dehumidifier test rig. Cooling system was installed to carry away the additional latent heat and sensible heat of humid/hot air. In this system, ground water or cooling tower is designed to produce cooling water to cool hot and strong desiccant.

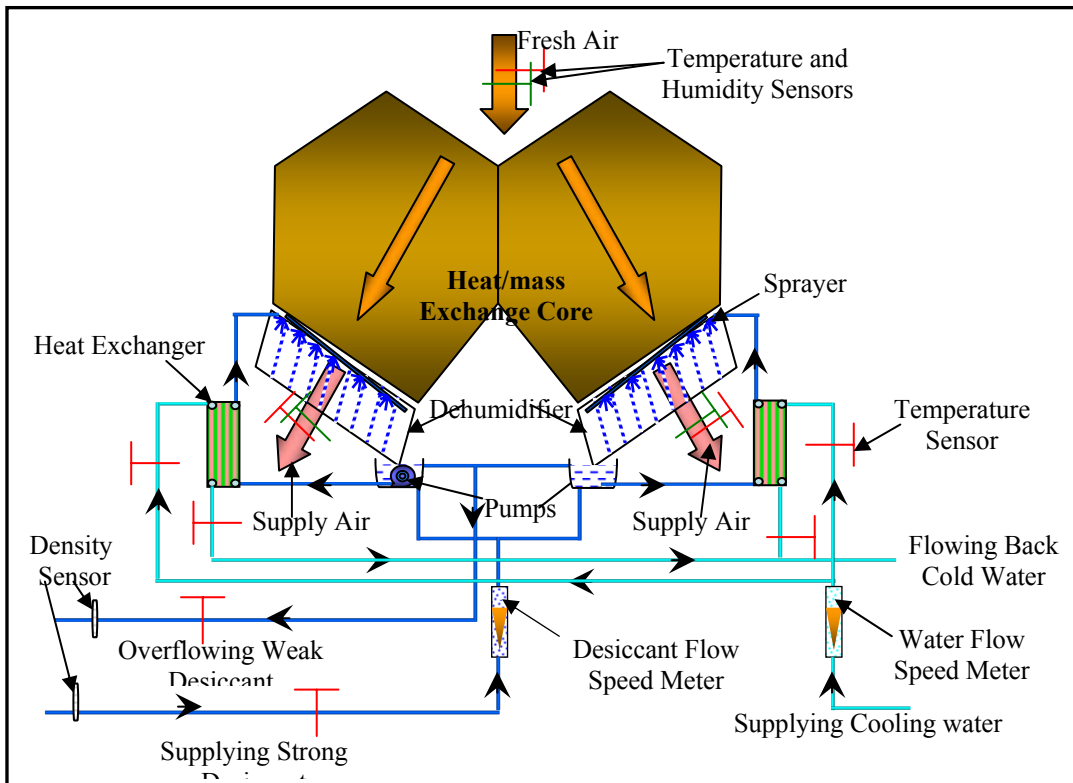


Figure 5-14 Schematic diagram showing the principle and layout of the test rig

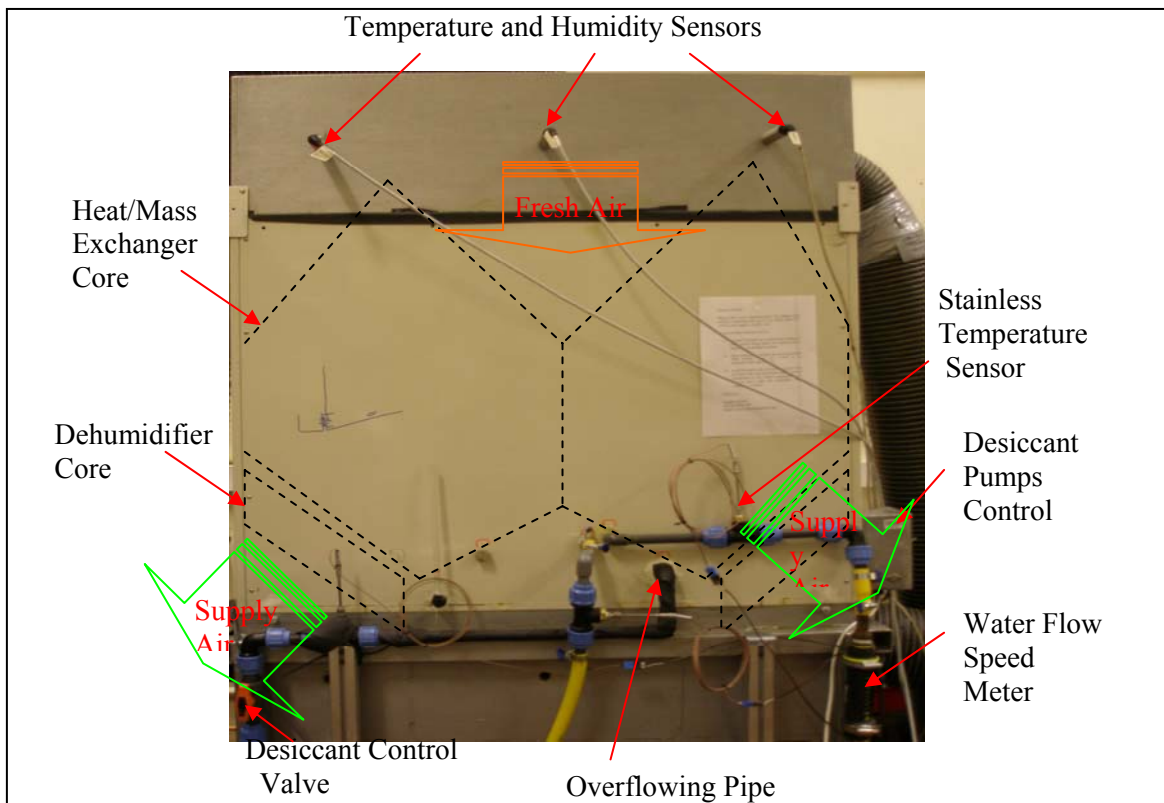


Figure 5-15 View of test rig — Liquid desiccant dehumidifier

It took 30~60 minutes to gain a steady air stream from the air controller, and about 30~40 minutes testing results were recorded in the computer (the computer record once per minute). The results used in these analyses are all the averages of each series testing results. It took 2~3 days to carry one series of testing regarding the air flow speed, air temperature and humidity, desiccant flow rate, concentration and temperature respectively.

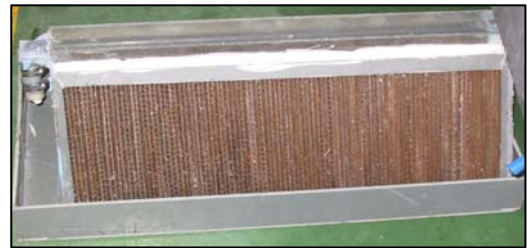
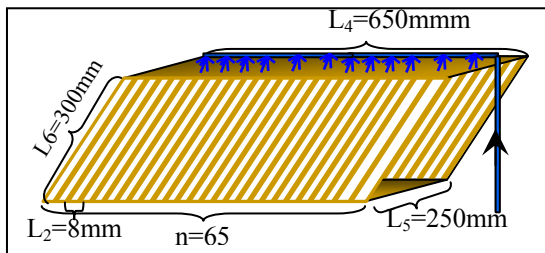


Figure 5-16 Schematic diagram of dehumidifier core Figure 5-17 Prototype of dehumidifier core

Figure 5-16 and 5-17 are the schematic diagram and prototype of the dehumidifier core utilized in this testing rig. The length of the core L_5 is 250mm, width L_4 is 650 mm and length L_6 is 300mm, and channel height is 8mm. Each channel is made of two fibre membranes investigated in Chapter 3 and the structure of each membrane is described in figure 5-1 (b).

5.5.2 Measuring Equipments

Owing to the strong causticity of the liquid desiccant, polythene or stainless pipes, sprayers, valves, and tanks, pumps were utilized in this system. All the sensors and related connecting components used in the test rig as shown in figures 5-14 and 5-15 were stainless. Stainless flat heat exchanger was employed to take the heat transfer between cooling water and hot desiccant. The same thermal anemometer shown in figure 4-13 was used in the dehumidifier performance testing.

Figure 5-18 is a floater flow meter to measure the liquid desiccant flow rate employing the gravity and flowing pressure. This kind floater meter must be installed vertically, and the measured liquid is clean. In general, the floater flow meter is calibrated at 20 °C according to

the water's density and dynamical viscosity. Hence, in this project, the observational results have to be rectified according to the liquid desiccant parameters. Equation 5-10 expresses accuracy fluid flow volume rate based one the observed value.

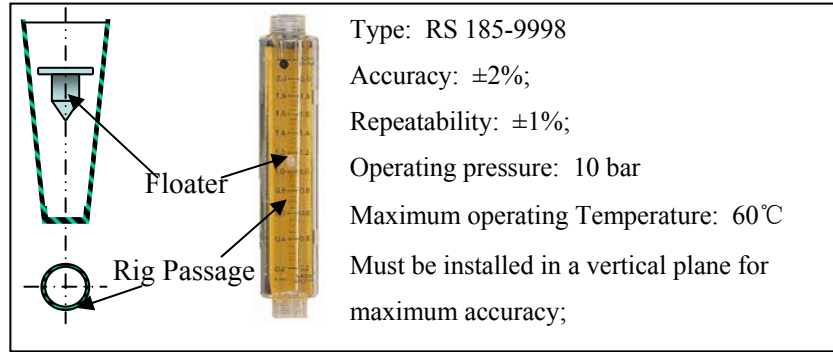


Figure 5-18 Schematic structure and view of liquid flow indicator



Figure 5-19 Stainless thermocouples



Figure 5-20 GP hydrometers

$$V_{fluid} = \omega_{floater} \omega \Delta F \sqrt{\frac{2g(m_{floater} - V'_{floater} \rho_{fluid})}{\rho_{fluid} F_{floater}}} \quad (5-10)$$

The volume flow rate of the liquid corresponds with the length scale on the cone outside wall. Then the regulated scale for the liquid desiccant to the water is expressed in the following equation:

$$V_d = V_{water} \sqrt{\frac{(m_{floater} - V'_{floater} \rho_d) \rho_{water}}{(m_{floater} - V'_{floater} \rho_{water}) \rho_d}} \quad (5-11)$$

For this water floater flow meter, the floater weight $G_{floater}$ is 2.1×10^{-3} kg, and the floater volume $V_{floater}$ is 0.25×10^{-6} m³.

The heat recovery effectiveness and moisture absorption capacity per litre solution per second are calculated through the equations 5-5 and 5-6 respectively and the testing errors are 6.7%, and 4.6% respectively (Law of Error Propagation) (A.A.Clifford, 1973)

5.5.3 Testing Results

From the numerical simulations, it has been concluded that desiccant solution flow rate, temperature and concentration, and humid air flow speed, temperature and humid affect the heat and mass transfer greatly. Hence, four series of experimental tests were carried out regarding these factors, when the dehumidifier core size was defined as described in figure 5-16.

Desiccant Temperature

Desiccant concentration in these series of tests were about 30% and corrected flow rate was 4.521×10^{-3} L/s. Humid air flow speed was controlled at 0.355m/s and the air temperature and relative humidity were in the range of 35~36°C and 65~68% respectively. Cooling water temperature was about 16~17°C and its flow rate was from 5 to 15L/min, corresponding desiccant temperatures were from 18°C to 26°C. The testing results are shown in Figure 5-21. Moisture absorption capacity and heat recovery effectiveness all increase with the desiccant temperature dropping and then decrease. In the desiccant temperature range of 22~24°C, we could gain the best dehumidification and cooling performance.

Humid Air Temperature

Desiccant solution flow rate, temperature and concentration were 4.521×10^{-3} L/s, 29°C and 24.5% respectively. Humid air flow speed was 0.885m/s and relative humidity varied from 50 to 60%. Changing the humid air temperature from 32.86~36.66°C resulting in the moisture content varying in the range of 0.014918~0.02035193 kg/kg dry air. The testing results are shown in the Figure 5-22. It was obvious that the moisture absorption capacity increases but heat recovery effectiveness decreases with the fresh air temperature increasing. For the fixed desiccant temperature, concentration, and fresh air relative humidity, when the fresh air temperature is

high, the vapour pressure is possible lower than the solution, which causes the moisture transferred from the desiccant to fresh air stream and negative moisture absorption capacity of the solution is gained as shown in Figure 5-22. With the fresh air temperature drops, the vapour pressure increasing results in the moisture transferred from the air side to the solution and positive absorption capacity. When fresh air temperature was higher than 33.4°C, moisture is evaporated out of the solution to the air stream causing latent heat absorbed from the solution and air stream. Therefore, the heat recovery effectiveness is high and positive. When the fresh air temperature is lower than 33.4°C, moisture is transferred in the contrary direction and latent heat is released into the air stream and solution resulting in the air temperature increasing and negative heat recovery effectiveness.

Humid Moisture Content

Desiccant solution flow rate, temperature and concentration were 4.521×10^{-3} L/s, 28°C and 29% respectively. Humid air flow speed was 0.356m/s and air temperature fluctuated around 35~35.7°C. Changing the air relative humidity from 19.96~67.80% resulted in the moisture content varying in the range of 0.0070706~0.0224536kg/kg dry air. Testing results are shown in Figure 5-23. Moisture absorption capacity increases but heat recovery effectiveness decreases with the fresh air relative humidity increasing. For the fixed desiccant temperature, the increasing fresh air relative humidity induces in high moisture content, which leads more moisture absorbed by per litre desiccant solution. However, with large numbers of moisture condensed into the solution, more latent heat is released to the fresh airflow and heats up the air temperature at some degree. Hence, when the cooling capacity of the solution could not cover the released latent heat, the heat recovery is negative as shown in Figure 5-23.

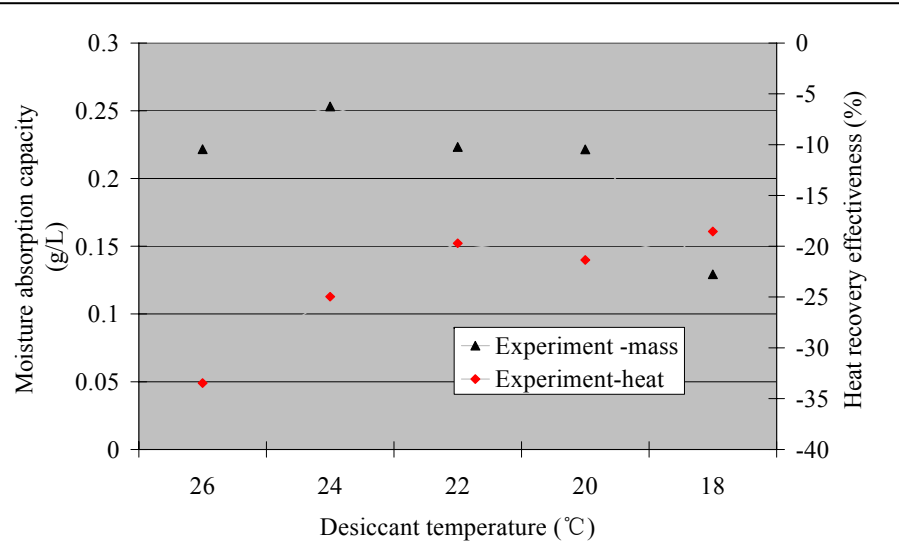
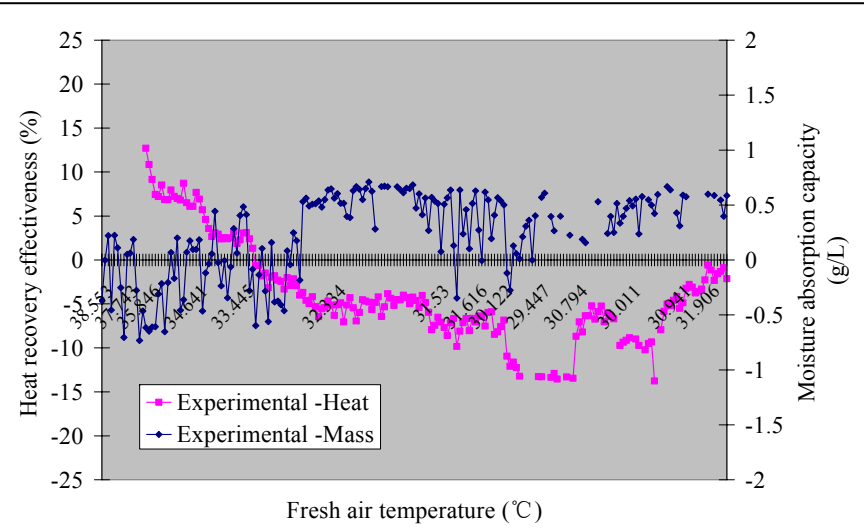


Figure 5-21 Dehumidification performance vs. desiccant temperature



Desiccant Concentration

Desiccant solution flow rate and temperature were 4.521×10^{-3} L/s and 29°C respectively. Humid air flow speed, temperature and relative humidity were 0.771 m/s, 35°C and 60%. Changing the desiccant solution concentration from 32.86~36.66%, results are presented in Figure 5-24. It is obvious that the dehumidifier core absorption capacity increases with the desiccant concentration increasing.

5.6 Comparisons between the Numerical Simulation and Testing Results

Four series of numerical simulation were carried out under the pre-set conditions according to experiments. The comparison results are shown in Figure 5-25 to 5-31

5.6.1 Desiccant Temperature Influence on Dehumidifier Performance

From the testing and simulation results shown in Figures 5-25 and 5-26, it can be found that the heat recovery effectiveness of testing results is closer to the simulation results than moisture absorption capacity. As mentioned in Chapter 3 that the fresh air temperature and humidity supplied from the air control system fluctuated in small ranges, this affects the testing results. Numerical simulation is carried out under the pre-set conditions, which is the average value of the tests, so there are contrast between the testing and modelling results.

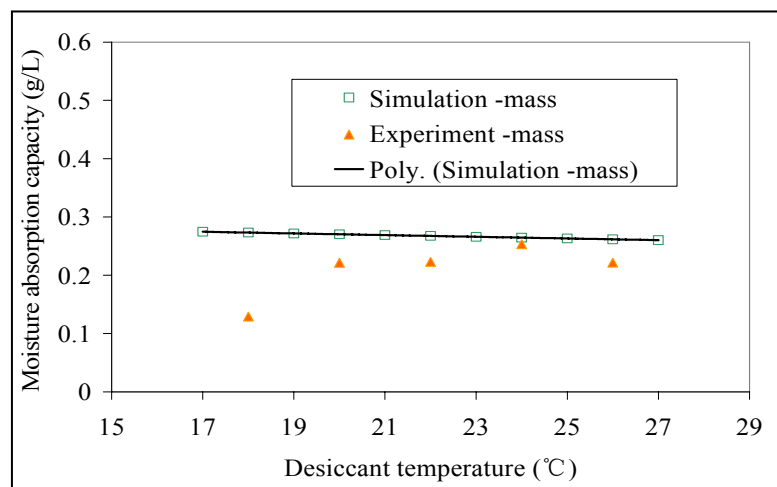


Figure 5-25 Comparison of testing and simulation results — moisture absorption capacity .vs. desiccant temperature

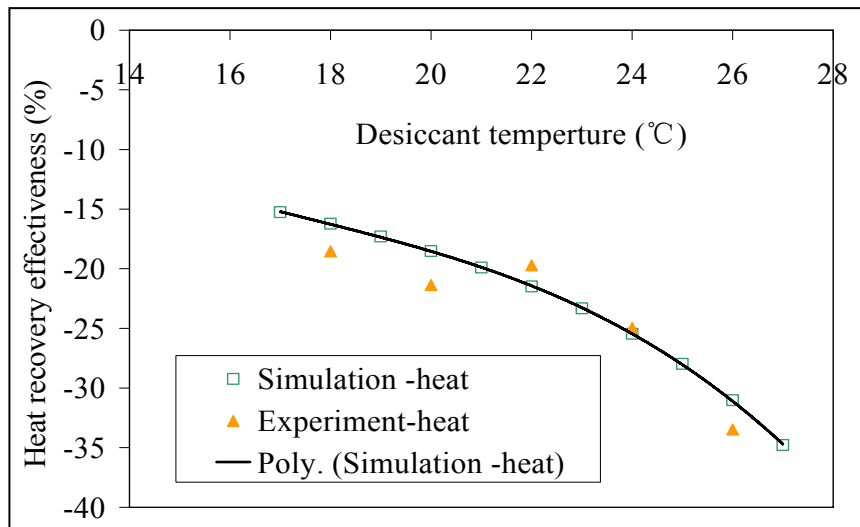


Figure 5-26 Comparison of testing and simulation results — heat recovery effectiveness .vs. desiccant temperature

5.6.2 Humid Air Temperature Influence on Dehumidifier Performance

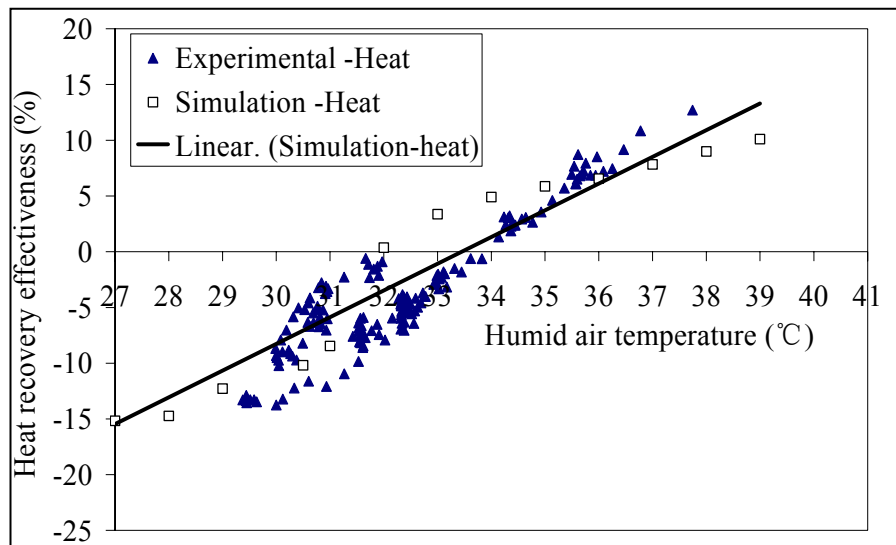


Figure 5-27 Comparison of testing and simulation results — heat recovery effectiveness .vs. humid air temperature

Comparison was made between experiential and simulation results. It was found that the experiment results fluctuated around the fitting curves of the simulation results as shown in Figures 5-27 and 5-28. And the numerical simulation and experimental results have the similar changing trend. This is because that the numerical simulations were carried under the pre-set conditions of steady moisture content and desiccant solution concentration, however, in the

testing, the moisture contents from the chamber were unsteady and the desiccant solution concentration also varied in a small range of 24.0~25%. All these factors make the testing results unfitting the modelling results perfect but fluctuating around it.

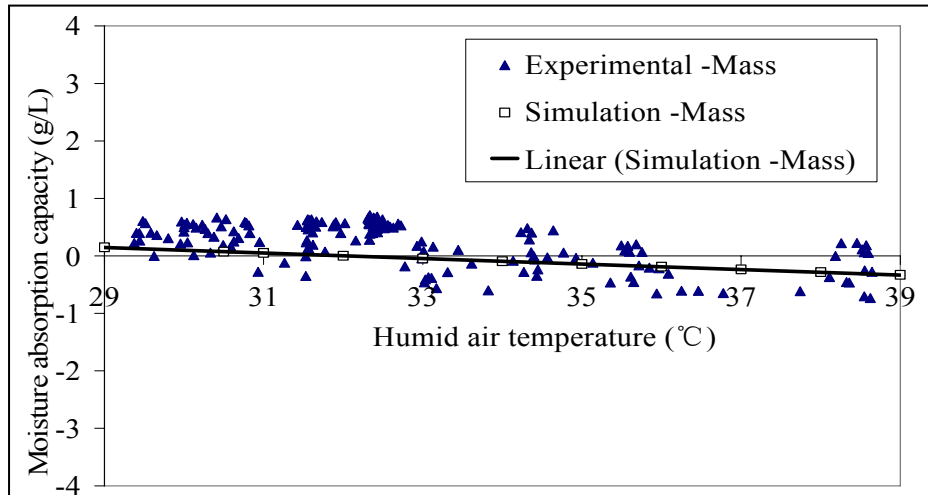


Figure 5-28 Comparison of testing and simulation results — moisture absorption capacity .vs. humid air temperature

5.6.3 Air Relative Humidity Influence on Dehumidifier Performance

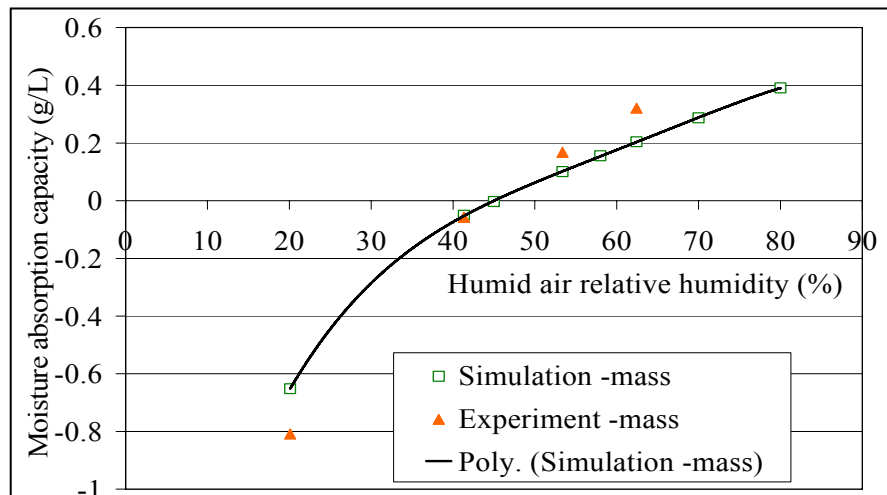


Figure 5-29 Comparison of testing and simulation results — moisture absorption capacity .vs. humid air relative humidity

In Figures 5-29 and 5-30, testing results of moisture absorption capacity and heat recovery effectiveness both are close to the simulation results. Only when the relative humidity of testing air is about 62.42%, the testing result is a little away from the simulation results. This is because

the pre-set desiccant concentration of the simulation was about 29%, but in the practical testing it reached 31% at the point of air relative humidity being 62.42%. This caused the higher moisture absorption capacity and heat recovery effectiveness.

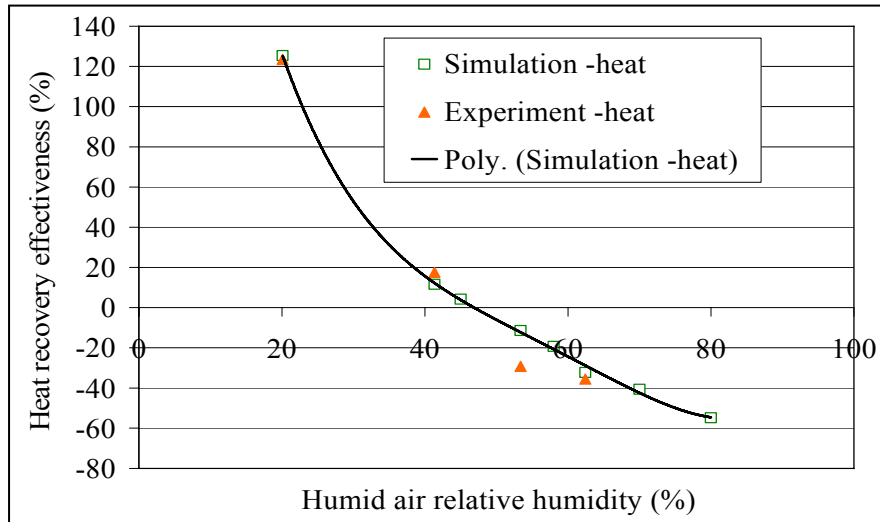


Figure 5-30 Comparison of testing and simulation results — heat recovery effectiveness .vs. humid air relative humidity

5.6.4 Desiccant Concentration Influence on Dehumidifier Performance

Numerical simulations were carried out under the similar pre-set air and solution conditions as the experiments and the comparisons results are shown in Figure 5-31

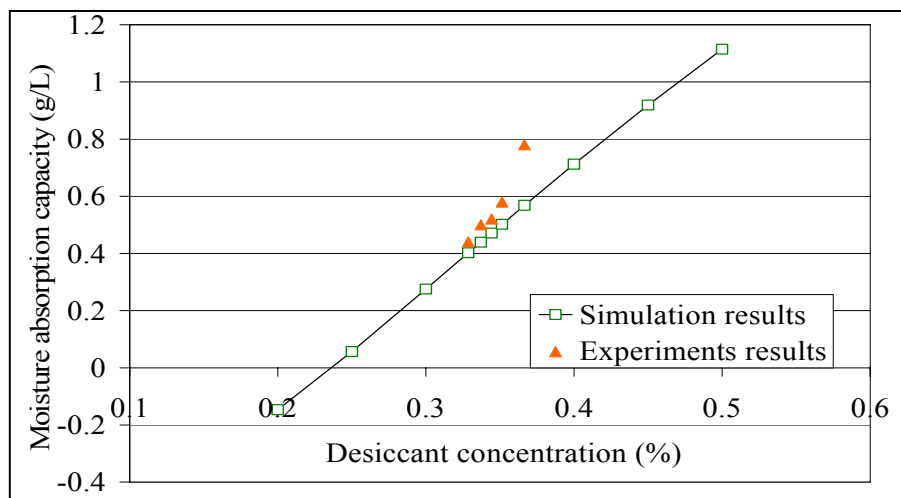


Figure 5-31 Comparison of testing and simulation results — moisture absorption capacity .vs. desiccant concentration

The moisture absorption capacity average difference between the experiments and modelling results is 14%, and the highest difference is 27.1%, which is caused by the unsteady humid air moisture content and temperature. As described in Chapter 3, the air humidity is controlled by a water valve and electrical controller, which supplies air stream with the moisture content and temperature changing in a small fluctuant range. But in the simulation the fixed air temperature and humidity were assumed, when the average moisture contents were higher than the values in the testing, the simulation results will be higher than the simulation one.

5.6.5 Reasons for the Difference between Simulations and Testing Results

From the comparison of the testing and numerical simulation results on the aspects of desiccant concentration, temperature and humid air temperature and relative humidity, it can be concluded that the simulation results are in a general agreement with the testing results. However, there are still some small difference between the simulation and experimental results, which are caused by the following reasons:

- (1) Average values of testing conditions were employed into the simulations, which caused results different from the testing in some degree;
- (2) The air flowing keeps a small angle with the desiccant falling direction in the practical testing, however, for predigesting it was assumed parallel in the numerical simulation. This induces the errors between the simulation and testing results;
- (3) Assumptions made before set-up the modelling possibly impact the testing results;
- (4) The simulation accuracy limit affects the simulation results;
- (5) When doing the test, all the parameters such as cooling water temperature, desiccant concentration, temperature and flow rate, air stream flow speed, temperature and humidity are variations. Testing errors may cause the difference from the numerical simulation.

The first two reasons are the main influencing factors, and the first one is unavoidable, the second one can be improved in the further research. Although there are difference between the numerical and testing results, the errors in the acceptable range. So, the numerical model is capable to predict operation characteristics of the dehumidifier and can be employed in Chapter 7 to predict the thermal performance of the whole system.

5.7 Summary

A numerical simulation was developed based on the pre-designed dehumidifier core shape. The numerical model has been proven to give a reasonable accuracy for predicting dehumidifier operation characteristics. Numerical simulations were carried out regarding the following six factors in the dehumidification performance: Desiccant solution sorts (LiCl, LiBr and CaCl₂), dehumidifier core channel size (height and length), solution concentration, temperature and flow rate, and air stream temperature, humidity and flow speed.

It was concluded based on the simulation results that:

- Under the same pre-set simulation assumptions, LiCl solution performs better absorption capacity than other two kind solutions, but lowest heat recovery effectiveness.
- Under the same pre-set simulation assumptions, to gain the same absorption capacity $\varepsilon_{De}^{moisture} = 0.0125$ g/L, at 29°C, LiCl solution concentration is 30%, LiBr solution is 50% and CaCl₂ is over 55%. Absorption capacity of the three solutions increases and heat recovery effectiveness decreases with the solution concentration increasing.
- Dehumidifier channel height affects heat recovery effectiveness more heavily than moisture absorption. Under the pre-set air and desiccant solution conditions, when the channel height is 25mm, the heat recovery effectiveness reaches the highest value of 47.22%, and when it is 35mm, the moisture absorption achieves the highest value of

0.027236. For gaining the desired supplying air as well as high heat/mass transfer performance, the channel height is preferable in the range of 10~15mm.

- Moisture absorption capacity and heat recovery effectiveness changes in the contrary direction with the channel length rising. Under the pre-set air and desiccant solution conditions, channel length in the range of 0.2~0.3m is the preferred size to obtain good moisture absorption and heat recovery as well as supplying air.
- Moisture absorption capacity and heat recovery effectiveness both decrease with desiccant temperature increasing. When the desiccant temperature is higher than the air dew point temperature, it can still offer an acceptable absorption capacity. This indicates that cooling tower can offer the cooling source for the hot strong solution.
- Moisture absorption capacity declines and heat recovery effectiveness increases with the desiccant flow rate increasing. Desiccant flow rates changing from 0 to 4.8L/s impacts the moisture absorption and heat recovery effectiveness greatly, and influences on the latter more. Hence it is concluded from the figures 5-9 and 5-10 that desiccant flow rates from 0.01L/s to 0.1L/s afford excellent dehumidification and cooling performance as well as satisfying supplying air.
- Increasing the air flow speed enhances the moisture and heat transfer load to the fixed desiccant solution and results in higher moisture absorption capacity and lower sensible heat recovery effectiveness. For the desiccant absorption capacity $\varepsilon_{De}^{moisture} = \rho_f v_f (d_f - d_s) / L_d$ based on the defined desiccant solution flow rate, temperature and concentration, L_d is fixed, increasing the air flow speed v_f leads $\varepsilon_{De}^{moisture}$ being improved.
- Under fixed air relative humidity, increasing air temperature results in higher moisture content, which strengthens the absorption ability per litre solution. When air temperature and its vapour pressure are lower than desiccant solution, moisture transfers from solution to air steam and if the evaporative latent heat fetches up the transferred

sensible heat to the air, air temperature is reduced, otherwise it is increased. When air temperature is higher and its vapour pressure is lower than desiccant solution, moisture moves from solution to air, evaporative latent heat is absorbed from air and its temperature is reduced by some degree. When air temperature and vapour pressure are both higher than solution, moisture and sensible heat both transfer to desiccant solution. The air temperature is increased when the transferred out sensible heat can't over take the absorbed condensed latent heat.

- Increasing the moisture content results in the higher moisture load to the fixed desiccant solution, this enhances the solution's absorption capacity. More absorbed moisture increases the condensate latent heat released to the air and reduces the heat recovery effectiveness.

Hence, for a defined air flow, a lower desiccant temperature, higher flow rate and concentration with the appropriate dehumidifier core channel height and length will achieve an excellent supply air with a good moisture absorption capacity and heat recovery effectiveness.

Laboratory testing was carried to investigate the operating characteristics of a dehumidifier. Fours series of tests were operated according to the influencing factors to dehumidifier: desiccant concentration, temperature, and air temperature, relative humidity.

Comparison between numerical predications and testing results were carried out. It was found that the results from tests are in general agreement to the numerical prediction when the simulation assumptions were close to the testing conditions. Ignoring the slight errors caused by the numerical simulation pre-set conditions and assumptions, the unsteady air control system and desiccant solution concentration, the testing results proved the validity of the numerical modelling, which can be employed in the theoretical model in Chapter 7.

Chapter 6. Performance Investigations of Desiccant Regenerator

6.1 Introduction

In Chapter 5, the performances of liquid desiccant dehumidifier have been investigated by the methods of numerical simulation and experimental testing. It was found that the fibre core dehumidifier could progress a good dehumidification, as well as a cooling performance. However, the solution was diluted by the humid air and needed to be regenerated before circle using. This chapter focuses on the performances of the regenerator, and the optimal solution and regeneration capacity, as well as running conditions, will be defined.

As described in Chapter 1, solar energy is purposed to offer the regeneration energy. Investigations have proved that a solar water collector could service hot water above 80°C, which is the highest water temperature requirement for this research. Therefore, the solar water collector is not the main aim of this project, and is substituted by an electrical boiler in the practical testing.

An air-to-air cross flow exchanger is employed in the regenerator to save energy from the exiting air. The proper size and ratio of its width to length is defined by the numerical simulations, which are proved in acceptable errors by experimental results.

Three desiccant solutions were invested in Chapter 5, and it was found that the LiCl solution produced a higher absorption capacity in the concentration range of 35% ~ 65%. In this chapter, the regeneration performances of three solutions are revealed, and the optimal absorbent is ascertained by interactively considering the dehumidification and regeneration capacity. The relationships between the regeneration capacity with the regenerator structure and size, fresh air and desiccant solution parameters, and hot water temperature and flow rate were investigated by numerical simulations and experimental testing.

6.2 Description of the Regenerator and Working Mathematical Theory

6.2.1 Description of the Regenerator

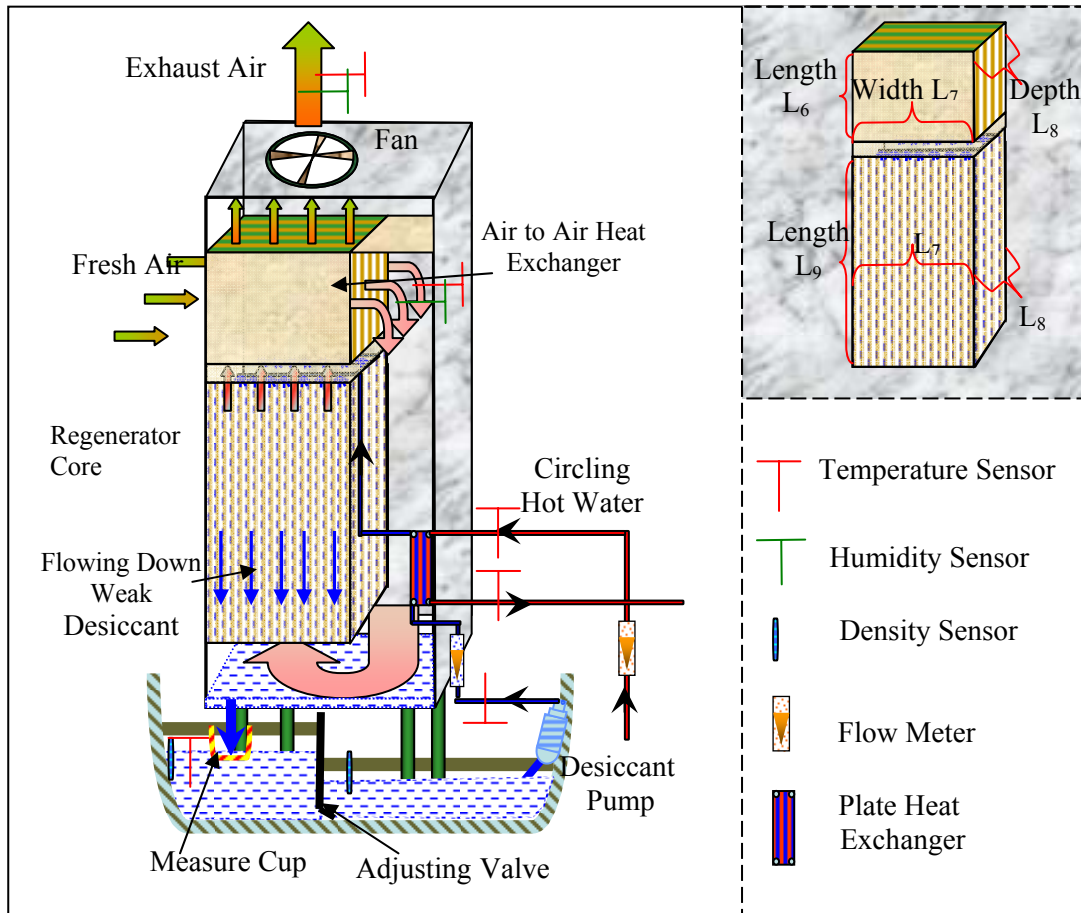


Figure 6-1 Sketch diagram of the desiccant regenerator

Figure 6-1 shows the structure of the desiccant regenerator, which is constituted of an air-to-air heat exchanger, a cellulose fibre regenerator core, and a solution circle/sink and heating water circle. For the solution circle, weak desiccant coming back from the dehumidifier is heated up by the hot water in the flat heat exchanger, and then is pumped to the top of the cellulose regenerator core. During the weak and hot solution is proportionally sprayed and falls down along the cellulose fibre membranes, moisture and sensible heat are transferred into the flowing upward air stream. Finally, the concentrated solution is collected into the storage sink and supplied again to the dehumidifier. For the air circle, the environment air is forced through the air-to-air heat exchanger, recovers sensible heat from the exiting air, and then flows through the

tunnel in the right side of the regenerator to the bottom of the core. Then the preheated air stream moves upward through the cellulose core channel and absorbs moisture and heat from the falling down solution film. Finally the hot and humid air stream existing out regenerator core release sensible heat to the incoming environment air in the air-to-air exchanger and exist out. Solar energy is proposed to provide the heating energy, but for simplifying the testing rig, an electrical heater replaced the solar collector.

6.2.2 Mass and Heat Transfer between Air Stream and Desiccant Film

Regenerating the dilute solution is a reversion progress of dehumidification. Hence, its sensible and mass transfer mechanism is similar to the dehumidification, and the calculating equations are the same as the equations used in the dehumidifier model. However, there is a more accurate calculating method for the convective mass-transfer coefficient k^l , which is suitable for the falling down wetted-wall columns mass transfer. In this wetted-wall column, the air stream moves upwards from the bottom of the tube, as shown in Figure 6-2, which is similar to the air and the solution contacting way in this regenerator. Vivian and Peaceman developed a correlation correction for the convective mass transfer coefficient of this gaseous solute into a falling liquid film, evenly wetting the inner surface of a tube, based on the equations 3-5, 3-12, and 3-13, expressed in Chapter 3. The developed equation for k^l is as the following (J.R.Welty, et al, 2000):

$$k^l = 0.433(Sc)^{1/2} \left(\frac{\rho_{fluid}^2 g z^3}{\mu_{fluid}^2} \right)^{1/6} (Re)^{0.4} \frac{D_{AB}}{z} \quad (6-1)$$

$$Re = \frac{4m_{fluid}}{\pi D \mu_{fluid}} \quad (6-2)$$

$$Sc = \frac{\mu_{fluid}}{\rho_{fluid} D_{AB}} \quad (6-3)$$

6.2.3 Performance Definition of the Regenerator

The sensible heat recovery effectiveness of the air-to-air cross-flow cellulose fibre exchanger is expressed as:

$$\varepsilon_{Cr}^{Se} = (t_s - t_f) / (t_e - t_f) \quad (6-4)$$

The moisture evaporated out from the dilute solution, per kilojoules, is defined as the regeneration capacity of the regenerator as shown in the following equation:

$$\varepsilon_{Re}^{moisture} = m_{desorb}^{moisture} / Q_{hot} \quad (6-5)$$

$$m_{desorb}^{moisture} = \rho_{weak} V_{weak} (\theta_{strong} - \theta_{weak}) / \theta_{strong} \quad (6-6)$$

$$Q_{hot} = c_{water} m_{hot} (t_{hot}^{in} - t_{hot}^{out}) \quad (6-7)$$

Counter-flow plate heat exchanger effectiveness is defined as the following:

$$\eta = \frac{C_{weak} (T_{weak}^{out} - T_{weak}^{in})}{C_{min} (T_{hot}^{in} - T_{weak}^{in})} = \frac{C_{hot} (T_{hot}^{in} - T_{hot}^{out})}{C_{min} (T_{hot}^{in} - T_{weak}^{in})} \quad (6-8)$$

6.3 Numerical Model

The regeneration core is similar to the dehumidifier core in the manufacturing material and structure, except for its' size being enlarged, and the air stream flowing in the contrary direction to the solution falling down route, which is parallel in the dehumidifier. As pointed out in section 6.2.2, the convective mass-transfer coefficient is corrected to meet the changing of air flow direction. Therefore, the numerical simulation method of the regenerator core is similar to the dehumidifier and its channel distribution and simulation assumptions are all the same as the dehumidifier model. Therefore, only the air-to-air heat exchanger simulation method is to be detailed in section 6.3.1.

6.3.1 Channel Distribution and Assumptions of Air-to-Air Cross-flow Exchanger

From the figure 6-1, it can be seen that the air-to-air heat exchanger is designed to save energy from the exhaust air, so its performance details are investigated. The environment air flows in a cross-direction with the exhaust air. The calculating grids are distributed as shown in Figure 6-3.

The calculating cell size is $0.01 \times 0.01 \text{m}^2$, there are a total of $m \times n$ pieces of calculating cells in each layer, and the layer number, $s = L_8 / H_3$, of the air-to-air exchanger is decided by the depth L_8 of the core and the channel height H_3 between the two layers. The heat balance calculation of each cell is the same as the heat exchange modelling in Chapter 4. The fresh air channel length is L_7 and the exhaust air is L_6 .

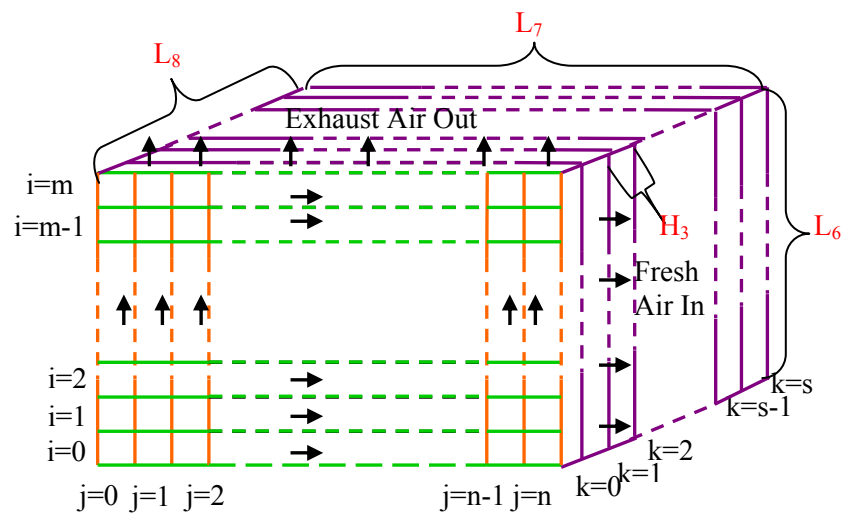
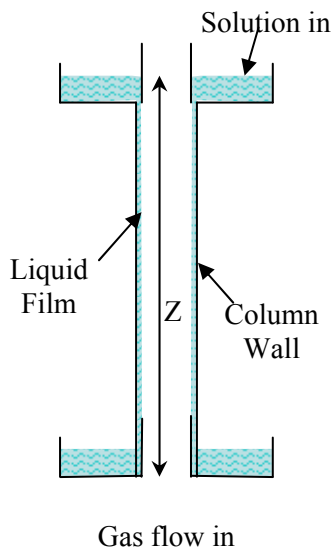


Figure 6-2 Wetted - wall column for mass transfer between gas and liquid Figure 6-3 Calculating cell sketch diagram of air-to-air heat exchanger

In this three-dimensional model, the fresh air and exhaust air only have a cross sensible heat exchange through the cellulose fibre membranes. To simplify the numerical simulation, assumptions were made as following:

- The fresh and exhaust air flow speed, temperature, and moisture content, at the start of each channel are assumed to be the same respectively.
- Heat transfer occurs vertically between the fibre paper membranes and airflow speed, and no heat transfers along the airflow direction.
- In each solution section, each cell has a uniform membrane surface, and the fresh and exhaust air have a uniform temperature respectively.
- The exhaust air has the same volume flow speed as the fresh air.

6.3.2 Simulation Base Conditions for Air-to-Air Heat Exchanger

The pre-set conditions for carrying numerical simulations are presented as following:

- Channel size of cellulose fibre exchanger: length L_6 was 0.5m, width L_7 was 0.6m, and depth L_8 was 0.5m respectively, channel height H_3 was 5mm.
- Cellulose fibre thickness was 0.3mm, and thermal conductivity was 0.5W/m ·K.
- Fresh air flow rate was 540m³/h.
- Fresh and exhaust air temperature and relative humidity were 35°C and 40°C and relative humidity was 50% and 70% respectively.

6.3.3 Air-to-Air Heat Exchanger Modelling Results

I . Influence of Exchanger Size on Recovery Effectiveness

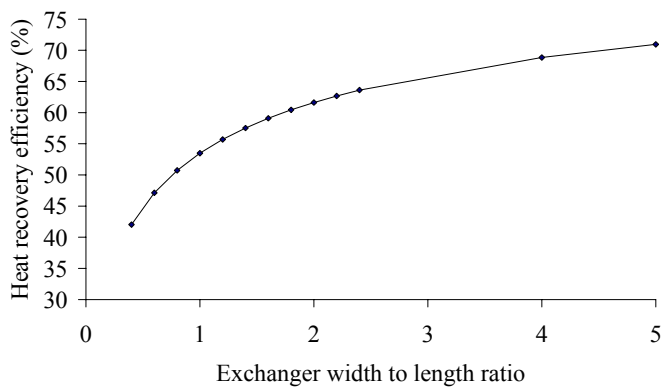


Figure 6-4 Heat recovery efficiency vs. ratio of fresh air to exhaust air channel length

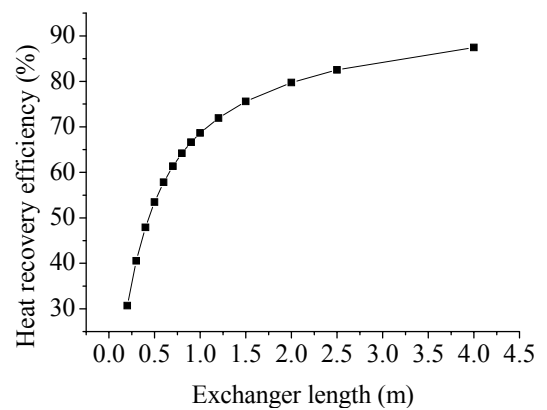


Figure 6-5 Heat recovery efficiency vs. exhaust and fresh air channel length

Exhaust air existing out of the regenerator core was 40°C and the fresh air was kept at 35°C.

Changing the exchanger width L_7 from 0.2 to 1.2 m, and keeping the other parameters unvaried, the simulation results are presented in Figure 6-4. Keeping the width to length ratio 1:1 unchanged, and increasing the exchanger size in the length and width, the simulation results are displayed in Figure 6-5.

From the Figure 6-4 and 6-5, it can be seen that the air-to-air heat exchange efficiency increases when the exchanger size is enlarged. High channel length ratio of fresh air to exhaust air induces high recovery efficiency. However, when the exhaust air channel is too short, only increasing the fresh air channel length can not improve the heat recovery efficiency greatly. Hence, to gain a high recovery efficiency it is necessary to increase the channel length in both the fresh and exhaust air sides, and to save as much energy from the exhaust air, the fresh air channel should be longer than the exhaust air. For this case, when the fresh air channel size is 1.0 m and the fresh to exhaust air channel length ratio is 1.0~2.0, the air-to-air heat exchanger will save the most energy as possible from the exhaust air effectively with a compact size.

II. Impact of Air Flow Rate and Temperature on Recovery Effectiveness

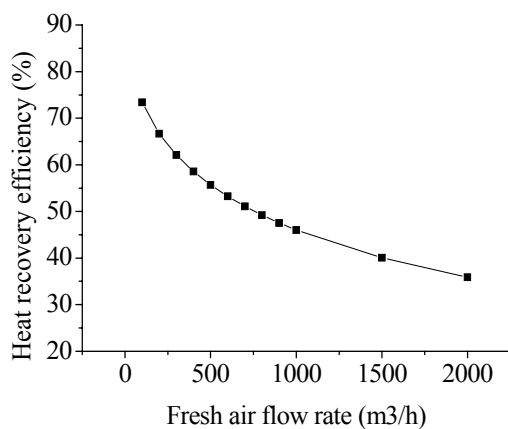


Figure 6-6 Heat recovery efficiency vs. air flow speed

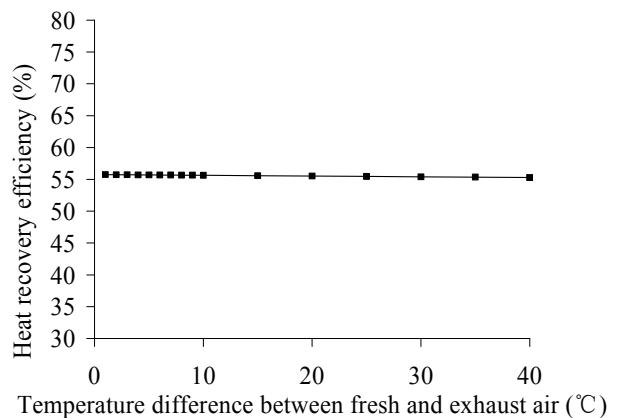


Figure 6-7 Heat recovery efficiency vs. air temperature

- (1) By keeping the exchanger size and air temperature unchanged, and varying the air flow rate from 100 to 2000m³/h, gave the simulation results shown in Figure 6-6.
- (2) Keeping the exchanger size, fresh air temperature, and flow speed unvaried, changing the exhaust air temperature from 36°C to 75°C, gave the simulation results shown in Figure 6-7.

Heat recovery efficiency decreases heavily with the air flow speed increasing, but when the air flow rate is over 1000m³/h, the decreasing trend becomes slower as shown in figure 6-6.

Results presented in figure 6-7 indicated that the air temperature difference between fresh air and exhaust air slightly influences the heat recovery efficiency.

III. Influence of Materials' Thermal Conductivity

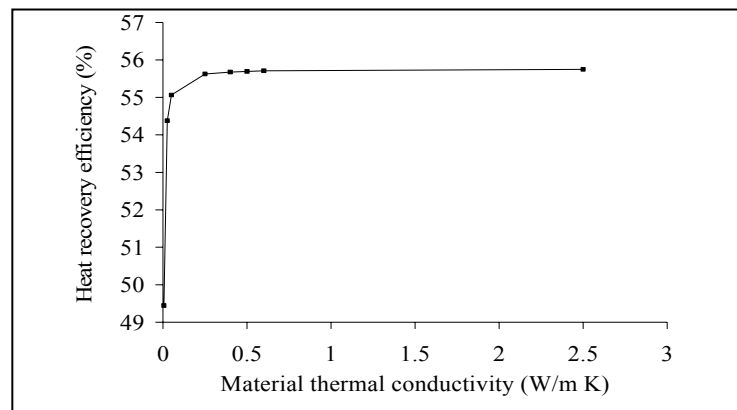


Figure 6-8 Heat recovery efficiency vs. material thermal conductivity

Unchanging any base conditions of the air-to-air exchanger, the materials' thermal conductivity was changed from 0.0025 to 2.5W/mK. Simulation results indicate that the thermal conductivity influences the heat recovery efficiency slightly when it is over 0.25W/mK, as shown in Figure 6-8. Hence, both fibre paper and metal perform the similar recovery efficiency for the same designed exchanger. Therefore, in this case, the paper is the preferred material to reduce the cost as well as the manufacturing difficulty. These numerical simulation results verify the theoretical analysis in Chapter 3. Thermal conductivity played an inessential effect on the sensible heat exchanger in the air-to-air exchanger, compared with convective heat exchange.

6.3.4 Simulation Base Conditions for the Regenerator

- The regenerator core length L_9 was 0.8m, and the width L_7 , depth L_8 was 0.5m and 0.6m, the same as the air-to-air heat exchanger, and the channel height H_3 was 8mm.
- The fresh air temperature was 35°C, relative humidity was 30%, and the flow rate was 540m³/h.
- Hot water temperature from the solar collector was 60°C and flow rate was 0.2L/s.

- The heat exchanger effectiveness of the desiccant to the water plate heat exchanger was 0.8.
- Table 6.1 shows the solutions' flow speed, concentration, and temperature, Henry's law constant was set for simulations.

Table 6.1 Parameters of three kinds of desiccant solutions

Desiccant solution	Temperature (°C)	Mass Concentration (%)	Desiccant flow Rate (l/s)	Henry's law constant (Appendix III)
LiCl+H ₂ O	35	25	0.25	$-0.00256t^2 + 0.86125t + 67$
LiBr+H ₂ O	35	35	0.25	$-6.25 \times 10^{-4}t^2 + 0.2125t + 58$
CaCl+H ₂ O	35	45	0.25	$0.995t + 59.5$

6.3.5 Regenerator Modelling Results

I . Influence of Desiccant Solution Concentration Regeneration Capacity

Keeping the pre-set simulations, such as fresh air temperature 35°C, and relative humidity 30%, the regenerator size and structure, desiccant temperature, and hot water temperature and flow rate unchanged, and varying the desiccant solution concentration from 15% to 40%, gave three kinds of solutions simulation results, which are presented in Figure 6-9.

CaCl₂ gives the best regeneration capacity with the regeneration temperature at about 68°C, and LiBr performs better than LiCl when its concentration is over 27.5%, but needs the highest regeneration temperature to be at about 69.5°C. From the simulation results presented in Figure 5-4 in Chapter 5, it is obvious that for the same dehumidification capacity $\varepsilon_{Re}^{moisture} = 0.0125 \text{ g/L}$, the LiCl solution concentration is about 30%, LiBr is 50% and CaCl₂ is 55%. If they absorbed the same moisture from the humid air in the dehumidifier, and their concentrations were reduced to about 25%, 45% and 50% respectively, the LiCl solution would have the best regeneration capacity, as shown in figure 6-9. Furthermore, the LiCl solution requires the lowest hot water temperature at 60°C, which is conveniently gained from the solar collector. To achieve the same effective regeneration capacity, LiBr needs the hot water temperature to be

80°C, and CaCl₂ needs the hot water temperature to be at least 75°C, which requires a highly effective solar collector and solar radiation. Therefore, LiCl is the preferred solution in our simulations and experiments, and the investigation results are detailed in the following sections.

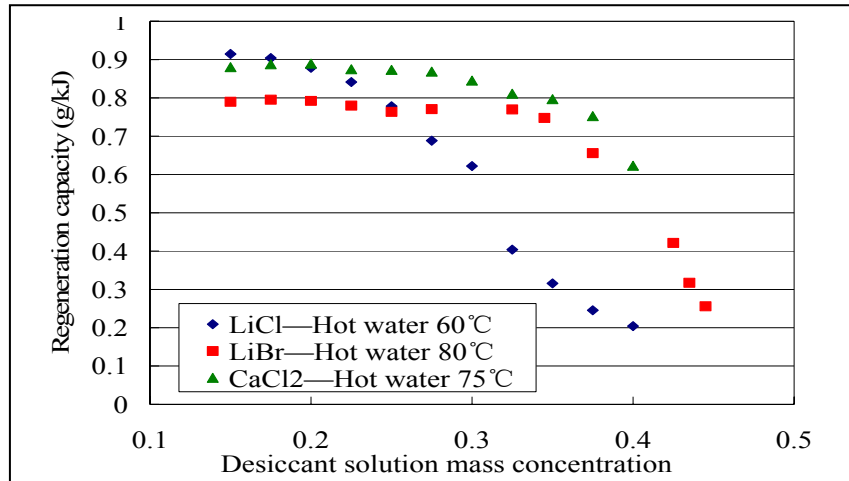


Figure 6-9 Regeneration capacity vs. desiccant solution mass concentration

II. Influence of Channel Length on the Regeneration Capacity

Changing the channel length from 0.4 to 3m, and keeping the other conditions, such as the fresh air temperature and the relative humidity, the desiccant temperature and concentration, and hot water temperature and flow rate were unvaried.

Figure 6-10 indicates that the regeneration capacity and condensed solution concentration both increase slightly with the regenerator channel length increase. Lengthening the channel, results in enlarging the contact surface between the fresh air stream and the solution film. However, for the fixed fresh air temperature, humidity, flow speed and desiccant temperature, concentration and flow rate, the vapor pressure difference between them is defined. With the air flowing along the channel, superfluous moisture is absorbed gradually into the desiccant film, and the vapor pressure difference is depressed, which induces less moisture is transferred. When the channel is over 1m, the vapor pressure in air stream is close to the one in solution and the

regeneration capacity improves very slowly. A proper channel length of 1m. is selected to achieve a compact regenerator core with a higher regeneration capacity.

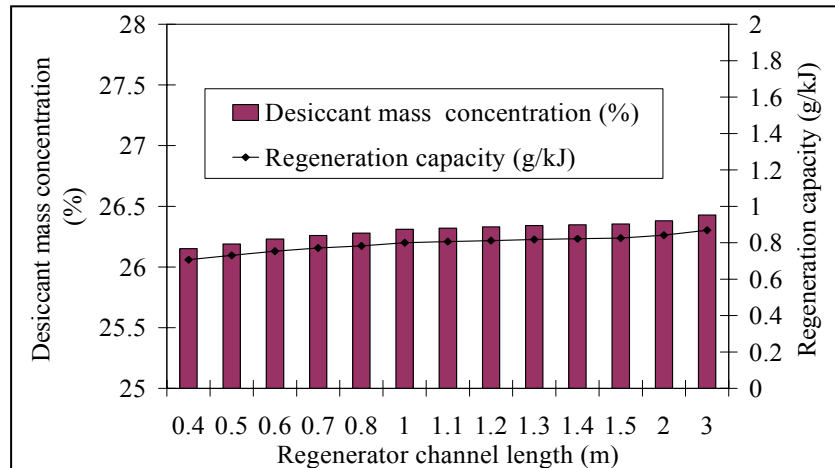


Figure 6-10 Regeneration capacity vs. channel length

III. The Influence of Channel Height on Regeneration Capacity

Changing the channel height from 2 to 15mm, and keeping the other conditions, such as the fresh air temperature and relative humidity, the desiccant temperature and concentration, and the hot water temperature and flow rate are unvaried.

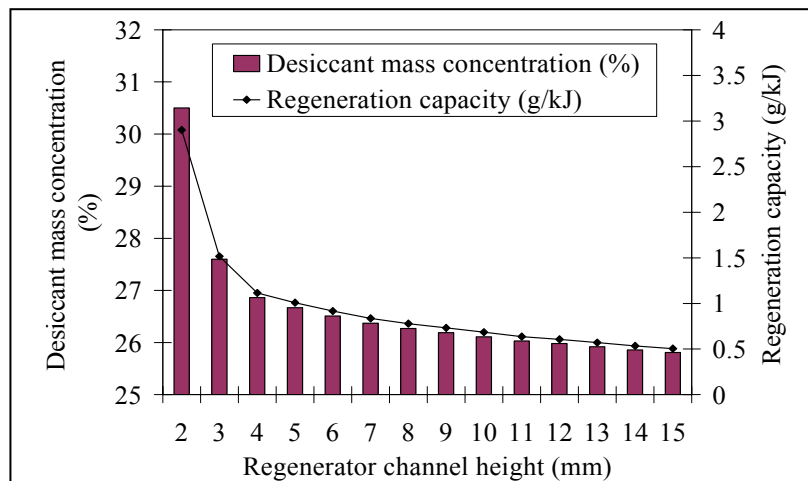


Figure 6-11 Regeneration capacity vs. channel height

It can be seen in Figure 6-11, that the regeneration capacity and the condensed solution concentration both decrease heavily with the regeneration channel height increasing. From

equation 6-1 and 6-2, it is known that a lower channel height results in a higher convective mass transfer coefficient, which results in a higher amount of moisture evaporated. For the fixed solution and hot water temperature and flow rate, the increase of the evaporated moisture leads to the higher regeneration capacity. However, a lower channel height causes higher airflow resistance, and manufacturing difficulties. A channel height of about 5~8mm is preferred for a fiber regenerator core, which could be manufactured of fiber paper conveniently with a relative lower frictional resistance.

IV. Influence of Desiccant Temperature on Regeneration Capacity

Keeping the pre-set conditions, such as fresh air parameters and flow speed, regenerator core size, hot water flow rate/temperature, and desiccant solution concentration/flow rate unchanged, varying the desiccant temperature from 28 to 55°C, gave the simulation results shown in Figure 6-12.

The regeneration capacity increases, with the desiccant temperature increasing sharply, when its temperature is over 50°C, but the condensed desiccant concentration rises at a small quantity, as shown in figure 6-12. For a fixed supply of hot water (with the temperature and flow rate unchanged), increasing the desiccant temperature will decrease the hot energy consumed, and also increase the desiccant temperature leaving the heat exchanger. A higher desiccant temperature induces high vapor pressure, which enhances the moisture evaporated out. As expressed in equation 6-5, more evaporated moisture $m_{moisture}$ and less consumed energy Q_{hot} results in a higher regeneration capacity $\varepsilon_{Re}^{moisture}$. For a defined hot water source and flat-plate exchanger, when the solution mass multiplying the thermal capacity C_{weak} is smaller than the hot water C_{water} , the consumed energy is slightly affected by the cold weak solution temperature T_{weak}^{in} , as shown in equation 6-8. Hence, the desiccant temperature out of heat

exchanger is increased by some degree, which induces evaporation moisture improved by a small amount. Therefore the condensed desiccant solution concentration increases with the cold weak solution temperature increasing slowly.

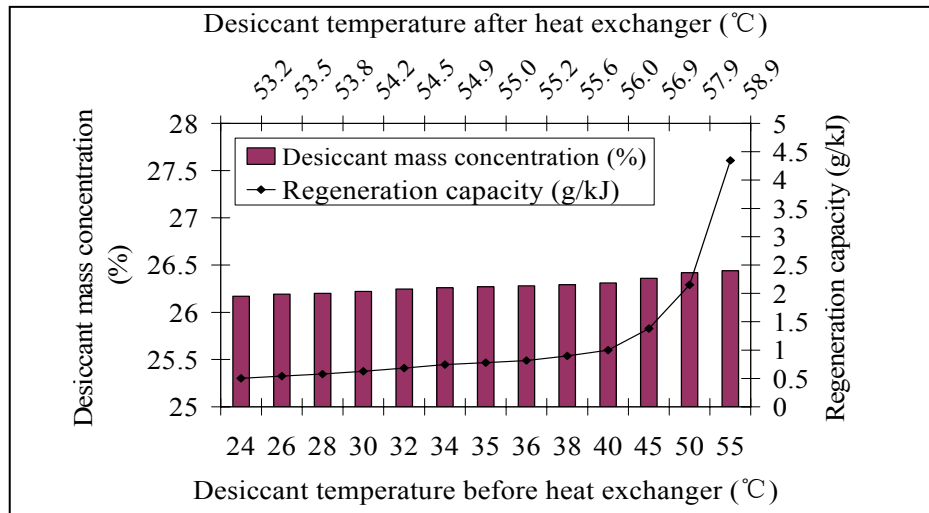


Figure 6-12 Regeneration capacity vs. desiccant temperature

V. Influence of Desiccant Flow Rate on Regeneration Capacity

When changing the desiccant flow rate from 0.1 to 0.6L/s, and keeping the other pre-conditions unvaried, the relationship between the regeneration capacity and the desiccant flow rate is presented in Figure 6-13.

The condensed desiccant mass concentration and the regeneration capacity both decrease with the desiccant flow rate increasing. For a fixed hot water source, the increasing desiccant solution flow rate results in a lower desiccant temperature. This depresses the vapour pressure in the solution, leading to the depressed moisture evaporating. At the same time, the increasing desiccant flow rate decreases its contact time with the airflow in the regenerator core. This causes the evaporated moisture to decrease. Hence, for the defined regenerator and hot water source, the increasing desiccant flow rate induces the declining condensed desiccant mass concentration and regeneration capacity. Therefore, a lower desiccant flow rate is preferred for a good regeneration performance.

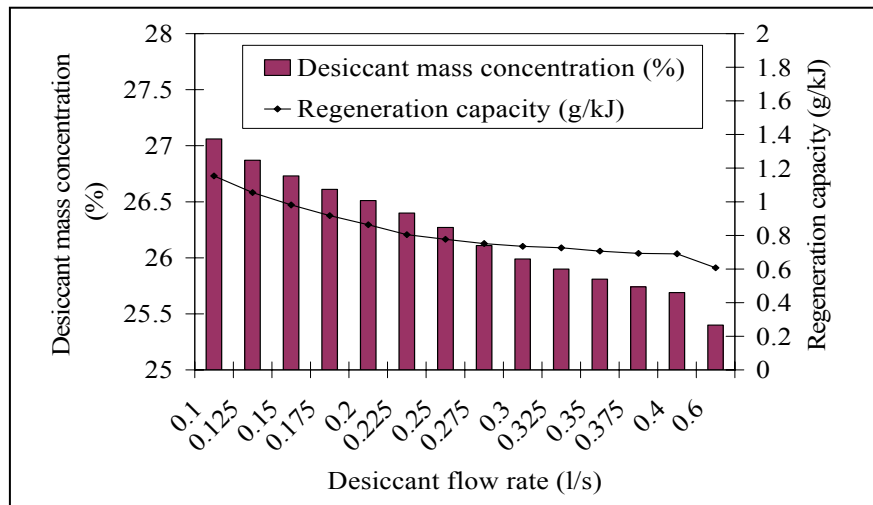


Figure 6-13 Regeneration capacity vs. desiccant flow rate

VI. Influence of the Air Flow Speed on Regeneration Capacity

Varying the air flow speed from 0.1 to 3m/s, and keeping the other conditions, such as the weak desiccant and hot water flow speed and temperature, air stream temperature and humidity unchanged.

The regeneration capacity and the condensed desiccant concentration, both increase with the air flow speed increasing until it reaches 1.0m/s, where they start to decrease, and keep the similar changing trend as shown in Figure 6-14. Because the desiccant and hot water flow speed and temperature are all fixed, the consumed energy is unvaried. A bigger air flow speed increases the convective mass transfer effectiveness, resulting in more moisture being evaporated and higher regeneration capacity. But with the air flow increasing, the influence of cold air flow on the temperature of the regenerator core and sprayed solution are becoming gradually heavier, which induces the lower vapor pressure between the air stream and solution, and lower moisture to be transferred. Hence, for a defined air stream and desiccant solution temperature, there is an optimal air flow speed for obtaining the highest regeneration capacity and condensed solution concentration, for instance, under the pre-set condition in this case, the air flow speed of 1.0m/s is optimal.

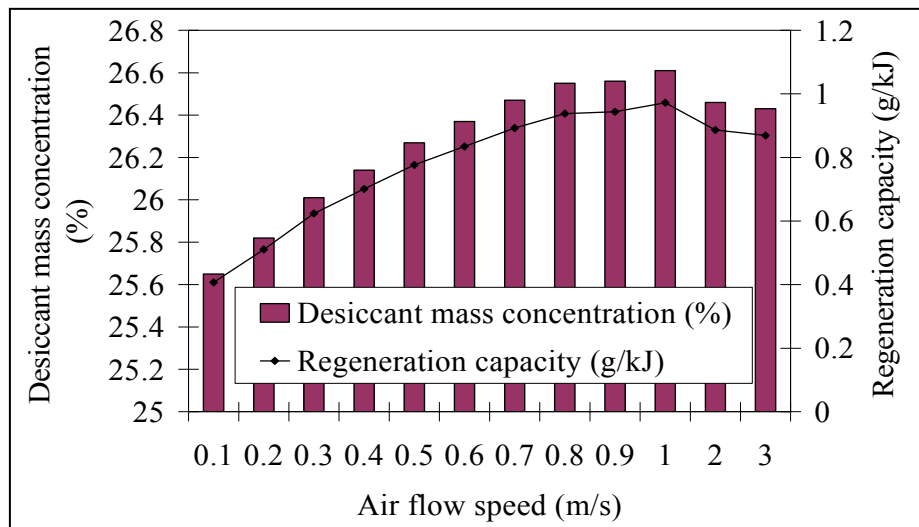


Figure 6-14 Regeneration capacity vs. air flow speed

VII. Influence of Air Temperature on Regeneration Capacity

Varying the air temperature from 24 to 46°C with the same relative humidity of 30%, and keeping the other conditions, such as the weak desiccant, and hot water flow speed and temperature, the air flow speed is unchanged. The simulation results are shown in Figure 6-15.

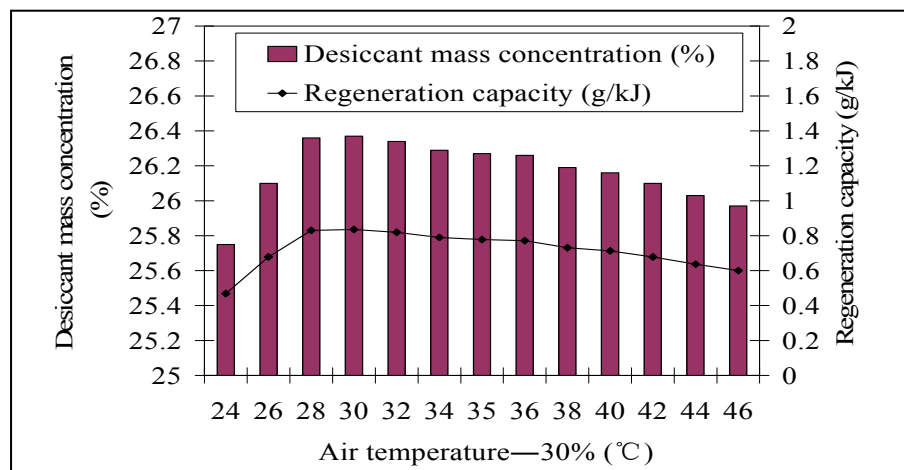


Figure 6-15 Regeneration capacity vs. fresh air temperature (relative humidity 30%)

The regeneration capacity and condensed solution concentration both increase with the air temperature in a short temperature range, and then decline in the remainder as shown in Figure 6-15. From 24 to 28°C, the air temperature considerably lower than the desiccant solution, and

with it increasing, its vapor pressure increases by a small percentage, resulting in the regeneration capacity and condensed solution concentration increasing. However, with the temperature continually increasing, the higher air temperature has more moisture content and lower vapor pressure with the invariable relative humidity. Hence, the evaporative moisture starts reducing slowly, resulting in a lower regeneration capacity and a mass concentration.

VIII. Influence of Air Humidity on Regeneration Capacity

Varying the air relative humidity from 5 to 65 under the temperature of 35°C, and keeping the other conditions, such as a weak desiccant and hot water flow speed and temperature, and the air flow speed unchanged gave the simulation results shown in Figure 6-16.

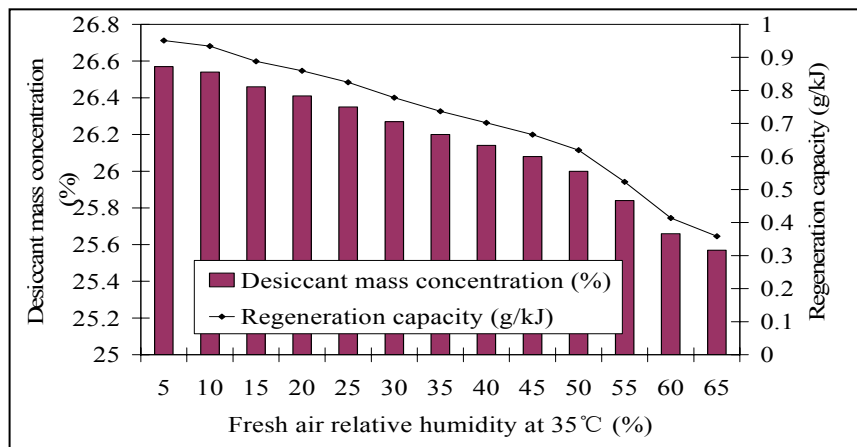


Figure 6-16 Regeneration capacity vs. fresh air relative humidity at 35°C

It is obvious in Figure 6-16 that the regeneration capacity and the condensed desiccant concentration both reduce with the air relative humidity increasing. Under the pre-settled air temperature increasing the air relative humidity results in a higher moisture content and lower vapor pressure difference from the desiccant solution. As described previously, the fixed desiccants, and hot water temperature and flow rate, indicate unchanged energy consumption. Decreasing the evaporative moisture induces a declining regeneration capacity and desiccant concentration.

IX. Influence of Hot Water Temperature on Regeneration Capacity

Varying the hot water temperature from 40 to 95°C, at a flow rate of 0.2L/s, and keeping the other conditions, such as weak desiccant flow speed and temperature, and air temperature, relative humidity and flow speed unchanged.

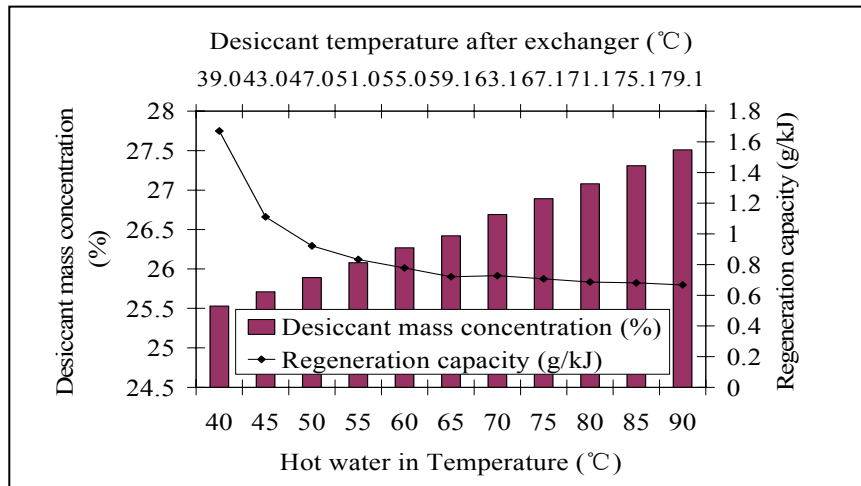


Figure 6-17 Regeneration capacity vs. hot water temperature

The regeneration capacity decreases when the hot water temperature increases, but the condensed desiccant concentration changes contrarily. A higher hot water temperature results in a higher desiccant temperature, which increases the vapor pressure at the solution side, and then induces more moisture to be absorbed out by the flowing air stream. So the condensed solution mass concentration is increased. As shown in Figure 6-17, the regeneration capacity decreases sharply with the hot water temperature increasing before 60°C. When the hot water temperature is over 60°C the regeneration capacity declines slowly. This is because when the hot water temperature is below 60°C, the energy consumed by the desiccant solution is low and the weak desiccant temperature is high enough to evaporate the moisture. With the hot water temperature increasing, the solution temperature is increased, and its regeneration ability per second is increased, which results in the higher condensed desiccant concentration. However, with the desiccant temperature increasing, more heating energy is consumed, and it is wasted with the

falling down solution in the regenerator. Hence, to save energy as well as gaining a high desiccant concentration, the preferred hot water temperature is 60°C for the fixed LiCl solution.

X. Influence of Hot Water Flow Rate on Regeneration Capacity

Varying the hot water flow rate from 0.05 to 0.4L/s at the temperature of 60°C, and keeping the other conditions, such as a weak desiccant, hot water and air stream flow rate and temperature unchanged. The simulation results are shown in Figure 6-18.

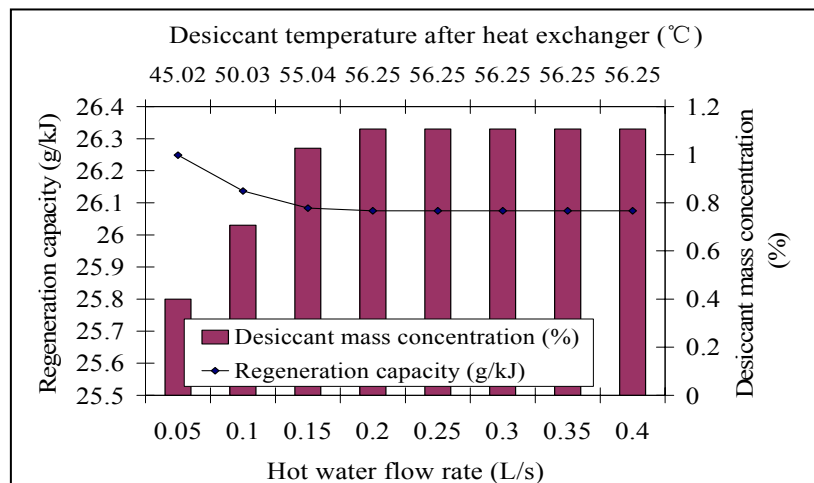


Figure 6-18 Regeneration capacity vs. hot water flow speed

The regeneration capacity decreases, and the condensed desiccant concentration increases with the hot water flow rate increasing, before it reaches 0.15L/s. When the hot water flow rate is lower than 0.15L/s, the C_{water} (mass multiplying thermal capacity) is smaller than the weak desiccant C_{weak} . The minimal one C_{min} in equation 6-8 is water C_{water} , and increasing the water flow rate induces the higher desiccant temperature as well as energy consumption. Hence the condensed desiccant concentration increases but the regeneration capacity reduces. When the hot flow rate is over 0.15L/s, the one C_{min} in equation 6-8 is the solution's mass multiplying thermal capacity C_{weak} , and the desiccant temperature and consumed energy is unchanged, resulting in the regeneration capacity and desiccant concentration being unvaried. Hence, for a

steady regeneration capacity and desiccant concentration, a hot water flow rate of 0.15L/s is preferred for the pre-settled desiccant and air stream conditions.

6.3.6 Summary of Simulation Results

Table 6.2 Factors and their influences on regenerator performance

Influence factors	Changing range	Regeneration capacity (g/kJ)		Condensed desiccant solution concentration (%)	
Channel width (mm)	2~15	2.9026 ~0.5052 (-82.56%)	↓	30.5~25.81 (-15.38%)	↓
Channel height (m)	0.4~3	0.2615~0.2643 (1.15%)	↑	26.15~26.43 (1.07%)	↑
Desiccant mass concentration (%)	20~40	0.9145~0.0204 (97.76%)	↑	—————	
Desiccant temperature (°C)	24~55	0.5014~4.3465 (766.87%)	↑	26.17~26.44 (1.03%)	↑
Desiccant Flow rate (L/s)	0.1~0.6	1.1537~0.6073 (-47.39%)	↓	27.06~25.4 (-6.13%)	↓
Air flow speed (m/s)	0.01~1~3	0.5882~0.9721~0.8693 (65.27%)	↑ ↓	25.95~26.61~26.43 (2.54%)	↑ ↓
Air temperature (°C)	24~30~46	0.4688~0.8363~0.6012 (238.65)	↑ ↓	25.75~26.37~25.97 (2.41%)	↓ ↓
Air relative humidity (%)	5~75	0.9511~0.3465 (-63.57%)	↓	26.57~25.55 (-3.84%)	↓
Hot water temperature (°C)	40~80	1.6708~0.5852 (-64.97%)	↓	25.53~27.39 (7.29%)	↑
Hot water flow rate (L/s)	0.1~0.45	0.998~0.767 (-23.15%)	↓	25.8~26.33 (2.01%)	↑

Form Table 6.2, it is seen that the desiccant temperature is the main factor influencing the regeneration capacity, by increasing the regeneration performance 7.0 times of the lowest one; the air temperature takes the second position affecting the regeneration, and is followed by the solution concentration, channel width, air flow speed, and hot water temperature, and the air relative humidity. Channel length has the least effect on the regeneration capacity, by only 1.15% increasing when lengthening the channel from 0.4 to 3 meters. For the condensed mass concentration, there is not a big difference amongst these impacting factors, except for channel width, which improves the solution concentration from 25.81% to 30.5%, whilst reducing its value from 15 mm to 2mm. Therefore, by improving the temperature of the desiccant solution, air stream and hot water is an effective way of enhancing the regeneration performance.

6.4 Experimental Testing

6.4.1 Test Rig

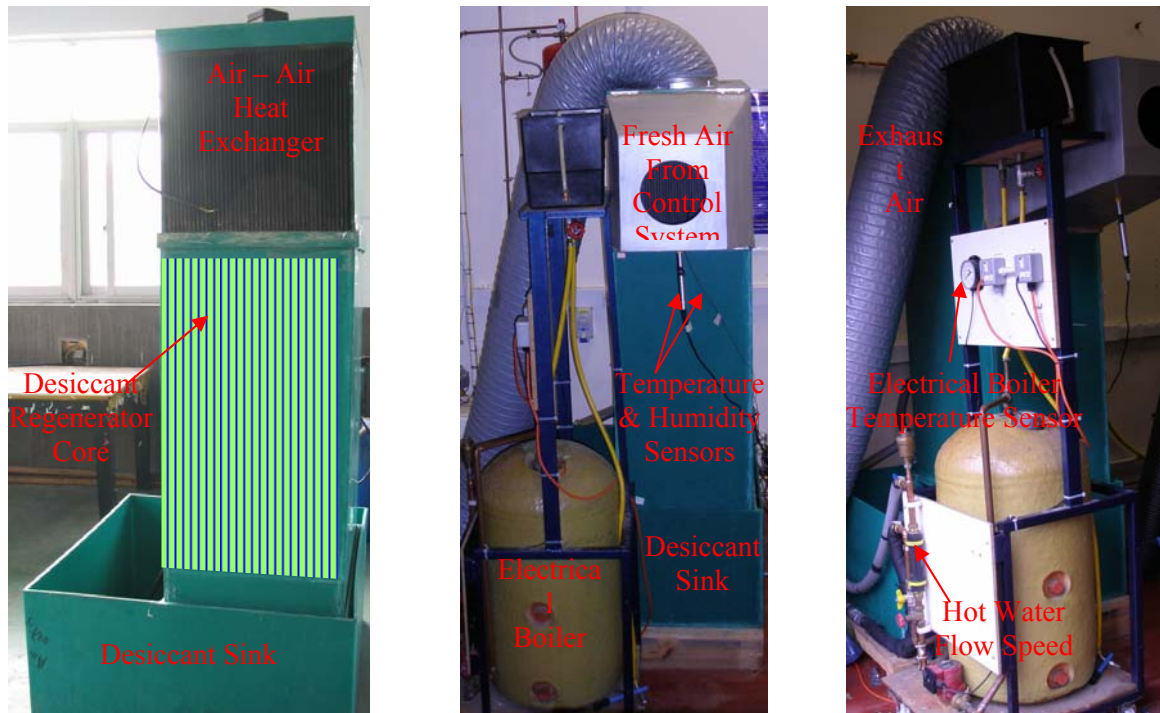


Figure 6-19 View of the test rig — liquid desiccant regenerator

A test rig was set up as shown in Figure 6-19 to test the operational performance of the liquid desiccant regenerator, utilizing the cellulose fibre pack as the carrier. Figure 6-1 is the schematic diagram showing the principle of the test rig. Temperature, humidity sensors, GP hydrometers and anemoscope are the same apparatus described in Chapters 4 and 5, and they were positioned in the test rig as shown in Figures 6-1 and 6-19. The air control system described in Chapter 3 was employed to produce the hot and dry air stream for regeneration. For simplifying the testing rig, an electrical boiler replaced the solar collector, to service the hot water and heat up the cold dilute solution.

The testing apparatus and methods are similar to those of the dehumidifier tests. The average values of the recorded results for each series of testing were used for the analyses. Factors including air temperature, humidity and flow rate, desiccant concentration, temperature and

flow rate, and hot water temperature and flow rate, were all considered in this experiment. The testing results are detailed in Tables 6.3 to 6.6.

The air-to-air cross-flow exchanger sensible heat recovery effectiveness, regeneration capacity of the regenerator and counter-flow plate exchanger are calculated through the equations 6-4 , 6-5 and 6-6 respectively and the testing errors are 5.2%, 6.16% and 6.24% respectively (Law of Error Propagation) (A.A.Clifford, 1973)

6.4.2 Air-to-Air Heat Recovery Testing Results

From the numerical simulation, it is concluded that the air-to-air heat exchanger size, airflow rate and thermal conductivity all heavily affect the heat recovery, but the air temperature difference between fresh and exhaust air slightly influences the recovery efficiency. For a designed heat recovery, the air-to-air heat exchanger structure and its manufacture material has been defined. Hence, the air flow rate and temperature impacting on the recovery performance were tested as shown in Figures 6-20 (a) and (b).

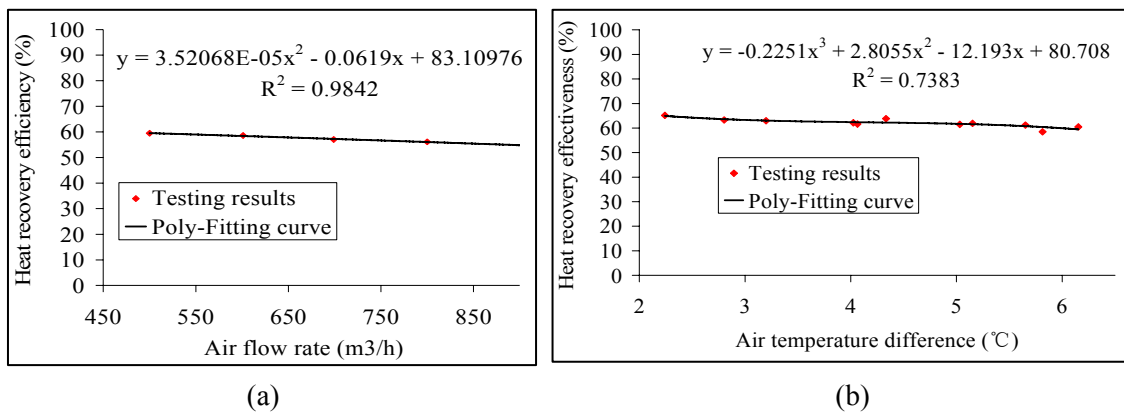


Figure 6-20 Testing results of the air-to-air heat exchanger

Testing results indicate that the heat recovery effectiveness decreases when the airflow rate increases, but the declining slope is small. Recovery effectiveness under different fresh and exhaust air temperature differences keep almost the same, only about 2% increasing rate when the air temperature difference increases one degree. However, the air-to-air heat recovery

effectiveness is low and needs to be improved in order to save maximal energy from the exhaust energy.

6.4.3 Desiccant Regenerator Testing Result

Desiccant Flow Rate VS. Regeneration Capacity

Table 6.3 Testing performance of regenerator vs. desiccant flow rate

Case number	1	2	3	4	5
<i>Desiccant flow rate (ml/min)</i>	950	1000	1100	1275	5520
Fresh air flow rate (m ³ /h)	540	540	540	540	540
Fresh air temperature (°C)	32.68	32.35	32.41	32.70	32.53
Fresh air relative humidity (%)	25.89	25.61	25.56	25.66	24.97
Desiccant mass content before regeneration (%)	27.8	28.21	29.1	27.85	32.97
Desiccant temperature before heated (°C)	35.24	36.60	35.53	40.29	40.5
Desiccant mass content after regeneration (%)	33.15	32.07	32.57	32.07	34.13
Desiccant temperature after regeneration (°C)	37.68	37.50	38.13	40.32	40.35
Hot water temperature in (°C)	61.83	60.25	59.30	62.53	58.83
Hot water temperature out (°C)	60.32	58.53	57.66	60.52	55.80
Hot water flow rate (L/min)	11.8	11.8	11.8	11.8	11.8
Regeneration capacity (g/kJ)	2.509	1.877	1.713	1.540	1.495

Table 6.3 shows the testing results gained from the regenerator under the settled running conditions: air temperature and relative humidity were in the range of 32.35°C~32.7°C and 24.97%~25.5%, and the air flow rate was 540m³/h; the hot water temperature and flow rate were 58.8°C to 61.5°C and 11.8L/min; the desiccant temperature before heating was 35.5°C~40°C. The performances of the regenerator under the desiccant flow rates of 950, 1000, 1100, 1275, 5520ml/min were tested. Testing results shown in Table 6-3 approximately indicate that a higher desiccant flow rate causes a lower regeneration capacity. The desiccant flow rate needs to be controlled at an acceptable value in order to gain the high regeneration capacity, as well as a short regeneration period.

Air Flow Rate VS. Regeneration Capacity

Testing conditions: air temperature and relative humidity were in the range of 32.20°C~33.41°C and 37.1%~42.46% respectively; the hot water temperature and flow rate were 59.35°C to 61.45°C and 11.8 L/min; the desiccant temperature before heating was 40.85°C~46.99°C, and its flow rate was 0.84L/min. Tests were carried out to investigate the performance of the regenerator under different airflow rates, such as 277, 307, 368, 500, 601, 699 and 806, 900m³/h. It is found that the higher airflow rate could improve the regeneration capacity until it reaches a value of 600m³/h. But the regeneration capacity is low, and it is only 0.156g/kJ for the highest regeneration capacity. Technologies need to be developed to enhance the regeneration capacity of the regenerator.

Table 6.4 Testing performance of regenerator vs. air flow rate

Case number	1	2	3	4	5	6	7	8
Fresh air volume flow rate (m ³ /h)	227	307	368	500	601	699	806	900
Fresh air temperature (°C)	33.41	32.74	32.47	33.01	33.03	33.13	32.62	32.20
Fresh air relative humidity (%)	42.46	39.54	37.50	37.27	37.02	37.14	37.76	39.55
Desiccant mass content before regeneration (%)	31.84	30.26	29.83	31.38	28.44	28.52	29.0	29.2
Desiccant temperature before heated (°C)	46.99	45.42	43.51	40.85	40.96	41.78	42.33	42.98
Desiccant mass content after regeneration (%)	32.78	31.69	31.67	33.97	30.86	20.96	31.69	32.29
Desiccant temperature after regeneration (°C)	47.89	46.74	44.79	41.99	40.99	42.56	43.07	43.59
Desiccant flow rate (ml/min)	840	840	840	840	840	840	840	840
Hot water temperature in (°C)	60.44	60.12	61.45	60.09	59.35	59.24	61.43	62.24
Hot water temperature out (°C)	58.27	57.19	57.78	55.78	55.78	56.99	56.79	56.79
Hot water flow rate (L/min)	11.8	11.8	11.8	11.8	11.8	11.8	11.8	11.8
Regeneration capacity (g/kJ)	0.218	0.3861	0.3164	0.635	0.622	0.413	0.463	0.428

Air Temperature and Humidity VS. Regeneration Capacity

Testing conditions: the air flow rate was 540m³/h; the hot water temperature and flow rate were 60.1°C to 63.3°C and 11.8L/min; the desiccant temperature before heating was 42.8°C~44.7°C,

and its flow rate was 0.84L/min. Testing was carried out according to the air temperature and moisture content varied in the range of 32.57~38.66°C and 7.6~8.9g/kg dry air. It was found that the regeneration capacity increased with the fresh air temperature increase, under the condition that the moisture content increased synchronously. For the case 2, the fresh air with temperature at 33.6°C and relative humidity at 27.53% leads higher regeneration capacity comparing to case 3 with lower relative humidity 27.04% as shown in Table 6.5. The testing results of the regeneration capacity varied in a range, which was caused by the unsteady testing conditions.

Table 6.5 Testing performance of regenerator vs. air temperature and humidity

Case number	1	2	3	4	5	6	7	8
Fresh air temperature (°C)	32.57	33.65	33.64	34.69	35.66	36.80	37.55	38.66
Fresh air relative humidity (%)	28.79	27.53	27.04	25.24	23.29	20.26	19.34	18.25
Fresh airflow volume (m ³ /h)	540	540	540	540	540	540	540	540
Desiccant mass content before regeneration (%)	31.54	30.03	30.06	30.15	32.97	33.8	32.45	32.45
Desiccant temperature before heated (°C)	40.74	42.14	42.67	42.89	42.57	42.39	42.85	43.48
Desiccant mass content after regeneration (%)	33.58	32.42	32.92	32.99	35.66	36.6	35.65	35.68
Desiccant temperature after regeneration (°C)	42.85	44.13	44.16	44.85	44.0	43.93	44.36	44.70
Desiccant flow volume (L/min)	0.84	0.84	0.84	0.84	0.84	0.84	0.84	0.84
Hot water temperature in (°C)	63.35	63.87	63.52	64.44	60.38	60.12	60.54	61.11
Hot water temperature out (°C)	58.03	58.20	58.21	59.12	55.07	54.79	55.22	55.79
Hot water flow speed (L/min)	11.8	11.8	11.8	11.8	11.8	11.8	11.8	11.8
Regeneration capacity (g/kJ)	0.075	0.0931	0.111	0.110	0.1105	0.111	0.125	0.145

Desiccant Mass Concentration VS. Regeneration Capacity

Testing conditions: air temperature and relative humidity were in the range of 30.46°C~31.1°C and 24.08%~24.9%, and the airflow rate were 540m³/h respectively; the hot water temperature and flow rate were 60.48°C to 62.0°C and 11.8L/min; the desiccant temperatures before being heated were 32.95°C~35.81°C, and its flow rate was 0.84L/min. Tests were carried out

according to the desiccant mass concentrations, which changed from 30.7% to 33.7%. It was found in Table 6.6 that the desiccant mass concentration heavily influenced the regeneration capacity. In the practical testing, the desiccant mass concentration was measured by the GP hydrometers, which gave the maximal accuracy when the solution was cooled to about 20°C. But in the practical testing, the desiccant temperatures were not exact at 20°C when read and recorded the value. Hence, there were some measuring errors in the testing, which possibly affected the results at some degree.

Table 6.6 Testing performance of regenerator vs. desiccant mass concentration

Case	1	2	3	4	5	6	7
Desiccant mass content before regeneration (%)	<i>30.7</i>	<i>31.3</i>	<i>31.34</i>	<i>32.34</i>	<i>33.33</i>	<i>33.63</i>	<i>33.73</i>
Fresh air temperature (°C)	30.75	30.93	30.88	31.09	30.92	31.10	30.46
Fresh air relative humidity (%)	24.74	24.43	24.65	24.08	24.22	24.89	24.71
Fresh air flow rate (m³/h)	540	540	540	540	540	540	540
Desiccant temperature before heated (°C)	32.95	33.22	34.08	34.9	35.81	35.55	35.43
Desiccant mass content after regeneration (%)	40.19	40.50	37.9	40.28	42.39	42.35	42.76
Desiccant temperature after regeneration (°C)	42.85	44.13	44.16	44.85	44.0	43.93	44.36
Desiccant flow rate (ml/min)	840	840	840	840	840	840	840
Hot water temperature in (°C)	60.75	60.79	61.66	61.02	62.0	62.20	<i>60.48</i>
Hot water temperature out (°C)	49.34	49.08	44.91	45.36	46.20	45.82	<i>44.83</i>
Hot water flow rate (L/min)	11.8	11.8	11.8	11.8	11.8	11.8	11.8
Regeneration capacity (g/kJ)	<i>0.215</i>	<i>0.178</i>	<i>0.173</i>	<i>0.169</i>	<i>0.159</i>	<i>0.121</i>	<i>0.112</i>

6.5 Comparisons of the Modelling and Experimental Results

6.5.1 Comparisons for the Air-to-air Heat Exchanger

Numerical simulations were carried out under test conditions, and the comparison of the testing and simulation results were made, as shown in Figure 6-21 (a) and (b). The heat recovery effectiveness of testing and simulation results has a similar varying trend in both of the two testing conditions: one is changing the airflow rate and the other is varying the air temperature

difference. However, the testing results are about 10% higher than the simulation. This may be caused by the following three reasons: firstly, the numerical simulation limit accuracy influences the simulation results; secondly, the simulation didn't consider the extra energy, the air stream gained from the water to the desiccant heat exchanger in the regenerator unit as shown in Figure 6-1; thirdly, the testing sensors accuracy could cause some errors.

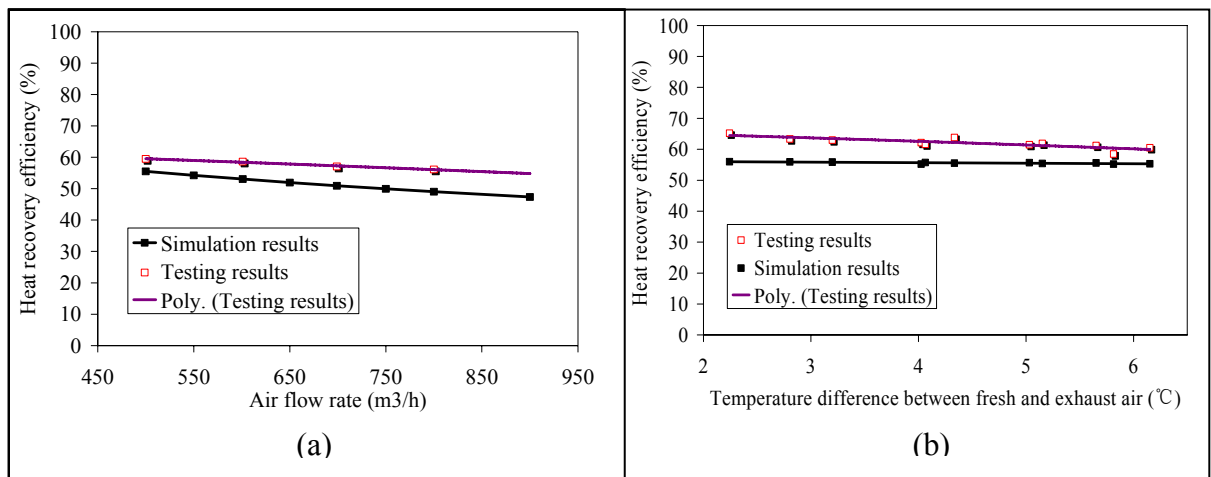


Figure 6-21 Comparisons of testing and simulation results of the air-to-air heat exchanger

6.5.2 Comparisons for the Desiccant Regenerator

Different numerical simulations were carried out under the testing conditions presented in Table 6.3 to 6.5. The average values of each series of fluctuant testing conditions were employed in the numerical simulations, an example for the case of the desiccant flow rate influencing the regeneration capacity, the simulations pre-set conditions: air temperature, relative humidity and flow rate were 32.6°C, 25.5% and 540m³/h respectively; the hot water temperature and flow rate were 61.5°C and 13L/min; the desiccant temperature before being heated was about 35.5°C. Each data is the average value of the corresponding data shown in Table 6.2. The same method was employed in the others simulations regarding different impacting factors.

Comparisons were carried out between the numerical modeling and testing results, regarding the impacting factors of the air flow rate, air temperature, desiccant flow rate and desiccant

concentration. The results were summarized in Figure 6-22 (a), (b), (c) and (d), respectively. It is seen that the theoretical regeneration capacities are close to the corresponding testing results at a fixed percentage in all of the series of comparisons, and they have a similar changing trend. The reasons causing this discrepancy between the simulations and testing results were investigated and summarized as follows:

(1) In the modeling the extra energy transferred into the air stream from the hot water heat exchanger was ignored in the theoretical calculation. This caused the energy consumption is lower than the practical experiments.

(2) In the modeling, the latent heat for the evaporating moisture out of the weak solution was assumed to be absorbed from both the solution and the air flow. However, the testing results indicated that the desiccant solution offered a smaller proportion to the evaporation heat.

(3) The equations calculating the solution parameters, such as thermal conductivity, dynamical viscosity, density, thermal capacity, vapor pressure etc, expressed in appendix II, were mostly concluded from the experimental results. Hence, their accuracy has the potential affecting the modeling results.

(4) The numerical simulation size for the regenerator, such as channel length 0.8m, channel height 8mm, and regenerator core width 0.6m, depth 0.5m were all measured from the outside of the regenerator unit. There were some hidden discrepancies between the practical channel sizes, for example, the channel constituted of fibre membranes is reshaped under long time running, which probably shortens the channel height.

(5) The base conditions employed in the simulation were the average values of the testing conditions. However, in the experiments the testing conditions such as air temperature/humidity, desiccant flow rate and concentration and hot water temperature, varied in a small range. Hence, the pre-set conditions cause some errors in the modeling.

(6) The limit of the model's accuracy causes the errors in the modeling.

(7) The testing accuracy and methods had the potential causing errors.

Reasons (1) and (2) are the main factors which caused the difference between the simulation and testing results. For the first reason, it has been found that the recovery effectiveness tested through experiments of the air-to-air exchanger is higher than the modelling results, which may be caused by the external heat from the plate exchanger (hot water to desiccant plate heat exchanger) in the regenerator unit. Because the desiccant to water plate exchanger is installed inside the regenerator unit as shown in Figure 6-1, the flowing air stream contacts directly with the exchanger, which absorbs energy from the heat exchanger. By comparing the out let hot water temperature between the simulations and experiments; it is found that the heating energy consumption in the practical testing is higher than the modeling results calculated by the equation 6-8. For the second reason, it is found that the condensed desiccant temperature in the experiments is higher than the simulation results, this caused more heating energy is wasted with the falling out solution. The fiber regenerator's distortion causes two resistances to the regeneration: one by reducing the contacting surface between the solution falling film with the flowing stream, and the other by damaging the uniform distribution of solution which soaked into the fiber membranes, forcing the solution to fall down in wisps.

The comparisons results were shown in Figure 6-22 (a), (b), (c) and (d), it is found that the modeling results approach the testing results and keep a small difference at about 10%, 5.2%, 4.0% and 2.81% corresponding to different affecting factors. The main errors are caused by the factor one, which can be avoided if we insulate the water-to-desiccant plate exchanger from the flowing air stream. Hence, when the equipment is good insulated and the fibre core is undamaged, the modeling can give a prediction of the performance of the regenerator with acceptable errors.

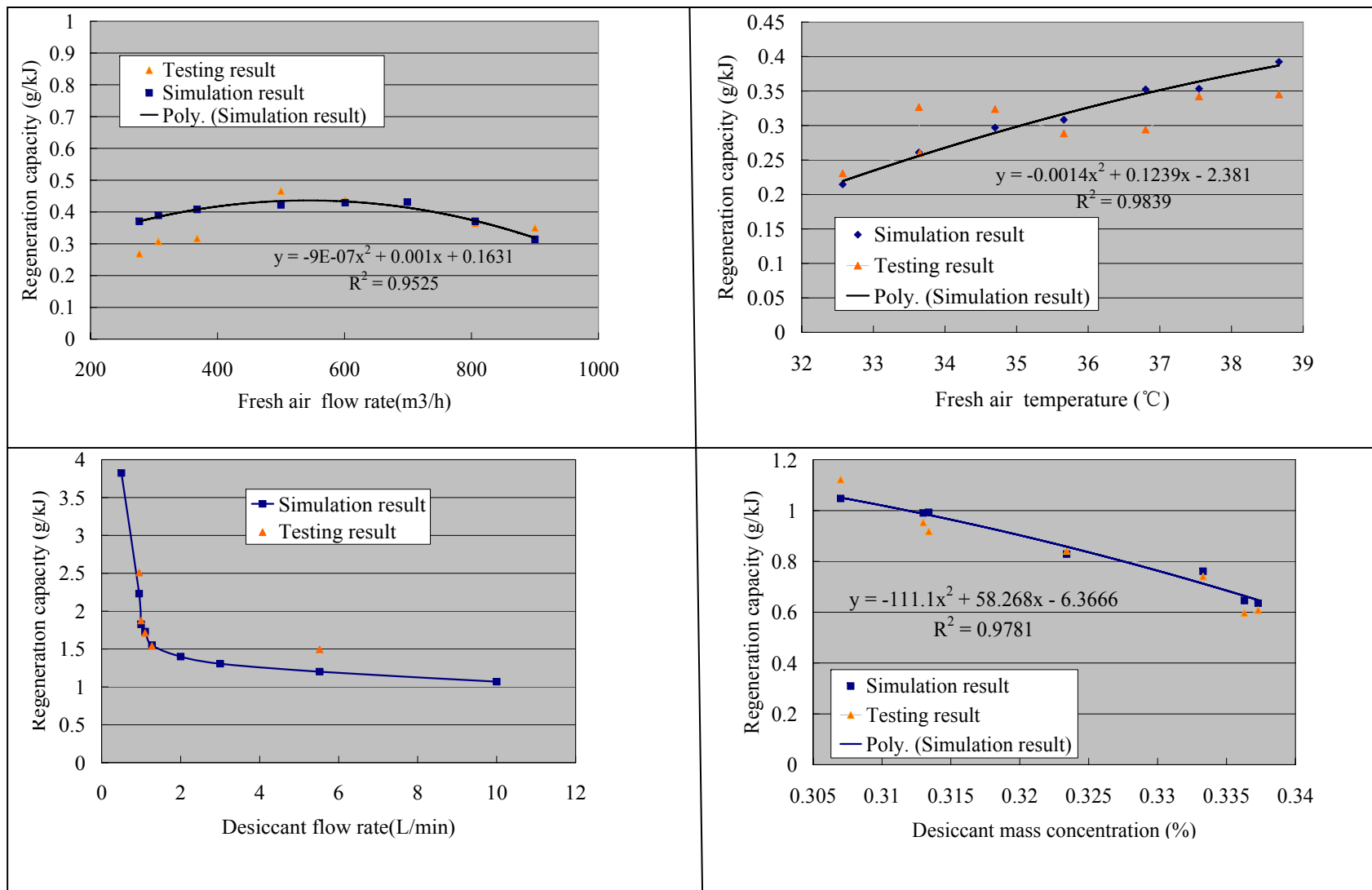


Figure 6-22 Comparisons of testing and simulation results of desiccant regenerator

6.6 Summary

The two main parts of the regenerator: the air-to-air heat exchanger and the fiber regenerator core were investigated in this chapter by the methods of numerical simulation and experimental testing. For the air-to-air heat exchanger performance, three influencing factors were studied, such as the exchanger size and structure, the ratio of the fresh to exhaust air flow rate, and the thermal conductivity of material. For the regenerator performance, four series of impacting factors were investigated, such as the exchanger size and structure (channel length and height), desiccant solution parameters (mass concentration, temperature and flow rate), and fresh air parameters (temperature, humidity and flow rate), hot water parameters (temperature and flow rate). These researched results were presented as the following:

Air-to-air heat exchanger

- A high channel length ratio of fresh air to exhaust results in high recovery effectiveness, but a too short exhaust air channel could not save the maximum energy from the exiting air. Suggested channel length of fresh air channel is 1m and the exhaust air channel is 1.0 to 0.5 times of fresh air channel length.
- The temperature difference between the fresh air and exhaust air slightly affects the effective recovery, but the air flow rate influences it heavily. Lower air flow rate is preferred.
- The recovery effectiveness quickly increases with the thermal conductivity when it is below 0.25W/mK, and then keeps almost unchanged. The thermal performances of the exchanger made of materials such as fibre paper, metal, zeolite et al are all similar. Hence, the cheapest material-fibre is selected in this research.

Desiccant regenerator

- Under the pre-condition that three kinds of solutions, LiCl, LiBr, and CaCl₂, effectively absorbed the same moisture in the dehumidifier, the LiCl solution at a lower mass

concentration, performs the best regeneration capacity and needs the lowest hot water temperature. Hence, LiCl is selected as the working solution in our project. Its regeneration capacity reduces with the weak desiccant mass concentration increasing. When the solution mass concentration is higher, the vapor pressure is reduced and the evaporation ability declines accordingly.

- The regeneration capacity increases little with the increase in the channel length. This is because when the desiccant and air stream parameters were settled, the vapor pressure difference between the air stream and solution is determined. Along with the direction of the channel, the vapor pressure of air decreases and approaches to the desiccant film. Hence, the increasing of the regeneration capacity increasing with a slow ratio. The preferred regenerator channel length is 1m for the pre-set conditions.
- The channel height considerably affects the regeneration capacity, especially when the channel height is lower than 8mm. Also, a lower channel height induces a high condensed solution concentration, which is important for the performance of better dehumidification in the next circle. But with the channel height reduced, the air flow resistance and manufacturing difficulty are improved. Hence for a compact and effectiveness regenerator core, the channel height in the range of 5~8 mm is preferred.
- A higher desiccant temperature results in higher regeneration capacity, but impacts the condensed mass concentration less. If the solution needs to be regenerated repeatedly to reach the required concentration, it is better to keep the desiccant temperature at a high value. However, if the solution is regenerated once through the regenerator core to obtain the desired concentration and then is stored in the sink, or delivered to the dehumidifier, a lower desiccant solution could save the hot energy as well as reducing the cooling energy in the dehumidification process.
- A lower desiccant flow rate leads to a higher regeneration capacity and condensed solution concentration. This is because the lower desiccant flow rate increases the

contact time with the airflow, which creates more opportunity for the superfluous moisture to evaporate. Hence, for a fixed regenerator size and airflow parameters, a lower desiccant flow rate is preferred, under the conditions that the regeneration energy is defined and protected by insulation.

- Regeneration capacity and condensed solution mass concentration increase with the fresh air flow rate increasing and then decline. This is because that the higher air flow speed enhances the convective mass transfer between the solution film and air stream, as well as aggravating the carrying out of the regeneration energy. When the energy being carried is too heavy to impact the vapor pressure difference between the air stream and solution film, the regeneration capacity and condensed solution concentration is receded. Hence, when the heating energy is fixed, air and desiccant parameters, an optimal air flow speed can be worked out by this modeling, for instance, in this studied case the optimal air flow speed is 1m/s.
- Similar to the air flow speed, there is an optimal air temperature to obtain the best regeneration capacity and desiccant concentration as shown in Figure 6-15. When keeping the relative humidity unchanged, increasing the air temperature enhances the moisture content and vapor pressure, as well as the solution film temperature. When the influence is towards the air moisture content and vapor pressure rather than to the solution temperature, the vapor pressure difference between the air stream and solution film is reduced and less moisture is evaporate out. Hence, for the defined air relative humidity, heating energy source and desiccant conditions, the best air temperature 28°C was concluded by this theoretical modeling.
- Owing to its lower vapor pressure, dry air performs a better regeneration capacity in the regeneration, showing its ability to absorb more moisture from the dilute solution, as shown in Figure 6-16.

- Higher hot water temperature produces a higher condensed solution at a lower regeneration capacity as shown in Figure 6-17. The reasons are these: higher hot water temperature results in a higher desiccant temperature and vapor pressure, which evaporate more moisture out of the dilute solution; at the same time, higher hot water and desiccant temperature lead to a higher energy consumption with the solution falling out of the regenerator; Because the increasing evaporation moisture cannot cover the rising of the consumed energy, the regeneration capacity declines. Hence, for LiCl solution at a temperature of about 35°C, and a concentration of about 25%, the hot water at 60°C could service a good regeneration performance.
- With the hot water flow rate increasing, the regeneration capacity decreases and the condensed solution concentration firstly increases, and then keeps unchanged. This is because, for the fixed water to desiccate plate heat exchanger and water/desiccant temperature, when the desiccant flow rate is over 0.15L/s, the desiccant temperature is steady after the exchanger, as is the consumed energy. Hence, for reducing the energy waste on the delivering route, the optimal hot water flow rate 0.15L/s can be produce a high concentration solution at a steady regeneration capacity.

Hence, for a defined air temperature/humidity and dilute solution concentration/temperature, the optimal regenerator size and running condition could be concluded. For instance, for this researched case, the optimal air-to-air exchanger fresh air channel length is 1m and exhaust air channel is 1~0.5m; regenerator core air channel length is 1m and height is 5~8mm; best fresh air temperature is 28°C with the relative humidity of 30; hot water is 60°C and flow rate is 0.15L/s.

Laboratory experiments were carried out to investigate the performance of the designed desiccant regenerator and the air-to-air heat exchanger. Two series of testing were performed, regarding the relationship between the fibre air-to-air exchange performance with the air

temperature and flow rate. Four series of testing, focusing on the performance of the regenerator were carried out, and the impacting factors, such as fresh air temperature and flow rate, desiccant solution flow rate, and concentration, were investigated.

Comparisons between the experimental and simulation results were carried out. For the air-to-air exchanger, two series of testing were processed, and it was found that the testing result was about 10% higher than the simulation results, which was caused by the additional hot energy from the hot water plate exchanger. For the fibre regenerator, it was found that all testing results kept the same gap with the simulation results. Detailed investigation found out that the consumed hot energy in practical testing is higher than the theoretically calculated ones. It is obvious that part of the heating energy is absorbed and carried away by the flowing airflow. Hence, the gap between the numerical simulation and experimental testing is mainly caused by unconsidered this part energy (carried out by air) into the simulation. Although, there are discrepancies between the testing and simulation results, they have the same changing trend with the varying factors such as air temperature, flow speed and desiccant concentration and flow rate. When the plate heat exchanger is insulated and the regenerator core is undamaged, there are less energy lost in the experimental, and the errors between the numerical and testing in an acceptable range. Therefore, simulation modeling could give a prediction for the fiber regenerator in the good running condition: no energy lost, no regenerator — core shaped and heating energy is protected by insulation.

Chapter 7. Performance of Heat Recovery/Desiccant Cooling System

7.1 Description of Heat Recovery/Desiccant Cooling System

Figure 1-1 shows the schematic of the desiccant cooling system, which is designed to fit within a windcowl or windcatcher. In this system, the solar collector and cooling tower are purposed to service hot and cold water to the regenerator and dehumidifier, respectively. The solar collector and cooling tower are both mature technologies, so for simplifying the testing rig, the electrical boiler was substituted for the solar collector, and tap water (below 15°C) replaced the cooling tower. Therefore, a simplified system as shown in Figure 7-1 includes a novel heat/mass fibre exchanger, a dehumidifier core to remove the superfluous moisture from the pre-cooled/dehumidified fresh air, a regenerator to desorb weak desiccant, and three plate heat exchangers (hot water-to-weak desiccant, weak desiccant-to-strong desiccant, strong desiccant-to-cold water). One desiccant cycle and two air cycles constitute the whole heat recovery/desiccant cooling system.

The desiccant cycle consists of a desiccant dehumidifier, a desiccant regenerator and store system (DRSS), three heat exchangers and desiccant sprayers, strong/weak solution sinks, and piping connections. The strong desiccant pumped from the regenerator loses its sensible heat in the desiccant to desiccant heat exchanger to the upcoming diluted desiccant solution, resulting in a certain degree of temperature drop. It then flows to the dehumidifier sink, where it is cooled by the cooling coil, pumped to the top of the fibre exchanger/dehumidifier core, and then sprayed equably. The strong and cold desiccant soaked in the fibre membranes absorbs the moisture as well as condensation heat from the passing humid air and flows back to a separate desiccant sink, where the diluted solution is accumulated and is ready to be delivered back to the DRSS for regeneration. The weak solution is delivered back to the regenerator through the desiccant-to-desiccant heat exchanger, where it obtains some heat from the upcoming strong

desiccant. The pre-heated solution is further heated up in a heating coil, and then pumped to the top of the fibre pack and sprayed over the core. The down-flowing solution is soaked by the fibre membranes and desorbed by the contacting/flowing air stream. Hot and condensed solution is collected and stored in the sink, which is large enough to contain plenty of solutions for at least 24 hours of dehumidifier working.

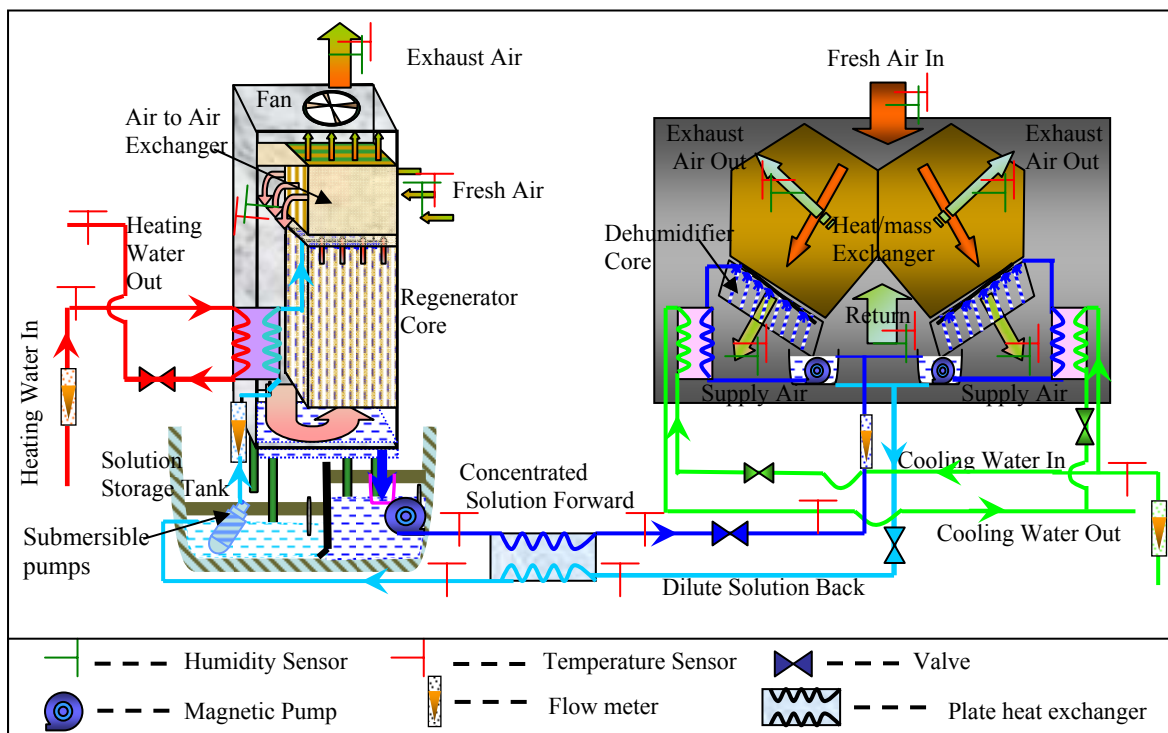


Figure 7-1 Schematic diagram of the heat recovery/desiccant cooling system

In the dehumidifier unit, firstly, the fresh air from the environment has heat/mass exchanges with the returning air from the air conditioning room through the fibre exchanger unit, and then flows into the dehumidifier channels, where it loses the superabundant moisture to the strong solution. Then the well-treated cold and dry air is supplied to the serving room.

In the regenerator unit, the forced in fresh air exchanges heat with the exhaust air, and flows to the bottom of the fibre pack, where it starts to absorb moisture from weak desiccant until it moves upwards to the top of the pack and exits.

7.2 Heat and Mass Transfer and COP of Whole System

7.2.1 Desiccant Circle Thermal Process on Duhring Diagram

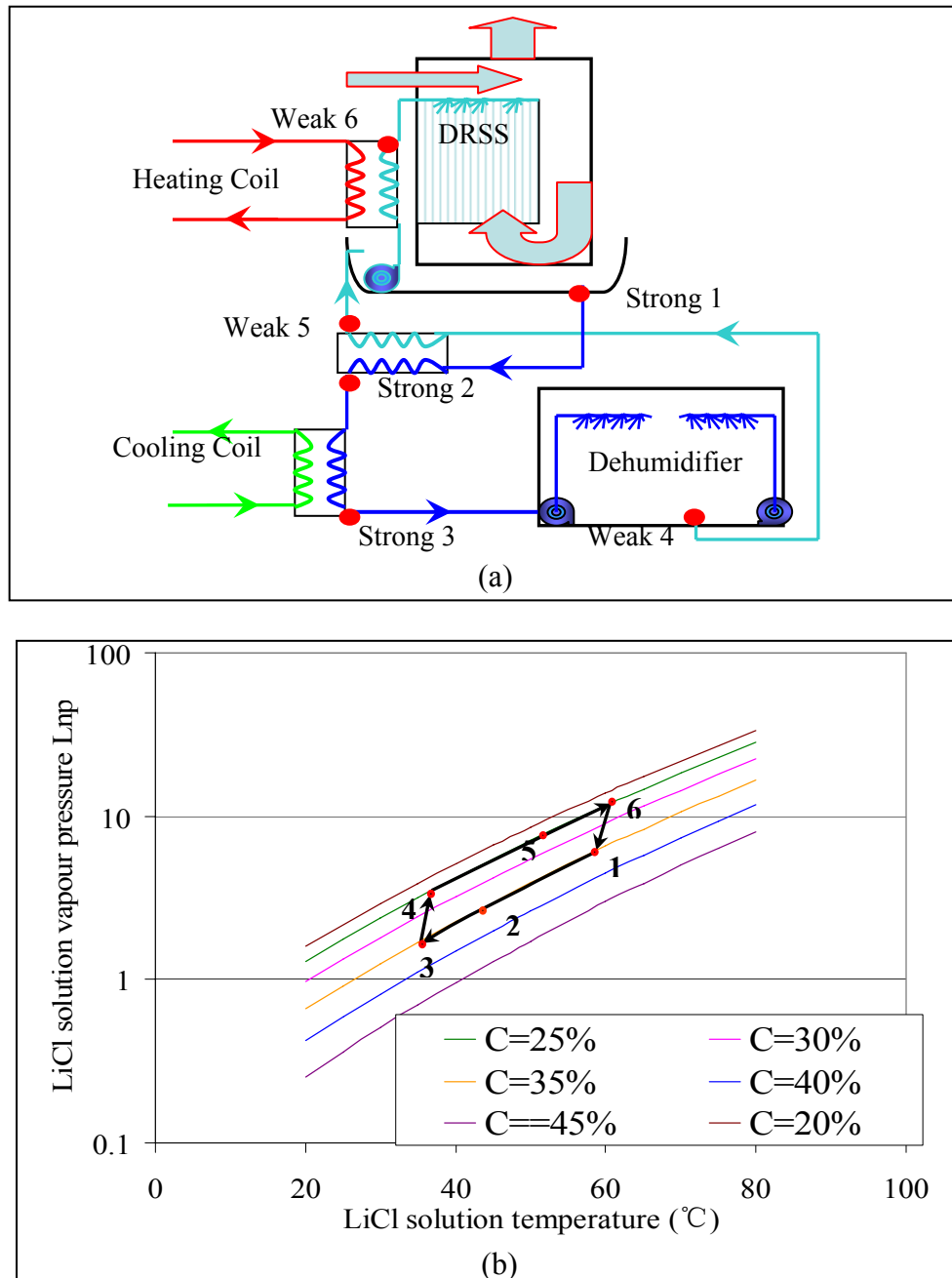


Figure 7-2 (a) Sketch diagram of the desiccant cycle (b) thermal process on Duhring diagram

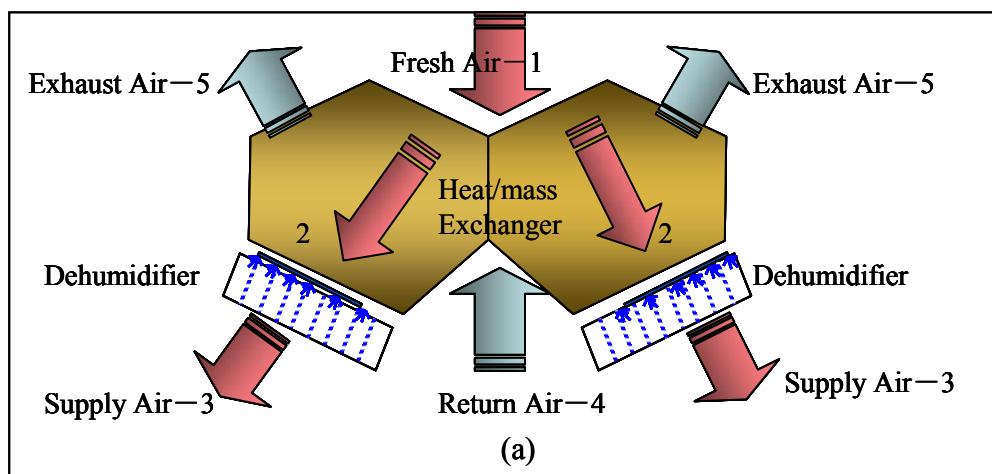
Figure 7-2 (a) and (b) show the desiccant cycle diagram and its process on the Duhring diagram.

The strong desiccant solution from the DRSS (state 1) is passed through a heat exchanger,

where it transfers heat to the upcoming weak solution, resulting in a lowered temperature state to point 2. The desiccant is further cooled via a desiccant-to-water heat exchanger prior to entering the absorber, resulting in a change from point 2 to 3. In the dehumidifier core, the desiccant absorbs moisture from the passing air and part of the heat released from vapour condensation, resulting in its' change from point 3 to 4. The diluted desiccant solution is then delivered to the regenerator. However, on the way to the regenerator, it experiences a temperature rise due to absorbing heat from the strong-to-weak solution heat exchanger (4 to 5). When entering the regenerator, the solution is heated by a hot water coil to state 6, which enables the evaporation of moisture from the solution. Thereafter, the solution is cooled and condensed to point 1 by a passing exhaust air flow.

7.2.2 Air Circle Thermal Process on Psychrometric Chart

Figure 7-3 presents the heat/mass changing process of the novel heat/mass fibre exchanger. In this designed air conditioning system the fresh air only take the latent heat load in the air conditioning room. The fresh air releases heat and mass to the existing air in the fibre heat/mass exchanger, and it is pre-cooled and dehumidified from point 1 to point 2 as shown in Figure 7-3, and then flows into the desiccant dehumidifier core, where it is further cooled and dehumidified until point 4. Exhaust air temperature and humidity is changed from point 7 to 8 through the air-to-air heat/mass exchanger and then exits.



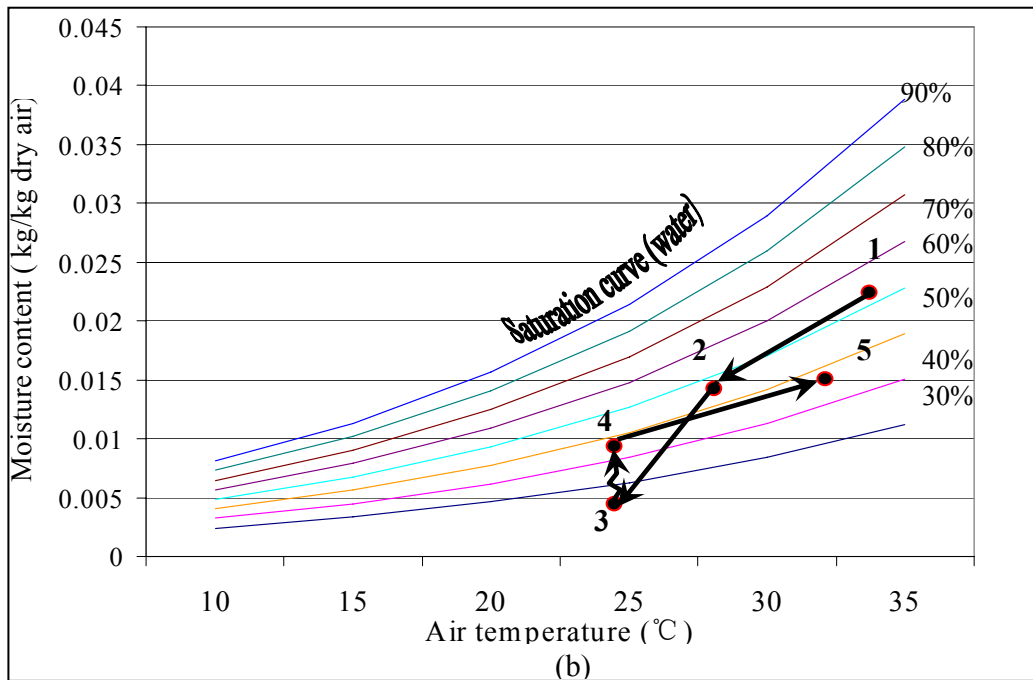


Figure 7-3 (a) Sketch diagram of the air processes (b) Air conditioning processes on the psychrometric chart

7.2.3 Heat and Mass Transfer

Desiccant Solution Cycle heat/mass transfer

Desiccant from the strong solution storage transfers sensible heat to the upcoming weak desiccant as shown in Figure 7-2. This results in lowered temperature of the desiccant flow, which is further cooled by the circulating cooling water from the cooling tower, which in turn creates a cooling water flow, with the temperature approaching the wet bulb point of the atmosphere. In the process from point 1 to 3, only heat exchange occurs, but no moisture transfer, hence, the desiccant temperature in this process can be written as follows:

$$T_{strong}^2 = T_{strong}^1 - \eta_1 C_{min}^1 (T_{strong}^1 - T_{strong}^4) / C_{strong}^1 \quad (7-1)$$

$$C_{min}^1 = \min(C_{strong}^1, C_{strong}^4) = \min(c_{strong}^1 m_{strong}^1, c_{weak}^4 m_{weak}^4)$$

From point 2 to point 3, the strong desiccant solution is cooled by the cooling water in the cooling coil, where its temperature is reduced but its concentration retains unchanged.

$$T_{strong}^3 = T_{strong}^2 - \eta_2 C_{min}^2 (T_{strong}^2 - T_{cold}^{in}) / C_2 \quad (7-2)$$

$$C_{min}^2 = \min(C_2, C_{cold}) = \min(c_{strong}^2 m_{strong}^2, c_{water}^{in} \rho_{cold}^{in} V_{cold})$$

From point 3 to point 4, the strong solution has heat and mass exchange with the flowing air stream, and its temperature and concentration is changed from T_3 and θ_{strong} to T_4 and θ_{weak} respectively. The absorbed moisture from the fresh air is described as the following:

$$m_{absorb} = \frac{(p_f^3 - p_d^3)}{RT \left(\frac{1}{k_f^l} + \frac{H}{k_d^l} \right)} A_{De} \quad (7-3)$$

p_f and p_d can be calculated through equations in Appendix I and II respectively. Then the dilute solution concentration is calculated as follows:

$$\theta_{weak} = (\rho_{strong}^1 V_{strong} \theta_{strong}) / (\rho_{strong}^1 V_{strong} + m_{absorb}) \quad (7-4)$$

Sensible heat transfers include two parts: one is from the hot air, and another is from the latent heat released by the condensation moisture. Hence, the solution temperature can be calculated by the following equation:

$$T_{weak}^4 = T_{strong}^3 + ((t_f^3 - T_{strong}^3) / (\frac{1}{k_f^s} + \frac{1}{k_d^s}) A_{De} + m_{absorb} (2500 - 2.35 T_{strong}^3)) / (\rho_{strong}^1 m_{strong}^3) \quad (7-5)$$

From point 4 to point 5, the dilute solution absorbs sensible heat from the advancing strong solution. The solution temperature is expressed as follows:

$$T_{weak}^5 = T_{weak}^4 + \eta_1 C_{min}^1 (T_{strong}^1 - T_{weak}^4) / C_4 \quad (7-6)$$

$$C_{min}^1 = \min(C_1, C_4) = \min(c_{strong}^1 m_{strong}^1, c_{weak}^4 m_{weak}^4)$$

The dilute solution is further heated up by the hot water in the desiccant-to-hot water flat plate heat exchanger before it is condensed. The heated-up dilute solution temperature is expressed as follows:

$$T_{weak}^6 = T_{weak}^5 + \eta_3 C_{min}^3 (T_{hot}^{in} - T_{weak}^5) / C_5 \quad (7-7)$$

$$C_{min}^2 = \min(C_5, C_{hot}) = \min(c_{weak}^5 m_{weak}^5, c_{water}^{in} \rho_{hot}^{in} V_{hot})$$

Hot weak desiccant is regenerated from point 6 to 1. The desorbed moisture and condensed solution concentration are expressed as the following:

$$m_{desorb} = \frac{(p_{weak}^5 - p_f^5)}{RT \left(\frac{1}{k_f^l} + \frac{H}{k_d^l} \right)} A_{Re} \quad (7-8)$$

$$\theta_{condense} = (\rho_{weak}^5 V_{solution} \theta_{weak}) / (\rho_{weak}^5 V_{solution} - m_{desorb}) \quad (7-9)$$

Because the air temperature is lower than the solution, and the specific capacity of the solution is about 3 times that of the air steam, the latent heat is assumed to be absorbed from the solution side. Hence the condensed solution temperature is expressed as the following:

$$T_{condense} = T_{weak}^6 - ((T_{weak}^6 - T_{air}^6) / (\frac{1}{k_f^s} + \frac{1}{k_d^s}) A_{Re} + m_{desorb} (2500 - 2.35t_6)) / (\rho_{weak}^6 m_{weak}^6) \quad (7-10)$$

For the whole desiccant circle (from the dehumidifier to regenerator) heat and mass balance, the moisture absorbed by strong solution equals the moisture desorbed out from the weak solution, and the condensed desiccant concentration equals the supplying strong desiccant, it is described as the following:

$$m_{desorb} = m_{absorb} \quad (7-11)$$

$$\theta_{condense} = \theta_{strong} \quad (7-12)$$

Air Cycle Heat/mass Transfer

Fresh air has heat and mass transfer with the exhaust air in the air-to-air heat exchanger, and its temperature and moisture content drops from point 1 to 2, as shown in Figure 7-3. The supply air temperature and moisture content is expressed as the following:

$$T_f^2 = T_f^1 - (T_f^1 - T_E^4) / (\frac{1}{k_f^s} + \frac{\delta}{k} + \frac{1}{k_e^s}) A_{Ex} / c_{air} \rho_{air} V_f^1 \quad (7-13)$$

$$d_f^2 = d_f^1 - \frac{(p_f^1 - p_e^4) / RT}{(\frac{1}{k_f^l} + \frac{\delta}{k_{mass}} + \frac{1}{k_d^l})} A_{Ex} / \rho_{air} V_f^1 \quad (7-14)$$

Then the air stream is further dehumidified and cooled by the strong/cold solution in the dehumidifier core, the desired air temperature and moisture content at point 3 is described as the following:

$$T_s^3 = T_f^2 - (T_f^2 - T_s^3) / \left(\frac{1}{k_f^s} + \frac{1}{k_d^s} \right) A_{De} / c_{air} \rho_{air} V_f^2 \quad (7-15)$$

$$d_s^3 = d_f^2 - \frac{(p_f^2 - p_s^3)}{RT \left(\frac{1}{k_f^l} + \frac{H}{k_d^l} \right)} A_{De} / \rho_{air} V_f^2 \quad (7-16)$$

Performance of the Whole Desiccant Cycle Process

Because the working performances of air-to-air heat exchanger, dehumidifier and regenerator have been investigated in detail in Chapters 4, 5 and 6, the performance of the whole system is the main research object in this chapter. Coefficient of performance (COP) is imported to describe the working performance of the novel heat recovery/desiccant cooling system. As the definition of COP, it is the input energy divided by the producing energy. The input energy in this system includes three parts: cold energy cooling hot/strong desiccant offered from the cooling tower, hot energy heating the cold/weak desiccant provided by the solar collector, and electrical energy driving the pumps and running the fans.

Consumption of the cooling energy is calculated by the equation as follows:

$$Q_{cold} = c_{water} m_{cold} (t_{cold}^{in} - t_{cold}^{out}) = c_{strong}^2 m_{strong}^2 (T_{strong}^2 - T_{strong}^3) \quad (7-17)$$

Consumption of the heating energy is calculated by the following equation:

$$Q_{hot} = c_{water} m_{hot} (t_{hot}^{in} - t_{hot}^{out}) = c_{weak}^5 m_{weak}^5 (T_{weak}^6 - T_{weak}^5) \quad (7-18)$$

Electrical energy consumed in this system is mainly for driving the pumps and fans, which require a small amount of energy with the maximal value of about 500W (There are 6(30W) pumps and 3 (100W) fans). $Q_{electrical} \approx 500W$

The output energy (cooling capacity) is energy reduction from the fresh air to supply air as shown in the following:

$$Q_{output} = m_f^1 h_f^1 - m_s^1 h_s^1 \quad (7-19)$$

In this proposed system, natural energy such as solar energy, and cooling tower energy, is utilised for the heating/cooling of the weak/strong desiccant, and the windcowl/catcher supplies the natural ventilation. Hence, the best COP should be considered in two conditions: when natural energy is unavailable, and natural energy is sufficient.

When no renewable energy is utilized, the COP of the whole system is:

$$COP_1 = \frac{Q_{output}}{(Q_{hot} + Q_{cold} + Q_{electric})} \quad (7-20)$$

When renewable heating and cooling energy are utilized, the COP of the whole system is:

$$COP_2 = \frac{Q_{output}}{Q_{electric}} \quad (7-21)$$

7.3 Theoretical Modelling

7.3.1 Modelling Set-up

This whole system modelling is constituted of four main numerical modules and three flat plate heat exchangers. The four models include the air-to-air heat/mass exchanger model, dehumidifier core models, the air-to-air cross-flow heat exchanger model, and the regenerator core model. Three flat plate heat exchangers are hot water to strong solution exchanger, solution to solution exchanger and cold water to solution exchanger.

In Chapter 4, the air-to-air heat/mass exchanger model was set up, and heat/mass transfer coefficients employed in this model were corrected by the experimental results. It was further approved by testing results that the numerical model utilizing the correction coefficients could predict the recovery working performance with acceptable errors.

In Chapter 5, the model of the desiccant dehumidifier was built up, based on the heat/mass transfer mechanism, and experimental results approved that the simulation results agreed with the experiments with acceptable errors.

In Chapter 6, the air-to-air heat recover model was built up and its performance was researched. It was found that the simulation results were higher than the testing results. It is because the extra energy absorbed from the hot water exchanger was not calculated in the numerical simulation. Also a regenerator model has been developed in this chapter, and the results kept a steady gap with the testing results in all of the series of comparison. It is mainly caused by energy waste in the testing with the following air stream and the falling down desiccant solution. However, the simulation results showed agreement with the testing results with acceptable errors.

Therefore, these four numerical simulation models were employed in the theoretical simulation as four calculating modules. Desiccant to desiccant and cold water to the strong desiccant flat plate exchanger are the calculating points connecting these four models. The hot water to weak desiccant flat plate exchanger had been considered in the regenerator modules, so it was not repeated again.

7.3.2 Base Conditions for Whole System Theoretical Modelling

Simulation pre-set conditions were presented as the following:

- (1) Fresh air temperature and relative humidity were 30°C and 50% respectively; return air temperature and relative humidity were 24°C and 50% respectively; fresh and exhaust air flow rates were the same 500m³/h; the fresh air flow speed into regenerator was 800m³/h.
- (2) LiCl solution was selected as the working liquid and its strong concentration of 35%, flow rate of 15L/min and temperature of 30°C equaled the temperature of the environment.

- (3) The cooling water temperature was 18.5°C (equal to the dew point temperature) and the flow rate was 18L/min.
- (4) The heating water temperature was 60°C, and the flow rate was 13L/min.
- (5) The air-to-air heat/mass exchanger, dehumidifier core, air-to-air cross-flow heat exchanger, and regenerator core size were described in Chapters 4, 5, and 6.
- (6) Desiccant to desiccant flat plate heat exchanger effectiveness was assumed at 80%, which was to be proved by experiments in the next section.
- (7) The same type flat plate heat exchangers were used for the desiccant to desiccant, desiccant to hot/cold water heat exchanger, at the assumed effectiveness of 80%.

7.3.3 Modelling Results of Heat Recovery/Desiccant Cooling System

As investigated in Chapters 4, 5, and 6, the main influencing factors of the air-to-air exchanger are the air humidity and flow speed; for the dehumidifier are the fresh air temperature/humidity, air flow rate, desiccant concentration and flow rate; for the regenerator are the desiccant and air temperature. For saving cooling and heating energy, the working solution temperature in the strong/weak store sink was assumed to be same as in the environment. The synthetically considered impacting factors for the COP research for the whole system, the affecting factors of air temperature, humidity, flow rate and desiccant concentration and flow rate were investigated. In all of the simulations, the air flow speeds into the regenerator were kept unchanged.

Air Temperature Influence on the COP

By varying the air temperature from 26 to 36°C at the relative humidity of 50%, the corresponding cooling water temperature equalling the dew point temperature, and the desiccant temperature in the storage sink equalling the environment temperature were changed respectively. The air flow, desiccant solution and heating/cooling water flow rate, and heating

water temperature, desiccant working concentration were kept unchanged. The influences of air temperature on the COP of the whole system are presented in Figure 7-4.

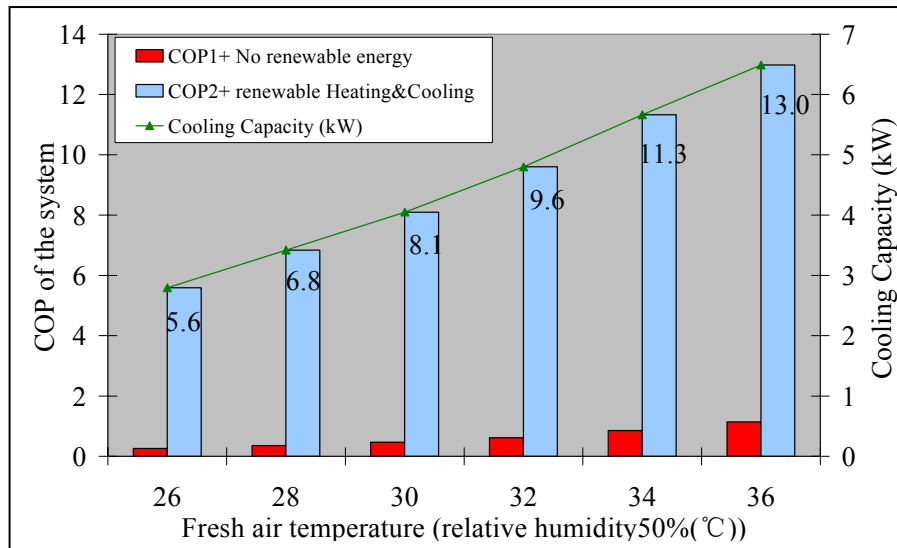


Figure 7-4 COP of the system vs. air temperature

From Figure 7-4 it can be seen that the air temperature greatly influenced the COP, when the air temperature is 26°C, the COP₁ without renewable energy is as low as 0.25, but it rises quickly to 1.14 when the air temperature reaches 36°C. When the renewable heating and cooling energy are both available, the COP₂ of the system is 13.0. The cooling capacity of the system increases with the fresh air temperature rising as presented in Figure 7-4, and the highest value is 6.5kW. The cooling tower could produce the cooling energy, and the solar collector could afford the heating energy with the proper temperature, which has been proved in Chapters 5 and 6 respectively. Hence, this heat/mass recovery and desiccant cooling system is applicable in the hot and humid climate with a good solar radiant.

Relative Humidity Influence on the COP

Varying the air relative humidity from 35 to 70% at the temperature of 30°C, the corresponding cooling water temperature equalling the dew point temperature was changed. The desiccant temperature in the storage sink equalled to the environment temperature of 30°C. The air flow

rate, desiccant solution and heating/cooling water flow rate, and heating water temperature, desiccant working concentration were kept unchanged. The influences of air relative humidity on the whole system COP are presented in Figure 7-5.

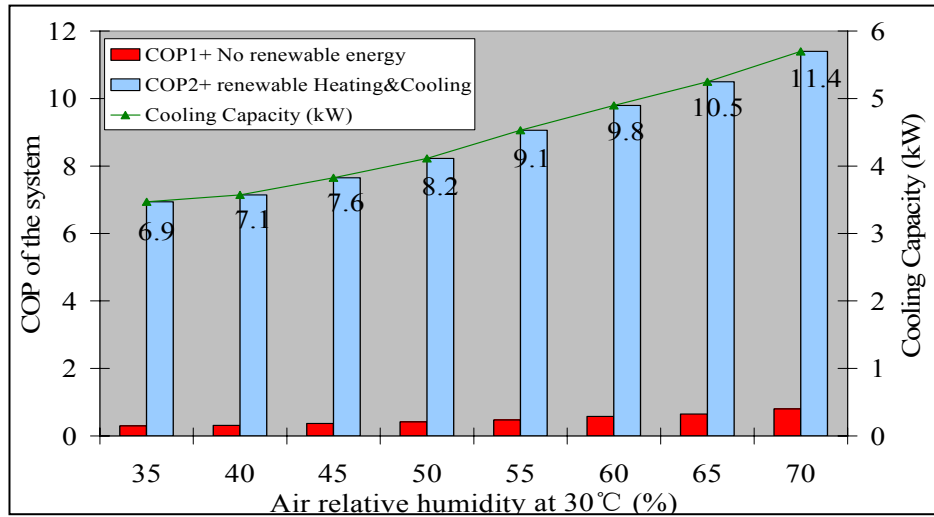


Figure 7-5 COP of the system vs. fresh air relative humidity

COP of this heat recovery/desiccant cooling system and cooling capacity, both increase with the fresh air relative humidity increasing. It's obvious that when no renewable energy is utilized, the COP₁ of this system is very low in the range of 0.3 ~ 0.8. However, when the cooling and heating energy both are substituted by renewable energy, the COP₂ is in quite a high range of 6.94 ~ 11.39. Dehumidification capacity increases and regeneration capacity decreases with the fresh air moisture content increasing as shown in figures 5-13 and 6-16 respectively. Because the cooling capacity rise could cover the regeneration capacity decline, the COP of the system rises. If the fresh air relative humidity is as high as 70%, the system can supply a cooling capacity of 5.7kW. Hence, this system performs higher COP in a humid region than in a dry place.

Air Flow Rate (into the Heat/mass Exchanger and Dehumidifier) Influence on the COP

By varying the air flow rate into the heat/mass exchanger from 300 to 900m³/h, the corresponding cooling water temperature equalled the dew point temperature of 18.5°C, and the

desiccant temperature equalled the environment temperature 30°C. By keeping the air temperature, relative humidity, desiccant and heating/cooling water flow rate, and heating water temperature, the desiccant working concentration remained unchanged. The influences of air flow rate on the whole system COP are shown in Figure 7-6.

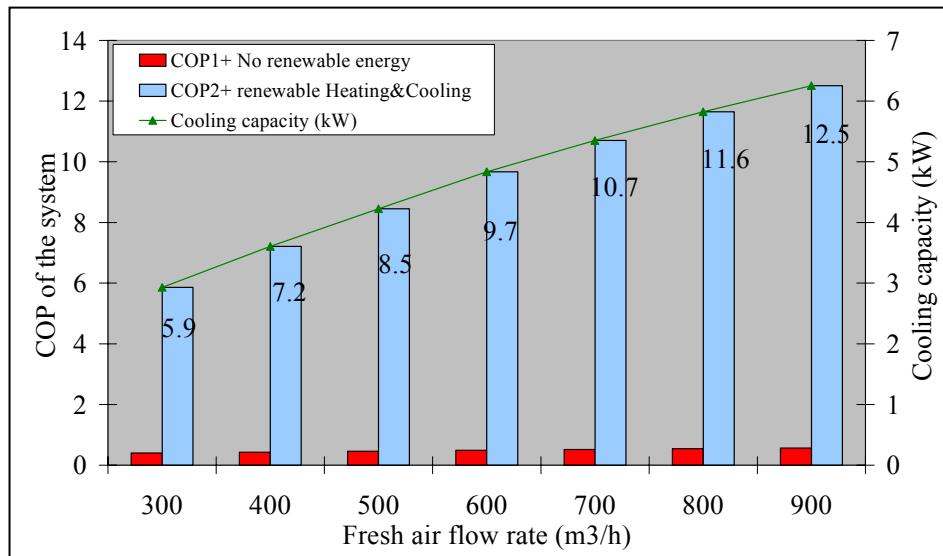


Figure 7-6 COP of the system vs. fresh air flow rate

As shown in Figure 7-6, the higher air flow rate results in a higher cooling capacity, but when the cooling capacity increases, the consumed regeneration energy is enhanced. Hence the COP changing trend is minimal, when there is no renewable energy available. This is because the greater air flow rate results in a higher dehumidification capacity, as illustrated in Chapter 5 (Figure 5-11), which induces more heating energy required to condense the dilute solution in the regenerator unit. The most part of the increased dehumidification capacity is counteracted by the rising heating energy, so the increase of COP₁ is almost ignorable. When renewable heating and cooling energy are both employed in this system, the COP₂ is enhanced from 5.9 to 12.5, with the air flow rate increasing. Therefore, for the regions with available renewable heating and cooling energy, a large amount of air ventilation gives good air quality as well as high COP.

Desiccant Working Concentration Influence on the COP

By changing the working solution concentration from 25% to 40%, and keeping the other pre-set conditions, such as air temperature, relative humidity, flow rate, and desiccant solution, the heating/cooling water flow rate, and heating water temperature remained unchanged. The corresponding cooling water temperature equals the dew point temperature 18.5°C, and the desiccant temperature equals the environment temperature 30°C. The impacts of the desiccant working concentration on the whole system COP are shown in Figure 7-7.

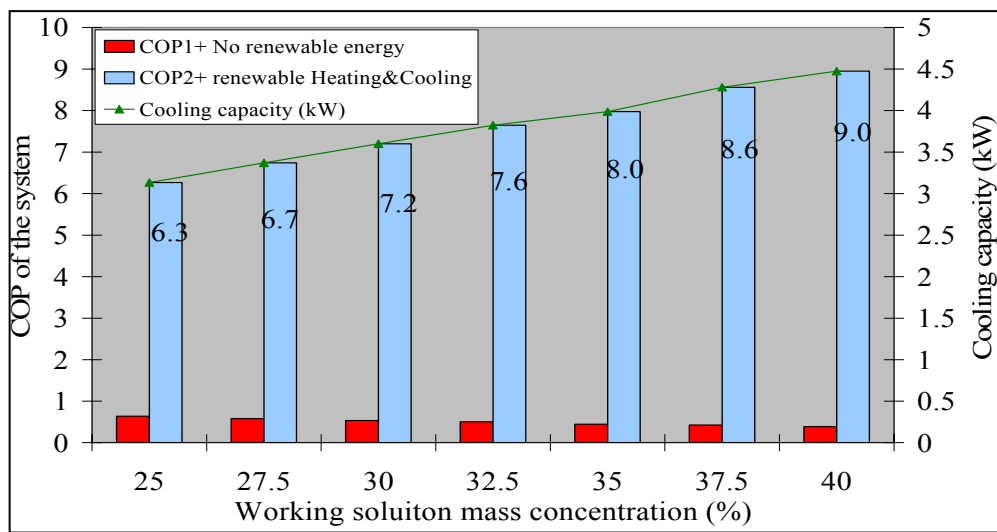


Figure 7-7 COP of the system vs. working solution mass concentration

From Figure 7-7 it can be seen that the cooling capacity increases from 3.1 to 4.5, with the solution mass concentration increasing from 25 to 40%, and the COP₁ of the system decreases with the working solution mass concentration increasing when no renewable energy is available. When the working solution concentration increased from 25% to 40%, the cooling capacity and dehumidification capacity increase as analyzed in Chapter 5, but the regeneration capacity is reduced in Chapter 6. As analyzed in Chapters 5 and 6, with the working solution mass concentration increasing, the heat recovery effectiveness decreased, inducing more consumption of cooling energy, and simultaneously, more regeneration energy and a high regeneration temperature was demanded to condense out the absorbed moisture as shown in figure 6-9. Hence, the COP₁ of the system decreases with the working LiCl solution concentration

increasing when no natural energy is available. However, when the cooling and heating energy are both substituted by renewable energy, such as solar energy/waste heat, natural cooling water from cooling tower/ground water, the COP₂ of the system increases with the increase of the working solution concentration.

Desiccant Flow Rate Influence on the COP

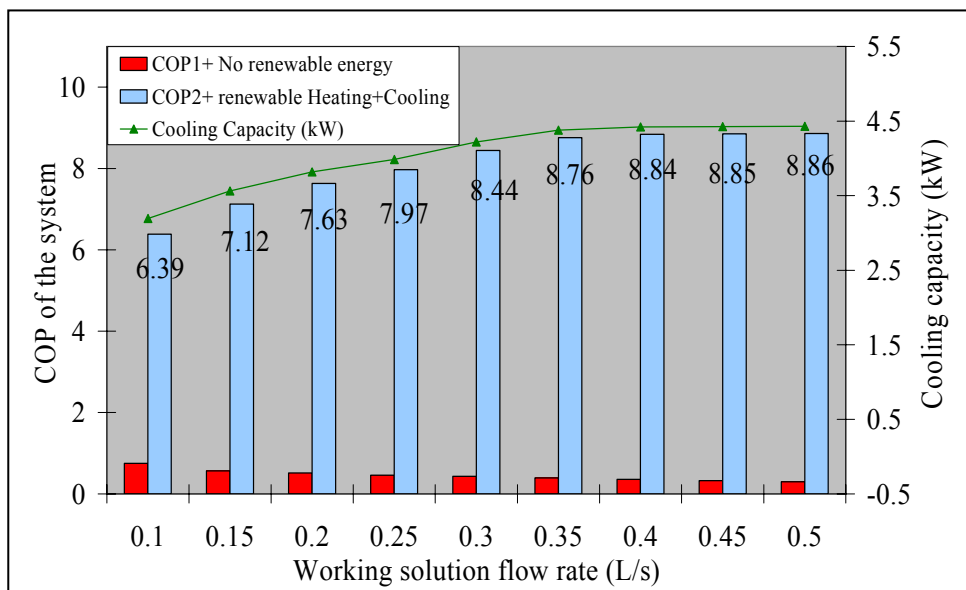


Figure 7-8 COP of the system vs. working solution flow speed

By changing the working solution flow rate from 0.1 to 0.5L/s, and keeping the other pre-set conditions such as air temperature, relative humidity, flow rate, and heating/cooling water flow rate and heating water temperature, the solution working concentration remained unchanged. The corresponding cooling water temperature equalled the dew point temperature 18.5°C, and the desiccant temperature equalled the environment temperature 30°C. The effects of the desiccant working concentration on the whole system COP are shown in Figure 7-8.

In figure 7-8, the cooling capacity of the system increases by 33% when the desiccant flow rate increased from 0.1 to 0.5L/s. The COP₁ of the system decreases with the working solution flow rate increasing when no renewable energy is available. This is because, with the desiccant flow

rate increasing, the dehumidification capacity and regeneration capacity both decrease, as expatiated in Chapters 5 and 6. Although the cooling capacity rises, the increasing speed can't cover the consumed energy increase. Moreover, when the renewable cooling and heating energy is existent, the COP₂ gradually increases to the value of 8.86 and then keeps to a very low rising speed at about 0.1% when the flow rate is over 0.35L/s. When only electrical energy is consumed, a higher desiccant flow rate results in more moisture being absorbed and supply air being more dehumidified. For this case, the cooling energy is enhanced, but the energy consumption is not accounted, so the COP₂ is high. But for the fixed air parameters and desiccant concentration and temperature, the superfluous moisture available for transferring from the air stream to the solution film is unalterable. When the increasing solution flow rate reaches the level of 0.35L/s, the absorbed moisture gradually approaches the maximal value. Then the COP₂ is close to the highest value and keeps slowly increasing. Hence, when natural cooling/heating energy exists, the higher desiccant solution flow rate of 0.35L/s is preferred to service good air supply conditions, with a high COP and cooling capacity. When renewable energy is absent, it was clear that the lowest desiccant flow rate could offer a high dehumidification capacity, and regeneration capacity, as well as COP, but it has the lowest cooling capacity, as shown in figures 5-9, 6-13 and 7-8. Hence, for achieving high COP and cooling capacity, the sprayed desiccant quantity to the dehumidifier core (in the dehumidifier small circle) is indicated, more than the solution circulating the whole circle (from dehumidifier to regenerator).

7.3.4 Summary of Theoretical Simulation Results

Figure 7-9 shows the system COP and cooling capacity changing trend when the affecting factors such as desiccant concentration, flow rate and fresh air temperature, relative humidity and flow rate were changed in range. The fresh air parameters impact the cooling capacity more heavily than the solution, especially the fresh air temperature and flow rate. It was obvious that when no renewable energy is utilized, the fresh air flow rate least affects the system COP₁, the

fresh air temperature heavily impacts the system COP₁, and the fresh air relative humidity takes the second impacting role. The impact of the desiccant flow rate and mass concentration on the COP₁ is similar to each other. When the cooling and heating energy are both replaced by renewable energy, the COP₂ is heavily affected by the fresh air parameters in the order of air temperature, flow rate, and humidity and the desiccant solution takes the smallest impact on the COP₂ as shown in Figure 7-9.

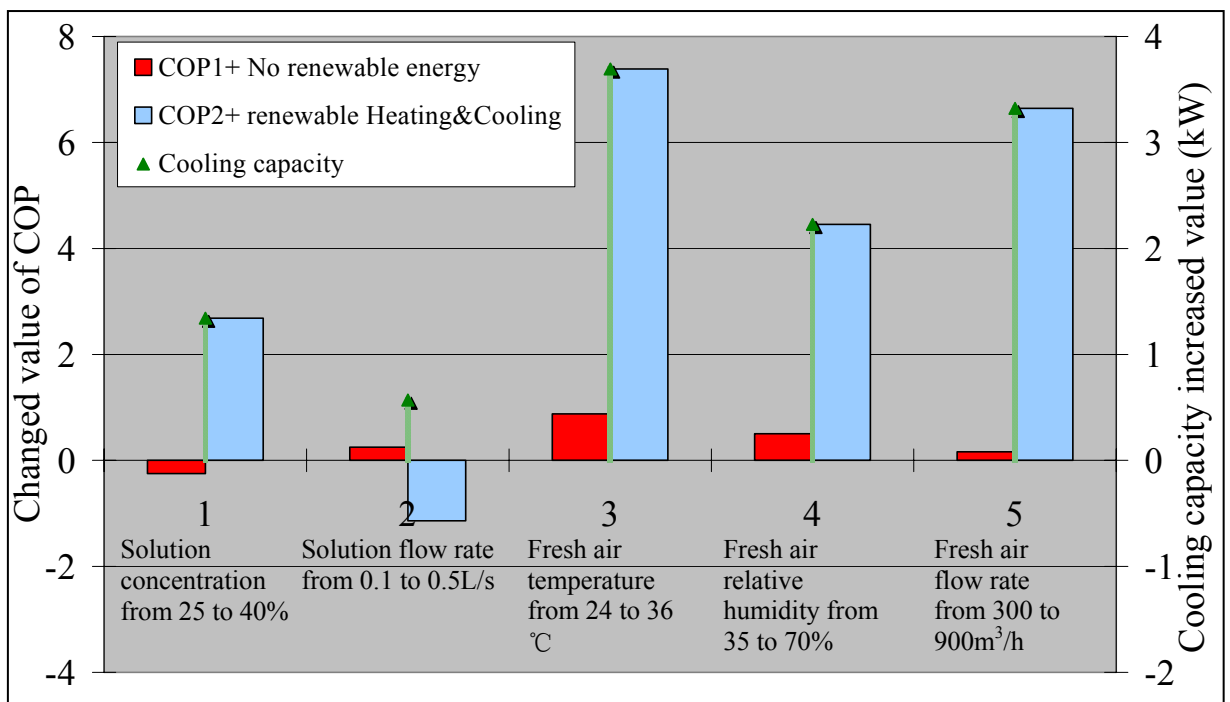


Figure 7-9 Comparisons of the different factors influencing on the system COP

Briefly, the fresh air temperature has most impact on the cooling capacity and COP in all the conditions (with/without renewable energy), and regions with a hot and humid climate are more suitable to use this system with high COP. Especially for hot/wet regions with plenty of sunshine, this heat recovery/desiccant cooling system has the ability to save lots of cooling energy and reduce the emission of CO₂. Furthermore investigations have found that if the heat/mass exchanger and dehumidifier unit is installed into the windcowl/catcher, the electrical energy driving the fans could be saved and the COP could reach as high as 21.6 under the conditions that air temperature is 36°C, with the relative humidity of 50%.

7.4 Experimental Testing of Heat Recovery/desiccant Cooling System

7.4.1 Test Rig of Heat Recovery/desiccant Cooling System

The novel heat recovery/desiccant cooling system testing rig is shown in Figure 7-10. It has been detailed in Chapters 4, 5, and 6, regarding the heat/mass exchanger, dehumidifier, regenerator unit and the two air control systems. All the testing apparatus and sensors utilized in this testing rig and the testing methods are the same as presented in Chapters 4, 5, and 6. Fresh air from the air controller was supplied to the top of the heat/mass exchanger unit, and then had the heat/mass exchanger with the upwards return air, which was controlled at about 24 °C and 50%. At the same time, air flow with the same temperature and humidity as supplied to the heat/mass exchanger, was forced into the regenerator unit, and regenerated out moisture from the weak solution.

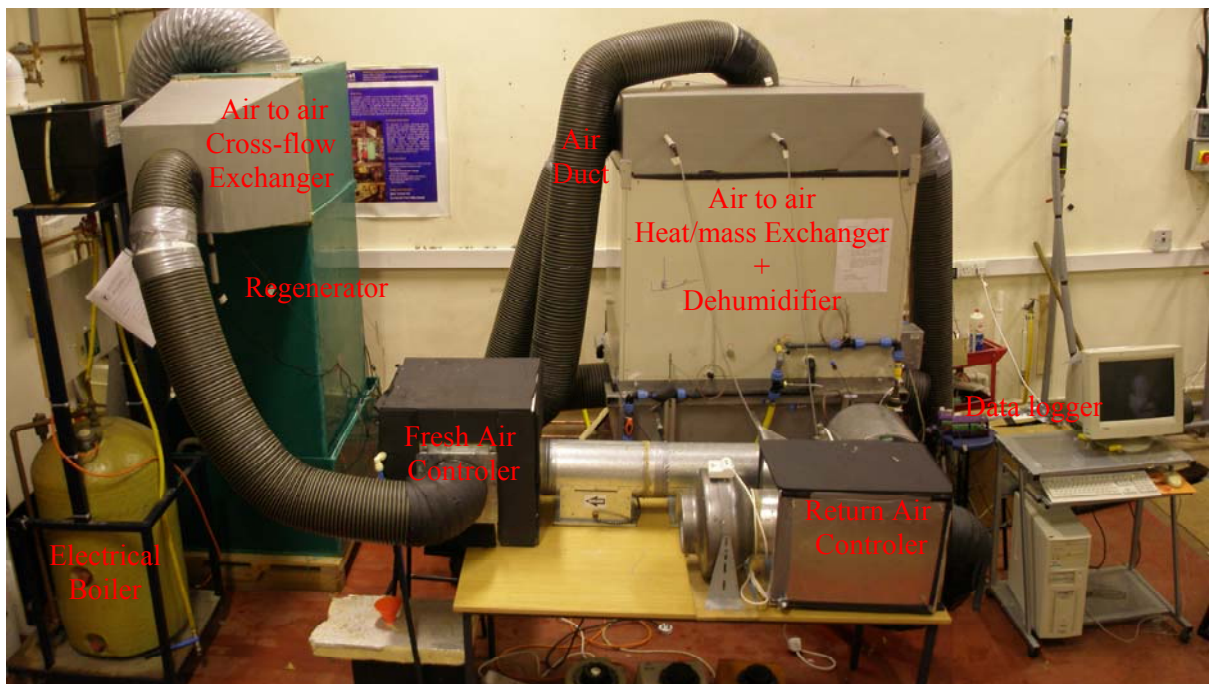


Figure 7-10 View of the testing rig — whole system

Cooling water was replaced by tap water in the experiments, and one 3kW electrical heater substituted for the solar energy, to supply hot water at about 60°C, as shown in Figure 7-10.

The data logger obtained the inspected data from the sensors and delivered it into the computer, as shown in figure 7-10. The testing results were recorded per minute by the computer. It took 2 hours to adjust the air stream and desiccant solution parameters waving in a small range before each series of resting, and at least 20 to 60 minutes testing results were recorded. Average values of each series of testing were used into the COP theoretical calculations.

7.4.2 Tests of Flat Plate Heat Exchanger

A series testing the flat plate heat exchanger, used as the desiccant to desiccant, desiccant to heating/cooling water exchangers, was performed, and the results are shown in Table 7.1. Nine cases were investigated, and it was found the average effectiveness was about 80.72%, very close to the assumed value –80% of the flat plate heat exchanger employed in the simulation of regenerator, dehumidifier and whole system models.

Table 7.1 Tested flat plate heat exchanger effectiveness

	Desiccant temperature from regenerator (°C)	Desiccant temperature to dehumidifier(°C)	Desiccant temperature out dehumidifier(°C)	Desiccant temperature to regenerator(°C)	Heat recovery effectiveness (%)
Case 1	37.09	29.90	27.78	31.83	77.23
Case 2	36.95	30.62	28.58	32.30	75.64
Case 3	36.61	28.90	26.72	30.73	77.88
Case 4	34.25	26.42	24.56	28.29	80.87
Case 5	36.57	27.00	25.18	31.73	84.04
Case 6	36.14	26.74	25.03	30.95	84.58
Case 7	35.40	28.54	27.08	31.28	82.42
Case 8	33.87	27.23	25.88	30.53	83.07
Case 9	31.91	25.63	24.69	27.62	86.99
Average value	35.86	28.17	26.35	30.95	80.72

7.4.3 Testing Results of Heat Recovery/Desiccant Cooling System

In the practical testing, the air and desiccant flow speed were kept unchanged in the regenerator for each series of testing. Cooling water was supplied from tap water, its temperature varied with the environment, and it was lower than the designed dew point temperature. Fresh air

supplied into the regenerator and dehumidifier were all from the fresh air controller as shown in figure 7-10, but because the supplying duct on the regenerator side was longer, and some heat was lost, the regenerator fresh air temperatures were lower than the dehumidifier side to a small degree.

In this testing rig, the regenerator had a bigger regeneration capacity than the dehumidifier demand per second. This is for regenerating and storing more energy when the solar energy is plentiful and it keeps supplying a strong solution to the dehumidifier when there is a shortage of solar energy. Hence, the consumed heating energy should be the energy regenerating out of the moisture absorbed in the dehumidifier.

COP_1 and COP_2 are calculated through the equations 7-20 and 7-21 respectively and the testing errors are 8.7% and 7.28% respectively (Law of Error Propagation) (A.A.Clifford, 1973). Because the heating and cooling energy were both consumed in the experiments, the COP was calculated by equation 7-21 (no renewable energy was utilized).

Influence of Fresh Air Temperature to COP

Testing was carried out regarding the air temperature's influence on the COP of the whole system. Return air temperature and relative humidity were controlled at about 24.3°C and 50% respectively; the cooling water was about 17°C (tests were carried out in winter in the UK), and flow rates were about 9L/min; the 3kW electrical heater supplied hot water at about 61.5°C with the flow rate of 10L/min; fresh and return air flow rates were the same 509m³/h; the working solution concentration in the dehumidifier was about 35%. Testing results are shown in Table.

7.2

Experimental results indicate that the COP and cooling capacity of the system decrease when the air temperature declines. Although the temperature of case 7 is lower than case 6, they have the same COP, owing to the higher moisture content than case 6. From the table 7.2 it can be

seen that the waving cooling water and heating water temperature impact the COP of the testing to some degree. The average COP and cooling capacity of this system are about 0.74 and 3.9kW and the highest values are about 0.89 and 5.35kW respectively.

Table 7.2 Influence of fresh air temperature changing to the COP of the system

Case number	1	2	3	4	5	6	7
Fresh air temperature (°C)	36.18	34.61	33.73	32.58	31.68	30.64	29.49
Fresh air moisture content (g/kg dry air)	15.01	14.56	14.30	14.37	13.47	15.04	15.54
Fresh air enthalpy (kJ/kg)	75.06	72.29	70.71	69.70	66.46	69.40	69.48
Return air temperature (°C)	23.78	24.53	24.44	24.57	24.51	24.25	24.50
Return air relative humidity (%)	49.86	49.90	49.47	49.60	49.42	50.67	50.54
Supply air temperature (°C)	25.77	25.70	25.94	26.04	25.72	26.19	26.24
Supply air moisture content (g/kg dry air)	10.53	10.08	10.00	9.70	9.61	9.89	10.01
Supply air enthalpy (kJ/kg)	52.87	51.63	51.68	51.01	50.45	51.66	52.01
Air flow rate to dehumidifier (m³/s)	509	509	509	509	509	509	509
Cooling water in (°C)	18.17	15.93	18.95	16.22	17.92	15.80	15.85
Cooling water flow rate (L/s)	0.23	0.23	0.23	0.23	0.23	0.23	0.23
Cooling energy (kW)	1.07	0.95	0.92	0.87	0.99	1.02	1.09
Heating water in (°C)	63.65	61.59	61.11	61.50	61.28	61.30	61.35
Heating water flow rate (L/s)	0.15	0.15	0.15	0.15	0.15	0.15	0.15
Heating energy (kW)	2.73	2.95	2.91	3.25	2.71	3.66	3.50
Cooling capacity (kW)	5.35	5.75	4.53	3.85	3.26	3.21	3.19
COP— No renewable energy	0.89	0.83	0.79	0.743	0.69	0.63	0.63

Influence of Fresh Air Humidity to COP

Testing was carried out regarding the air humidity’s influence on the COP of the whole system. Return air temperature and relative humidity were controlled at about 24.6°C and 56.7% respectively; the cooling water was about 16.8°C equaling the environment temperature (winter in UK), and flow rates were about 13.8L/min; the 3kW electrical heater supplied hot water at about 63.4°C with the flow rate of 9L/min; fresh and return air flow rate were the same 509m³/h; the working solution concentration into the dehumidifier was about 35%. Testing results are shown in Table. 7.3

Testing results shown in Table 7.3 indicate that the moisture content of the fresh air heavily affects the COP of the system. With the same air temperature, the highest moisture content 16.84g/kg dry air resulted in the highest COP of 0.57 and a cooling capacity of 4.14kW but a lower fresh air temperature drop. Hence, this system is effective for utilization in humid regions.

Table 7.3 Influence of fresh air moisture content changing to the COP of the system

Case number	1	2	3	4
Fresh air temperature (°C)	30.47	29.90	30.30	30.61
Fresh air moisture content (g/kg dry air)	<i>11.43</i>	<i>12.54</i>	<i>14.88</i>	<i>16.84</i>
Fresh air enthalpy (kJ/kg)	59.99	62.23	68.64	73.98
Return air temperature (°C)	24.60	24.88	24.75	24.33
Return air relative humidity (%)	54.58	56.98	58.04	56.70
Supply air temperature (°C)	25.90	26.36	26.13	26.93
Supply air moisture content (g/kg dry air)	7.31	7.81	9.17	9.46
Supply air enthalpy (kJ/kg)	52.93	53.48	53.83	52.07
Air flow rate to dehumidifier (m ³ /s)	509	509	509	509
Cooling water in (°C)	16.63	16.77	16.62	16.10
Cooling water flow rate (L/s)	0.23	0.23	0.23	0.23
Cooling energy (kW)	0.87	0.32	0.37	0.71
Heating water in (°C)	63.54	63.20	63.20	63.70
Heating water flow rate (L/s)	0.18	0.18	0.18	0.18
Heating energy (kW)	7.92	6.18	5.59	6.12
Cooling capacity (kW)	<i>2.83</i>	<i>2.94</i>	<i>3.45</i>	<i>4.14</i>
COP— No renewable energy	<i>0.31</i>	<i>0.40</i>	<i>0.50</i>	<i>0.57</i>

Influence of Fresh Air Flow Rate to COP

Testing was carried out regarding the air flow rate's influence on the COP of the whole system. Return air temperature and relative humidity were controlled at about 24.5°C and 50.8% respectively; the cooling water was about 12.9°C, and flow rates were about 10L/min; the 3 kW electrical heater offered the hot water at about 60.0°C with the flow rate of 11.5L/min; working solution concentration into dehumidifier was about 35%. Testing results are shown in Table. 7.4

Experimental results reveal that the fresh air flow rate into the dehumidifier impacts on the COP of the system, but the influence is not large like the moisture content and temperature dose compared with Tables 7.2 and 7.3. However, it heavily impacts on the cooling capacity. The maximal air flow rate produced the highest COP 0.76 and cooling capacity 3.73kW of the system. But under a similar cooling water temperature, the higher air flow rate induced the lower temperature drop of the fresh air. For the instance of case 4, the fresh air dropped 4.69°C, which was 0.21°C higher than case 5.

Table 7.4 Influence of fresh air flow speed changing to the COP of the system

Case number	1	2	3	4	5
Fresh air temperature (°C)	30.25	30.35	30.40	30.64	30.73
Fresh air moisture content (g/kg dry air)	12.71	12.90	13.22	13.31	13.42
Fresh air enthalpy (kJ/kg)	58.13	60.81	64.48	64.98	64.63
Return air temperature (°C)	24.60	24.51	24.30	24.57	24.71
Return air relative humidity (%)	44.91	50.75	52.87	54.52	50.88
Supply air temperature (°C)	24.97	25.58	25.47	25.95	26.25
Supply air moisture content (g/kg dry air)	8.07	8.84	9.22	10.38	10.22
Supply air enthalpy (kJ/kg)	46.54	49.77	49.21	52.92	52.35
Air flow rate to dehumidifier (m ³ /s)	322	500	600	700	800
Cooling water in (°C)	12.94	12.88	13.67	12.32	12.58
Cooling water flow rate (L/s)	0.167	0.167	0.167	0.167	0.167
Cooling energy (kW)	1.66	1.58	2.38	1.60	1.60
Heating water in (°C)	60.01	60.13	57.80	63.30	58.93
Heating water flow rate (L/s)	0.192	0.192	0.192	0.192	0.192
Heating energy (kW)	2.54	2.66	2.86	2.14	2.76
Cooling capacity (kW)	1.99	2.77	3.30	3.02	3.73
COP— No renewable energy	0.42	0.58	0.59	0.71	0.76

Influence of Desiccant Mass Concentration to COP

Testing was carried out regarding the desiccant concentration's influence on the COP of the whole system. Return air temperature and relative humidity were controlled at about 24.4°C and 49% respectively; the cooling water was about 14°C, and flow rate was about 13.8L/min; the 3

kW electrical heater provided hot water at about 63.2°C with the flow rate of 11L/min. Fresh and return air flow rates were the same 509m³/h. Testing results are shown in Table. 7.5

From the results presented in table 7.5, the influence of the desiccant concentration to the COP and cooling capacity are not obvious. The reasons for this include the working concentration of the solution changed in a small range from 31.59 to 35.57%; the testing conditions, such as the cooling and heating water temperature, fresh air and return air temperature and moisture content fluctuated in small range, which could have affected the testing results. Hence, the COP of the system were the similar value of 0.46~0.5 and the cooling capacity was about 3kW with the working solution mass concentration varying in the range of 33~36%

Table 7.5 Influence of working solution mass concentration to the COP of the system

Case number	1	2	3	4	5
Fresh air temperature (°C)	32.68	32.30	32.63	32.55	32.80
Fresh air moisture content (g/kg dry air)	15.04	14.68	14.21	14.41	14.39
Fresh air enthalpy (kJ/kg)	66.64	66.23	61.28	61.72	63.45
Return air temperature (°C)	24.17	24.19	24.47	24.60	24.39
Return air relative humidity (%)	52.78	53.58	42.92	47.36	48.68
Supply air temperature (°C)	25.06	25.39	25.51	26.02	26.08
Supply air moisture content (g/kg dry air)	10.58	10.18	9.48	9.69	9.84
Supply air enthalpy (kJ/kg)	53.80	54.28	47.48	48.27	48.71
Desiccant mass concentration (%)	33.19	34.60	34.87	35.17	35.57
Cooling water in (°C)	14.18	14.93	13.66	13.79	13.37
Cooling water flow rate (L/s)	0.23	0.23	0.23	0.23	0.23
Cooling energy (kW)	1.98	1.98	2.07	2.15	2.18
Heating water in (°C)	63.54	63.20	63.20	63.70	62.10
Heating water flow rate (L/s)	0.183	0.183	0.183	0.183	0.183
Heating energy (kW)	3.60	3.88	4.64	4.26	4.57
Cooling capacity (kW)	3.02	2.92	3.49	3.37	3.33
COP— No renewable energy	0.50	0.46	0.48	0.49	0.46

7.5 Comparison of Theoretical Simulation and Testing Results

Comparisons between the theoretical simulation and experimental results of the heat recovery/desiccant cooling system performance were carried out, and the results are shown in figures 7-11 and 12 regarding the factors of fresh air temperature, flow rate, moisture content and working desiccant concentration. The running conditions input to the theoretical modelling were the average values of the testing conditions. For instance of the case—air temperature influencing the COP, the average values of the testing results shown in Table 7.2 were employed in the corresponding simulation. These average values were the cooling and heating water temperature (17°C and 61.5°C respectively), flow rate (509m³/h), and return air temperature (24.3°C), moisture content (50%) and solution concentration (35%). The same method was used for other series of theoretical simulation. It was found that the experimental and theoretical simulation results show a similar changing trend, but there are discrepancies between them. The main reasons causing these are as follows:

- 1) The pre-set conditions of the theoretical simulation were the average value of the fluctuating testing conditions. This is the key factor inducing the difference between the theoretical simulation and experimental results.
- 2) The four numerical simulation modules constituting the theoretical model were researched in Chapters 4, 5, and 6. It was proved that they could predict the performance of the corresponding working unit in acceptable errors. These errors caused the differences between the theoretical results and experimental values.
- 3) The whole system tests were carried out in September and October in 2007, in Nottingham University, and the cold environment caused some energy loss in the testing.
- 4) There were unavoidable measuring errors in the testing, such as desiccant temperature, flow rate, concentration, air streams temperature, relative humidity and flow rate, hot/cold water temperature, flow rate.

- 5) The fresh air into the regenerator was a few degrees lower than the fresh air into the dehumidifier in the experimental testing. But in the theoretical simulation, it was assumed to be the same as the fresh air into the dehumidifier. This caused more energy consumption in practical testing than in the theoretical simulation.
- 6) The limit accuracy of the theoretical model simulation was another probability causing errors.

Although there are differences between the theoretical and experimental results, they have the similar COP changing trend. The average COP difference between the experimental and theoretical simulation results are 3.7%, 7.3%, 1.0% and 6.4 % for the factors of air temperature, flow rate, moisture content and solution mass concentration respectively as shown in Figures 7-11 (a), (b), (c) and (d). The cooling capacity difference between the experimental and theoretical simulation results are 13.8%, 12.2%, 10.7% and 9.9 % respectively, as presented in Figure 7-12. Therefore, the theoretical model predicted the COP of the system closer to the experimental results (a), (b), (c) and (d). The theoretical system was constituted of four numerical models, each of them having simulation errors to the experiments, and there are over 20 testing parameters in the whole system synchronously, so the discrepancy between the theoretical simulation and testing are unavoidable. Furthermore, the theoretical simulation and experimental results show the similar varying trend and the average difference percentage between them to be less than 14%, which is acceptable for the whole system theoretical modelling. Hence, the theoretical modelling can give a prediction of the system COP and cooling capacity within agreement errors. This is very useful when evaluating the feasibility of the heat recovery/desiccant cooling system for a different climate.

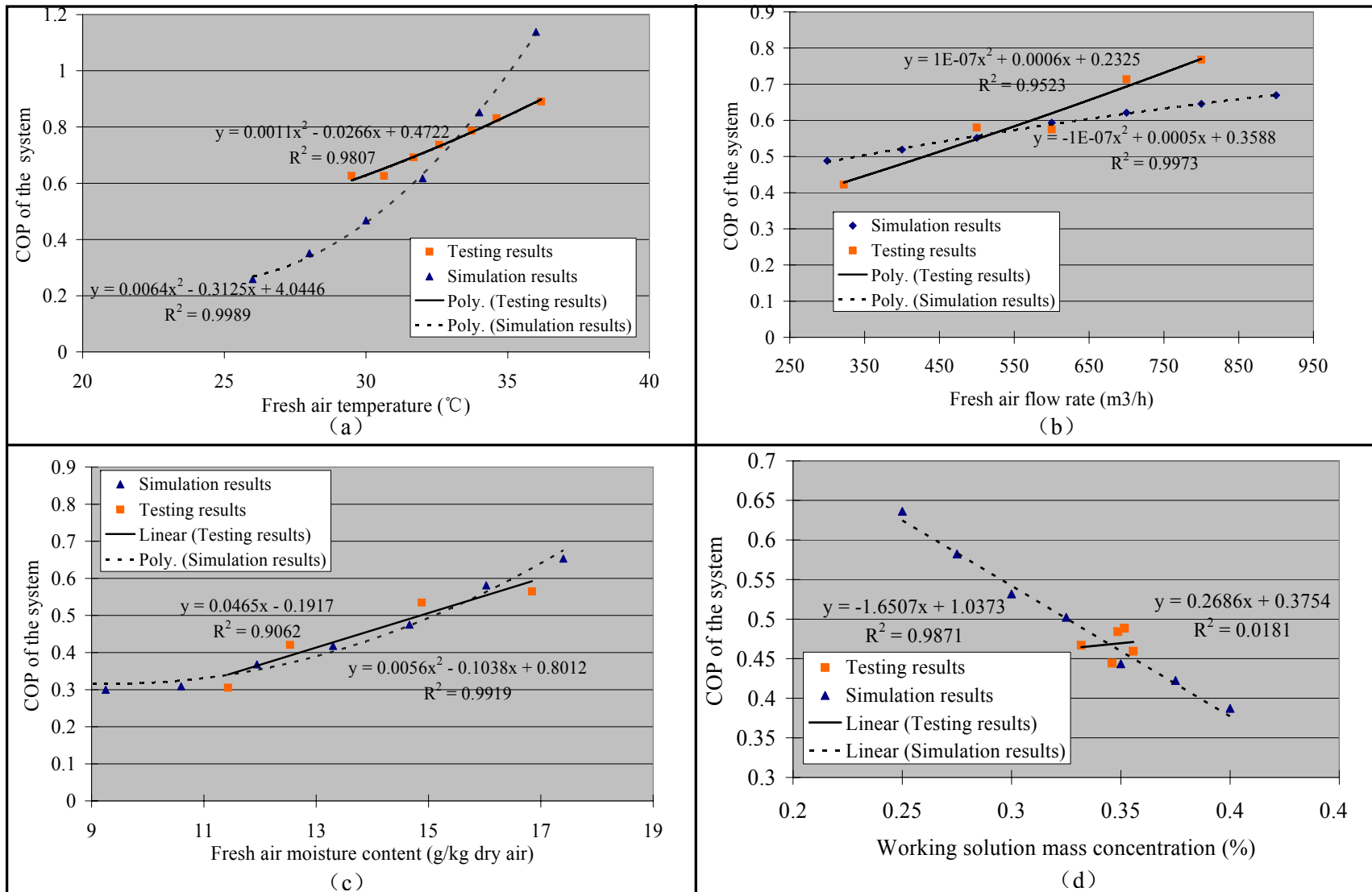


Figure 7-11 COP comparisons between the theoretical and testing results of the heat recovery/desiccant cooling system

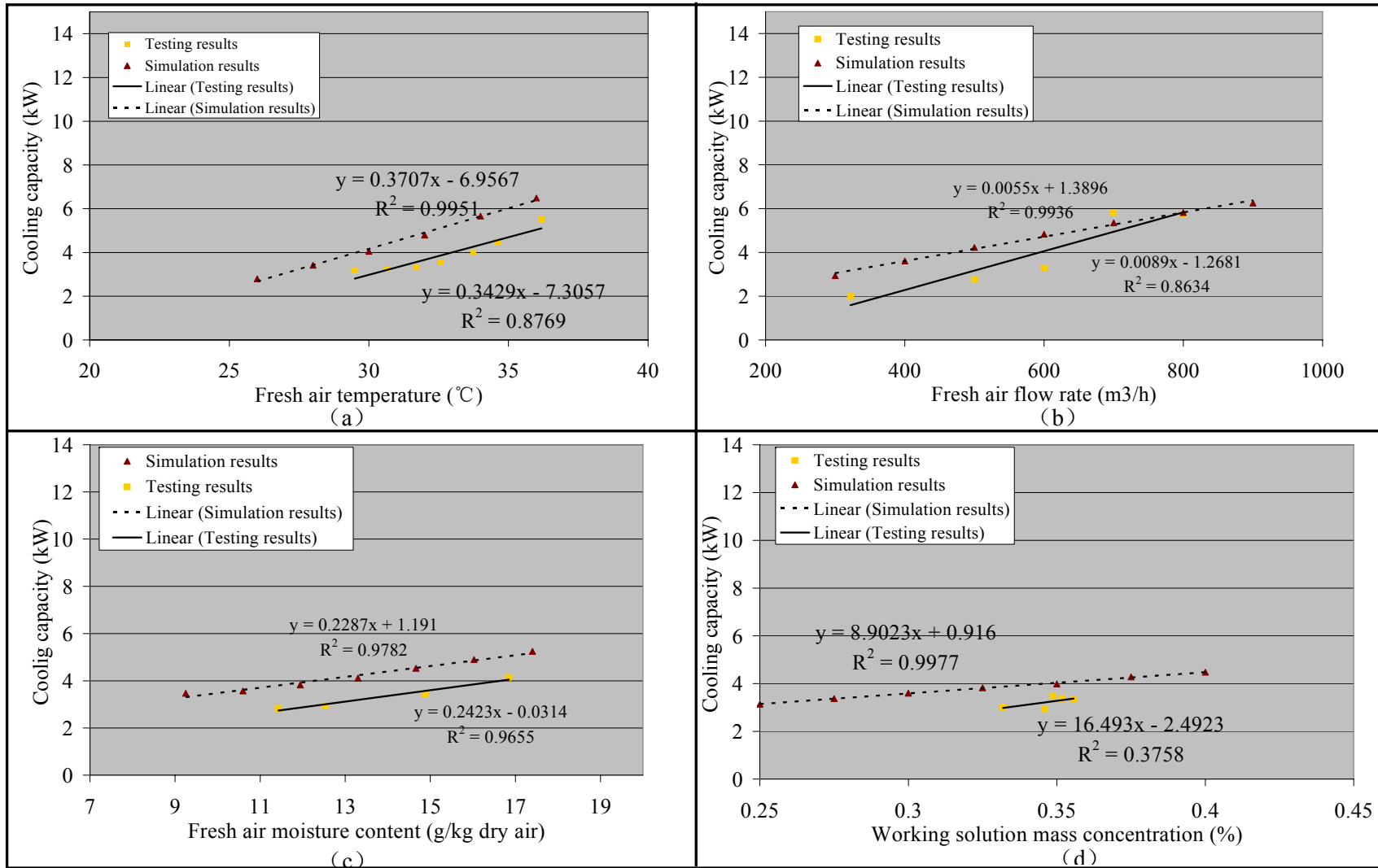


Figure 7-12 Cooling capacity comparisons between the theoretical and testing results of the heat recovery/desiccant cooling system

7.6 Summary

The whole heat recovery/desiccant cooling system was illuminated and the working processes of desiccant and air circle were described in the duhring diagram and psychrometric chart respectively. The coefficients of performance (COP) of the system were defined according to two energy conditions: no renewable energy and both cooling/heating energy available. The cooling capacity and COP of the novel system were investigated by both theoretical simulation and experimental testing. Conclusions summed up from the theoretical simulations were as follows:

- The cooling capacity and COP of the system increases with the increase in the fresh air temperature, especially in the case of utilizing renewable energy for cooling/ heating the strong/dilute solution, as COP_2 is heavily affected by air temperature. Therefore, this system is very suitable for use in hot/humid places. The highest cooling capacity 6.5 kW and COP_2 13.0 were achieved when the fresh air temperature rose to 36°C, with the relative humidity 50% and renewable energy available.
- Air moisture content influences the cooling capacity and COP less than the air temperature, but it is still an important factor impacting on the system. As investigated in Chapters 5 and 6, it can be found that high moisture content results in high dehumidification capacity but a lower regeneration capacity, only when the first is higher than the latter, the COP_2 of the system increases with the moisture increase. For the case of air temperature 30°C and relative humidity 70%, the cooling capacity and COP_2 of the system are 5.7kW and 11.4 respectively.
- When no renewable energy exists, the COP_1 changes are few with the air flow rate increasing. This is because a higher air flow rate results in more moisture absorbed into the solution, which accordingly needs more heating energy to evaporate it. But when renewable energy is available, such as solar energy, the COP_2 increases to 12.5 and the

cooling capacity rises to 5.9kW with the air flow rate reaching 900m³/h. This is because the cooling capacity increased, but the increasing cooling and the heating energy is not calculated

- Increasing the solution concentrations results in little change of COP₁, when no renewable energy is utilized. When renewable energy is employed, the cooling capacity and COP₂ increase with the concentration rises, due to the unconsidered heating energy. When renewable energy is utilized, the highest solution concentration results in the highest cooling capacity and COP₂ as shown in figure 7-7. But if there is no natural energy to be utilized, the lowest solution concentration 25% is preferred in order to gain the highest COP₁ 0.63 and cooling capacity 3.1kW.
- The cooling capacity and COP change slowly with the solution flow rate increasing. In figure 7-8, it can be seen that COP₂ of using renewable heating energy continues to change in a minor manner when the solution flow rate is over 0.35L/s. When there is no renewable energy, the lowest desiccant flow rate 0.1L/s performed the best with COP₁ 0.74 and the cooling capacity 3.19kW. But when the renewable energy is available, the flow rate of 0.35L/s is optimal to produce the higher COP₂ 8.0 and the cooling capacity 3.95kW with the lower circulating solution quantity.

Hence, under a defined air temperature and humidity for achieving an effective cooling and dehumidification system, the sizable dehumidifier and regenerator, proper desiccant concentration and flow rate and air flow speed can be calculated by this theoretical model before producing the equipment, and installing the system.

Laboratory tests were carried out to investigate the novel heat recovery/desiccant cooling system by the testing rig shown in figure 7-10. The influence of the fresh air temperature, moisture content, and flow speed, as well as the desiccant concentration to the system COP and cooling capacity were tested and the results are shown in Tables 7.2 to 7.5.

Comparisons between the experimental and theoretical simulation results were carried out. It was found that there are differences between the testing and simulation results as shown in figures 7-11 and 7-12. The reasons causing the discrepancy were analyzed and the main reasons include pre-set conditions utilized in the theoretical simulation, errors of each module employed in the theoretical model, the cold environment which caused energy loss in the testing, unavoidable measuring errors in the testing and reading data, and theoretical calculation limit accuracy. Because of the complexity of the theoretical model of the whole system, the assumptions settled in the simulation, and the unavoidable influence in the experiments, errors between the theoretical simulation and testing results are acceptable, and the model can approximately predict the system running conditions.

From the experimental and theoretical simulation results, we can see that the heat recovery/desiccant cooling system can perform a COP as high as 12.5, when the renewable heating/cooling energy is available. And the testing and numerical simulations in Chapters 5 and 6 proved that the solar collector and cooling tower could service sufficient energy at the required temperature. Furthermore, the high COP of 21.6 can be achieved, when the natural ventilation in the windcowl/catcher is available. This is significant for saving cooling energy in summer and reducing the CO₂ emission.

Chapter 8. Economic Analysis of the Whole System

8.0 Introduction

From the previous Chapters 3,4,5,6, and 7, the heat recovery/desiccant cooling system was investigated in details. It was found the system could be driven by the natural energy provided from the equipments such as solar collector, cooling tower and windcowl/catcher. The analyses were carried out and results proved that the heating energy for regeneration and cooling energy for strong solution heavily influence the COP. So in this system, renewable energies utilizing is the key to save the fossil-fuel energy and reduce the CO₂ emission. Therefore, the economic and environment benefits of utilizing this system are expressed in this chapter.

8.1 Required Cooling and Heating energy

It was assumed that the novel heat recovery/desiccant cooling system was installed to treat a 200 m² office room in London in summer. From the air conditioning criteria in England, it is regulated that the indoor air condition for the educational buildings, offices and libraries has the similar air temperature and air ventilation requirement listed in Table 8.1 (CIBSE, 1999).

Table 8.1 Recommended comfort criteria for specific applications

	Educational buildings	Offices	Libraries	Retailing	Building societies	Hotels (bed room)
Air temperature (°C)	21~23	22~24	21~23	21~23	21~23	21~23
Suggested air supply rate (L/s· person)	8	8	8	8	8	8

From the Table8.1, it is clear that for the most buildings the recommended comfort temperature is from 21 to 24°C and air supply is 8L/s per person. We supposed the servicing office room is for twenty people sitting inside, the design indoor air temperature is 22°C and air supply rate is 160L/s. As presented in CIBSE that the relative humidity in the range of 40~70% is acceptable for people comfort requirement. In our economic analysis the value of 50% is selected as the

criteria. The design outside air conditioning parameters for London in UK in summer is shown in Table 8.2 (CIBSE). Furthermore, the ventilation air volume for the working room per hour is 576m^3 . For balance the air pressure in the room, the commensurate exhaust air is released out.

Table 8.2 Design outdoor and indoor air parameters

	Dry temperature (°C)	Wet temperature (°C)	Dew point temperature (°C)	Relative humidity (%)	Moisture content (g/kg dry air)	Enthalpy (kJ/kg)
Indoor air	22	15.36	11.15	50	8.225	43.02
Outdoor air	27.4	18.7	13.9	43.5	9.9063	52.81

In general, the sensible cooling capacity caused by building fabric, solar radiation and equipment, people is treated separately from the fresh supply air conditioning. Hence in our economic analyses only the fresh air cooling capacity and latent heat load aroused by the people working inside are considered. For the air ventilation, there is total $18\text{L/s} \times 20 (0.16\text{m}^3/\text{s})$ fresh air which need to be treated from the outside environment state to the indoor state as shown in Figure 1-1. As the criterion regulated in the CIBSE, the latent heat caused by the working people in the office is $46\text{W} \times 20 (0.368\text{g/s moisture})$ (CIBSE)

For the traditional air conditioning system, the ventilation fresh air has sensible heat exchange with the exhaust air and its temperature will be about 22.81°C , and the moisture content keeps unchanged (sensible heat recovery effectiveness is assumed at about 85%). Therefore, the total sensible and latent heat cooling load are about 169W and 0.715g/s (there is 0.347g/s moisture form the fresh air and 0.368g/s moisture caused by the people working inside). To deal with the latent cooling load, the $0.16\text{m}^3/\text{s}$ of fresh air is cooled below 7.5°C by the traditional HVAC system to condense out the superfluous moisture and then is reheated to 22°C again. In this over-cooling and re-heating progress, the cooling and heating capacity are 4.11kW and 2.99kW respectively.

For the novel heat/recovery desiccant cooling system, the ventilation fresh air has heat/mass exchanger effectively with the exhaust air and its temperature and moisture content will be reduced to 22.81°C and 8.4772g/kg(dry air) respectively (Chapter 4: sensible and latent heat recovery effectiveness is about 85%). Hence the total sensible heat cooling load is 169W and latent heat cooling load is 0.420g/s (there is 0.052g/s moisture form the fresh air and 0.368g/s moisture caused by the people working inside). Superfluous moisture (0.420g/s) is absorbed in the dehumidifier, and the sensible heat (169W) from the supply air and latent heat (1028W) released by the condensed moisture are treated by the cooling tower. The dehumidification capacity of the liquid desiccant is about 0.2g/L (Chapter 5), so the required desiccant flow speed is 2.1L/s and the least desiccant mass in the solution circle is about 60Kg. The average regeneration capacity gained in Chapter 6 is about 0.7g/kJ, for regenerate 0.420g moisture, the solar collector energy power is 600W. The monthly mean irradiation in London area in July is about 426.3kWh/m² (CIBSA Gide A), and the stand flat plate solar collectors' efficiencies are about 50% (S.B.Riffat, et al, 2000), so the demanded solar collector area is at least 3m². Table8.3 shows the monthly mean irradiation of stated inclination from horizontal.

Table 8.3 Monthly mean daily irradiation on inclined planes: London area

Month	Mean irradiation (W·h·m ⁻²) for stated inclination from horizontal (°)														
	Beam					Diffuse					Total				
	0	30	45	60	90	0	30	45	60	90	0	30	45	60	90
East:															
Jan	223	216	212	200	156	467	443	408	358	228	690	668	640	592	453
Feb	440	424	406	380	284	857	813	748	656	417	1298	1255	1191	1101	832
Mar	771	733	692	632	458	1428	1355	1250	1093	696	2199	2117	2007	1836	1374
Apr	1552	1464	1362	1227	858	2093	1989	1845	1627	1039	3644	3502	3314	3036	2263
May	2034	1866	1709	1512	1010	2578	2442	2263	1992	1262	4612	4370	4107	3734	2733
Jun	1929	1763	1596	1392	897	2874	2711	2508	2198	1380	4802	4538	4245	3831	2758
Jul	2116	1930	1757	1542	1013	2699	2553	2365	2078	1312	4815	4547	4263	3861	2807
Aug	1868	1765	1636	1465	1016	2319	2206	2043	1804	1153	4187	4026	3801	3479	2588
Sep	1250	1176	1101	996	712	1626	1548	1438	1264	811	2877	2763	2623	2404	1811
Oct	637	621	596	556	413	1009	960	886	779	498	1646	1603	1531	1417	1076
Nov	309	299	289	272	209	575	546	503	441	281	884	857	818	758	579
Dec	155	147	146	136	108	377	356	328	287	182	532	510	489	450	344
Mean	1107	1034	958	859	594	1575	1493	1382	1215	772	2682	2563	2419	2208	1635

8.2 Equipments Capital and Running Cost

Table 8.4 Equipments capital and running cost

	Traditional HVAC system		Heat recovery/desiccant cooling system	
Capital cost	£2500 (Web 8.1)		Dehumidifier +Regenerator unit	£1050.0 (Web 8.2)
			Solar collector (collector area 3.58m ²)	£360.0 (Web 8.3)
			Cooling tower	£1257.0 (Web 8.4)
			Working solution (60kg)	£550 (Web 8.6)
			sum	£3217
Maintain cost	£250		Dehumidifier +Regenerator fibre core	£250 (changing once time per year)
			Solar collector	Free (Web 8.3)
			Cooling tower	£49.0 (Web 8.5)
			sum	£299
Cooling capacity	Cooling capacity	4.11 kW	Cooling capacity	1.197 kW
	Heating capacity	2.99 kW	Heating capacity	0.6 kW
COP	Cooling COP	3.0	8.0	
	Gas boiler effectiveness	80%		
Total Input energy	Electricity	1.37 kW	0.225 kW	
	Gas	3.74 kW		
Energy price (Web 8.7)	Electricity	19.03 p/kWh	Electricity 19.03 p/kWh	
	Gas	4.183 p/kWh		
Annual running hours	8 hours per day for 3 months (720hrs)		8 hours per day for 3 months (720hrs)	
Annual running cost	£300.35		£30.82	
Pay back year	3.25 years			

The maximal COP value of the traditional vapour compression air-conditioning system is 3.0, which is quoted into the calculation of input energy (S.B. Riffat and Guoquan Qiu, 2004) and the gas boiler effectiveness is about 80%. The COP of the novel heat recovery/desiccant cooling system is obtained in Chapter 7 and when renewable energy is utilized, it reaches to 8.0 approximately. It is assumed that the air conditioning system running 8 hours per day to cool the office and there are total 3 months (June, July and August) utilizing air conditioning during each

year in UK. The heat recovery/desiccant cooling system can save 824.4kWh electric and 2692.8kWh gas energy per year comparing to the tradition vapour pressure HVACE system. The base capital of the novel heat recovery/desiccant cooling system is expensive than the traditional HVAC system. And because the heat/mass recovery and dehumidifier/regenerator core are made of fibre, which will be reshaped for long term running, the cores are all replaced each year. This replacement will cost £250 each year. Therefore, the pay back time of the novel system is about 3.25 years detailed in Table 8.4.

Additional, the solar collector can service living water and heating energy for the office in the rest time during the year. The dehumidification system could deal with the superfluous moisture from the fresh air in the winter. Figure 8-1 shows the energy gained by the 3.58m² solar collectors, which offer the heating energy/ living water in the winter (the 45° inclination from horizontal is selected). Therefore the solar collector can totally provide 29.9kW heating energy to the working room from December to May every year.

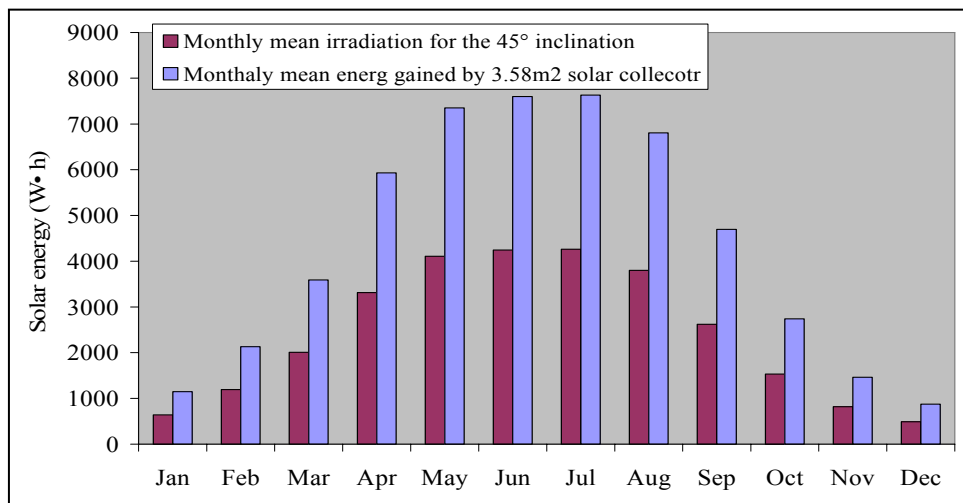


Figure 8-1 Monthly mean Irradiation for 45° inclination in London area and gained energy by 3.58m² solar collector

As pointed out that this system can save 824.4kWh electrical and 2692.8kWh gas energy per year compared with the traditional HVAC system. For the fossil -fuels energy, 0.6083 kg CO₂ is

released to produce 1kWh power. Hence, this system can prevent at least 2139.5kg CO₂ emission into the atmosphere (Web 8.8).

8.3 Summary

Energy consumptions of the traditional HVAC system and the novel heat recovery/desiccant cooling system were investigated based on a 200m² working office in London. It is known that the latter can save at least 824.4kWh electric and 2692.8kWh gas energy than the traditional HVAC system. The base capital of the novel heat recovery/desiccant cooling system is 717 pounds higher than the traditional HVAC system. For keeping the heat/mass recovery, dehumidifier/regenerator working effectively in the novel system, all the cores need to be replaced each year, which caused its maintaining cost about 50 pounds higher than the traditional HVAC system. Although it will take 3.25 years for the novel heat recovery/desiccant cooling system to pay back the high base capital, it is an effective way to save fossil-fuels energy as well as reduce CO₂ emission.

Chapter 9. Conclusion

9.1 Conclusions

9.1.1 Optimal Material Selection for Heat/mass Transfer

For the air-to-air heat/mass transfer membrane, only when the pore size was controlled in the range of $2.75 \times 10^{-10} \text{ m} < d_{\text{pore}} < 3.2 \times 10^{-7} \text{ m}$, it could allow liquid water across, and prevent gaseous air penetration. Investigation results indicated that most of the porous materials could offer the proper pore size at a high porosity, except for metals. Based on considering the other evaluating criterions, such as durability, Young's modulus and cost, fibre was selected as the preferred material. This is because of its' strong adsorption, compatible pore size, and lowest price which could cover its' disadvantages, such as lower durability and Young's modulus.

9.1.2 Performance of the Air-to-Air Heat/Mass Exchanger

Theoretical analyses indicated that the liquid desiccant soaked fibre membranes performed better than the clean and solid desiccant coated FPEM. The great improvement in the mass transfer of liquid desiccant soaked FPEM was thanks to its' mass transfer progress, which was caused by the concentration difference in the solution film. Corrections to the heat and mass transfer coefficients were made out and then the numerical simulation of liquid desiccant soaked FPEM were carried out. From the simulation and experimental results these were found that: (1) Enthalpy recovery effectiveness is a function of heat and mass transfer, and is heavily influenced by the latter; (2) The exchanger channel length greatly affects the heat/mass recovery effectiveness; (3) A lower exchanger channel height results in better energy recovery effectiveness, but leads to friction force, manufacturing difficulty, and cost increase; (4) The air temperature difference between fresh and exhaust air slightly affects the heat, mass and enthalpy recovery effectiveness; (5) Energy recovery effectiveness decreases heavily when the air flow

speed increases, but the decline trend slows down when the air flow speed is over 4m/s, as shown in Figure 4-19; (6) Heat transfer is slightly influenced by the moisture content difference, but mass transfer increases when the moisture content difference absolute value increases, as shown in Figure 4-20; (7) When the fresh air flow speed equals the exhaust air (ratio=1.0) the enthalpy recovery is as high as 86.34% with an acceptable supply air condition, and a high percentage of exhaust air energy is saved.

9.1.3 Performance of the Liquid Desiccant Dehumidifier

The performance of the desiccant dehumidifier was investigated by numerical simulation and experimental testing, and these are the conclusions from the results: (1) LiCl solution executes a better absorption capacity than LiBr and CaCl₂ solutions, but a lower heat recovery effectiveness; (2) The absorption capacity of the three investigated solutions increases, and the heat recovery effectiveness decreases, with the solution concentration increasing; (3) For the same dehumidification capacity $\varepsilon_{De}^{moisture} = 0.0125$ g/L at 29°C, the LiCl solution concentration is 30%, the LiBr solution is 50%, and CaCl₂ is more than 55%; (4) The channel height of the dehumidifier heavily affects the heat recovery effectiveness, but less to the moisture transfer; (5) The moisture absorption capacity increases, and the heat recovery effectiveness decreases with the channel length rising. (6) A higher desiccant temperature results in a lower recovery effectiveness in both heat and mass transfer, and a higher supply air temperature; (7) When the desiccant flow rate increases the moisture absorption capacity per litre solution declines, and the heat recovery effectiveness increases, as shown in Figure 5-9; (8) Increasing the air flow speed results in the higher moisture absorption capacity and lower heat recovery effectiveness; (9) Under fixed air relative humidity, increasing the air temperature results in a higher moisture content, which strengthens the absorption ability per litre solution; (10) Higher moisture content of fresh air results in higher absorption capacity but lower heat recovery effectiveness.

9.1.4 Performance of the Liquid Desiccant Regenerator

Two parts were investigated in Chapter 6, one is the air-to-air cross-flow heat recovery, and the other is the liquid desiccant regenerator. From the numerical simulation and experimental results, these were the conclusions:

For the air-to-air heat exchanger: (1) A high channel length ratio of fresh air to exhaust results in high recovery effectiveness, but a too short exhaust air channel works against saving the maximum energy from the exiting air; (2) The temperature difference between the fresh air and the exhaust air slightly affects the effective recovery, but the air flow rate heavily influences it. (3) Thermal conductivity slightly affects the recovery effectiveness; (4) The recovery effectiveness of the tested exchanger is only 50% to 65%, which needs to be improved.

For the desiccant regenerator: (1) LiCl is selected as the working solution in our project owing to its middle regeneration performs and lowest temperature requirement of the hot water; (2) The channel length of the dehumidifier slightly influences the regeneration capacity; (3) The channel height considerably affects the regeneration capacity, especially when the channel height is lower than 8mm; (4) A higher desiccant temperature results in a higher regeneration capacity, but it impacts less with the condensed mass concentration; (5) A lower desiccant flow rate leads to a higher regeneration capacity, and a condensed solution concentration; (6) The regeneration capacity and the condensed solution mass concentration increase with the fresh air flow speed increasing and then decline; (7) Similar to the air flow speed, there is an optimal air temperature necessary to obtain the best regeneration capacity and desiccant concentration; (8) A dry air stream performs a better regeneration capacity in the regenerator; (9) Higher hot water temperature produces a higher condensed solution at a lower regeneration capacity, as shown in Figure 6-17; (10) With the hot water flow rate increasing, the regeneration capacity decreases and the condensed solution concentration firstly increases, and then stays unchanged.

9.1.5 Performance of the Whole Heat Recovery/Desiccant Cooling System

Through the investigations of the coefficient-of-performance (COP) of the system, by the theoretical simulation and experimental studies, these conclusions were achieved: (1) The COP of the system increases with the fresh air temperature and moisture content increasing, especially in the case of utilizing renewable energy for cooling and heating strong and dilute solutions; (2) When no renewable energy is available, the COP₁ changes little with the air flow rate increasing. But when renewable energy is available, the COP₂ increases with the air flow rate; (3) When no renewable energy is utilized, the COP₁ slightly decreases with the solution concentration increasing. However, when the renewable heating energy is practicable, the COP₂ increases with the concentration rising; (3) When renewable energy is absent, the COP₁ decreases with the solution flow rate increasing; when renewable energy is present, the COP₂ increases until the desiccant flow rate is over 0.35L/s.

9.1.6 Economic Analysis of the Whole System

Capital and running cost comparisons between the traditional HVAC system and the novel heat recovery/desiccant cooling system were carried out. It was found, for a 200m² working office in London, the latter could save least 824.4kWh electric and 2692.8kWh gas energy as well as prevent 2139.5kg CO₂ emission per year. Although the base capital and maintaining cost of the novel system is higher than the traditional system, the running cost is low. Its pay back time is 3.25 years. Hence, the novel heat recovery/desiccant cooling system is an effective technology to produce cooling energy as well as reduce energy consumption and CO₂ emission.

9.2 Further Work

Although substantial work has been carried out during this research, there are still quite a few problems needing to be solved, and the performance of the system can still be improved to some degree. These potential chances to improve the performance are in the following:

Heat/mass Recovery Unit

Because the heat/mass recovery and dehumidifier/regenerator cores are all produced of fibre, which is difficult to keep the shape for long term, the rigidity needs to be improved. So, producing one kind material constituted of fibre and carbon and finding the proper combinatorial percentage is a feasible way to achieve effective heat/mass transfer material as well as durability and cheaper.

Dehumidifier and Regenerator Unit

It was noticed that the LiCl solution could produce dehumidification and regeneration effectively than the other solutions and demand the lowest regeneration temperature. However, some researchers found the vapor pressure in the mixture solution such as LiCl+LiBr, LiCl+CaCl₂, and LiBr+CaCl₂, etc, are changed (Koo, Kee-Kahb, 1998). Hence, the working performance of the mixture solution in this system is another potential to improve the COP.

Heat Recovery/Desiccant Cooling System

For the whole system, the research of the system running in other seasons is another direction to create satisfying indoor air condition and save heat energy. Instance for the winter in UK, the weather is moist and cold, hence it is advantageous to recovery the heating energy from the existing warm air and to dehumidify the fresh air before it is forced into the room. The heat/mass recovery between the warm and cold air streams is similar to summer condition. However, the dehumidification and regeneration running processes in the cold condition need to be designed and tested carefully. In this situation, the higher solution concentration and colder solution concentration is needed to absorb the moisture form the cold/humid air and the existing warm air from the room is utilized in the regeneration. Furthermore, the solar collector can service energy for both heating and living hot water.

References

A

- A.A.Clifford, Multivariate error analysis, A handbook of error propagation and calculation in many-parameter systems, Applied science publishersm, LTD, London, 1973
- A.A.M. Hassan, M. Salah Hassan, Dehumidification of air with a newly suggested liquid desiccant, Renewable Energy, 2008
- A.G. Straatman, N.C. Gallego, B.E. Thompson, H. Hangan, Thermal characterization of porous carbon foam—convection in parallel flow, International Journal of Heat and Mass Transfer 49 (2006) 1991–1998.
- A. Hachemi, Experimental study of thermal performance of offset rectangular plate fine absorber-plates, Renewable Energy, 17 (1999), 371-384
- A. Hoque, M. K. Alamb, G. G. Tibbetts, Synthesis of catalyst particles in a vapor grown carbon fiber reactor, Chemical Engineering Science 56 (2001) 4233–4243
- AKIO KODAMA, an Energy Flow Analysis of a Solar Desiccant Cooling Equipped with a Honeycomb Adsorber, Springer Science + Business Media, 11(2005) 597-602
- Alexander Wanner, Elastic modulus measurements of extremely porous ceramic materials by ultrasonic phase spectroscopy, Materials Science and Engineering A248 (1998) 35–43
- A.M. Hamed, Experimental investigation on the natural absorption on the surface of sandy layer impregnated with liquid desiccant, Renewable Energy 28 (2003) 1587–1596
- Ana Espert, Francisco Vilaplana, Sigbritt Karlsson, Comparison of water absorption in natural cellulosic fibres from wood and one-year crops in polypropylene composites and its influence on their mechanical properties, Composites: Part A 35 (2004) 1267–1276
- Arshad Y. Khan, Cooling and dehumidification performance analysis of internally-cooled liquid desiccant absorbers, Applied thermal engineering, 18, 1998, 265-281
- A. Schulz, G.N.Akapiiev, V.V.Shirkova, H.Rösler, S.N.Dmitriev, A new method of fabrication of heat transfer surfaces with micro-structured profile, Nuclear Instruments and Methods in Physics Research B 236 (2005) 254–258
- ASHRAE Handbook—HVAC Systems and Equipments Chapter 44, 2004
- A.W.T.Barenbrug, Psychrometry and Psychrometric Charts, Cape& Transvaal Printers Ltd, 1974

B

- B.Nait-Ali, K.Haberko, H.Vesteghem, J.Absi, D.S.Smith, Thermal conductivity of highly porous zirconia, Journal of the European Ceramic Society 26(2006) 356703574

C

- Chung TW, Ghosh TK, Hines AL, Novosel D, Dehumidification of moist air with simultaneous removal of selected indoor pollutants by triethylene glycol solutions in a packed-bed absorber, Sep, Sci Technol, 30, 1995, 1809-32
- Charles K. Hersh, MOLECULAR SIEVES, New York, Reinhold publishing corporation, Chapman & Hall , Ltd, London, 1961
- Christos J.Tsenoglou, Sylvia Pavlidou, Constantine D. Papaspyrides, Evaluation of interfacial relaxation due to water absorption in fiber-polymer composites, Composites Science and Technology 66(2006) P2855-2864
- C.J.Tsenoglou, et al, Evaluation of interfacial relaxation due to water absorption in fiber-polymer composites, Composites science and technology 66(2006)2855-2864.
- CIBSE Guide A, Environmental design, Chart 7-2, 1999
- C.X.Jia, Y.J.Dai, J.Y.Wu, R.Z.Wang, Analysis on a hybrid desiccant air-conditioning system, Applied Thermal Engineering, 26(2006) 2393-2400

D

- D. Metin, F. Tihminlioglu, D. Balköse, S.Ülkü, The effect of interfacial interactions on the mechanical properties of polypropylene/natural zeolite composites, Composites: Part A 35 (2004) 23–32
- Douglas E.Burkes, Guglielmo Gottoli, John J.Moore, Mechanical properties of porous combustion synthesized $Ni_3Ti-TiC_x$ composites, Composites Science and Technology 66(2006) 1931-1940
- D.Pietruschka, U.Eicker, M.Huber, J.Schumacer, Experimental performance analysis and modelling of liquid desiccant cooling systems for air conditioning in residential buildings, Internation Journal of Refrigeration, 29(2006) 110-124
- Duan P. Chen, Le Xu, Ashutosh Tripathy, Gerhard Meissner, and Bob Eisenberg, Selectivity and Permeation in Calcium Release Channel of Cardiac Muscle: Alkali Metal Ions, Biophys J, 76.3 (1999) 1346-1366

F

- F.A.Al-Sulaiman, P.Gandhidasan, S.M.Zubair, Liquid desiccant based two-stage evaporative cooling system using reverse osmosis (RO) process for regeneration, Applied Thermal Engineering, 27 (2007) 2449-2454

- F. Frusteri, V. Leonardi, S. Vasta, G. Restuccia, Thermal conductivity measurement of a PCM based storage system containing carbon fibers, *Applied Thermal Engineering* 25 (2005) 1623–1633
- F.N.Ani, E.M.Badawi, K.S.Kannan, The effect of absorber packing height on the performance of a hybrid liquid desiccant system, *Renewable Energy* 30 (2005) 2247-2256.
- Francey, J. L. A. Golding, P. Optical characteristics of swimming pool covers used for direct solar heating, *Solar Energy*, 1981, 26(3) 3, 259-263.

G

- G.A.Longo, A.Gasparella, Experimental and theoretical analysis of heat and mass transfer in a packed column dehumidifier/ regenerator with liquid desiccant, *International Journal of Heat and Mass Transfer*, 48(2005) 5240-5254
- G.Krauß, J.Kübler and E.Trentini, Preparation and properties of pressureless infiltrated SiC and AlN particulate reinforced metal ceramic composites based on bronze and iron alloys, *Materials Science and Engineering A337(2002)* 315-322
- Ghosh TK, Hines AL, Novosel D, Dehumidification of moist air with simultaneous removal of selected indoor pollutants by triethylene glycol solutions in a packed-bed absorber, *Sep, Sci Technol*, 30, 1995, 1809-32
- Giuseppe Pezzotti, Ikuko Kamada, Sadao Miki, Thermal conductivity of AlN/polystyrene interpenetrating networks, *Journal of the European Ceramic Society* 20 (2000) 1197-1203.
- Grossman G, Solar-powered systems for cooling, dehumidification and air-conditioning, vol. 1. 2002, P 53-62.
- Gur Mittelman, Abraham Kribus, Abraham Dayan, Solar cooling with concentrating photovoltaic/thermal (CPVT) systems, *Energy Conversion and Management* 48 (2007) 2481–2490

H

- H.A. Zondag, Flat-plate PV-Thermal collectors and systems: A review *Renewable and Sustainable Energy Reviews*, 12 (2008) 891–959
- Hersh CK. In: *Molecular sieves*. New York, London: Reinhold Publishing Corporation; Chapman & Hall Ltd.; 1961.
- H- M. Henning, T.Erpenbeck, C.Hindenbunrg, I.S.Santamaria, The potential of solar energy use desiccant cooling cycles, *International Journal of Refrigeration*, 24(2001)220-229
- H.Pelletier, Predictive model to estimate the stress-strain curves of bulk metals using nanoindentation, *Tribology International* 39(2006) 593-606

Hyunjo Jeong and David K.Hsu, Quantitative estimation of material properties of porous ceramics by means of composite micromechanics and ultrasonic velocity, *NDT&E International*, Vol.29.No.2(1996) 95-101

I

Igor Sevostianov and Mark Kachanov, Connection between elastic moduli and thermal conductivities of anisotropic short fiber reinforced thermoplastics: theory and experimental, verification *Materials Science and Engineering A360* (2003) 339_ 344

J

Jae-Weon Jeong, Stanley A. Mumma, Practical thermal performance correlations for molecular sieve and silica gel loaded enthalpy wheels *Applied Thermal Engineering* 25 (2005) 719–740

James R. Welty, Charles E. Wicks, Robert E. Wilson and Gregory Rorrer, Fundamentals of momentum, Heat, and Mass Transfer, John Wiley & Sons, USA, Inc, 2000, P288~326 and P500~589

Jae-Weon Jeong and Stanley A. Mumma Practical thermal performance correlations for molecular sieve and silica gel loaded enthalpy wheels *Applied Thermal Engineering* 25 (2005) 719–740

James R. Gaier, Yvonne Yoder Vandenberg, Steven Berkebile, Heather Stueben, Frederick Balagadde, The electrical and thermal conductivity of woven pristine and intercalated graphite fiber-polymer composites, *Carbon* 41 (2003) 2187–2193

James R. Sand, John C. Fischer, Active desiccant integration with packaged rooftop HVAC equipment, *Applied Thermal Engineering*, 25 (2005) 3138–3148

J.E. Parrott and Audrey D. Stuckes, *Thermal conductivity of solids*, Pion Limited, 1975, p 92,123,144

J. F. Despois, et al, Influence of the infiltration pressure on the structure and properties of replicated aluminium foam, *Materials Science, A* 462 (2007) 68-75

John Banhart, Manufacture, characterisation and application of cellular metals and metal foams, *Progress in Materials Science* 46 (2001) 559–632

J.Luo and R.Stevens, Porosity-dependence of elastic moduli and hardness of 3Y-TZP ceramics, *Ceramics International* 25 (1999) 281-286

J. P. Masse, et al, Influence of relative density on the architecture and mechanical behaviour of a steel metallic wool, *Scripta materialia* 54 (2006) 1379-1383

J. Hirunlabh, R. Charoenwat, J. Khedari, Sombat Teekasap, Feasibility study of desiccant air-conditioning system in Thailand, 2005, *Building and Environment*, 1-6

- J.L.Niu, L.Z.Zhang, H.G.Zuo, Energy saving potential of chilled-ceiling combined with desiccant cooling in hot and humid climates, *Energy and Buildings*, 34(2002)487-495
- Jörg Frauhammer, Harald Klein, Gerhart Eigenberger and Ulrich Nowak, Solving moving boundary problems with an adaptive moving grid method: Rotary heat exchangers with condensation and evaporation, *Chemical Engineering Science*, Vol. 53, No. 19, pp. 3393-3411, 1998
- Jose Ortiz and Christine Pout, Go Figure, *Building Service Journals (UK)*, November, 2006, 38-40

K

- K.Daou, R.Z.Wang, Z.Z.Xia, Desiccant cooling air conditioning: a review, *Renewable and Sustainable Energy Reviews*, 10(2006) 55-57
- K.Gommed, G.Grossman, A liquid desiccant system for solar cooling and dehumidification, *Journal of Solar Energy Engineering*, 126(2004) 879-885
- Kiyoshi Itatani , Tsuyoshi Tanaka , Ian J. Davies, Thermal properties of silicon carbide composites fabricated with chopped Tyranno[®] Si- Al- C fibres, *Journal of the European Ceramic Society* 26 (2006) 703–710
- Kiyoshi Okada, Shaunsuke Matsui, Toshihiro Isobe, Yoshikazu Kameshima, Akria Nakajima, Water-retention properties of porous ceramics prepared from mixtures of allophone and vermiculite for materials to counteract heat island effects, *Ceramics international* 34 (2008) 345-350.
- Koo, Kee-Kahb; *Journal of Chemical and Engineering Data*, Sep-Oct, 1998, v 43, n 5, p 722-725
- K.R. Kistler, E.L. Cussler, Membrane modules for building ventilation, *Chem. Eng. Res. Des.* 80 (2002) 53–64.

L

- Lacroix C, Ramany Bala P, Feidt M. Evaluation of the effective thermal conductivity in metallic porous media submitted to incident radiative flux in transient conditions. *Energy Conversion and Management* 40 (1999) 1775–81.
- L.A. Sphaier and W.M. Worek Analysis of heat and mass transfer in porous sorbents used in rotary regenerators, *International Journal of Heat and Mass Transfer* 47 (2004) 3415–3430
- L.C.S.Mesquita, S.J.Harrison, D.Thomey, Modeling of heat and mass transfer in parallel plate liquid-desiccant dehumidifiers, *Solar Energy* 80 (2006) 1475-1482

- Li-Wu Fan, Ya-Cai Hu, Tian Tian, Zi-Tao Yu, The prediction of effective thermal conductivities perpendicular to the fibres of wood using a fractal model and an improved transient measurement technique, *International Journal of Heat and Mass transfer* 49 (2006) 4116-4123
- Li-Zhi Zhang, Heat and mass transfer in plate-fin sinusoidal passages with vapour-permeable wall materials, *International Journal of Heat and Mass Transfer*, 51 (2008) 618-629
- L.M. Manocha, Ashish Warriar, S. Manocha, D. Sathiyamoorthy, S. Banerjee, Thermophysical properties of densified pitch based carbon/carbon materials—I. Unidirectional composites, *Carbon* 44 (2006) 480–487
- L. Mei, Y.J. Dai, A technical review on use of liquid-desiccant dehumidification for air-conditioning application, *Renewable and Sustainable Energy Reviews*, 2006
- L.Tadrist, M. Miscevic, O. Rahli, F. Topin, About the use of fibrous materials in compact heat exchangers, *Experimental Thermal and Fluid Science* 28 (2004) 193-199
- L.Z. Zhang, Y. Jiang, Heat and mass transfer in a membrane-based energy recovery ventilator, *J. Membr. Sci.* 163 (1999) 29–38.
- L.Z.Zhang, Heat and mass transfer in a cross-flow membranes-based enthalpy exchanger under naturally formed boundary conditions, *International Journal of Heat and Mass Transfer* 50(2007) 151-162
- L.Z.Zhang, Heat and mass transfer in plate-fin sinusoidal passages with vapour-permeable wall materials, *International Journal of Heat and Mass Transfer* 51(2008) 618-629
- L.Z. Zhang, J.L. Niu, Effectiveness correlations for heat and moisture transfer processes in an enthalpy exchanger with membrane cores, *ASME J. Heat Transfer* 122 (5) (2002) 922–929.

M

- Manocha LM, et al. Thermophysical properties of densified pitch based carbon/carbon materials, part I. Unidirectional composites. *Carbon* 2006;44:480–7.
- Manuel R. Conde, Aqueous solutions of lithium and calcium chlorides: — Property formulations for use in air conditioning equipment design, *M.CONDE ENGINEERING*, 2004
- Melda Özdinç, Çarpinlioglu, Murtaza Yildirim, A methodology for the performance evaluation of an experimental desiccant cooling system, *International Communications in Heat and Mass Transfer* 32(2005) 1400-1410
- M. Idicula, et al, Thermophysical properties of natural fibre reinforced polyester composites, *Composites Science and Technology* 66(2006)2719-2725
- Michael Piggott, *Load Bearing Fibre Composites*, 2ed Edition, KLUWER ACADEMIC PUBLISHERS, 2002

Moran Wang, Jihuan He, Jiangyong Yu and Ning Pan, Lattice Boltzmann modelling of effective thermal conductivity for fibrous materials, *International Journal of Thermal Science*(2006)

Mehmet Kanoğlu, Melda Özdiñç, Çarpınlioğlu, Murtaza Yıldırım, Energy and exergy analyses of an experimental open-cycle desiccant cooling system, *Applied Thermal Engineering* 24 (2004) 919–932

Michael D. Larson, Carey J. Simonson, Robert W. Besant, Phillip W. Gibson, The elastic and moisture transfer properties of polyethylene and polypropylene membranes for use in liquid-air energy exchangers *Journal of Membrane Science* 302 (2007) 136–149

N

N.A. Eltekova , D. Berek , I. Novak , F. Belliardo, Adsorption of organic compounds on porous carbon sorbents, *Carbon* 38 (2000) 373–377

N. Ghodsipour and M. Sadrameli, Experimental and sensitivity analysis of a rotary air pre-heater for the flue gas heat recovery, *Applied Thermal Engineering* 23 (2003) 571–580

O

Oberg V, Goswami DY, Experimental study of the heat and mass transfer in a packed bed liquid desiccant air dehumidifier, *Solar Energy Engineer*, 120 (1998), 4, 289-297

P

P.A. Davies, P.R. Knowles, Seawater bitterns as a source of liquid desiccant for use in solar-cooled greenhouses, *Desalination* 196 (2006) 266–279.

P.A.Davies, A solar cooling system for greenhouse food production in hot climate, *Solar energy*, 79(2005) 661-668

Pabst W, et al. Elasticity of porous ceramics—a critical study of modulus–porosity relations. *Journal of the European Ceramic Society* 2006;26:1085–97.

Peng Donggen, Zhang Xiaosong, Yin Yonggao, Theoretical storage capacity for solar air pre-treatment liquid collector/regenerator, *Applied Thermal Engineering* xxx (2007) 1–8

P.Mazzei, F.Minichiello, D.Palma, Desiccant HVAC system for commercial buildings, *Applied Thermal Engineering*, 22(2002) 545-560

P.Mavroudaki, C.B.Beggs, P.A.Sleigh, S.P.Halliday, The potential for solar powered single-stage desiccant cooling in Southern Europe, *Applied Thermal Engineering*, 22(2002) 1129-1140

Q

Qun Cui, Haijun Chen, Gang Tao, Huqing Yao, Performance study of new adsorbent for solid desiccant cooling, *Energy*, 30(2005)273-279

R

Ramasamy Sivakumar, Shuqi Guo, Toshiyuki Nishimura and Yutaka Kagawa, Thermal conductivity in multi-wall carbon nanotube/silica-based Nanocomposites, *Scripta Materialia* 56 (2007) 265–268

R.M. Lazzarin, A. Gasparella, G.A. Longo, Chemical dehumidification by liquid desiccants: theory and experiment, *International Journal of Refrigeration* 22 (1999) 334–347

R.M. Lazzarin and F. Castellotti, A new heat pump desiccant dehumidifier for supermarket application, *Energy and Buildings* 39 (2007) 59–65

R. Yamada, N. Igawa, T. Taguchi, Thermal diffusivity/conductivity of Tyranno SA fiber- and Hi-Nicalon Type S fiber-reinforced 3-D SiC/SiC composites, *Journal of Nuclear Materials*

R. Z. Wang, J. Y. Wu, Y. X. Xu, Y. Teng and W. Shi, Experiment on a continuous heat regenerative adsorption refrigerator using spiral plate heat exchanger as adsorbers, *Applied Thermal Engineering* Vol. 18. P13-23, 1998

S

S. Alizadeh and W. Y. Saman, An experiment study of a forced flow solar collector/regenerator using liquid desiccant, *Solar Energy*, 73(2002) 345-362

S. Alizadeh, Performance of a solar liquid desiccant air conditioner –An experimental and theoretical approach, *Solar Energy*, (2007)

Sankar Nair, Samir Verma, S. C. Dhingra, Rotary heat exchanger performance with axial heat dispersion, *International Journal of Heat and Mass Transfer* 41 (1998) 2857-2864

Sanjeev Jain, P.L.Dhar, S.C.Kaushik, Experimental studies on the dehumidifier and regenerator of a liquid desiccant cooling system, *Applied Thermal Engineering*, 20(2000) 253-267

S.B. Riffat and Guoquan Qiu, Comparative investigation of thermoelectric air-conditioners versus vapour compression and absorption air-conditioners, *Applied Thermal Engineering* 24 (2004) 1979–1993

S.B.Riffat, Doherty P.S. and Abdel Aziz E.I., Performance testing of different types of liquid flat plate collectors, *Internal Journal of Energy Research*, 24, 1203-1215

Schweitzer Philip A., *Metallic Materials, Physical, Mechanical and Corrosion Properties*, Marcel Dekker, INC, USA, 2003.

- S.Liu, S. Riffat and X. Zhao, Investigation of the Performance of a Low-cost Fibre Air-to-Air Heat/Mass Exchanger, SET 2007
- Shahab Alizadeh, Performance of a solar liquid desiccant air conditioner –An experimental and theoretical approach, Solar Energy (2007)1–9
- S Ginestet, P Stabat D Marchio, Control design of open-cycle desiccant cooling systems using a graphical environment tool, Building Serv. Eng. Res. Technol. 24, 4 (2003) 257-269
- S. S. Elsayed, Y. Hamamoto, A. Akisawa, T.Kashiwagi, Analysis of an air cycle refrigerator driving air conditioning system integspeedd desiccant system, International Journal of Refrigeration,14(2005)1-10
- S. Techajunta, S. Chirarattananona, R.H.B. Exell, Experiments in a solar simulator on soliddesiccant regeneration and air dehumidi_ cation for air conditioning in a tropical humid climate, Renewable Energy 17 (1999) 438_457

T

- Thomas Fend, Bernhard Hoffschmidt, Robert Pitz-Paal, Oliver Reutter, Peter Rietbrock, Porous materials as open volumetric solar receivers: Experimental determination of thermophysical and heat transfer properties, Energy 29 (2004) 823–833
- Toshihiro Isobe, Yoshikazu Kameshima, Akira Nakajima, Kiyoshi Okada, Yuji Hotta, Gas permeability and mechanical properties of porous alumina ceramics with unidirectionally aligned pores, Journal of the European Ceramics Society 27(2007)53-59
- Toshihiro Isobe, Takahiro Tomita, Yoshikazu Kameshima, Akira Nakajima, Kiyoshi Okada, Preparation and properties of porous alumina ceramics with oriented cylindrical pores produced by an extrusion method, Journal of the European Ceramic Society 26 (2006) 957–960
- T. Taguchi, N. Igawa, R. Yamada, S. Jitsukawa, Effect of thick SiC interphase layers on microstructure, mechanical and thermal properties of reaction-bonded SiC/SiC composites, Journal of Physics and Chemistry of Solid 66(2005) 576-580
- T.W.Clyne and F.Simancik, Metal Matrix Composites and Metallic Foams, EUROMAT-Volume 5, Weinheim.New York.Chichester, 2000

W

- Wiwut Tanthapanichakoon, Anawut Prawarnpit, New simple mathematical model of a honeycomb rotary absorption-type dehumidifier, Chemical Engineering Journal, 86(2002)11-15
- W.Y.Saman and S.Alizadeh, An experimental study of a cross-flow type plate heat exchanger for dehumidification/cooling, Solar Energy, 73 (2002)59-70

Welty J. R., Wicks C. E., Robert E. Wilson, Gregory L. Rorrer, Fundamentals of Momentum, Heat, and Mass Transfer, John Wiley & Sons, Inc, 2001, 723–724.

Willi Pabst, Eva Gregorov'a, Gabriela Tich'a, Elasticity of porous ceramics—A critical study of modulus–porosity relations, Journal of the European Ceramic Society 26 (2006) 1085–1097

X

X.Zhao, Shuli Liu and Saffa Riffat, Optimal Study of the Heat and Mass Exchanging Materials for the Indirect Evaporative Cooling Systems, Built and Environment accepted, 2007

X. Fu and D. D. L. Chung, Effects of silica fume, latex, methylcellulose, and carbon fibers on the thermal conductivity and specific heat of cement paste, Cement and Concrete Research, Vol. 27. N0.12.pp.1799-1804, 1997

X.H.Liu, Y..Zhang, K.Y.Qu, Y.Jiang, Experimental study on mas transfer performances of cross flow dehumidifier using liquid desiccant, Energy Conversion and Management, 2005

X.H.Liu, K.Y.Qu, Y.Jiang, Empirical correlations to predict the performance of the dehumidifier using liquid desiccant in heat and mass transfer, 2005

X.L. Wang, H.M. Zhang, J.L. Zhang, H.F. Xu, Z.Q. Tian, J. Chen, H.X. Zhong, Y.M. Liang, B.L. Yi , Micro-porous layer with composite carbon black for PEM fuel cells, Electrochimica Acta 51 (2006) 4909–4915

X. Py, E. Daguerre, D. Menard, Composites of expanded natural graphite and in situ prepared activated carbons, Carbon 40 (2002) 1255–1265

Y

Y. Hamamotoa, K.C.A. Alamb, B.B. Sahac, S. Koyamac, A. Akisawab, T. Kashiwagi Study on adsorption refrigeration cycle utilizing activated carbon fibers. Part1. Adsorption characteristics, International Journal of Refrigeration 29 (2006) 305–314

Y.J. Dai, H.F. Zhang, Numerical simulation and theoretical analysis of heat and mass transfer in a cross flow liquid desiccant air dehumidifier packed with honeycomb paper, Energy Conversion and Management 45 (2004) 1343–1356

Y.J.Dai, R.Z.Wang, H.F.Zhang,J.D.Yu, Use of liquid desiccant cooling to improve the performance of vapour compression air conditioning, Applied Thermal Engineering,21(2001)1185-1202

Y.J.Dai, R.Z.Wang, Y.X.Xu, Study of a solar powered solid adsorption desiccant cooling system used for gain storage, Renewable Energy,25(2002)417-430

Y.J.Dai, K.Sumathy,R.Z.Wang,Y.G.Li, Enhancement of natural ventilation in a solar house with a solar chimney and solid adsorption cooling cavity, Solar Energy,74(2003)65-75

Yonggao Yin, Xiaosong Zhang, Geng Wang, Lei Luo, Experimental study on a new internally cooled/heated dehumidifier/regenerator of liquid desiccant systems in international journal of refrigeration xxx (2007) 1–10

Yanxiang Wang, Shouhong Tan, Dongliang Jiang, The effect of porous carbon preform and the infiltration process on the properties of reaction-formed SiC, Carbon 42 (2004) 1833–1839

Z

Zhaokun Ma, Jingli Shi, Yan Song, Quanguo Guo, Gengtai Zhai, Lang Liu, Carbon with high thermal conductivity, prepared from ribbon-shaped mesophase pitch-based fibers, Carbon 44 (2006) 1298–1352

Zhenyi Liu, Guoding Zhang, Hong Li, Jinliang Sun, Musu Ren, Al infiltrated C–C hybrid composites, Materials and Design 26 (2005) 83–87

Zurigat YH, Abu-Arabi MK, Abdul-Wahab SA, Air dehumidification by triethylene glycol desiccant in a packed column, Energy Convers Manage, 45 (2004), 141-155

Websites:

Web1.1 http://en.wikipedia.org/wiki/Global_warming

Web1.2 <http://search.live.com/images/>

Web1.3 http://en.wikipedia.org/wiki/Energy_policy_of_the_United_Kingdom

Web2.1 <http://www.cooling-pads.usgr.com/cooling-pads.html>

Web3.1 <http://www.lsbu.ac.uk/water/molecule.html>

Web3.2 http://cai.tongji.edu.cn/wanluokecheng/p03/ch08/example/exa08_09_01

Web3.3 http://www.ifam-dd.fraunhofer.de/fhg/ifam_dd/EN/gebiete/schaum/index.jsp

Web3.4 <http://www.briwax-online.com/GMTStainless.html>

Web3.5 http://www.coleparmer.co.uk/catalog/Product_Index.asp?search=Aluminum+nitride

Web8.1 <http://gohvacsupply.com/store.php?cid=53>

Web8.2 <http://www.isaw.com.cn>

Web8.3 <http://www.eco-nomical.co.uk/SolarWaterProduct.htm>

Web8.4 <http://www.coolingtowersystems.com/listpriceguide/coolingtowerlistprice.html>

Web8.5 <http://www.isa.org/PrinterTemplate.cfm?Section=Training&Template=/Ecommerce/ProductDisplay.cfm&ProductID=8535>

Web8.6 www.levelclark.demon.co.uk

Web8.7 <http://www.edfenergy.com/html/showPage.do?name=welcome.til>

Web8.8 <http://en.wikipedia.org/wiki/R-744>

Appendixes

Appendix I —Thermal Parameters of Air

Vapour pressure, moisture content and enthalpy calculating equations based on the air temperature and relative humidity (A.W.T.Barenbrug, 1974):

$$p = 0.61078 \exp\left(\frac{17.269 \times t}{237.3 + t}\right) \quad (1)$$

$$d = 0.622 \frac{\phi\% \times p}{P - \phi\% \times p} \quad P=101.325\text{kPa} \quad (2)$$

$$h = 1.01t + (1.84t + 2500)d \quad (3)$$

Air parameters included specific heat C_p , thermal diffusivity α , kinematic viscosity ν and density ρ , dynamical viscosity μ , thermal conductivity k can be calculated by the equations as the followings (Web, 1, 2007):

$$T = t + 273.15$$

$$\nu = -1.1555\text{E-}14 \times T^3 + 9.5728\text{E-}11 \times T^2 + 3.7604\text{E-}08 \times T - 3.4484\text{E-}06 \quad (R^2= 0.99997) \quad (4)$$

$$k = 1.5207\text{E-}11 \times T^3 - 4.8574\text{E-}08 \times T^2 + 1.0184\text{E-}04 \times T - 3.9333\text{E-}04 \quad (R^2= 0.99993) \quad (5)$$

$$\rho = 360.77819 \times T^{-1.00336} \quad (R^2= 0.99997) \quad (6)$$

$$C_p = 1.9327\text{E-}10 \times T^4 - 7.9999\text{E-}07 \times T^3 + 1.1407\text{E-}03 \times T^2 - 4.4890\text{E-}01 \times T + 1.0575\text{E+}03 \quad (R^2= 0.99961) \quad (7)$$

$$\alpha = 9.1018\text{E-}11 \times T^2 + 8.8197\text{E-}08 \times T - 1.0654\text{E-}05 \quad (R^2= 0.99987) \quad (8)$$

Appendix II —Thermal Parameters of LiCl, CaCl₂ and LiBr Solutions

Thermal parameters of LiCl solution includes: enthalpy h specific heat C_p , thermal diffusivity α , density ρ , and dynamical viscosity μ , thermal conductivity k (Manuel R.Conde, et al, 2004)

Density of LiCl /CaCl₂ solution

$$\rho_{LiCl} = \rho_{H_2O}(\tau) \left(\sum_{i=0}^3 \rho_i \left(\frac{C^{Cl}}{1 - C^{Cl}} \right)^i \right) \quad (9)$$

$$\rho_{H_2O}(\tau) = \rho_{c, H_2O} \left(1 + B_0 \tau^{1/3} + B_1 \tau^{2/3} + B_2 \tau^{5/3} + B_3 \tau^{16/3} + B_4 \tau^{43/3} + B_5 \tau^{110/3} \right) \quad (10)$$

Where $\tau \equiv 1 - \theta$ and ρ_{c, H_2O} is the density of water at the critical point (322kg/m³)

Table 1 Parameters of the density equation for LiCl-H₂O solutions

	ρ_0	ρ_1	ρ_2	ρ_3
LiCl solution	1.0	0.540966	-0.303792	0.100791
CaCl solution	1.0	0.836014	-0.436300	0.105642

Table2 Parameters of the density equation for LiCl-H₂O solutions

B_0	1.993 771 843 0	B_3	-1.761 912 427 0
B_1	1.098 521 160 4	B_4	-44.900 548 026 7
B_2	-0.509 449 299 6	B_5	-723692.261 863 2

Dynamic Viscosity of LiCl /CaCl₂ solution

$$\mu = \mu_{H_2O}(\theta)e^{\mu_1\zeta^{3.6} + \mu_2\zeta + \mu_3\frac{\zeta}{\theta} + \mu_4\zeta^2} \quad (11)$$

Where ζ is defined as $\zeta = \frac{C_{Cl}}{(1-C_{Cl})^{0.6}}$ (12)

$$\mu_{H_2O} = \mu_{H_2O,0}(A + B\theta^{0.02} + C\theta^{0.04} + D\theta^{0.08} + E\theta^{2.85} + F\theta^8) \quad (13)$$

$\mu_{H_2O,0}$ is the dynamic viscosity of water at 0 °C.

Table 3 Parameters of the dynamic viscosity equation for LiCl-H₂O solutions

A	B	C	D	E	F
1.026 186 2	12 481.702	-19 510.923	7 065.286	-395.561	143 922.996

Specific Thermal Capacity of LiCl /CaCl₂ solution

Table 4 Parameters of the specific thermal capacity equation for solutions

	A	B	C	D	E	F	G	H
LiCl solution	1.429 80	-1.243 17	-0.120 70	0.128 25	0.629 34	58.522 5	-105.634 3	47.794 8
CaCl ₂ solution	1.637 99	-1.690 02	1.051 24	0.0	0.0	58.522 5	-105.634 3	47.794 8

$$C_{P, Cl} = C_{P, H_2O}(T)(1 - f_1(C_{Cl})f_2(T)) \quad (14)$$

$$C_{P, H_2O}(T) = 88.7891 - 120.1958\theta^{0.02} - 16.9264\theta^{0.04} + 52.4654\theta^{0.06} + 0.10826\theta^{1.8} + 0.46988\theta^8 \quad (15)$$

$$\theta = \frac{T}{228} - 1 \quad (16)$$

$$f_1(C_{Cl}) = AC_{Cl} + BC_{Cl}^2 + CC_{Cl}^3 \quad (C_{Cl} \leq 31\%) \quad (17)$$

$$f_1(T) = D + EC_{Cl} \quad (C_{Cl} > 31\%) \quad (18)$$

$$f_2(T) = F\theta^{0.02} + G\theta^{0.04} + H\theta^{0.06} \quad (19)$$

Vapour pressure of LiCl /CaCl₂ solution

$$p_{LiCl} = A_{25}f(C^{Cl}, \theta) + f(water) \quad (20)$$

$$\theta \equiv \frac{T}{228} - 1 \quad (21)$$

$$f(C^{Cl}, \theta) = A + B\theta \quad (22)$$

$$A = 2 - \left(1 + \left(\frac{C^{CL}}{A_0}\right)^{A_1}\right)^{A_2} \quad B = \left(1 + \left(\frac{C^{CL}}{A_3}\right)^{A_4}\right)^{A_5} - 1$$

$$A_{25} = 1 - \left(1 + \left(\frac{C^{CL}}{A_6}\right)^{A_7}\right)^{A_8} - A_9 e^{\frac{-(C^{CL}-0.1)^2}{0.005}} \quad (23)$$

$f(water)$ is the vapour pressure above the normal water surface at different temperature, the fitting curve is gain from the Figure 1(web1).

Vapour pressure on the water surface

$$\ln(p/p_c) = (a_1\tau + a_2\tau^{1.5} + a_3\tau^3 + a_4\tau^{3.5} + a_5\tau^4 + a_6\tau^{7.5})T_c/T, \quad (24)$$

Where p is the pressure, $T = T_{90}$, and subscript c indicates the values at the critical point; $\tau = 1 - T/T_c$. The values for substitution in the equation are:

$$T_c = 647.096K \quad p_c = 220.64 \text{ kPa} \quad a_1 = -7.85951783 \quad a_2 = 1.84408259$$

$$a_3 = -11.7866497 \quad a_4 = 22.6807411 \quad a_5 = -15.9618719 \quad a_6 = 1.80122502$$

Table 5 Parameters of the vapour pressure equation for solutions

	A ₀	A ₁	A ₂	A ₃	A ₄	A ₅	A ₆	A ₇	A ₈	A ₉
LiCl solution	0.28	4.3	0.6	0.21	5.1	0.49	0.362	-4.75	-0.4	0.03
CaCl ₂ solution	0.31	3.698	0.6	0.231	4.584	0.49	0.478	-5.2	-0.4	0.018

Diffusion Coefficient of water into Solutions

$$D_{AB} = D_0 \left(1 - \left(1 + \left(\frac{\sqrt{C^{Cl}}}{B_1}\right)^{B_2}\right)^{B_3}\right) \quad (25)$$

$$D_0 = \frac{0.11353 \times 10^{-16} RT_{water} \Lambda_c^{2/3}}{\mu_{water} \Lambda_{water}} \quad (26)$$

$$\mu_{water} = 2.414 \times 10^{-5} \times 10^{247.8/(T_{water}-140)} \quad (27)$$

(<http://en.wikipedia.org/wiki/Viscosity>)

$$\Lambda_c = 0.05559 \text{ m}^3/\text{mol} \quad \Lambda_{water} = 0.018 \text{ m}^3/\text{mol}$$

Table 6 Parameters of the water diffusion coefficient equation into solutions

	A ₀	A ₁	A ₂	A ₃	A ₄	A ₅	A ₆	A ₇	A ₈	A ₉
LiCl solution	0.28	4.3	0.6	0.21	5.1	0.49	0.362	-4.75	-0.4	0.03
CaCl ₂ solution	0.31	3.698	0.6	0.231	4.584	0.49	0.478	-5.2	-0.4	0.018

The enthalpy of the LiBr solution at temperature t^{Br} and concentration C^{Br} can be gained by the group of the following equations [3]:

$$X = C^{Br} / 76 \quad (28)$$

$$T = t^{Br} / 191 \quad (29)$$

$$E_1 = 4.2676X - 1.2627T - 1.4966 \quad (30)$$

$$F_1 = 1/(1 + e^{-E_1}) \quad (31)$$

$$E_2 = -3.1227X + 1.0459T - 0.93206 \quad (32)$$

$$F_2 = 1/(1 + e^{-E_2}) \quad (33)$$

$$E_3 = 5.6623X - 3.7293T - 2.6641 \quad (34)$$

$$F_3 = 1/(1 + e^{-E_3}) \quad (35)$$

$$E_4 = 1.7248X - 0.47757T + 0.6311 \quad (36)$$

$$F_4 = 1/(1 + e^{-E_4}) \quad (37)$$

$$E_5 = 12.7082X - 8.7818T + 8.483 \quad (38)$$

$$F_5 = 1/(1 + e^{-E_5}) \quad (39)$$

$$E_6 = -0.064516X + 7.2131T + 2.5795 \quad (40)$$

$$F_6 = 1/(1 + e^{-E_6}) \quad (41)$$

$$E_7 = 0.026916X - 63.5969T - 1.6957 \quad (42)$$

$$F_7 = 1/(1 + e^{-E_7}) \quad (43)$$

$$E_8 = -39.5995X + 37.9497T - 40.4815 \quad (44)$$

$$F_8 = 1/(1 + e^{-E_8}) \quad (45)$$

$$E_9 = -12.2997F_1 + 57.3418F_2 - 3.0813F_3 + 111.869F_4 - 2.4623F_5 + 27.0311F_6 - 44.8749F_7 + 44.213F_8 - 112.8907 \quad (46)$$

$$h^{Br} = 810/(1 + e^{-E_8}) \quad (47)$$

Because the desiccant solution is soaked into the fibre paper membranes, one thin saturated desiccant layer covering on the membranes surfaces contacts with air flow directly. The vapour pressure of the desiccant solution is considered as the saturated vapour pressure of the thin desiccant layer at temperature t^{Br} and concentration C^{Br} :

$$A_0 = -2.00755$$

$$B_0 = 124.937$$

$$F = 7.05$$

$$A_1 = 0.16976$$

$$B_1 = -7.71649$$

$$D = -1596.49$$

$$A_2 = -3.133362 \times 10^{-3}$$

$$B_2 = 0.152286$$

$$E = -104095.5$$

$$A_3 = 1.97668 \times 10^{-5}$$

$$B_3 = -7.9509 \times 10^{-4}$$

$$T^{Br} = \frac{(t^{Br} - \sum_0^3 B_n C^{Br^n})}{\sum_0^3 A_n C^{Br^n}} \quad (48)$$

$$p^{Br} = 10^{(F+D/T^{Br}+(E/T^{Br^2}))} \quad (45 < C^{Br} < 70\%) \quad (49)$$

$$p^{Br} = -9.12555 + 0.3836610T^{Br} \quad (C^{Br}=45\%) \quad (50)$$

$$p^{Br} = -9.38706 + 0.44817T^{Br} \quad (C^{Br}=40\%) \quad (51)$$

$$p^{Br} = -9.64088 + 0.51466T^{Br} \quad (C^{Br}=35\%) \quad (52)$$

$$p^{Br} = -11.34804 + 0.59145T^{Br} \quad (C^{Br}=30\%) \quad (53)$$

$$p^{Br} = -15.15182 + 0.78107T^{Br} \quad (C^{Br}=0\%) \quad (54)$$

Enthalpy and vapour pressure mathematical analyses for the LiCl solution

The enthalpy of the LiCl solution at temperature t^{Cl} and concentration C^{Cl} can be gained from the group of the following equations [3]:

$$X = C^{Cl} / 51 \quad (55)$$

$$T = t^{Cl} / 121 \quad (56)$$

$$E_1 = -5.143X + 2.6514T - 6.2915 \quad (57)$$

$$F_1 = 1/(1 + e^{-E_1}) \quad (58)$$

$$E_2 = -0.76695X - 6.5859T - 6.3701 \quad (59)$$

$$F_2 = 1/(1 + e^{-E_2}) \quad (60)$$

$$E_3 = -5.3177X + 2.7087T - 5.1454 \quad (61)$$

$$F_3 = 1/(1 + e^{-E_3}) \quad (62)$$

$$E_4 = 1.8305X + 0.98974T - 9.7099 \quad (63)$$

$$F_4 = 1/(1 + e^{-E_4}) \quad (64)$$

$$E_5 = 13293.5116F_1 - 2545.7435F_2 - 4095.9176F_3 + 4560.039F_4 - 2.0774 \quad (65)$$

$$h^{Cl} = 451/(1 + e^{-E_5}) \quad (66)$$

Equilibrium moisture content of LiCl solution can be calculated by the following equations exported out from the Lithium Chloride equilibrium humidity ratio chart showed in ASHRAE 2000 [2].

$$1) C^{Cl} \leq 20$$

$$d^{Cl} = 2.46935e^{(t^{Cl}/14.79138)} - 0.20779 \quad (67)$$

$$2) 20 < C^{Cl} \leq 25$$

$$d^{Cl} = (2.46935e^{(t^{Cl}/14.79138)} - 0.20779) - (2.46935e^{(t^{Cl}/14.79138)} - 0.20779 - 1.43248e^{(t^{Cl}/14.31737)} - 0.14869)/5 \times (25 - C^{Cl}) \quad (68)$$

3) $25 < C^{Cl} \leq 30$

$$d^{Cl} = (1.43248e^{(t^{Cl}/14.31737)} - 0.14869) + (2.46935e^{(t^{Cl}/14.79138)} - 0.20779 - 1.43248e^{(t^{Cl}/14.31737)} - 0.14869)/5 \times (30 - C^{Cl}) \quad (69)$$

4) $30 < C^{Cl} \leq 35$

$$d^{Cl} = (1.43248e^{(t^{Cl}/14.31737)} - 0.14869) - (1.43248e^{(t^{Cl}/14.31737)} - 0.14869 - 1.3372e^{(t^{Cl}/22.12633)} - 0.81576)/5 \times (35 - C^{Cl}) \quad (70)$$

5) $35 < C^{Cl} \leq 40$

$$d^{Cl} = (1.3372e^{(t^{Cl}/22.12633)} - 0.81576) + (1.43248e^{(t^{Cl}/14.31737)} - 0.14869 - 1.3372e^{(t^{Cl}/22.12633)} - 0.81576)/5 \times (35 - C^{Cl}) \quad (71)$$

5) $C^{Cl} > 40$

$$d^{Cl} = 1.3372e^{(t^{Cl}/22.12633)} - 0.81576 \quad (72)$$

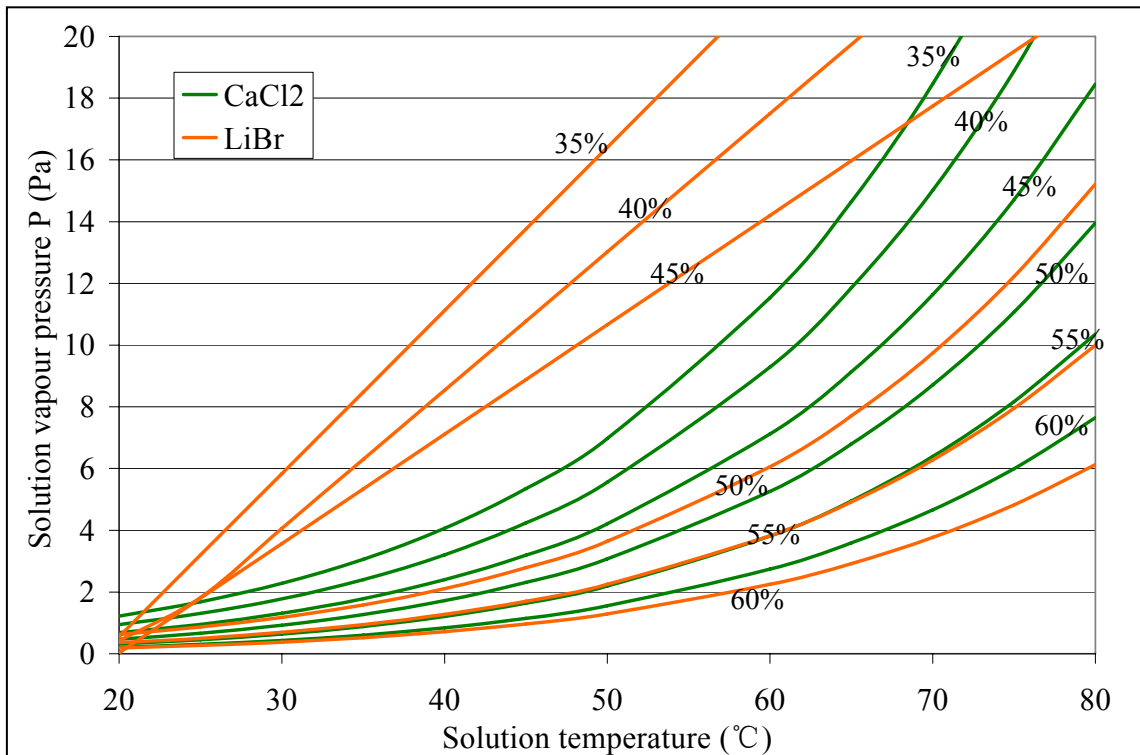


Figure 1 Dühring diagram of LiBr and CaCl₂ solution

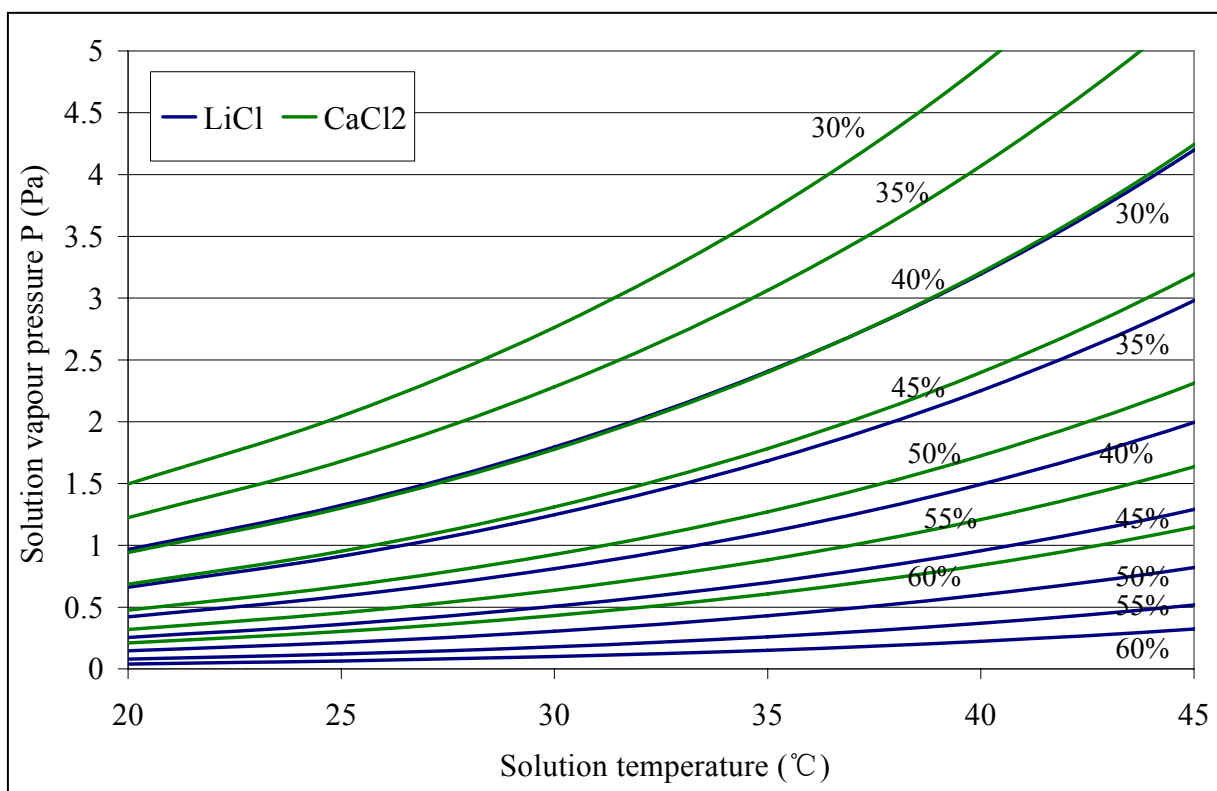


Figure 2 Dühring diagram of LiCl and CaCl₂ solution

Appendix III —Henry’s Law Constant of the Aqueous Solutions

Henry’s law constant *H* for different solution at varying temperature under the Atmospheric pressure (101.325kPa) are listed in Table 7.

Table 7 Henry’s law constant of the solutions into water

Temperature (°C)	0 (°C)	20 (°C)	100 (°C)
Solution/100 g water			
LiCl solution	67	83.2	127.5
CaCl solution	59.5	_____	159
LiBr solution	58	62	73

$$H_{LiCl} = -0.00256t^2 + 0.86125t + 67 \quad (\text{Atmospheric pressure is } 1.01325 \text{ kPa})$$

$$H_{LiBr} = -6.25 \times 10^{-4}t^2 + 0.2125t + 58 \quad (\text{Atmospheric pressure is } 1.01325 \text{ kPa})$$

$$H_{CaCl_2} = 0.995t + 59.5 \quad (\text{Atmospheric pressure is } 1.01325 \text{ kPa})$$

Web 1 <http://baike.baidu.com/view/570939.htm>

Web 2 <http://baike.baidu.com/view/162685.htm>